THE EFFECT OF MICROALLOY ADDITIONS ON FERRITIC WELD METAL MICROSTRUCTURES.

BY

CHRISTOPHER SMITH BSc.

Doctor Of Philosophy

THE UNIVERSITY OF ASTON IN BIRMINGHAM

SEPTEMBER 1986

THE UNIVERSITY OF ASTON IN BIRMINGHAM

THE EFFECT OF MICROALLOY ADDITIONS ON FERRITIC WELD METAL MICROSTRUCTURES.

SUMMARY

Christopher Smith, Doctor Of Philosophy, 1986.

The objective of this research was to gain a further understanding of ferritic steel weld metal microstructures and the compositional factors affecting their formation. Continuous cooling transformation (CCT) diagrams have been produced isolating the effects of low and high concentrations of the microalloying elements vanadium, titanium, niobium and aluminium on the development of as-deposited and reheated weld metal microstructures, with low oxygen contents. The effects of carbon and oxygen content have also been considered. In order to achieve this, thermal analysis and dilation techniques were used for simulating as-deposited and reheated weld metal.

The type and proportions of ferritic constituents were significantly affected by the addition of microalloying elements, even at low concentations. The transformation temperatures were depressed and the phase field on the CCT diagrams displaced to longer times.

In the simulated as-deposited weld metal, low microalloy additions suppressed primary ferrite(PF) and ferrite side plate(FSP) growth, initially increasing the proportion of acicular ferrite(AF) and at faster cooling rates, lath ferrite(LF). High AF contents could be achieved in low oxygen content weld metal, in the absence of a suitable oxide inclusion population, to act as nucleation sites. High microalloying elements significantly increased the proportions of LF, even at slow cooling rates. High titanium and niobium concentration refined the prior austenite grain size, promoting PF at slow cooling rates.

Reduced carbon content increased the transformation temperatures, favouring PF, FSP and AF formation. LF only formed at very high cooling rates. High oxygen contents refined the prior austenite grain size and the microstructures were dominated by PF and FSP constituents.

In reheated weld metal, refined equi-axed prior austenite grains were formed, as opposed to the large columnar grains seen in the simulated as-deposited material. The proportions of AF were reduced by microalloy additions and were significantly lower than in the as-deposited alloys, at similar cooling rates. PF, FSP and LF constituents dominated the microstructures.

The microphase contents and hardness were increased and microstructures refined, by microalloy additions and faster cooling rates.

KEY WORDS: WELD METAL MICROSTRUCTURES.
FERRITIC STEEL.
MICROALLOY ADDITIONS.
LOW OXYGEN CONTENT.

ACKNOWLEDGEMENTS.

The author would like to thank the Science And Engineering Research Council for funding this project and Professor R.H. Thornley, Head of the Department of Mechanical and Production Engineering, for providing the laboratory facilities.

The work of Mr K.A.A. Mills in building the arc melting apparatus and the practical assistance of Mr A. Smith must be acknowledged and was appreciated.

The Author would also like to thank Dr M.F. Jordan as supervisor during the three year research project and the subsequent assistance of Mr L. Crane and Professor Thornley for advice during the writing of this thesis.

CONTENTS.

TABLES.

FIGURES

CHAPTER 1 - INTRODUCTION.

CHAPTER 1. INTRODUCTION.

The present scale of welded construction is immense, with deep sea oil platforms, pipelines stretching hundreds of miles, giant storage tankers and pressure vessels to name but a few examples. The materials used in these constructions have to meet the high standards required in terms of strength, toughness, corrosion and fatigue, but most importantly they have to possess good weldability. These demands have provided a major impetus to the development of high strength low alloy (HSLA) steels.

In the past HSLA steels were designed on tensile strength and carbon was often used to obtain this strength. However the introduction of welding as a major fabricaton process has led to a progressive lowering of the carbon, so that now steels are available with strengths much greater than that obtained previously, but with carbon contents as low as 0.03%wt. The use of welding has also created a greater awareness of the importance of steel toughness in the presence of sharp cracks and it was readily shown, that the toughness of steel at low temperature could be improved by low carbon contents. The key to the development of these materials lies in the refinement of the ferrite grain size. During steel fabrication grain refinement of the austenite and therefore the ferrite can be achieved by additions of the microalloying elements alumimium(Al), niobium(Nb), vanadium(V) or titanium(Ti) either singularly or in combination. All but Al can also introduce some precipitation hardening by carbo-nitrides. To achieve the finest possible austenite grain size and also employ a high

solution temperature, so as to provide maximum precipitation potential, many modern HSLA steels are controlled rolled at low finishing temperatures.

A wide range of welding processes are available, but by far the most important technique used in welding construction today is fusion welding. In one of the most common fusion welding processes, manual metal arc(MMA), the heat source is provided by an electric arc, a high current and a low voltage discharge in the range of 10-2000A and 10-50V. The electrode consists of a core of filler wire coated with flux. During welding the flux melts to form slag which provide protection from atmospheric contamination. Other welding processes such as submerged arc(SA) employ separate slag feeding processes, but the principle is essentially the same. With metal and tungsten inert gas (MIG and TIG) processes, a protective atmosphere is generated using an inert gas. A wide range of welding variables have to be considered when choosing the process required, eg. heat input, welding speed etc. and these have to be designed to the specific task in hand. Many structural joint are also produced by "laying down" a number of weld runs, to build up welds in thick plate and reduce problems associated with distortion and residual stresses. Under these circumstances the weld metal will consist of as-deposited and reheated material.

During the welding process, in the heat affected zone (HAZ), the thermo-mechanical requirements for the development of a fine ferrite grain size are lost, with resultant degradation of the mechanical properties. However microalloying elements may also enter the weld pool as a

result of dilution and particularly for high dilution processes, such as SA welding, the concentrations may be as high as 70% of the parent plate content. Although beneficial to parent plate properties, under welding conditions these elements may adversely affect the properties of the weld metal.

There is widespread agreement that mechanical properties of weld metal are determined by the gross microstructure, although other factors such as oxide inclusion population are also important. In fact, in the case of low carbon structural steels it is confidently stated that the optimum conbination of strength and toughness is given by an acicular ferrite microstructure, although this is only one of a number of microstructural constituents which may be present. There is extensive evidence that the presence of microalloying elements in weld metal significantly influence toughness. Whether the effect is beneficial or detrimental would appear to depend on the type and concentration of microalloying element present and welding conditions.

A low inclusion population also increases weld toughness and there is therefore an increasing trend to reduce the oxygen content of weld metal. Ideal weld metal would therefore be achieved with low inclusion population and a microstructure consisting of a high proportion of acicular ferrite. However, although it is recognised that the factors governing the microstructure are composition and cooling rate, the necessary detailed information relating microstructure, composition and cooling rate is not available, particularly for low oxygen content conditions.

Thus the need was recognised for a research programme to clarify the effects of microalloying elements on microstructural development and gain further understanding on the mechanisms operating. Microalloying elements enter the weld pool via the parent plate or the welding wire/flux and the main types usually present in HSLA steel weld metal are V,Ti,Nb and Al. The influence of these alloys were thererfore investigated. Since the concentration may have a significant affect on toughness, typical low and high levels were studied for each microalloy type. The microalloying elements were also added to the weld metal individually in order to isolate their effects and avoid problems with interactions. The microalloyed weld metal was compared with a typical plain carbon, manganese, silicon base alloy. Because of the importance of producing low oxygen content weld metal for good toughness, the major proportion of the investigation was directed towards the influence of microalloying elements under low oxygen conditions. However some work was also carried out to determine the effect of higher oxygen levels.

A useful method for relating the effect of composition and cooling rate to microstructure, is by constructing continuous cooling transformation (CCT) diagrams. These diagrams provide information on the transformation temperature and the relative position of the phase fields with respect to cooling rate and can be used to facilitate prediction and control of the weld metal microstructures, by appropriate choice of welding consumables and parameters. However it is particularly difficult to systematically control the composition of weld metal and also produce an adequate range

of cooling rates, for constructing CCT diagrams. Therefore simulative techniques were used to reproduce the conditions and microstructures in weld metal.

Since weld metal may consist of both as-deposited and reheated material, techniques were used to simulate each type. An arc melting technique was used, to reproduced the solidification conditions of the weld pool and the microstructures present in as-deposited weld metal. For the reheated weld metal, a reheating technique was used which simulated the thermal cycle in the coarse grained region. Similar compositions were used for the as-deposited and reheated alloys to allow direct comparison. Using these simulative techniques, CCT diagrams were produced in which the only significant difference in composition was that of the microalloy addition and for cooling rates in the range 3 to 60°C/sec.

Extensive quantitative metallography was conducted to determine the influence of microalloy type/concentration and cooling rate, on type and proportions of ferrite constituents, prior austenite grain size, microphase content and ferrite grain size. Hardness tests results were also related with the microstructures observed. By comparing the effect of microalloying elements on the transformation temperatures and microstructures produced, it was possible to determine some of the mechanisms operating. Also by assuming that a high proportion of acicular ferrite in the microstructure was required for good toughness, the changes in microstructure observed could also be related to potential effects on toughness.

CHAPTER 2 - LITERATURE SURVEY.

CHAPTER 2. LITERATURE SURVEY.

2.0 INTRODUCTION.

The presence of microalloying elements in HSLA steel weld metal can influence the ferritic microstructures formed and consequently the mechanical properties. Although the transformation from austenite to ferrite is directly influenced by the composition and cooling rate the mechanisms are complex. The development of the ferrite structure is dependent on a number of factors including:

1. Solidification structure.
2. Prior austenite grain size.
3. Hardenability.
4. The degree of undercooling.
5. Solute diffusion rate.
6. Heterogeneous nucleation on second phase particles.
7. Growth rate of the ferrite phases.

These are inter-related and also influenced by the process variables.

In the following sections the factors influencing the microstructures formed in ferritic weld metal will be reviewed, with particular emphasis on the effects and mechanisms associated with microalloying elements.

2.1 WELD METAL MICROSTRUCTURE AND TERMINOLOGY.

In any study of phase transformation it is essential to define the microstructures observed. Even a brief review of the literature dealing with welded ferritic steels, would indicate that the terminology used to describe weld metal microstructures has been the subject of much debate. It is also clear that the wide range of terms used has probably led to considerable confusion.

Early classifications of ferritic microstructures were produced by Dube(1) and later Aaronson(2) for isothermal transformation from austenite to ferrite. Although the proposed morphologies were uniquely identifiable for isothermally transformed specimens, the structures of continuously cooled weld metal were found to be less distinct.

Cochrane(3) attempted to classify weld microstructures using the Dube terminology, while also indicating the factors thought to control ferrite growth. It was concluded that the problems associated with this terminology reflected the difficulty in describing a three dimensional structure, in terms of a two dimensional section.

Widgery(4) suggested that classification of weld metal microstructures presented the investigator with a choice:

1. To use a simple system, relying on the use of a light microscope, which would permit quantitative measurements of good reproducibility.
2. To use a complex system, which would describe the transformation products accurately, but would make reproducible quantitative measurements

difficult ie. use of an electron microscope. Having found that it was possible to correlate mechanical properties with quantitative metallographic data produced using a light microscope, it was concluded that this simple classification was the best technique for undertaking quantitative analysis of weld metal microstructures.

Abson and Dolby(5) recently proposed a scheme for quantitative description of weld metal microstructures, again utilising the light microscope. It was suggested that since electron microscopes were only available to a limited number of workers, a scheme based on optical microscopy would have a wider application. However it was also recognised that by using a light microscope only, certain constituents of similar appearance may be grouped together despite having differences in detailed microstructure. A collaborative effort is currently in progress at the Welding Institute to further refine the terminology and microstructural descriptions proposed by this scheme. Based on work from this programme (6), a flow chart has been proposed, for use by workers investigating weld metal microstructures, which may be used to characterised the major microstructural constituents, fig. 2.1.

The microstructural constituents found in ferritic steel weld metal will now be discussed in more detail. The terminology used by various authors will be indicated and the confusion arising from this will be highlighted.

2.1.1 PRIMARY FERRITE.

In the IIW Sub-commission IX Scheme(6) primary ferrite can occur in two forms. If present as "veins" outlining the

prior austenite grain boundaries, it may be defined as grain boundary ferrite(GBF), fig. 2.2. This constituent is pro-eutectoid in nature and has been reported to form in the temperature ranges:

a. 1000-750 °C, (7)

b. 770 -680 °C, (8)

c. 700 -625 °C, (9).

If the ferrite colony is three times the average intragranular lath size (6), the constituent may be termed polygonal ferrite. Cochrane(3) described this constituent as ferrite islands. Polygonal ferrite is similar in nature to GBF, being pro-eutectoid, but it may form intragranularly, fig. 2.2. Cochrane(3) suggested that polygonal ferrite may arise in as-deposited weld metal due to the short time available for recovery and grain grow. However it is more readily observed in reheated weld metal

2.1.2 FERRITE SIDE PLATES.

Other terms used to describe this phase have been upper bainite(10), lamellar product(4) and ferrite with aligned second phase(6). This constituent has been subject to much confusion in the literature as a result of its similarity in appearance to a structure that forms at lower transformation temperatures. This phase generally appears as single or multiple plates growing continuously from primary ferrite aligning the prior austenite grain boundaries.

As an example of the apparent confusion surrounding this phase, Glover et al(10) found that at faster cooling rates the proportions of this constituent, termed "upper

bainite", increased in preference to acicular ferrite, while Dolby(11) predicted exactily the opposite. Choi and Hill(7) later observed that a structure which was optically similar to this phase, also formed at a lower transformation temperature to acicular ferrite. Therefore the term "upper bainite" had been used to describe two different transformation products, one forming at higher temperatures than acicular ferrite and the other at lower temperatures.

Since the IIW scheme(6) for weld terminology is only based on a light microscope, these two transformation products are not distinguished and are termed ferrite with aligned second phase, fig. 2.2. The constituent is described as adjacent parrallel laths. Harrison(12) distinguished between the high and low temperature transformation products using the terms ferrite side plates(FSP) and lath ferrite, respectively. Transmission electron microscopy(TEM),(7) has indicated that ferrite side plate structures are characterised by a low dislocation density, which is said to be indicative of a high transformation temperature. The transformation ranges which have been quoted for FSP formation are:

a. 750-650 °C (7),

b. 700-500 °C (8),

c. 625-600 °C (9).

2.1.3 ACICULAR FERRITE.

This structure has also been called bainitic ferrite(8). It consists of fine interlocking grains of aspect ratio greater than 4 to 1 (6), which form intragranularly, fig.

2.2. The fine grain size and high angled grain boundaries associated with this phase, provide a high resistance to crack propagation and consequently high toughness. Which accounts for the general requirement for high proportions of acicular ferrite(AF) in weld metal microstructures.

The nucleation and growth mechanism of this constituent is still not fully understood. Ricks(13) suggested that it was a form of Widmanstatten ferrite, while Ito(8) concluded that it was formed by a bainitic reaction. TEM(7) has indicated that AF grains have a high dislocation density. The transformation temperature ranges reported for this constituent are:

a. 650-600 °C (7),

b. 600-575 °C (8),(14).

2.1.4 LATH FERRITE.

Due to the reported difficulty in distinguishing this constituent fron FSP structures, using an optical microscope, the IIW scheme(6), would also group lath ferrite(LF) as ferrite with aligned second phase, fig. 2.2. LF has be described as fine parallel laths, which form between AF or FSP (12), although in the absence of higher transformation products the microstructure may consist entirely of this lath structure. Choi and Hill(7) noted that LF formed at low temperatures(<500 °C), below the AF transformation range and contained a very high dislocation density, with carbide films between the laths. This they suggested indicated that this phase was a form of bainite.

2.1.5 FERRITE CARBIDE AGGREGATE.

This is the term used to describe structures which form

in the later stages of transformation, in the carbon enriched regions between the ferrite grains. If the colony size is less than the average ferrite grain size then the constituent is classified as a microphase in accordance with the IIW scheme(6). A degenerate form of pearlite, which may also be describe using the term ferrite carbide aggregate(FC), has been observed in weld metal adjacent to primary ferrite, fig. 2.2. TEM examination has revealed that this pearlite was not lamellar, but consisted of carbides distributed in regular arrays of spherical or rod shaped particles(15).

2.1.6 MARTENSITE.

Colonies of martensite are rare in high strength low alloy steel weld metal, deposited by normal arc welding techniques. If present it may be either twinned or lath. Garland(16) found that lath martenite was particularly associated with solidification boundaries in submerged-arc welds and was deleterious to toughness. Martensite is however normally present as a microphase in weld metal.

2.1.7 MICROPHASES.

Microphases tend to form between ferrite grains, as the final products of transformation. As a result of carbon redistribution from the ferrite during transformation, these regions transform to martensite-austenite(M-A) structures or carbides. It is possible to observe the distribution of these microphases using a light microscpe, with a picral etch, although identification usually requires an electron microscope (6). However Garland and Kirkwood(16) have differentiated between two types of

microphases using a picral etch and a light microscope. They suggested that dark etching microphases were predominantly carbides, fig. 2.3a, while light etching phases surrounded by a dark band could be classified as lath martenite, fig. 2.3b.

2.1.8 TRANSFORMATION SEQUENCE.

The transformation temperature ranges reported for the formation of each microstructural constituent appeared to vary considerably, from one investigation to another, which probably reflects the differences in composition and conditions used. However there appears to be a general agreement on the transformation sequence in submerged arc weld metal, which should also apply to other processes. Quenching weld metal from temperatures in the range 1000 to 500 °C (3,17) has indicated the transformation sequence, in descending order of temperature as:

1. Primary ferrite.
2. Ferrite side plate.
3. Acicular ferrite.
4. Lath ferrite.
5. Ferrite carbide aggregate.
6. Microphases.

2.2 THE EFFECT OF MICROSTRUCTURE ON WELD PROPERTIES.

The properties of weld metal are determined to a large exent by the microstructure. It has been established that the best weld properties in terms of strength and toughness are associated with weld metal containing a high proportion of AF (18). The fine grain size of this constituent together with high angled grain boundaries and high

dislocation density, give increased strength and resistance to crack propagation. Other microstructural constituents give poor toughness properties as a result of their large effective grain size and low angled boundaries, which do not provide an effective barrier to crack propagation. The Hall-Petch relationship(19):

$$\sigma = \sigma_0 + k \times d^{-1/2}$$

were σ_0 and k are constants for the material, may be used as a simple guide to the influence of grain size(d) on material strength(σ), while the effect on toughness is clearly demonstrated in fig. 2.4.

Microphases may also influence the toughness of the weld metal. Microcracks can nucleate at grain boundaries within the microphase and subsequently propagate through the grains (20). In this context lath martensite microphases have been shown to be particularly detrimental to weld toughness (16).

Tuliani(18) found that the flux type could also affect weld metal toughness, by influencing the oxide inclusion population, size and distribution. The fluxes were classified using a basicity index, in which higher values denote basic fluxes and generally produce lower oxygen content weld metal, with a low oxide inclusion population. It was found that improved toughness was achieved with more basic fluxes, fig. 2.5. The requirement for improved toughness, has provided the impetus for the development of high basicity fluxes, which reduced the oxygen content of the weld metal and corresponding inclusion population.

2.3 SOLIDIFICATION OF WELD METAL.

The structure formed during solidification of weld metal determines to a large extent the segregation patterns of alloying elements and inclusions. This alloy segregation and inclusion distribution may play a significant role in determining the ferrite microstructure on subsequent cooling

During welding it is essential that the base metal is melted to some degree, thus removing oxides and other impurites from the fusion zone. The similarity in composition produced by this dilution results in good "wetting" of the base metal by the molten weld metal and consequently a low energy barrier to solidification. This effectively means that no undercooling is required prior to solidification and the weld crystal forms uniformly over the whole grain of the base metal by "epitaxial" growth. The consequence of this epitaxial growth mechanism is that the initial grain size of the weld metal may be determined by the grain size of the unmelted fusion boundary.

It is the absence of this energy barrier to solidification in weld metal which differentiates it from solidification in cast metal. In casting the composition of the molten metal and the mould wall are completely different and as a result of poor wetting, a high degree of undercooling is required prior to solidification.

2.3.1 SOLIDIFICATION STRUCTURE

The solidification structure is determined by a number of factors including:

1. Solute concentration gradient,

2. Degree of solute partitioning,

3. Temperature gradient.

During the solidification of alloys, it is well established that solute partitioning occurs between the solid and liquid phases. For steels the partition coefficient(k):

$$k = Xs/Xl$$

were Xs and Xl are the solute contents of the solid and liquid respectively, is less than one and therefore there is a "build up" of solute ahead of the solid-liquid interface. Savage(21) suggested that a boundary layer would exist at the solid-liquid interface in which the solute concentration was governed by diffusion. It therefore followed that a concentration gradient would exist ahead of the solid-liquid interface, the magnitude of which was found to increase with higher heat input weld processes, eg SA welding.

The degree of segregation may be influenced by the growth rate of the weld crystal, with higher rates reducing the width of the concentration gradient resulting in a higher solute level at the solid-liquid interface. The alloying elements present may also influence segregation, were in general elements or impurities that tend to widen the solidification range or reduce the partition coefficient, increase the amount of segregation. Increased solidification range as a result of the fast cooling rates found in welding would also increase segregation.

Increased solute content ahead of the solidification interface lowers the solidification temperature, compared to the melting temperature of the solid. This region of

lower solidification temperature is said to be constitutionally supercooled. The degree of constitutional supercooling is determined by segregation. The consequence of constitutional supercooling on the solidification mode and sub-structure has been discussed extensively by Easterling(22). The temperature gradient is particularly important in determining the solidification mode and in general it is increased with arcs of higher heat intensity. The solidification substructure as a function of the solidification parameter and solute content (23) is shown schematically in fig. 2.6, which indicates that decreased temperature gradient tends to produce a more dendritic structure. Since the temperature gradient decreases towards the weld centre line, the sub-structure may also progressively change from planar at the fusion boundary to dendritic at the centre.

The degree of segregation at the cell or dendrite boundaries is dependent on the cell or dendrite arm spacing. Generally the finer the cell spacing the more homogenious the segregation. It has been found that for most metals the arm spacing S can be related to the temperature gradient G and the growth rate R by the relationship(22)

$$S = 1/GR$$

Factors which increase R and G such as high welding speed, high melting point alloys, low thermal conductivety etc., produce a finer arm spacing with a more even distribution of alloying elements.

2.3.2 SEGREGATION OF ALLOYING ELEMENTS AND INCLUSIONS DURING SOLIDIFICATION.

The segregation of various alloying elements and impurities depends not only on their partition coefficient, but also on their diffusion rates in ferrite or austenite. It has been estimated that the diffusion rate in ferrite is one hundred times faster than in austenite. Therefore whether a steel solidifies as delta ferrite or austenite may be significant in affecting the subsequent degree of segregation.

Fredriksson(24) argued that although the initial segregation was determined by the partition coefficient of the solute element, "back diffusion" could occur after solidification, due to the fast diffusion rates possible in delta ferrite, increasing the homogeneity of the material. However it was also indicated that segregation was dependent on the cooling rate, with faster rates giving less time for "back diffusion" to occur. Estimates suggested that even at fast cooling rates the segregation of vanadium and niobium was significant. But at cooling rates less than 30 °C/sec., back diffusion of carbon in delta ferrite could occur, although at rates encountered in welding segregation would still be significant.

Using X-ray microanalysis, Vasiljec(25) indicated that solute segregation at cell boundaries and solidification fronts was significant in weld metal. Marked heterogeneity in the distribution of inclusions within the weld metal was also observed, with two regions apparent:

1. A narrow band adjacent to the fusion line, which

was characterised by a low inclusion population, probably corresponding to planar growth.

2. The bulk of the weld metal with a non-uniform distribution of inclusions, which appeared to be located at cell boundaries and solidification fronts.

Keville(26) also noted the presence of inclusions at the delta ferrite and cell boundaries.

However Wardell(27) suggested that in most cases inclusions were overtaken by the solid-liquid interface and were therefore randomly distributed within the weld metal and not specifically present at solidification boundaries.

2.3.3 THE EFFECT OF MICROALLOYING ELEMENTS ON SOLIDIFICATION STRUCTURE.

Ohashi(28) and Nishio(29) have indicated that non-metallic inclusions and particles may significantly influence solidification in castings and weld metal respectively. Ohashi(28) found that oxides of aluminium, silicon and manganese could produce heterogeneous nucleation of delta ferrite in castings, with alumina inclusions being the most potent sites.

Nishio(29) suggested that carbides and nitrides of titanium, niobium, zirconium and boron were stable in the weld pool and could influence the solidification mode. It was shown that the addition of 0.03%wt of titanium or niobium could change the solidification mode from columnar to a finer columnar dendritic structure, with titanium being the most effective. Thaulow(30) also found that when the titanium content of weld metal exceeded 0.06%wt,

titanium carbide particles were formed which refined the microstructure.

Turnbull and Vonnegut(31) determined that compounds with small disregistry act as sites for heterogeneous nucleation. Disregistry (Dr) is the ratio of lattice parameters between the compound and delta ferrite and is determined using the relationship:

$$Dr = a \times 100\% / \Delta a$$

were "aΔ" is the difference in lattice parameters between the compound and delta ferrite and "a" is the lattice parameter of the delta ferrite. Nishio(29) calculated the disregistry between various oxides, nitrides, carbides and delta ferrite and confirmed the low disregistry of the titanium compounds, found to influence solidification.

Other investigators (32,33) have suggested that heterogeneous nucleation in castings and subsequent grain refinement was not possible since all potential nuclei would be soluble in the molten metal. However Bailey(33) also noted that because of the limited melting and cooling time available in welding some particles may survive.

2.3.4 THE EFFECT OF HAZ GRAIN SIZE ON SOLIDIFICATION.

A number of workers have suggested that since solidification in weld metal is epitaxial, the initial grain size of the delta ferrite formed is closely related to the heat affected zone(HAZ) grain size(34,35). Cochrane et al(35) noted that the initial grain size in weld metal was similar to the coarse grained austenite of the HAZ. A relationship between the weld metal and HAZ grain size may suggest an influence of the latter on subsequent ferrite

transformation.

Theoretical considerations based on equalibrium diagrams have suggested that between the molten metal and the coarse grained region of the HAZ there is a partially melted region (36). This region results from segregation which reduces the effective solidus(39) particularly at the austenite grain boundaries, which become "decorated" with a liquid film. The presence of this film arrests austenite grain growth and therefore the weld metal grain size could be inherited from the finer grains of the partially melted region, rather than the coarse grained zone of the HAZ(37).

2.4 PHASE TRANSFORMATION.

Phase transformation may be divided into two basic types:

1. Nucleation and growth,
2. Martensitic.

However in steels it is possible for transformation processes to possess characteristics of each type.

With transformation by nucleation and growth, the new phase grows at the expense of the old by the migration of the phase boundary, as a result of atom by atom transfer across this boundary. The growth may occur by one of two mechanisms. Firstly the growth may be controlled by processess in the immediate vicinity of the interface boundary and is independent of diffusion. This type of growth is common in single phase materials for processes such as grain growth, recrystallization and during initial nucleation of a new phase. If the boundary divides regions of different composition, which is the case when austenite transforms to ferrite, then the motion of the boundary requires long range transport of atoms towards or away from the growth region and is therefore diffusion controlled.

Martensitic type transformations utilize a cooperative movement of many atoms instead of the independent movement of individual atoms. It is diffusionless and descrete regions of the solid usually transform suddenly with very high velocity.

The driving force for any transformation process is the difference in Gibbs free energy of the initial and final phases. Classical nucleation theory for the formation of a nucleus suggest that an energy barrier exist between nucleation and continuous growth of a new phase. This energy

barrier is the result of the positive free energy change due to the creation of a new surface, which opposes the negative free energy change from the formation of the initial nucleus. The driving force for nucleation G may be expressed by the relationship:

$$\Delta G = -\Delta Gv + \Delta Gs + \Delta Ge - \Delta Gd$$

were ΔGv= chemical free energy of the nucleus,

ΔGs= increased surface energy of the nucleus,

ΔGe= increased strain energy due to lattice distortion,

ΔGd= free energy donated due to heterogeneous nucleation.

Because of the energy barrier, undercooling is required before it becomes energetically favourable for nucleation and growth to occur. Since the nucleus also has to attain a critical size prior to growth, some redistribution of solute atoms by diffusion must take place, suggesting that the degree of undercooling is dependent on the cooling rate. Easterling(22) has indicated that the faster the cooling rate, the less time there is available for the nucleus to attain critical size and consequently the greater the undercooling required.

Unless one is considering high purity material with no lattice defects, transformation can be assumed to occur by a heterogeneous nucleation mechanism(38) and the energy donated by this process is extremely important. The nucleation process is catalysed by reducing the net surface area required to form a nucleus. This occurs when the formation of the nucleus "embryo" involves the destruction of part of an existing surface, the free energy of which provides some of

the energy required for the formation of the new phase. The degree of free energy donated depends on the "potency" of the nucleation site. The most favourable sites for nucleation listed in descending order of free energy donated are:

1. Free surfaces,
2. Grain boundary corners,
3. Grain boundaries,
4. Inclusions,
5. Dislocations,
6. Vacancy clusters.

The orientation relationship of the new phase with the initial phase may also be important(38). If the new phase forms a low energy coherent boundary then the surface energy barrier to nucleation would be less, thus reducing the degree of undercooling required. Semi-coherent and incoherent boundaries have progressively higher energies and therefore present a greater barrier to nucleation.

In general the factors that determine the final volume of transformation products are:

1. Nucleation rate,
2. Growth rate,
3. Density and dispersion of nucleation sites,
4. Overlap of diffusion fields from adjacent products,
5. Impingement of adjacent phases.

2.4.1 DELTA FERRITE TO AUSTENITE TRANSFORMATION.

Ferritic steels can solidify initially as delta ferrite or austenite depending on the composition. The equilibrium diagram for the iron-carbon system(39) indicates that weld metal with carbon content less than 0.43%wt solidifies as

delta ferrite.

If delta ferrite is the initial phase to form, heterogeneous nucleation on inclusions or microalloy second phase particles could refine the grain size (28,29). Since austenite may nucleate at the delta ferrite grain boundaries, the effective austenite grain size could also be refined (40).

Cochrane(41) has also suggested that the inclusion type and distribution may further affect austenite grain growth on cooling. Since the flux type influences the inclusion size, distribution and type (42), current theories on inclusion controlled grain growth (43), would suggest that different fluxes could restrict austenite grain growth to varying degrees. This would appear to be confirmed by studies undertaken on SA weld metal (41) using acidic fluxes, which indicated that the columnar austenite grains were confined to the original delta ferrite boundaries and were finer compared to welds produced using basic fluxes. The effect of inclusions on transformation will be described more fully in section 2.5.3.

Widgery(15) has proposed two mechanisms to account for the formation of austenite from delta ferrite, which indicate that the austenite grain boundaries may not correspond to the original delta ferrite boundaries. Firstly austenite grains in the HAZ could grow epitaxially into the weld metal across the delta ferrite, which would therefore be destroyed, fig. 2.7a. However nucleation and growth may also occur on the delta ferrite boundaries ahead of the epitaxial growth region. If the nucleus grows into the two adjacent delta

ferrite grains the boundary would be destroyed, fig. 2.7b.

The development of austenite in weld metal would therefore depend upon the original solidification structure and the subsequent degree of coarsening in cooling.

2.4.2 AUSTENITE DECOMPOSITION.

On cooling of ferritic steel weld metal a temperature is eventually reached when the austenite becomes energetically unstable and transforms to ferrite. Quench techniques have been used to determine the sequence of transformation from austenite to ferrite and the order of transformation has been given previously in section 2.1.8. The mechanisms proposed for the formation of the ferrite constituents will now be given, considering the constituents in descending order of transformation temperature.

2.4.2.1 PRIMARY FERRITE.

Grain corners and boundaries are the most favourable sites for nucleation to occur because of their high energy (22). Primary ferrite(PF) therefore forms along the large angle prior austenite grain boundaries and subsequently thickens in a direction perpendicular to the boundary (41). Cell boundaries within the austenite grains are small angled boundaries consisting of dislocation networks with relatively low energy and provide unlikely sites for initial ferrite nucleation (22).

The formation of PF is a pro-eutectoid reaction, in which solute redistribution results in "build up" of solute elements ahead of the growth front. The magnitude of this "build up" is determined by the diffusion rate of the solute particles in austenite and the cooling rate. Easterling(22)

has suggested that at weld cooling rates segregation at the PF growth front could be extensive.

2.4.2.2 FERRITE SIDE PLATES.

Rasenen(36) has suggested that ferrite side plates(FSP) form as a result of carbon segregation ahead of the PF growth front. It is thought that this segregation leads to instability in the austenite-ferrite boundary resulting in pertubations from which FSP develop, fig. 2.8a. Townsend et al(44) proposed a different mechanism for the formation of these pertubations, suggesting that they were due to anisotropy in the surface tension in the ferrite-austenite interface, as the PF followed the curve of the austenite grain boundary, fig. 2.8b. As a result of the formation of pertubations and segregation at the phase interface, Rasenen(36) suggests that when the austenite undercools below the Widmanstatten formation temperature only ferrite needles can break though the carbon barrier. Subsequent growth of the FSP is rapid because solute is effectively redistributed to the sides of the growing tip, thus reducing the problems of solute build up.

2.4.2.3 ACICULAR FERRITE.

Intragranular nucleation of AF occurs below the temperature at which FSP develop (7) and the mechanism of formation is still subject to debate. However there is evidence to suggest that AF formation may be associated with nucleation on inclusions (8,13,45), although the factors of importance in terms of inclusion size, distribution and type are unclear (45).

Ricks(13) observed the presence of AF nucleated on inclusions in SA weld metal. However calculations suggested that the inclusion population was not sufficient to account for the number of AF grains observed. It was therefore proposed that the phase initially formed on inclusions, followed by sympathetic nucleation of further grains.

Further work by Ricks et al(13) has indicated that AF growth was associated with carbon partitioning and was therefore pro-eutectoid in nature. Since no carbide precipitation was observed at either the grain boundaries or within the grains it was also suggested that it was a form of Widmanstatten ferrite, rather than bainitic in character as proposed by other workers(8)

2.4.2.4 LATH FERRITE.

Abson et al(46) suggested that lath ferrite may form as a result of:

1. The inhibition of long range diffusion of carbon from the ferrite austenite boundary, into the austenite grain interior as a result of fast cooling rates.
2. The failure of AF to nucleate or grow to mutual impingement.

The formation of LF is thought to be an essentially interphase controlled reaction, with short range diffusion of carbon resulting in formation of carbides with an orientation relationship to the ferrite, indicative of a bainitic type reaction. Using electron microscopy Choi et al(7) observed a high dislocation density within the ferrite laths, with carbide films between them, which they suggested confirmed

that LF was bainitic in nature.

2.4.2.5 FERRITE CARBIDE AGGREGATE.

Rasenen(36) indicated that if the initial PF growth was rapid, carbon segregation at the ferrite-austenite interface would be high. Under these circumstances the austenite would become unstable with respect to ferrite and cementite and small regionsof ferrite-carbide aggregate would form. Widgery(11) suggested that this constituent was usually observed adjacent to PF, where it forms by a process of interphase precipitation. The growth mechanism is said to involve the formation of carbide precipitates at the ferrite boundary, followed by ferrite growth until the solute barrier was again formed and precipitation occurred once more.

2.4.2.6 MICROPHASES.

The microphases are formed as a result of carbon enrichment of the austenite, between the pro-eutectoid ferrite grains (7). This enriched austenite can transform to carbides or martensite-austenite (M-A) structures depending on the cooling rate. Increased cooling rate has been observed to increase the proportion of M-A microphases in preference to carbides(20).

2.5 FACTORS INFLUENCING TRANSFORMATION FROM AUSTENITE TO FERRITE.

Austenite to ferrite transformation is a competitive process in which the type and proportion of constituents is determined by the factors listed in section 2.4. If the conditions within the weld metal favour grain boundary nucleation and growth, PF and FSP may grow to mutual impingement and dominate the final microstructure. However

conditions which favour intragranular nucleation may result in the formation of high proportions of AF. In weld metal the microstructure can be influenced to a large extent by the:

1. Prior austenite grain size,
2. Cooling rate,
3. Composition,
4. Inclusion population,

and the effect of these parameters will now be reviewed.

2.5.1 PRIOR AUSTENITE GRAIN SIZE.

A number of investigators have demonstated the effect of prior austenite grain size on transformation from austenite to ferrite (47,48). Tests in which specimens were reheated to increasing peak temperatures in the range 900 to 1350°C, were found to transform at lower temperatures, which correlated with increased prior austenite grain size.

Christensen(48) also observed that coarser prior austenite grain size resulted in increased proportions of AF in reheated and as-deposited weld metal. This increase in intragranular transformation products, particularly AF has been noted by a number of workers (3,41,49). Inagaki(47) suggested that this effect was due to the reduced grain boundary area available for nucleation, together with increased diffusional distances, which effectively suppressed PF nucleation favouring transformation to intragranular constituents. The suppression of grain boundary nucleation would also lower the transformation temperatures.

Harrison(50) proposed a mechanism in which the prior austenite grain size, together with the amount of carbon rejection as the PF grows, influences the degree of

undercooling within the grain and subsequent transformation, fig. 2.9. If the austenite grain size is small and carbon enrichment of the austenite large, the grain interiors would be stabilised and would not readily transform. In such cases PF would dominate the microstructure. However with large austenite grains carbon rejection would not be significant and undercooling within the grains would reach the necessary state for intragranular transformation to occur. Therefore AF or lower temperature transformation products may dominate the microstructure.

2.5.2 WELD METAL COOLING RATE.

The cooling rate associated with weld metal is determined by a number of factors, with the heat input and plate size being particularly important. Weld cooling rates are normally determined for the 800 to 500°C temperature range, because it was thought that the major proportion of transformation occurred between these limits. For fusion welding the cooling rates generally vary from 3 °C/sec. for high heat input process, eg. SAW, to 60 °C/sec. with low heat input processes, eg. TIG.

Glover et al(10) varied the cooling rate of SAW metal from 3 to 60 °C/sec., by reducing the heat input from 10 to 0.74 KJ/mm. It was found that the dominant microstructure changed from PF to AF and then to LF as the cooling rate increased. This tendency towards lower temperature transformation products with faster cooling rates has also been noted by other workers.

Rasenen(36) explained the effect of cooling rate in terms of its influence on the diffusion of carbon within the

austenite. On PF formation, redistributed carbon segregates at the growth front. The degree of segregation is dependent on the cooling rate, with fast rates increasing the magnitude, as a result of reduced diffusion. By stabilising the austenite ahead of the PF growth front the carbon effectively forms a barrier to further growth, allowing other phases to nucleate and grow, fig. 2.8a.

Harrison(50) suggested that the cooling rate directly influenced the thermodynamics of transformation by altering the degree of undercooling, fig. 2.9. During cooling from the Ae3 temperature, the degree of undercooling was said to increase, until eventually the thermodynamic driving force was sufficient to produce detectible nucleation at the most favourable sites. If the cooling rate was slow, sufficient time may be available for grain boundary nucleated phases to grow to mutual impingement, before undercooling within the grains was sufficient for nucleation. However with fast cooling rates although the grain boundary phases may continue to grow, undercooling within the austenite grains would rapidly increase allowing intragranular nucleation to occur. In these circumstances grain boundary and intragranular nucleated phase would then grow simultaneously until mutual impingement.

2.5.3 NON METALLIC INCLUSIONS.

A number of recent investigations (49-53) have indicated that the size, shape, distribution and composition of non metallic inclusions in weld metal may influence transformation. These particles may either be oxide, nitrides or carbo-nitrides.

2.5.3.1 WELD METAL OXYGEN CONTENT.

The solubility of oxygen in ferrite is extremley low ie. less than 0.002%wt. It follows that oxygen present in weld metal must therefore be in the form of oxide inclusions. In tungsten inert gas(TIG) and metal inert gas(MIG) processes oxygen may be absorbed via the shielding gas(51), while in SAW and manual metal arc(MMA) the content is influenced by the flux type and wire composition(52). The flux type may be classified in terms of the basicity index calculated using the formula proposed by Tuliani(18), in which a value greater than 2.5 indicates a highly basic flux. It is reported that the oxygen content of weld metal deposited using acidic fluxes is higher than that present when basic fluxes are used (53).

The net oxygen content of weld metal has been reported to be a complex function relating to (53):

1. Composition, particularly the carbon, manganese, silicon, aluminium and titanium contents.
2. Gas evolution rate.
3. Welding parameters and process type.
4. Flux type.
5. Weld pool temperature and short reaction times.

Widgery(4) has suggested that the kinetics of coelescence and flotation of inclusions may also influence the weld oxygen content. But it was also stated that because of the short reaction times available during welding, the flotation of inclusions alone could not fully account for the removal of oxygen. It was therefore proposed that removal could also occur by inclusions, transported to the surface by

turbulence, impinging on and being held by surface tension.

2.5.3.2 THE EFFECT OF INCLUSIONS ON TRANSFORMATION.

Abson(46) indicated that the effect of inclusions on weld metal microstructures could be classified within three regimes, corresponding to low(<100ppm), intermediate(200 to 400ppm) and high(>500ppm) oxygen contents. This was demonstrated using three schematic CCT diagrams, fig. 2.10. Using a laser remelting technique to reduce the oxygen content to below 200ppm, Abson(54) found that LF was the dominant microstructural constituent. Cochrane et al(55) found that weld metal of intermediate oxygen content tended to form structures with high AF contents, while high oxygen contents promoted ferrite side plate structures.

The effect of oxygen on microstructural development is thought to be due to its influence on the size, number and distribution of inclusions(46). With low oxygen content, intragranular nucleation is said to be restricted because there are insufficient inclusions to act as nucleants. In the intermediate oxygen content regime an optimum inclusion population is formed to favour AF, while with high oxygen contents, inclusions lying at the prior austenite grain boundaries promote, PF nucleation(54).

Cochrane(55) and Abson(54) used different fluxes of varying oxygen potential to generate high and intermediate oxygen contents. However this technique has been critisised by Farrar et al(56), who suggested that changes in flux type would result in changes in the nominal composition of other alloying elements, as well as oxygen. This was suggested because the acidic and basic flux types, used to produce the

high and intermediate oxygen contents respectively, would also change the type of inclusions present. Manganese silicate fluxes (acidic) form inclusions of high manganese content, while alumina based fluxes (basic) form alumina or alumino silicate type inclusions. Therefore it was argued that although chemical analysis would indicate similar manganese contents in each case, with the acidic flux less manganese would be in solution, which would affect the hardenability of the two alloys.

The type of inclusions formed is also thought to significantly influence transformation (55). Pargeter(57) investigated the types of oxides formed in SA weld metal. The results indicated, that inclusions containing manganese and silicon predominated in welds produced using acidic manganese silicate and calcium silicate fluxes. With basic fluxes, aluminium and titanium were also observed in the inclusions, with the proportions present depending on the contents of these elements in the fluxes. Pargeter also noted an apparent association between the manganese-silicon type inclusions and PF and the titanium-aluminium type inclusions and AF. Boothby (58) has also reported a similar association.

Pargeter(57) has further suggested that if a suitable distribution of inclusions was not present, AF nucleation would not occur. However Terishima and Hart(59) stated that even if an apparently favourable distribution of inclusions was present, AF may still not form.

A number of workers have suggested that inclusions influence transformation by affecting the prior austenite grain size (35,60,61). Cochrane(35) proposed that inclusions

in high oxygen content weld metal "lodge" at the prior austenite grain boundaries and therefore encourage PF nucleation. Barrite(60) using an acidic and basic flux to produce high and low oxygen content weld metal, found that a finer austenite grain size was observed in the latter. Evidence of large inclusions at the austenite boundaries was said to confirm the mechanism proposed by Cochrane(35). However in work by Harrison(50) no difference in prior austenite grain size was observed between high and low oxygen content as-deposited weld metal and it was concluded that grain boundary pinning was not an important factor.

2.5.3.3 MECHANISMS OF INCLUSION SITE NUCLEATION.

Although it is fairly well established that inclusions influence weld transformation, the mechanism remain unclear. Inclusions may influence transformation directly by providing sites for nucleation of ferrite or indirectly by their effect on the austenite grain size.

It has been suggested that in high oxygen content weld metal, inclusions pin the prior austenite grain boundaries. This is thought to have two affects:

1. Increased inclusion distribution at the austenite boundaries may encourage PF nucleation on the boundary.
2. Finer prior austenite grains produced as a result of pinning, may increase the grain boundary area available, thereby encouraging PF nucleation.

Ricks et al(13) have recently shown that inclusions can act as a direct substrate for AF nucleation. They suggested that destruction of part of the austenite-inclusion interface by the formation of the ferrite nucleus, reduced the overall energy barrier to nucleation. But they also concluded that that heterogeneous nucleation at grain boundaries were more favourable.

Some investigators (54,62) have suggested that the composition of the inclusion may be an important factor in determining its potency as a site for ferrite nucleation. This would indicate some degree of crystallographic matching between the inclusion and ferrite was required. North(63) found that a close lattice matching occurred between ferrite and Ti or V nitride particles, which resulted in increased

AF nucleation.

Harrison(64) proposed that high dislocation densities may be associated with inclusions, as a result of strains produced by differential contraction between the austenite and inclusion, on cooling. They suggested that nucleation may therefore occur on these dislocations as opposed to the inclusion surface. Easterling(22) as however indicated that although nucleation on dislocations is more favourable than homogenious nucleation, it is less so than nucleation at boundaries or inclusion surfaces.

Inclusions may also influence ferrite nucleation by altering the surrounding matrix composition (56). Depletion of the matrix manganese content would reduced the local hardenability and therefore favour ferrite nucleation. However although some metallographic evidence is available to support this theory in steel ingots (65), Ricks et al(13) found no detectable variation of either manganese or silicon within 0.05μm of inclusions in weld metal.

2.6 THE EFFECT OF WELD COMPOSITION ON AUSTENITE DECOMPOSITION.

The composition of the weld metal is obviously important in determining the type and proportions of ferrite constituents formed on austenite decomposition. Generally the composition may affect the transformation in two ways:

1. Alloying elements present in solution may directly influence the hardenability.
2. Elements present may influence the size, distribution and type of second phase particles formed in the weld metal.

Many workers have attempted to isolate the effects of alloying elements on the microstructure formed in weld metal and corresponding toughness and a summary of these effects will now be presented.

2.6.1 MAJOR ALLOYING ELEMENTS.

2.6.1.1 Carbon.

The detrimental effect of carbon on weldability of steel has resulted in a reduction in the amounts present in weld metal. In HSLA steel weld metal, carbon contents may be in the range 0.03 to 0.2%wt. Carbon has limited solubility in ferrite, but depending on other alloying elements present, may be completely soluble in austenite, were it significantly increases hardenability.

Garland and Kirkwood(16) noted that it was difficult to isolate the effect of carbon on transformation, because changes in carbon content were difficult without influencing the level of other alloying elements present, particularly manganese.

Some investigators (66,67) have suggested that increased carbon reduced weld metal toughness, but unfortunately no metallographic information was given. Abson(68) indicated that an increase in carbon from 0.12 to 0.19%wt reduced the proportion of PF and also refined the AF. However this change in the major microstructural constituents was also accompanied by an increase in the proportion of M-A microphase content, which resulted in an overall reduction in toughness. A significant increase in nitrogen content was apparent in Absons(68) work, which could also have accounted for the reduced toughness. The effect of carbon on the type

and proportion of microphases has also been noted by Glover(10) and Pacey(20). It was suggested that for welds cooled at a particular rate, increased carbon content promoted the formation of carbides as opposed to M-A constituents. It was also found that increased cooling rate favoured M-A formation.

Recent work by Harrison(50) has indicated that increased carbon content depressed the transformation temperature at fast and slow cooling rates. This resulted in an increased proportion of AF, at the expense of PF and ferrite side plate structures.

2.6.1.2 Manganese.

Manganese is a strong austenite stabilising element, which when present in solution significantly increases hardenability. It may also be present as manganese silicate or sulphide inclusions.

Manganese is thought to be beneficial to weld metal toughness for contents up to 1.7%wt, as a result of the promotion and refinement of AF, at the expense of PF (7,69,70). However, although the microstructure continued to improve above this concentration, a marked reduction in toughness was recorded, which was said to be the consequence of increased M-A formation (70).

Harrison(50) found that increased manganese contents up to 2.12%wt depressed the transformation temperature and promoted AF at the expense of PF and ferrite side plate structures. It was suggested that manganese inhibited PF nucleation and growth by a solute drag mechanism, which allowed undercooling within the austenite grains to reach a

level at which intragranular nucleation would dominate transformation.

Barrite(60) proposed a different mechanism to acount for the influence of manganese, which suggested that increased concentration produced a decrease in oxygen content. This would reduced the inclusion population favouring a larger prior austenite grain size, which would in turn promote acicular ferrite.

The association of manganese silicate inclusions with prior austenite grain boundaries has been noted by Pargeter(57). It was suggested that the presence of these inclusions would lead to early nucleation of PF, which may subsequently dominate the microstructure. This would be in contrast to the previous reported increases in AF (50,60). Farrar and Watson(56) have proposed that increased oxygen content favoured the formation of manganese silicate inclusions, which would deplete the matrix manganese content and thus account for higher temperature transformation products.

2.6.1.3 Silicon.

Silicon is a ferrite stabilising element and tends to increase austenite to ferrite transformation temperature. It is also a strong deoxidant and may also occur in weld metal as silicate inclusions.

Tuliani(71) noted that an increased silicon content up to 0.2%wt, had a limited affect on weld metal microstructures. The microstructure of the weld metal studied being predominantly PF and FSP. However further increases up to 0.4%wt produced an increase in the proportion of AF, which

corresponded with increased weld metal toughness.

Recently Abson(68) has indicated that increased silicon content from 0.23 to 0.57%wt, did not significantly affect the major microstructural constituents. However there was an increase in the proportion of M-A microphases which reduced toughness, in contrast to the Tuliani(71) work.

2.6.1.4 Molybdenum.

Molybdenum is a strong ferrite forming element, which when in solution may significantly increase hardenability. Yoshino et al(72) and Abe(73) found that an increased molybdenum content was consistantly beneficial to weld toughness irrespective of the carbon, Nb content or flux basicity. The higher concentrations appear to increase hardenability and thereby suppress PF formation, promoting AF. An optimum weld toughness was found for molybdenum contents of 0.35%wt.

However Harrison(50) has also noted that increased molybdenum contents also promoted LF microstructures. It was suggested that higher concentrations increased the degree of undercooling to the point were LF formed, in a bainitic transformation process.

2.6.2 MICROALLOYING ELEMENTS.

Microalloying elements are transfered to the weld metal by two routes. In high dilution processes such as SA welding, the weld metal may contain up to 70% of the base metal microalloy content. Nb and V may be "picked up" as a result of diluton. Microalloying elements may also enter the weld metal via the welding wire or flux. For example Al and Ti, although they may also be present due to dilution, are

often added deliberately to deoxidise the weld metal. The concentration of microalloying elements in the weld metal is small compared to other elements, but their effect in solution or as second phase particles can significantly alter the microstructure.

2.6.2.1 Niobium.

Niobium is used widely in microalloyed steels to improve strength and toughness via grain refinement and precipitation hardening mechanisms. In solution Nb is a ferrite stabilising element and significantly increases hardenability. It may also occur as second phase particles, either carbides or carbo-nitrides.

Garland and Kirkwood(74) produced a model to account for the influence of Nb on weld transformation. They suggested that Nb increased hardenability and therefore would increase the proportion of AF, while inhibiting PF and ferrite side plate formation. It was also proposed that Nb would increase the proportion of microphases and precipitation of carbo-nitride particles in weld metal. The effects of Nb were indicated in a vector diagram(16), fig. 2.11a. However their subsequent experiment did not reveal any affect which could be directly attributed to Nb.

Levine and Hill(75) studied the effect of Nb in weld metal of basic composition 0.09%wt carbon, 1.7%wt manganese and 0.18%wt silicon. It was found that an increased Nb content up to 0.02%wt reduced the proportion of PF and increased AF formation which resulted in higher toughness levels. With higher Nb contents, FSP structures were promoted.

In contrast to the initial beneficial effect observed by Levine and Hill(75), a number of reports have suggested that Nb is deleterious to weld toughness at all levels. Sawhill(76) increased the Nb content of 0.06%wt carbon weld metal from 0 to 0.05%wt and found that the proportion of ferrite side plate structures increased at the expense of AF. Jesseman(77) also found that Nb contents as low as 0.01%wt, significantly increased ferrite side plate formation, resulting in reduced weld toughness.

In a review of the effects of Nb on weld metal microstructures and toughness, Dolby(78) concluded that Nb reduced the proportion of PF, but the proportion of AF and FSP may be increased or decreased depending on the weld consumables and conditions. It was further indicated that at high heat inputs, if the microstructure in the absence of Nb consisted of predominantly PF and FSP structures, then Nb additions would reduce toughness. This was said to be due to the higher proportions of M-A constituents and precipitation hardening, offsetting the improved toughness which should have occurred as a result of reduced PF formation. Dolby(78) summarised the effects of Nb on weld toughness using a vector diagram, fig. 2.11b, modified from that presented previously by Garland and Kirkwood(16)

In recent papers by Abson et al(79) and Watson et al(9,12), the effect of Nb was said to depend on the weld metal hardenability. Abson(79) found that an increase in Nb content from 0 to 0.07%wt, refined the weld microstructure and increased the yield strength, tensile strength and hardness. With fluxes that tended to form PF and ferrite

side plate microstructures, a high Nb concentration, increased the AF content from 10 to 30%. However the weld toughness decreased due to the higher yield strength. With fluxes that produced a microstructure with 60% acicular ferrite, high Nb concentration reduced the proportion of PF, while favouring a further increase in AF.

Watson et al(9) found that Nb increased the hardenability of weld metal, which resulted in reduced PF content, with increased and refined AF. With an acidic flux which produced low hardenability weld metal, Nb additions of 0.02%wt reduced the proportion of AF and promoted ferrite side plate structures.

2.6.2.2 Vanadium.

Vanadium is used in microalloyed steels to produce grain refinement and precipitation hardening. When present in solution V is a ferrite stabilising element, but it may also occur as carbide or carbo-nitride particles.

An early report by Kirkwood and Garland(80), suggested that an increase in V content from 0.005 to 0.12%wt progressively promoted the formation of AF, but the proportions of M-A microphases were also increased, which resulted in reduced toughness. However in later work (81), it was found that no significant change in microstructure was observed when V contents were increased up to 0.065%wt, although increased proof stress was said to indicate precipitation clustering of V nitride. At high levels of V ie 0.13%wt, Garland and Kirkwood(81) noted that the proportion of FSP and M-A phases was increased. This was said to be due to increased hardenability as a result of V

remaining in solution, when the available nitrogen and carbon required for pre-precipitation had been exhausted. Wegrzyn et al(82) agreed with Garland and Kirkwood(80) that increased V resulted in an increase in strength and a reduction in toughness in SA weld metal. They also concluded that the reduction in toughness was due to the precipitation of V carbides or carbo-nitrides.

In contrast to the above work, a number of investigators have suggested that small increases in V may improve weld toughness. Matrosov and Sorokin(83) found that weld toughness increased for V contents upto 0.04%wt, with other workers only indicating a deleterious affects above 0.05%wt(84,85) and 0.08%wt(86).

Abson et al (87) found that the effect of V was dependent on the hardenability of the weld metal. An addition of 0.06%wt to weld metal containing 1.2%wt manganese, increased the proportions of AF at the expense of PF. With higher levels of manganese the effect was less apparent due to the already high proportions of AF.

In a recent review by Dolby(88), it was concluded that the addition of V to weld deposits generally promoted AF and inhibited ferrite side plate structures. It was also noted that the influence on toughness depended on the welding conditions and the deposit alloying level. Dolby(88) has summarised the effects of V in a vector diagram, fig. 2.12, modified from that proposed previously by Kirkwood and Garland(89).

2.6.2.3 Titanium.

Titanium is a ferrite stabilising element, which when present in solution may significantly increase hardenability. It may also occur as second phase particles of carbides, nitrides or carbo-nitrides. A number of investigators have indicated that small additions of Ti upto 0.04%wt could have a beneficial effect on weld metal toughness (90,52). However with further additions, toughness was found to be continuously reduced.

Snyder et al(91) increased the Ti content in SA weld metal from 0 to 0.05%wt and found that its influence appeared to depend on the level of manganese present in the weld metal. With low manganese contents ie. 1.05%wt, a higher Ti concentration increased the proportion of PF. However with higher manganese levels the effect of Ti additions was weak. Snyder(91) suggested that at the low manganese contents, the effect of Ti as a ferrite stabiliser was dominant and therefore promoted PF. But this effect was overshadowed at higher manganese levels, were manganese effectively inhibited PF growth. In early work by Widgery(52) a similar increase in PF was noted.

Contrary to the effect observed by Snyder(91) and Widgery(52), Thaulow(30) found that an increase in titatium reduced the proportions of PF and improved toughness, with the optimum concentration 0.032%wt. However, although the microstructure was said to improved continually with Ti additions above 0.06%wt, the weld toughness decreased. An effect reported to be due to precipitaton hardening by Ti

carbo-nitride formation. Later work by Widgery(92) also indicated that Ti additions promoted AF at the expense of PF, although a corresponding reduction in weld toughness was said to be the result of solution hardening. Recent work by Bailey(33), also suggested that small increases in Ti content caused a change to an AF microstructure in high oxygen content weld metal, were such microstructures would not normally be expected.

Boothby(58) and Pargeter(47) both indicated that Ti based inclusions in weld metal were associated with AF nucleation. Boothby(58) suggested that Ti oxide or carbo-nitride could nucleate AF, while Ito et al(93) thought that Ti nitride particle promoted this phase. Since this work several investigators have suggested that titanium oxide inclusions form in both metal inert gas (94) and SA weld (95) processes, rather than titanium nitride.

No vector diagrams have been produced to show the effects of Ti on toughness, like those presented previously for Nb (78) and V (88). However from the papers reviewed, it is possible to construct a similar vector diagram, summarising the effects of Ti, fig. 2.13.

2.6.2.4 Aluminium.

Aluminium is a ferrite stabilising element. It may be present in solution in the weld metal, were it may increase hardenability, or in the form of oxide or nitride particles. There again appears to be conflicting evidence regarding the influence of Al on weld metal toughness. Some investigators (96,97) have suggested that Al was detrimental at all levels, although the results were often inconsistent. Others

have noted that Al may be beneficial to weld toughness for levels upto 0.02%wt(98) or 0.05%wt(99).

The presence of other alloying elements or flux basicity would appear to influence the effect of Al on weld transformation. North et al(63) noted that Al improved weld toughness for carbon-manganese steel, but reduced toughness for Nb microalloyed steel. Yoshino and Stout(72) found that Al was detrimental when using a basic flux, but beneficial with acidic fluxes. Although the explanation for these effects were said to be a coarsened structure, no metallographic details were given.

Widgery(92) observed that increased Al promoted AF at the expense of PF, although Terishima et al(100) showed that the proportion of AF decreased, while ferrite side plate formation increased, at high Al concentrations.

In a review of the influence of Al, Hannerz(101) indicated that the oxygen content of the weld metal was an important factor. With basic fluxes, producing low oxygen weld metal, Al would remain in solution and affect the microstructure via an influence on hardenability. However with acidic fluxes, the Al functions mainly as a deoxidiser, affecting the inclusion distribition, size and type, which subsequently influence transformation. Hannerz(101) has proposed a vector diagram, similar to those produce for Nb(78) and V(88), summarising the effects of Al on microstructural development and toughness, fig. 2.14.

In a similar manner to that described for Ti, a number of workers (47,59) have noted that Al inclusions were associated with AF nucleation. However, other work has also

suggested that Al additions reduced the titanium oxide population and subsequently inhibited AF formation, since the titanium oxide inclusions were nucleation sites.

2.7 THE EFFECT OF MICROALLOYING ELEMENTS ON TRANSFORMATION.

The preceeding section has given a brief summary of the influence of microalloying elements on ferritic transformation and toughness. The mechanisms by which these elements are effective will now be reviewed. The presence of microalloying elements may influence transformation in four basic way:

1. In solution, directly affecting hardenability.
2. By refinement of the prior austenite grain size.
3. Directly influencing austenite to ferrite transformation.
4. Affecting the type and proportion of second phase particles.

2.7.1 MICROALLOYING ELEMENTS IN SOLUTION.

All the microalloying elements reviewed are ferrite stabilising elements. It has been shown that in solution these elements may significantly increase hardenability, although the degree by which this occurs depends upon the type and concentration. However V, Nb and Ti also have a strong affinity to carbon and the resulting carbide formation may remove carbon from solution and consequently reduce hardenability (81).

2.7.2 THE INFLUENCE ON PRIOR AUSTENITE GRAIN SIZE.

The effect of microalloying elements on prior austenite grain size would appear to depend upon two mechanisms:

1. Carbides, nitrides, carbo-nitrides or oxides of

these elements may survive or are formed in the molten weld pool and subsequently act as sites for heterogeneous nucleation of delta ferrite during solidification.

2. Second phase particles may inhibit austenite grain growth during cooling, after solidification.

Ohashi(28) and Nishio(29) suggested that non metallic inclusions could significantly affect the solidification mode. Nishio(29) noted that carbides and nitrides of Ti and Nb could produce heterogeneous nucleation of delta ferrite. This was said to produce a much finer solidification structure and prior austenite grain size. Thaulow(30) has also reported that when the Ti concentration exceeded 0.06%wt titanium carbo-nitride particles formed, which refined the weld structure. However there is some debate as to whether second phase particles may survive in the weld pool. Grain growth diagrams have been constructed by Easterling et al (22), showing the influence of titanium nitride and niobium carbide on grain coarsening in HAZ weld metal, fig. 2.15. However these diagrams also indicate the dissolution temperatures for these particles in relation to the heat input. From these diagrams it is clear that titanium nitride particles can survive in the molten pool. Whereas niobium carbides dissolve at temperatures in the range 1090 to 1450°C, depending on the heat input and are therefore less likely to be present in the molten pool. The temperatures and times required for complete dissolution of vanadium and aluminium carbide/nitride particles(22), fig. 2.16, would suggest that these particles are very unlikely

to survive in the weld metal.

Particles which survive in the weld pool or form on cooling may also influence prior austenite grain size as the weld cools. The pinning action of these second phase particles depends upon there size and volume fraction (43). A large number of fine particles are more effective in inhibiting grain growth than coarser particles. Widgery(52) found that the inclusion size in weld metal ranged from 0.15 to 1.5 μm and the volume fraction was 0.3 to 0.7%wt, which according to Gladman(102) would be suitable for grain boundary pinning.

2.7.3 THE INFLUENCE ON AUSTENITE TO FERRITE TRANSFORMATION.

The direct influence of microalloying elements on austenite to ferrite transformation would appear to depends on two mechanisms:

1. The inhibition of PF growth.
2. Direct nucleation of AF on microalloy second phase particles.

A number of investigators (50,103) have indicated that the influence of microalloy additions on transformation depends on the hardenability of the weld metal. Harrison(50) suggested that PF growth was inhibited by interphase precipitation of niobium carbo-nitride particles. The subsequent influence of this effect, on the development of the ferritic microstructure, was said to depend on the hardenability. In high hardenablity weld metal with a relatively low transformation start temperature, inhibition of PF would allow the grain interiors to undercool sufficiently for AF to nucleate and grow. However with low

hardenability weld metal transformation may occur at high temperatures. In these circumstances PF growth may again be inhibited, but the austenite grains would not be sufficiently undercooled for AF to form and therefore FSP would develop. Harrison(50) has suggested that the degree of undercooling and the influence of cooling rate, composition etc. on this undercooling, can be used to explain the transformation mechanisms operating in weld metal. The proposed vector diagram summarising this is shown in fig. 2.9.

Other microalloying elements which readily form carbides or carbo-nitides may influence transformation in a similar manner to that reported for Nb (50). However the precipitation temperature would appear to be important. Dolby(88) noted that for weld metal of low hardenability (lean alloy content) or slow cooling rate, the start temperature for transformation would be high. Consequently with V additions, the precipitation temperature would be below this transformation temperature and therefore the influence on transformation would be relatively small, compared to elements which precipitated at higher temperatures.

Direct nucleation of AF on microalloy second phase particles has been proposed (13,60,63). Nucleation on oxide inclusions, particularly Ti or Al based, has been reviewed in section 2.5.3. However AF nucleation on titanium or vanadium nitride particle has also been proposed (63). The reason suggested for these particles acting as nucleation sites, was a reduction in nucleation energy, due to close

lattice matching between the particles and ferrite.

However, although inclusions are formed during solidification of weld metal, whether precipitation takes place, appears to be the subject of debate. Work by Tanino(104) indicated that precipitation of niobium carbide only occurred for cooling rates from 0.17 to 1.33°C/sec., determined for the 1000 to 700°C temperature range. Therefore the fast cooling rates present in weld metal, together with the limited amount of direct transmission electron microscopy evidence of precipitates, has led Gray(105) to suggest that precipitation does not occur.

Contrary to Grays opinion, Wegrzun(82) and Hannerz(97) have noted the presence of Nb and V precipitates of 40-200 Å in size, in as-deposited weld metal, although no cooling rates were given. Easterling(22) has also observed niobium carbide precipitates of 50-100 Å in SA weld metal. It is said that limited TEM evidence of precipitates in weld metal is due to the difficulty in imaging, as a result of their fineness(8). Garland(81) has stated that precipitation clusters of niobium carbo-nitride or vanadium nitride occur in as-deposited weld metal, but under no circumstances has the actual occurence of descrete precipitates been observed. Easterling(22) has further proposed that stresses induced in weld metal as a result of rapid cooling may be instrumental in forcing precipitation to occur.

2.7.4 THE INFLUENCE ON MICROPHASE CONTENT.

Microalloying elements present in weld metal may significantly affect the type, proportion and distribution of microphases observed (78,88). Garland and Kirkwood(16)

found that higher Nb contents increased the proportion and non-uniform distribution of M-A constituents and a similar affect has also been noted for V additions (81).

2.8 REHEATED WELD METAL.

In multi-pass welding techniques, the weld will consist not only of as-deposited weld metal, but also of metal which has been reheated during subsequent passes. The microstructure produced in this reheated weld metal would depend on the thermal cycle experienced.

Tweed(106) used a simulative technique to reheat as-deposted weld metal to peak temperatures of 900 and 1250°C. It was found that the reheated material had a similar inclusion distribution to the as-deposited metal, but the prior austenite grain size was much finer. This reduction in the prior austenite grain size favoured the formation of PF and ferrite side plate phases and resulted in the AF content decreasing from 87 to 57%.

Evans(69) also observed fine equiaxed austenite grains in reheated weld metal compared to the coarse columnar grains of as-deposited material. The reduced prior austenite grain size again appeared to promote PF at the expense of AF. Rodrigues(49) again noted the finer austenite grain size in reheated weld metal, but found that although the AF content was reduced, as reported in previous work, the proportions of FSP increased significantly as opposed to PF.

In reviews of the effect of Nb (103) and V (88), Dolby noted evidence of precipitation hardening in reheated weld metal. It was therefore concluded that a clear distinction should be made between tests on single pass un-reheated welds

and those on two pass or multi-pass welds, were the test specimen samples the reheated areas.

2.9 POST WELD HEAT TREATMENT.

Post weld heat treatment(PWHT) is normally applied to weld fabrications were the plate thickness exceeds 25mm. The British Standard 1515 (107) suggests that heat treatment should be carried out at 600°C for a period of one hour for each 25mm in section thickness. The aim is to minimise stresses which contribute to buckling or brittle failure. This removal of residual stresses is accompanied by various microstructural changes which may have opposing effects on the mechanical properties. The structural changes which may occur are:

1. Carbide spheroidization.
2. Carbide formation in carbon rich areas in the ferrite.
3. Dislocation recovery and ordering.
4. Precipitation hardening if any microalloying elements are present.

Garland and Kirkwood(108) have suggested that during PWHT of Nb bearing weld metal, precipitaion of niobium carbo-nitride may occur. This precipitation hardening would result in an increase in yield stress and reduction in toughness. Farrar et al(109) indicated that for Nb levels up to 0.02%wt, no increase in yield stress or microstructural hardening occurred and improved toughness was achieved, due to dislocation recovery and carbide spheroidisation. However Farrar et al(109) also noted that for Nb levels above 0.025%wt, niobium carbo-nitride precipitation could occur

offsetting any beneficial changes in microstructure. Fick and Rogerson(110) have also reported that weld metal containing 0.012%wt Nb, had improved toughness after PWHT.

Kirkwood(80) has suggested that precipitation hardening also occurs during PWHT of V bearing weld metal. Whether this precipitation was detrimental to toughness depended on the microstructural changes which occurred. It was said that PWHT resulted in the degradation of martensitic microphases to FC, which allowed the full potential of the AF structure to be achieved. If the V concentrations were less than 0.032%wt precipitation of vanadium carbo-nitride was not sufficient to offset the beneficial effect of this martensitic degradation. However with V contents in excess of 0.12%wt, precipitation hardening was sufficient to outweigh any beneficial change in microstructure.

2.10 CONTINUOUS COOLING TRANSFORMATION DIAGRAMS.

Although many CCT diagrams have been produced, very few can be directly applied to weld metal because of the low austenitisation temperatures used and the corresponding small prior austenite grain size of the materials studied. A large proportion of CCT diagrams which have been produced are for material with fine austenite grain size in the range 8 to 9 ASTM, as opposed to the coarse grained austenite (2 to 4 ASTM) found in weld metal. In recent years however a number of investigators have attempted to produce CCT diagrams said to be applicable to weld metal.

Abson et al(54) and Glover et al(10) produced schematic CCT diagrams for weld metal, figs. 2.10 and 2.17. Although these diagrams were not based on experimental evidence they

did suggest how variations in alloying elements, oxygen content and cooling rate may influence microstructural development. Glover attempted to determine the effect of cooling rate and composition by inserting thermocouples into the weld pool and subsequent metallographic examination. The schematic CCT diagram produced was divided into three phase fields corresponding to ferrite, bainite and martensite transformation products. The effect of cooling rate was thought to depend on the carbon content, with faster cooling rates generally producing lower temperature transformation products.

Abson(54) considered the influence of inclusions as sites for ferrite nucleation. A series of schematic CCT diagrams was produced, fig. 2.10, to indicate the effects of high, intermediate and low oxygen content regimes on the microstructures formed. It was suggested that with high oxygen contents (600ppm), PF and ferrite side plate structures were promoted and therefore the phase fields corresponding to these constituents moved to shorter times and higher temperatures. With lower oxygen concentrations the phase fields were moved to longer times and lower temperatures, with AF promoted at intermediate oxygen contents and LF with low oxygen contents. Therefore with these diagrams, Abson suggested that the microstructure for a weld cooled at a particular rate, was dependent on the oxygen content.

Harrison and Farrar(61) and Ito(93) used a simulative reheating technique to study transformation in as-deposited weld metal. With this technique specimens were machined from

as-deposited weld metal and subjected to a further heating cycle said to reproduce the coarse prior austenite grain size. During cooling the transformation temperatures were determined by dilatometry. Harrison et al(61) found that a reduction in oxygen content from 654 to 278ppm lowered the transformation temperature from 712 to 693°C. Ito(93) reported that reduced oxygen contents moved the phase fields to longer times and slightly higher temperatures. Increased manganese and Ti were found to have a similar effect on the position of the CCT diagrams.

Recent work by Harrison(12), again using a simulative reheating technique, has reported CCT diagrams said to show the influence of carbon, manganese, nickel and Nb on transformation, fig. 2.18. The specimens machined from as-deposited weld metal were subjected to a heating cycle of 1400 C for 10 seconds, which was said to reproduce a similar prior austenite grain size to the found in the weld metal. Increased alloy content was found to move the CCT diagrams to longer times and lower temperatures.

2.10.1 CONSTRUCTION OF CCT DIAGRAMS.

To construct a CCT diagram the temperatures corresponding to the start and finish of transformation have to be determined for specimens cooled at a series of rates. Most workers calculate the cooling rate for the temperature range 800 to 500°C, because it was thought that the majority of transformation occurred within these limits. The cooling rate ranges which have been used to construct CCT diagrams, said to be applicable to as-deposited weld metal, have been 0.6 to 20°C/sec(10) and 0.06 to 1200°C/sec.(12). Typical

metal cooling rates for arc welding processes are generally within the range 1 to 60 °C/sec.

Two technique have been used to determine transformation temperature:

1. Thermal analysis,
2. Dilatometry.

Thermal analysis utilises thermocouples to detect the arrest in the cooling curve, associated with the evolution of latent heat during transformation, fig. 2.19. With dilatometry, the volume change associated with transformation from austenite to ferrite on cooling, is measured using displacement transducers, fig. 2.20.

The cooling curves and corresponding transformation temperature are plotted onto temperature-log time axis and the phase field are constructed by dividing the cooling curve into the microstructural proportions determined by quantitative metallography.

2.10.2 THERMAL ANALYSIS.

A number of investigators have used thermal analysis to determine the transformation temperatures in simulated reheated (10,14,50,60) or as-deposited weld metal (4,15,49). Widgery(4) and Rodrigues et al(49) carried out limited thermal analysis of as-deposited weld metal. The thermocouple was either inserted by hand into the weld metal(4) or positioned at the weld root prior to welding (49). Widgery(4) also used electronic differentiation techniques on the thermocouple output, in an attempt to improve the determination of the transformation temperatures, although the success would appear to have been

limited.

Stembera et al(111) suggested that the strong electromagnetic field present during arcing, could have a deleterious affect on the sensitivity of the thermocouple, immersed in the weld pool. Therefore in their studies the arc was extinguished before the thermocouple entered the weld pool. However in work by Barlow(112) the thermocouple was placed in the weld metal during arcing, although no mention of precautions taken to avoid problems associated with the electromagnetic field were apparent.

Glover et al(10) and Christensen et al(48) used thermal analysis during simulative reheated studies of weld metal. Harrison(50) found that for cooling rates in excess of 80 °C/sec., dilatometry became impractical and therefore used thermal analysis during tests at faster rates.

2.10.3 DILATOMETRY.

All the CCT diagrams produced (10,12,45,46), which are said to be applicable to as-deposited weld metal, have been produced using simulative reheating techniques in association with dilatometry. The technique usually employed involves heating a specimen machined from weld metal to a pre-determined temperature and holding for a period of time. The peak temperature and dwell time used are said to allow the prior austenite grain size to coarsen to that observed in the weld metal. The heating cycles used have varied from one investigation to another.

Glover(10) used an austenitisation temperature of 1350 °C for 2 seconds. The resulting austenite grain size was much finer and equiaxed compared to the coarse columnar grain

size of the weld metal. It was also suggested that a fast heating rate was required, to ensure that all elements in solution, after initial preparation, remained in solution. A similar thermal cycle was employed by Ito(8).

Harrison(50) initially used a heating cycle of 1250 °C for five minutes with a Theta dilatometer, but then changed to 1400 °C for 10 seconds. These heating cycles produced a prior austenite grain size of 5.5 ASTM, which Harrison suggested was typical of weld metal. Harrison(64) also considered the effect of the equiaxed austenite grains produced by reheating compared to the columnar grains found in as-deposited weld metal. It was suggested that the ratio of grain boundary area to grain volume, may be used to determine the required prior austenite grain size. If this was the case the proportion of grain boundary phases would be correct, but the conditions within the grain would differ from real weld metal. However if the diffusional distances within the grains were thought to be more important, then the grain size of the reheated weld metal should be equal to the width of the columnar grains. But this would result in a higher proportion of grain boundary phases. Harrison(64) produced prior austenite grain sizes similar to the columnar grain width, which would obviously produce a higher proportion of PF in the microstructures and consequently higher transformation temperatures than might be expected in the weld metal.

Harrison(50) also concluded that it was important to ensure complete dissolution of precipitates during the heating cycle. The dissolution temperature for 0.03%wt Nb

was calculated using the solubility product for niobium carbo-nitride. This indicated that all the Nb was in solution above 1150 °C. However it was also stated that higher concentrations could significantly increase this temperature. Calculations also revealed that vanadium carbo-nitride and aluminium nitride particle would be completely soluble at temperatures below that determined for Nb, but Ti based compounds were more stable and therefore likely to be present at significantly higher temperatures.

Dilatometer specimens have either been gas quenched, air cooled or controlled cooled using a thermal programmer. A schematic dilatation trace is shown in fig. 2.20, indicating the transformation temperatures at the points of inversion. Eldis(113) suggested that the error associated with location of the start of transformation should not be greater that ±5 °C, if the cooling rate is slow. However due to the curvature of the dilatation curve, the error in determining the finish of transformation may be as high as ±35 °C. This curvature arises due to the variation in the expansion coefficient with temperature and alloy content.

Except for very slow cooling rates the dilatometric traces only indicate the start and finish of transformation. The temperature at which the individual phases transform within this range are not indicated.

2.11 SUMMARY.

Recent engineering requirements have resulted in an increasing need to improve the toughness of HSLA steel weld metal. The toughness is dependent on a number of metallurgical features including:

1. Type and proportion of ferrite constituents and microphases,
2. Inclusion population,
3. Grain size of the ferrite constituents.

The factors influencing the devolpment of the weld microstructure has become a subject for extensive investigation. The composition and cooling rate have been found to be particularly important, in determining the type and proportions of ferrite constituents formed in weld metal. The presence of microalloying elements have been reported to significantly influence weld microstructure and toughness.

Nb and V are normally present in the weld metal as a result of dilution of the parent plate. Their effect is said to depend on the original hardenability of the material and the concentrations of the elements present. It has been suggested that low levels of Nb ie.<0.02%wt, may improve weld toughness by increasing the proportions of AF, at the expense of PF. However it has also been stated that all levels of Nb reduce toughness by promoting ferrite side plate formation. V has been reported to promote AF or FSP. Some investigators have indicated that all concentrations reduce toughness, while others have suggested that a beneficial affect on toughness was observed at levels below

0.04%wt.

Ti and Al may be present in the weld metal due to dilution of the parent plate or specifically added to the weld pool via the welding wire or flux. It has been noted that low levels of these elements may improve toughness, with the optimum concentrations reported as 0.032%wt and 0.02%wt for Ti and Al respectively. Some investigators have noted that increased Ti promoted PF, while others have reported an increase in AF content, at the expense of PF. Higher Al contents have been found to raise the AF volume fraction, while reducing the proportion of PF. However a reduction in AF and an increase in the proportion of LF, have also been noted with Al additions. It has been suggested that in high oxygen content weld metal AF is promoted due to nucleation on Ti or Al oxide inclusions.

Microalloying elements may also affect the microphases formed in weld metal. V and Nb were reported to increase the proportions of microphases formed and also favour martensitic as opposed to carbide types. There is little information to indicate the influence of Ti or Al on microphase formation. It has further been suggested that microalloying elements may also refine the structures formed in weld metal. Nb has been found to refine the ferrite structure, but no detailed information is available to show the influence of V, Ti or Al, particularly under low oxygen content conditions.

The mechanism suggested to account for the effects of microalloying elements include:

1. Direct influence on the hardenability due to

microalloying elements present in solution.

2. Inhibition of PF growth as a result of precipitation or segregation to the ferrite growth front, producing boundary drag.
3. Direct nucleation of AF on microalloy second phase particles.
4. Refinement of the prior austenite grain size.

Two main techniques have been used to study the effects of composition on the development of ferritic weld microstructure. Direct examination of weldments have been used in a number of investigations. The composition was usually varied by changing the chemistry of the parent plate, welding wire or flux or in some cases ferro alloy powders were added to the weld pool. However systematic control of the weld composition is difficult and proposed changes in chemistry were often accompanied by un-required changes in other alloying elements.

In recent investigations the usefulness of CCT diagrams, to show the influence of microalloying elements is apparent. However it is difficult to produce these diagrams using actual welding processes. This is due to the difficulty in producing an adiquate range of cooling rates without changing the welding process, which would inevitably make composition control difficult. The difficulty in controlling the composition of weld metal, has often resulted in ambiguous and contradictory results for the effect of microalloying elements on transformation. Changes in carbon, manganese and oxygen may significanlty influence the microstructures formed and it is therefore important to

ensure the variation in the concentration of these elements are kept to a minimum, when studying small changes in microalloy content.

In an attempt to simulate the structures formed in weld metal a number of investigators have used simulative reheating techniques. With these techniques, specimens machined from weld metal are subjected to a further heating cycle and the transformation temperature generally determined using dilatometry. The CCT diagrams produced using this technique are said to be applicable to as-deposited weld metal, but a number of major differences are apparent:

1. The solidification processes of the weld metal are not reproduced by the reheating, which in fact destroys the distribution of alloying elements and second phase particles, produced in the weld metal by the solidification process.
2. Equiaxed grains are produced in the reheated specimens as opposed to the columnar grain structure of as-deposited weld metal. This either produces differences in the proportions of grain boundary area or diffusional distances, compared with as-deposited weld metal. In most of the CCT diagrams produced for as-deposited weld metal, equiaxed grains have been produced with similar grain diameters to the columnar grains in weld metal. This produces a greater grain boundary area, which would promote a higher degree of PF formation and consequently higher transformation

temperatures, compared to the real weld metal.

Recently some CCT diagrams, said to be applicable to as-deposited weld metal, have been constructed, using simulative reheating techniques. Diagrams have been produced for changes in carbon, manganese, nickel, Nb and Ti concentrations. However a number of differences in the concentrations of other elements in the alloys studied were apparent, which may be significant. Increased carbon, Nb and Ti were found to move the phase fields on the CCT diagrams to longer times and lower temperatures. With the CCT diagram said to show the influence of carbon on weld transformation, the carbon level was increased from 0.05 to 0.09%wt. However a corresponding decrease in the oxygen content from 411 to 233ppm was also apparent, which could also have accounted for the reduction in transformation temperature and rate noted. Other differences in composition were also apparent within these series of CCT diagrams. With the CCT diagrams presented to show the effect of increased Nb from 0 to 0.03%wt, an increase in carbon content from 0.09 to 0.13%wt was also apparent. According to the CCT diagrams to show the effect of carbon, from the same report, an increased carbon content of 0.04%wt could also account for the reduction in transformation temperature and rate, said to be due to Nb. The CCT diagrams produced to show the influence of Ti were for an increase of 0 to 0.05%wt. Differences in composition were also apparent between the CCT diagrams with the carbon, silicon, manganese and oxygen varying by 0.02, 0.04, 0.03%wt and 100ppm respectively.

Much of this work undertaken to show the influence of

microalloying elements on weld transformation, has been for material with oxygen contents in excess of 250ppm. Since the oxygen content is directly related to the inclusion population and consequently toughness, recent developments have been directed toward a reduction in oxygen content. However it has been suggested that under these low oxygen content conditions AF may not form because of the limited inclusion population, said to be a substrate for nucleation of this phase. Therefore any potential improvement in toughness, as a result of reduced inclusion content, may not be realised because a poor microstructure would form. However there is little available information on microstructural development under low oxygen content conditions, particularly for microalloyed materials.

In many structural welds multi-run techniques are used were the weldment consists of as-deposited and reheated weld metal. The microstructure produced in the reheated weld metal, is determined by the thermal cycle experienced as a result of subsequent weld runs and the composition of the material. Some work has been undertaken on carbon/manganese steel weld metal, were it was found that the prior austenite grain size was refined by reheating. This was said to promote PF and ferrite side plate structures at the expense of AF. However microalloying elements may again play a significant part in the development of the ferritic structure, but the relationship between composition, cooling rate and microstructure is not well understood.

Thus it can be seen that work is needed to gain a further understanding of the relationship between the composition,

in terms of the type and concentration of microalloying elements present, cooling rate and microstructure, particularly for low oxygen content as-deposited and reheated weld metal. For investigating as-deposited weld metal there is also a need to develop a simulative technique which overcomes the restrictions and problems associated with studying real weld metal, without resorting to the reheating methods used by previous workers. Hence this project studies the effect of low and high concentrations of the microalloying elements V, Ti, Nb and Al on the development of microstructures in ferritic steel weld metal. Simulative techniques are used to reproduce the microstructures observed in as-deposited and reheated weld metal and quantitative data is presented in the form of representative CCT diagrams.

CHAPTER 3 - APPROACH TO EXPERIMENTATION.

CHAPTER 3. APPROACH TO EXPERIMENTATION.

It is clear that microalloying elements may significantly affect the properties of HSLA steel weld metal and this is directly related to their influence on the type and proportions of ferrite constituents present in the microstructure. Structural weldments can consist of as-deposited and reheated weld metal and the different thermal cycle experienced by each may influence the mechanisms of microstructural development and the role of microalloying elements within the transformation process. However there is a need for a greater understanding of the factors relating microalloy composition, cooling rate and microstructure in as-deposited and reheated weld metal and this will therefore be studied.

The most common microalloying elements found in weld metal and therefore of most interest are V, Ti, Nb and Al, which may be "picked up" via the parent plate, filler wire or flux as described in chapter 2. In practical welding situations these elements are often found together in the weld pool, but resultant interactions make it difficult to isolate individual effects. It was therefore considered essential to study these elements in isolation. The effect of these elements would also appear to be influenced by the concentrations present. A number of investigators have suggested that low concentrations may be beneficial to weld metal toughness, while others indicated that all levels were detrimental. Therefore the alloys investigated, were chosen to reflect low and high concentrations of V, Ti, Nb and Al found in weld metal. For comparison with the microalloyed

materials, a base alloy consisting of typical concentrations of carbon, manganese and silicon, to that found in HSLA steel weld metal, was chosen. The compositions of the alloys selected for investigation are summarised in table 1.

Due to the potential advantages of improved weld toughness, as a result of low inclusion population, together with the need for greater understanding of the factors influencing the development of ferritic microstructures in low oxygen content weld metal, it was decided to study the influence microalloy composition and cooling rate, at low oxygen levels. The low oxygen content regime is classified by Abson(46) as levels below approximately 150ppm. It has been suggested that AF would not form under these low oxygen conditions because of the absence of an oxide inclusion population to act as nucleation sites. However, although AF has been shown to nucleate on oxide inclusions(17), the inclusion population is generally only sufficient to account for some of the ferrite grains observed and information relating microstructural development, composition and cooling rate in weld metal low oxygen levels is limited. By reducing the oxygen content of the weld metal to very low levels, below the solubility of oxygen in alpha Fe (20ppm), clearer understanding of the development of ferrite constituents in the absence of oxide inclusions may be achieved.

Also in many investigations differences were apparent in the oxygen content of the weld metal studied. Since the formation of inclusions would remove alloying elements from solution, the resultant differences in inclusion population

could affect transformation, by directly influencing the hardenability of the alloy. As this would obscure the effects of the alloying additions investigated, it is obviously essential to ensure consistant oxygen contents. Further, at higher oxygen contents some microalloying elements ie. Ti and Al could be removed from solution and may only influence transformation by affecting the type of oxides formed. Therefore with low oxygen levels the influence of these microalloy elements in solution or as other types of second phase particles could be determined. Therefore the majority of this work will concentrate on the influence of microalloying elements in weld metal with oxygen contents less than 20ppm, although some consideration will also be given to the effects of higher oxygen contents.

A useful method for relating composition and cooling rate to the microstructures formed in ferritic steel weld metal, is by construction of CCT diagrams. Many CCT diagrams have been produced for wrought materials, but these cannot be applied to weld metal because they represent to low an austenitisation temperature and take no account of element segregation due to solidification. A few CCT diagrams, said to be applicable to as-deposited weld metal, have been produced, but these are either schematic (14,58) or based on reheated simulative techniques(52), with the inherent problems, summarised in section 2.11, of not reproducing the solidification process and also forming equiaxed prior austenite grains. No CCT diagrams have been produced to show the influence of microalloying elements on reheated weld metal.

CCT diagrams will therefore be constructed to show the influence of microalloying elements and cooling rate on the microstructures formed in as-deposited and reheated weld metal. However to produce CCT diagrams isolating the effects of microalloying elements, it is necessary to systematically control composition and cooling rate. It would not possible to fulfil this criteria using real welding processes, because:

1. Systematic control of the weld pool composition is difficult. Problems associated with control of the composition have been highlighted in previous work, in that the desired changes in microalloy concentration have been accompanied by changes in other alloying elements and also oxygen content. This has made the isolation of the effect of microalloying elements difficult.
2. Producing an adequate range of cooling rates, to cover the arc welding cooling rate range of 1 to 60 C/sec., for constructing CCT diagrams, would not be possible without changing the welding process.
3. The harsh welding enviroment causes problems with sensitive temperature measuring equipment.

To overcome these problems, techniques will be used to simulate as-deposited and reheated weld metal.

For the as-deposited weld metal studies, a simulative arc melting technique will be used to reproduce solidification conditions in the weld pool, the columnar prior austenite grain structure and simulate the ferritic microstructures

produced in as-deposited weld metal, overcoming the problems associated with reheating methods used previously. The technique will also allow systematic control of the composition and cooling rates in the range required for arc welding processes.

Reheated weld metal is subjected to a wide range of thermal cycles depending on the proximity of the material to the subsequent weld run/s. Since the material adjacent to the final weld run experiences the most severe thermal cycle, it was decided to study the effects of microalloying elements and cooling rate on this region of the weld. Simulative reheating techniques have been used previously, but almost exclusively to study as-deposted weld metal. However although there are considerable limitations when used to study as-deposited weld metal, providing the thermal cycle produced is similar to that found in weld metal, the technique can be used for studying reheated weld metal. The composition used in the reheated alloys will be identical to those used for the as-deposited weld metal, to allow direct comparison of microstructural development.

In any investigation of the factors influencing microstructural development it is important to ensure that the types of ferrite constituents are correctly identified and the proportions determined accurately. The method of classification of the microstructures, will be primarily based on that proposed by the IIW Sub-commission IX (6) report. However with this scheme, the term "ferrite with aligned second phase" was used to identify two different transformation products. This was considered necessary

because of the difficulties associated with differentiating between these phases using a light microscope. However Choi(11) observed that the two microstructural features, encompassed by this term, formed at different transformation temperatures. These two ferrite phases, classified as FSP and LF by Harrison(12), formed at higher and lower transformation temperatures than AF. Therefore when constructing CCT diagrams it is important to distinguish between these phases.

The classification of phases identified in this investigation are:-

1. Primary ferrite: pro-eutectiod ferrite delineating the prior austenite grain boundaries.
2. Ferrite side plates: ferrite needles growing from primary ferrite and associated with high transformation temperatures.
3. Acicular ferrite: small interlocking ferrite grains with aspect ratios of <4:1.
4. Lath ferrite: ferrite with aligned M-A/ carbides not associated with primary ferrite.
5. Ferrite carbide aggregate : structures of ferrite + unresolvable carbides and martensite.
6. Pearlite : ferrite + lamellar carbides.

Representative photomicrographs of all these phases are

shown in fig. 3.1.

The most common technique used for quantitative metallography and recommended by the Welding Instituent is point counting. The technique involves superimposing a grid over a representative area of the microstructure and determining the phases present at the intersection of points on the grid.

Four possible sources of error may be identified with point counting ie.:

1. Careless specimen preparation.
2. Selection of a typical region of microstructure.
3. Difficulty in classification of phases.
4. Statistical errors.

In a statistical analysis of point counting by Gladman et al (114), it was found that for a constituent comprising either 90% or 10% of the microstructure, a statistical error of 1% was achieved when counting 1000 points, rising to 3% with 100 points. For constituents representing 50% of the microstructure, errors of 2% were present when counting 1000 points. The other sources of error noted are difficult to quantify, but could well exceed the statistical error. The errors noted in 1 and 2 can be reduced by careful specimen preparation and choice of sections. With the third type of error it has been reported that for microstructures that were difficult to classify, the magnitude could be as great as 20%. However consistant use of the classification scheme proposed and continual comparison with the standard microstructural types shown previously, the source of error in the current work should be only a few times the

statistical error. Also by constructing CCT diagrams, microstructures will be compared over a range of cooling rates and therefore consistent trends in microstructural development will be highlighted.

Other microstructural features may also be influenced by the microalloy concentration and cooling rate, including the prior austenite grain size, the type and proportions of microphases and the ferrite grain size. The prior austenite grain size may influence subsequent transformation, while the other features influence toughness. Therefore to fully understand the effects of microalloying elements these features will also be examined and quantified. Since AF is particularly important to toughness, ferrite grain size measurement will be directed towards this phase. The hardness of a material can also provide a useful parameter, in that high hardnesses may be associated with low toughness. Since it may also be possible to correlate the hardness with the type of microstructures present, this value will also be determined for each alloy.

CHAPTER 4 - EXPERIMENTAL EQUIPMENT, TECHNIQUE AND RESULTS.

CHAPTER 4. EXPERIMENTAL EQUIPMENT, TECHNIQUE AND RESULTS.

Three distinct areas were apparent in this work and therefore the following chapter is divided accordingly into sections covering:

1. Simulative arc melting technique used for studying the influence of microalloying elements on low oxygen content "as-deposited" weld metal.
2. Modified simulative arc melting, used for studying the influence of oxygen content on transformation in as-deposited weld metal.
3. Simulative reheating technique used for studying the influence of microalloying elements on low oxygen content reheated weld metal.

Each section will describe the materials, apparatus and methods used and list the experimental results determined.

4.1 SIMULATIVE ARC MELTING TECHNIQUE.

Generally, the technique involved melting a pre-prepared specimen in a water cooled copper hearth using a tungsten inert gas (TIG) torch. The specimen was produced by a powder metallurgy process. During melting the specimen was completely surrounded in an annealed borosilicate glass shroud, which was continually purged with high purity argon to prevent atmospheric contamination. When the specimen was completely molten, the arc was extinguished and a thermocouple fired automatically into the molten button. The temperature of the button was recorded during cooling, using a Commodore 8032 microcomputer, via an analog to digital converter. A schematic drawing of the assembly together with

a picture of the equipment is shown in figs 4.1 and 4.2.

4.1.1 COMPARISON OF SIMULATED AND REAL WELD METAL MICROSTRUCTURES.

An obvious difference between the simulated arc melting technique used and the behaviour of real weld metal, was the absence of a true heat affected zone, from which epitaxial growth could occur. Cochrane(37) has suggested that the initial grain size of delta ferrite formed in the weld metal, was closely related to the grain size of the HAZ and therefore the latter could influence weld metal transformation. A series of tests were therefore planned to determine how significant this difference would be and ultimately whether similar microstructures could be produced in the simulated and real weld metal.

RQT-500 steel was readily available and was used for these series of trials. The nominal composition of this material is shown in table 2. Blocks from the material were sectioned into a suitable size, fig. 4.3a and placed within the glass shroud. The central region of the blocks were melted using the TIG torch, fig. 4.3b and the corresponding cooling rate measured by inserting a thermocouple. Using this technique a cooling rate of 4 °C/sec. was determined for the melted material. Sections from the RQT-500 were then melted in the water cooled copper hearth and by control of the specimen size, a similar cooling rate was reproduced. Subsequent analysis of the melted material in each case revealed that deoxygenation had occurred, but the compositions were similar, table 2.

Using this technique the influence of the HAZ could be

assessed, although the conditions reproduced would be more akin to those found in the weld crater, at the end of a weld run. Photomicrographs of the simulated and real weld metal microstructures produced, are shown in fig. 4.4. Comparison revealed that marginally coarser prior austenite grains were formed in the simulated "as-deposited" buttons, although the type and proportions of ferrite constituents were very similar, table 3.

Further examination of the arc melted buttons revealed a zone of material, which would have been in contact with the water cooled copper hearth, of finer grain size, from which the columnar grain structure appeared to originate, fig. 4.5. This suggests that during melting, the material in contact with the copper hearth remained solid and on solidification, columnar grain growth occurred from this region in an epitaxial manner.

The relative similarity of the prior austenite grain size between the simulated and real specimens suggests that the the grain size was determined by factors within the weld pool and not by the epitaxial growth mechanism. The mechanism may relate to the heterogenious nucleation of delta ferrite within the molten material (31) or the formation of austenite on the delta ferrite boundaries ahead of the epitaxial growth front (19). The final prior austenite grain size would be influenced by these nucleation processess and by the degree of subsequent grain coarsening during cooling.

The similarity of microstructures produced in the arc melted buttons and the real weld metal, suggests that the

technique represented a useful simulative approach to determining the effect of changes in composition and cooling rate.

4.1.2 PRODUCTION OF SPECIMENS.

To produce consistent controlable starting material, with the required levels of alloying elements and low oxygen contents, a powder metallurgical approach was used. The required alloys were prepared by mixing high purity elemental powders, compacting and vacuum sintering to reduce the oxygen content.

The elemental constituents of each alloy were mixed in the proportions to give the required composition. Carbon is taken up to reduce oxide films on the particles during vacuum sintering and trials indicated that 0.08%wt of graphite, needed to be added to the mix in excess of the final compositional requirements. The alloy powders used were guaranteed 99.99%wt pure by the manufacturers, to lessen the possibility of adverse contamination. The iron powder used (Hoganas ASC.100) composed the bulk of the mixes and therefore provide the major source of potential contamination. Quantovac analysis was therefore undertaken to ensure the powder was free of any major impurities, table 4. Adsorbed gases on the surface of the powders are also sources of contamination. The degree of this contamination depends on the surface area of the powder and for a constant volume, is inversely proportional to the particle diameter. The iron powder was therefore sieved to a constant 150μm diameter, to ensure consistant surface contamination from batch to batch.

Initially, attempts were made to mix the powders automatically in a motorised barrel drum. However problems associated with agglomeration of the powders, preventing even distribution, meant that mixing had to be carried out manually. The technique used was that proposed by Hausner(115), to be most effective for achieving consistent mixing. The powders in a glass jar, approximately twice the volume, were rotated at an angle of 20 degrees to the horizontal for one half hour. Longer periods, were reported to result in de-mixing. When completely mixed the powders were divided into 30gm samples. Each sample was compacted in a 13mm diameter cylindrical die tool set, using a 500 kN Denison testing machine. To provide a sufficient green strength for handling a load of 130kN was used for compaction.

The compacted specimens had a significant oxygen content, due to surface contamination of the powders. The specimens were therefore vaccum sintered to reduced the oxygen content to low levels. The vacuum sintering was carried out at 1250 °C and $4X10^{-4}$ Torr., for one half hour, followed by furnace cooling to prevent contamination. During this process the oxides present in the compact were reduced by carbon and degassing occurred as carbon monoxide was removed by the vacuum pump. The major degassing occurred on heating during the temperature range 950 to 1150 °C. As mentioned earlier the carbon lost as a result of this process, was accounted for by adding excess graphite in the initial mixing. The final oxygen content of the compact after sintering was less than 50 ppm. While awaiting testing, the sintered compacts

were stored in a vacuum dessicator.

4.1.3 COMPOSITION OF ARC MELTED BUTTONS.

Initial tests were undertaken to ensure that the required material compositions could be produced consistently. A number of sintered compacts were prepared, corresponding to the required base composition and microalloy concentrations, table 1, using the powder metallurgy process described. The 30gm compacts were then melted in the water cooled copper hearth, with a purging gas flow rate of 0.80 cubic metres/hr. The composition of the buttons, determined by Quantovac analysis after arc melting, are shown in table 5. These tests indicated that for the conditions examined a consistent and reproducible composition could be achieved. The base C,Mn and Si elements remained constant in each series, with the carbon equivalent varying by less than 0.02, with the only change in analysis being that of the required microalloy concentration. The oxygen contents determined by vacuum fusion analysis were less than 10ppm in each series.

Further tests were carried out to determine the influence of purging gas flow rate, compact size and arcing time, on the composition. By varying the gas flow rate from 0.10 to 2.55 cubic metres/hr, it was found that the the only significant change in composition occurred with flow rates below 0.28 cubic metres/hr, in which oxygen contamination was apparent, table 6. Increasing the button size from 5 to 60gm and arcing time from 1 to 30 seconds did not appear to significantly influence the composition, when using effective gas purging conditions, table 7 and 8.

The specimens used for constructing the CCT diagrams for the base alloy and low and high microalloyed materials, were prepared using the powder metallurgy process. The base alloy was denoted series A, while the low and high V, Ti, Nb and Al alloys, B to I respectively. After arc melting and thermal analysis each button was analysed to ensure that it conformed to the required composition. The compositions for each series, together with the specimen identification, are summarised in table 9. In the V,Ti and Nb series the alloys produced conformed to the required composition, with the only significant change in each case being that of the required microalloy concentration. However in the low and high Al series, the carbon content of 0.174 and 0.178%wt respectively, were marginally higher than the base level. In the V, Ti and Nb alloys the oxygen contents were less than 10ppm, while in the Al alloys the contents were marginally higher at 20ppm.

4.1.4 ARC MELTING APPARATUS.

The simulative arc melting technique used was designed to overcome the problems associated with a study of real weld metal, by providing systematic control of composition, an adequate range of cooling rates and also a suitable enviroment for accurate measurement of thermal cycles. Analyses of the cooling curves produced, were used to determine the phase transformation temperatures of the alloys, cooled at various rates. This data together with subsequent quantitative metallography, were used to construct CCT diagrams.

As determined previously the arcing time did not

significantly influence the composition of the button, but to ensure that consistant conditions were used with each test, the arc was extinguished immediately the button was completely molten. On extinguishing the arc a thermocouple was fired automatically into the molten pool and the temperature of the button on cooling was recorded on a microcomputer.

4.1.4.1 Control Of Cooling Rate.

The cooling rate of a button was controlled by adjusting the button size and the flow rate of the purging gas. The flow rate of water through the copper hearth did not significantly influence cooling rate. A change in gas flow rate from 0.84 to 2.6 cubic metres/hr, could alter the cooling rate of a button of specific weight by 3 to 20 °C/sec., depending on size. However to produce faster cooling rates it was necessary to reduced the size of the button. With a combination of button size and gas flow rate, cooling rates could be controlled within the range 2 to 70 °C/sec. The cooling rates were determined for the 800 to 500°C temperature range and the influence of gas flow rate and button size on these rates, are summarised in fig. 4.6.

4.1.4.2 Temperature Measurement.

Recording the low level millivoltage output from thermocouples is difficult in the vicinity of an arc, due to the "noise" produced by the electromagnetic field. This "noise", together with the high frequency present when the arc is struck, can also damage the operational amplifiers in sensitive recording equipment. Thus the temperature of a

button was measured by automatically firing a thermocouple, through a small hole in the side of the glass shroud into the weld pool, immediately after the arc was extinguished.

A schematic diagram of the harpoon thermocouple arrangement used is shown in fig. 4.7. The thermocouple was in a twin bore alumina sheath, fixed within an outer metal tube. The spring loaded thermocouple was held in place prior to "firing " by a solenoid valve. The operation of the solenoid valve was controlled by the arc voltage. Exstinguishing the arc caused the solenoid to energise and trigger the firing of the thermocouple into the molten pool. If required, a timer switch at the arc relay could be used to delay the firing, although it was usually set to zero allowing the thermopcouple to fire immediately. The circuit diagram together with a description of the operation of the thermocouple control device is shown in fig. 4.7.

The thermocouple used was a tungsten-25%rhenium/tungsten-3%rhenium type of 0.25mm diameter. The advantages of using this type of thermocouple were:-

1. Rigidity, which allowed the thermocouple to penetrate to the centre of the molten pool, without deflection.
2. The high operating temperature range of 0 to 2300 °C.
3. The relatively high thermal voltage produced, which gives high accuracy and rapid response to small temperature changes.

Platinum-rhenium type thermocouples, which have been used by some workers to measure temperature in weld metal, were

particularly unsuitable, because their lack of rigidity resulted in deflection on penetrating the molten pool. The hot junction of the tungsten type thermocouple was formed by plasma arc fusion. To generate sufficient heat to melt the wires, a transfered arc mode was used and high purity argon prevented contamination. It was important to disconnect the thermocouple from the electronic recording equipment, prior to forming the hot junction, to prevent damage.

To isolate the thermocouple from the molten pool, a Koran 555 refractory coating was used. This zirconia based refractory was held in aqueous suspension and applied to the thermocouple using a brush. A bunsen flame was then used to harden the coating. Two coats gave an adherent refractory coating on the thermocouple, approximately 0.02mm thick. The advantage of this thin coating, in comparison to the refractory sheath often used, was that the thermocouple was more responsive to changes in temperature and also the heat sink was small enough to have no influence on the solidification characteristics of the molten pool.

To maintain the clarity of the thermocouple signal, limiting "noise", the recommended precautions (116) were taken ie. twisted pair compensating cables of the correct type, cable screening etc. However the high sensitivity of the microcomputer required that the gas control solenoid in the welding power source was removed and the thermocouple solenoid was switch off before recording the data. It was also important to ensure that similar electrical earths were used on each piece of equipment, to prevent problems associated with earth loops.

4.1.4.3 Recording Of Temperature.

The thermocouple output was recorded on a Commodore 8032 microcomputer, via an analog to digital(A-D) convertor. The A-D convertor had eight channels and a resolution of twelve bits. Since the output from the W-Rh thermocouple was 0 to 40mV, the channels used for the temperature, were configured for the range ±0 to 50mV. At these low signal levels the amplifiers in the A-D convertor produced a non-linear response to the input voltage. However since the response was consistent, the problem was overcome by calibration.

Using a voltage calibrator, a range of voltages from 0 to 40mV was input to a channel and the corresponding output recorded on the computer and related to temperature. The results were analysed on a main frame computer to provide the polynomial for the curve of best fit to the temperature/voltage data. A change of operational amplifier, for example due to damage, required re-calibration of each channel. The polynomials were then used to convert the thermocouple signal recorded on the computer, directly to temperature. The accuracy of the recording system was determined by the resolution of the A-D convertor. The 12 bit resolution of the A-D, gives a maximum range of 0 to 4096 increments ie. 2↑12. The A-D was also configured for bi-polar input and therefore zero millivolts corresponded to half the full scale increments ie, 2047. The digital value recorded was then converted to millivolts using the relationship:

mV= (DIGITAL VALUE-2047 X FULL SCALE) / 2048

Therefore, for the configuration used one digital increment

was equivalent to 0.024mV, giving a recording accuracy of ±2.1°C

A flow diagram for the computer program used to record the temperature of the button is shown in fig. 4.8a. The program selects the channels to be used, triggers the sample and hold amplifiers, initiates conversion and reads the result. The initial user inputs were the channel numbers to be used, the rate at which the data was to be sampled and the number of data samples required. By using machine code to increase the program speed, a sampling rate of 170 data sample/sec./channel was achieved. The more channels used the slower the maximum possible rate. The sampling rate and number of data samples required, depended on the cooling rate of the specimen tested. For slow cooling rates a sampling rate and number of 15/sec. and 2500 respectively was normally used. However with faster cooling rates a sampling rate and number of 25/sec and 1500 was required, to improved response. Once recorded the data was saved on floppy disc for further processing.

4.1.4.4 Processing Of Temperature Data.

The sequence used to process the temperature data is shown in fig. 4.8b. During testing the temperature was recorded and stored in digital form. Initial processing involved smoothing the data to remove any "noise" present on the signal. The program used to smooth the data, averages the data for a set of 30 sample points increments by one and repeats the routine. The smoothed digital data was then converted directly to temperature using the polynomials calculated during calibration of the channel. The program

also applies a cold junction compensation.

4.1.4.5 Determination Of Transformation Temperatures.

Recording the temperature using a microcomputer gave maximum flexibility and ease in the analysis of the cooling curves produced. An example of a cooling curve for the base alloy composition is shown in fig. 4.9a. To assist in determining the points corresponding to the start and finish of transformation, the cooling curves were plotted with expanded axis on a Hewlett Packard graph plotter, fig. 4.9b. The transformation from austenite to ferrite results in the evolution of latent heat, which produces a departure form the Newtonian cooling relationship. The transformation temperatures were therefore taken as the points where arrests occurred in the Newtonian curve, using the constructions shown in fig. 4.9b. The facilities available on the graph plotter, allowed the indicated transformation points to be directly read by the computer, overcoming problems associated with limited axis sizes on conventional chart recorders.

To further enhance the determination of the transformation temperature, software differentiation could be applied to the cooling curves. Applying first and second derivatives to the data, indicated the Ts and Tf temperatures as a point of inflection and minimum on the first derivative and a minimum and zero on the second derivative respectively, fig. 4.9c. However applying this differential technique, to improve the accuracy of determining the transformation temperatures was not successful in all cases. The success appeared to be

dependent on the shape of the cooling curve. Transformations showing sharp arrest usually produced clear points on the derivative curves. Cooling curves with less significant arrests, produced derivatives on which the transformation points were represented by a wide temperature range, becoming less clear than on the original curve. These effects are summarised in fig. 4.10. The derivative technique was most applicable for tests conducted in the intermediate temperature range ie. 6 to 25°C/sec. Assuming the transformation temperatures were based on 98% transformation an estimated accuracy of ±5 and ±10°C could be expected for determinations of Ts and Tf respectively, although at cooling rates above 25°C/sec. the accuracies were likely to be lower.

To construct the CCT diagrams, 15 to 20 tests at cooling rates from 3 to 60°C/sec, were conducted for each series. Each cooling curve was analysed to determine the temperatures corresponding to the start and finish of phase transformation and the result are summarised for series A to I in tables 10 to 18.

4.1.5 QUANTITATIVE METALLOGRAPHY.

Each button produced was sectioned in the transverse direction, fig. 4.11, and prepared using standard metallographic equipment, to a 1μm diamond finish. To examine the major microstructural constituents the specimens were etched in 2% nital. In general the macrostrucure of the buttons consisted of fine prior austenite grains at the base, from which columnar grain development was apparent. The majority of the button consisted of these columnar

grains, although a small region near the top was usually equi-axed in structure. A representaive macrograph showing the solidification structure of the button is shown in fig. 4.12.

Metallographic examination was always conducted in the central region of the buttons, fig. 4.13, in the vicinity were temperature measurements were taken, although the microstructures were usually consistent throughout a wide area of the specimens. Analysis of the microstructures included measurement of:

1. The prior austenite grain size.
2. The type and proportions of ferrite constituents.
3. The type and proportions of microphases.
4. The ferrite grain size.

4.1.5.1 Measurement Of Prior Austenite Grain Size.

The prior austenite grain size was apparent at slow and intermediate cooling rates by PF delineation. In the absence of this phase, at the faster cooling rates examined, Saspananses reagent was used, which preferentially etches the austenite boundaries. The transverse sections of the buttons were placed on an optical microscope and the image projected onto a screen. The size measured was that associated with the short transverse section of the elongated columnar grains, which equated to the shortest diffusional distance, fig. 4.14. Measurements were taken with the straight line at right angles to the austenite boundaries and the magnification was varied depending on the relative grain size. The grain size was measured in each button tested and the results for series A

to I are shown in table 10 to 18 and figs. 4.15a to d.

4.1.5.2 Determination Of The Type And Proportion Of Ferrite Constituents And Microphases.

Quantitative analysis of the type and proportions of ferritic constituents observed was carried out by taking six representative photomicrographs, selected randomly from the central region of each button. The constituents identified are shown in chapter 3.. The magnification used was either X145 or X300, depending on the microstructure examined. Higher magnifications were occasionally used if phases were difficult to resolve. Point counting was achieved by laying a grid, produced on clear plastic, over the micrograph, fig. 4.16 and identifying the phases at each intersection of the grid. 1000 points were counted for each button, giving a statistical error(114) of 1%, rising to 2% with the more complex structures produced. The results for series A to I are shown in tables 10 to 18. The influence of microalloy concentration and cooling rate on the type and proportions of ferrite constituents are compared directly with the base alloy in figs. 4.17 to 4.20 and in representative photomicrographs, figs. 4.21 to 4.29. The photomicrographs were chosen to represent comparible low, intermediate and fast cooling rates for each microalloy series. With each micrograph a histogram is also shown, directly indicating the type and proportions of ferrite phases present.

The proportions of microphases present in the buttons were also determined by taking representative photomicrographs from the central region of the button. The specimens were reprepared and etch in picral and

photographed at a magnification of X1200. Using a light microscope it was not possible to clearly distinguish the microphases present, but with a similar classification to that used by Garland and Kirkwood(4), two types were apparent:

1. Completely dark etch type, classified as carbides.
2. Light etching type surrounded by a dark band, classified as lath martensite.

Examples of these phases are shown in fig. 2.3. For each series the microphase content was determined for alloys cooled at 7°C/sec. At this cooling rate high proportions of AF were generally formed and therefore the influence of microphase content would be important, since any increase would impair toughness. Microalloy additions increased the microphase contents and also favoured lath martenite types, table 19 and figs. 4.30 to 4.33. The microphase content also increased with faster cooling rate, fig. 4.34.

For each series, the specimens cooled at 4°C/sec. were examined to determine the influence of microalloy additions on the AF grain size. The short transverse dimension of the ferrite grain was measured using a mean linear intercept technique. Increased microalloy additions were found to refine the AF grain size, table 20 and figs. 4.35 to 4.38. Examination of the micrographs produced for each series, figs. 4.21 to 4.29, show that the ferrite constituents are also generally refined with increasing cooling rate.

4.1.6 HARDNESS TESTING.

Vickers diamond pyramidal hardness tests were conducted on each of the buttons, using a 20kg load. Five impressions

were made on each specimens, again in the central region, corresponding to the positions were temperature measurement and quantitative metallography was carried out. The results for series A to I are summarised in tables 10 to 18 and figs. 4.39 to 4.42.

4.1.7 CONSTRUCTION OF CCT DIAGRAMS.

The CCT diagrams were constructed by computer plotting the cooling curves, determined during thermal analysis, onto temperature-log time axis, fig. 4.43a. The transformation temperatures determined, were plotted onto the cooling curves and the boundaries corresponding to the start and finish were constructed, fig. 4.43b. The phase fields, within the transformation boundaries, were constructed by dividing the cooling curves into the proportions, corresponding to the percentage of microstructural constituents determined by quantitative metallography. The assumed order of transformation, was that proposed by Choi(9) (see section 2.1.8).

Transformation is a "competitive" process and although the general order of formation applied, there would be some overlap of the temperature ranges in which individual phases formed. Also the rate of growth of phases may be different. Because of these anomalies the temperatures associated with phase field boundaries constructed, were only approximate. This does not however detract from their effectiveness in indicating the type and proportions of constituents formed, as a result of changes in composition, cooling rate or prior austenite grain size.

The CCT diagrams for the low and high microalloy series

are compared directly with the base alloy in figs. 4.44 to 4.47. Composite CCT diagrams have also been constructed, figs. 4.48 to 4.56, to give more information than normally presented on CCT diagrams in the literature. In these diagrams, together with the actual CCT diagram, plots relating to the prior austenite grain size, the type and proportion of ferrite constituents and hardness for each series, are also shown.

4.2 SIMULATED ARC MELTING WITH HIGH OXYGEN CONTENT.

The development of the ferritic microstructure in weld metal is influenced by the oxygen content(57). A series of tests were therefore initiated to determine the effect of oxygen content on the microstructures formed, using the simulative arc melting technique.

Two techniques were employed, in an attempt to increase the oxygen content of the buttons:

1. Oxygen was introduced to the arc atmosphere via the shielding gas.
2. Unsintered buttons were melted in association with sintered buttons, the oxygen deriving from dissociation of the oxides present in the unsintered button.

With the first method, an argon-2%oxygen shielding gas was used during the melting of sintered buttons, conforming to the base composition. Subsequent analysis revealed that the composition was influenced significantly by the arcing time. The longer the arcing time the higher the oxygen content of the buttons, but the carbon contents were also reduced, table 21. With arcing times up to 10 seconds the carbon contents were reduced to approximately 0.05%wt, although the Si and Mn concentration did not appear to be influenced significantly. The oxygen contents were approximately 300ppm. However arcing times longer than 10sec., reduced the proportion of all the alloying elements present, although the oxygen content did not appear to increase further. The button size was also found to influence the composition. Using an arcing time of 5 seconds, it was found that the

oxygen content increased and the carbon concentration was reduced, with decreasing button size, table 22.

Mixing unsintered buttons with sintered button, during melting, was found to have very little effect on the oxygen content, although some reduction in carbon concentration was apparent, table 23.

These results indicated that a limited increase in oxygen content could be achieved, using the oxygenated purging gas method. But reproducibility of composition was difficult, unless the arcing time and button size were standardised. As a result of these difficulties only a limited number of test were conducted. The conditions used were, a gas flow rate of 1.1 cubic metres/hr and an arcing time of 5 seconds. The initial button composition was similar to the base alloy used previously and was of 30gm weight. This produced specimens with cooling rates of 8 °C/sec. and a consistant composition, table 24.

The reduced carbon content of these buttons, prevented direct comparison with the previous series, in which the carbon levels were 0.15%. A CCT diagram was therefore constructed using the arc melting technique, for a material of similar Si and Mn contents to those used previously and also present in the higher oxygen alloys, but with a carbon content of 0.05% and low oxygen (denoted series J). The composition and composite CCT diagram, determined for this low carbon alloy are shown in table 25 and fig. 4.57, respectively. A comparison of the microstructures observed in the high and low oxygen buttons, produced at similar cooling rates, indicated some of the effects of oxygen

content on microstructural development. Comparison with the CCT diagram produced for the base alloy (series A), also provided information on the effect of carbon content on the microstructures formed.

An increase in oxygen content was found to refine the prior austenite grain size and promote the formation of PF structure, when compared to alloys of similar composition and cooling rate, but with lower oxygen contents, fig. 4.58. A comparison of the CCT diagrams produced for the low and high carbon alloys, series J and A respectively, are shown in fig. 4.59. Reducing the carbon content increased the transformation temperature and moved the CCT curve nose to a shorter time, resulting in increased PF and FSP formation fig. 4.60. Representative photomicrographs of the microstructures formed with low carbon content, at increasing cooling rate, are shown in fig. 4.61. The proportions of microphases were reduced, fig. 4.62 and the AF grain size increased, fig. 4.63, compared to the higher carbon alloy. The hardness was also reduced compared to the high carbon alloy, fig. 4.64. The thermal analysis, quantitative metallographic and hardness results, for the simulated low carbon weld metal, are summarised in table 26.

4.3 TECHNIQUE FOR SIMULATING REHEATED WELD METAL.

The simulative reheating technique used involved subjecting specimens, machined from arc melted buttons, to a similar heating cycle to that typical of reheated weld metal, followed by natural or gas cooling at a series of cooling rates. During cooling, the temperature and length of the specimens were recorded on a Commodore microcomputer, using a thermocouple and displacement transducer respectively. Testing was carried out in an inert atmosphere to prevent oxidation and decarburisation. Dilatometric analysis, together with quantitative metallography, were conducted on each specimen to provide data for constructing CCT diagrams, showing the influence of microalloying elements on transformation. A schematic diagram and photograph of the equipment are shown in figs. 4.65 and 4.66, respectively.

4.3.1 SIMULATIVE THERMAL CYCLE.

Since the material adjacent to the final weld run experiences the most severe thermal cycle, it was decided to study the effects of microalloying elements and cooling rate on this region of a weld. Measurements were therefore initiated to determine the thermal cycle experienced in this, the "coarse grained" region of reheated weld metal.

An RQT-500 steel was again used for this series of tests and the arc melting apparatus described earlier was employed. Blocks of the steel were positioned under the TIG torch, within the glass shroud, fig. 4.67a, which was purged with high purity argon during melting. The central region of the block was melted using the TIG torch and the harpoon

thermocouple fired on extinguishing the arc. The thermocouple was aimed to finish at a pre-determined position, at the centre of the pool and initially at a depth of 5mm from the surface, fig. 4.67b. A second region of the block was then melted, with the weld pool produced overlaping the first, fig. 4.67c. During this second melting, the temperature was monitored via the "in-situ" thermocouple, using a Maxsym minicomputer. The filtering provided on the input boards of this computer, allowed the temperature to be recorded during arcing and therefore the heating cycle of the material, produced by the second melting, could be monitored. The powerful basic provided by this computer allowed a simple analog input program to be written for achieving temperature measurement, fig. 4.67d. Subsequent sectioning and incremental polishing, was used to determine the proximity of the thermocouple, with respect to the coarse grained region produced by the second weld. After a number of trials, in which the arcing conditions were varied, a suitable thermocouple position was achieved in which the thermal cycle monitored was that of the reheated coarse grained region, fig. 4.67c. The arcing parameters, which produced this suitable pool size were 350 amps and 18 volts. The thermal cycle determined, shown in fig. 4.68, indicated that a peak temperature of 1350 °C was reached within 7 seconds, followed by a cooling rate of 4°C/sec.

Subsequent tests were carried out with the thermocouple positioned at 3 and 7.5 mm from the surface, to determine the influence of molten pool size and "heat input" on the thermal cycle. These tests indicated that the arcing

conditions did not appear to influence the peak temperature of 1350 °C achieved, although the time to reach this peak temperature was marginally faster in the smaller button size ie. 5 seconds, compared to 7 seconds at 7.5mm. However the cooling rates were affected, with the highest "heat input" and corresponding largest pool size, producing the slowest cooling rates of 3°C/sec, while the cooling rate increased with lower "heat input". The result of this series of tests are summarised in fig. 4.68.

4.3.2 COMPARISON OF REAL AND SIMULATED REHEATED WELD METAL.

The series of tests described in the previous section, were also a useful basis for comparing simulated and real reheated weld microstructures. In these tests the thermal cycle experienced, and the corresponding microstructural development of the coarse grained reheated weld metal was known. Therefore a comparison with simulated reheated weld metal, subjected to a similar thermal cycle, would indicate whether the simulative technique, reproduced the conditions present in the real weld metal and ultimately whether similar microstructures were formed.

Dilatometric specimens, machined from "as-deposited" RQT-500 steel, were subjected to a heating cycle of 1350 °C, followed by cooling at 4 °C/sec. Unfortunately the heating rate determined for the real weld, was marginally higher than that possible during simulation, which was 1350 °C in 9 seconds. However subsequent comparison of the microstructures observed in each case, were in good agreement, fig. 4.69, consisting of similar proportions of PF, FSP and LF phases. This general agreement in the

microstructures formed, would suggest that the simulative reheating technique was a useful approach for investigating the effects of microalloying elements and cooling rate on reheated weld metal transformation.

4.3.3 EXPERIMENTAL APPARATUS.

The high speed dilatometer used, consisted of an induction heating power source, electronic feed back temperature controller and an induction heating coil within a chamber. The dilatometer specimens were heated within the induction coil and the temperature and volume change were monotored on an X-Y chart recorder. The specimens were 10mm long X 6mm diameter bars. Gas quenching could be applied, via tubes placed close to the specimen surface.

Initial tests undertaken using this equipment highlighted a number of problems. The maximu cooling rate which could be achieved was only 15 °C/sec., which was slow in comparison to the rates required for simulating weld metal. Specimens also suffered from excessive oxidation and decarburisation at high peak temperatures and nickel plating, used previously to overcome this, was unsuitable above 800 °C. The capacitor discharge technique, used to weld thermocouples to the dilatometer specimens, was also suspect, with a high proportion of test failures as a result of detachment.

A number of modification were made to the equipment and specimen design, to produce the required parameters for simulating reheated weld metal. These modification will be reported in the following section, but can be summarised as:

1. A vacuum chamber was designed and built for testing in an inert atmosphere.

2. The specimen was re-designed to allow faster cooling rates to be achieved.
3. To give better bonding a microspot welding technique was adopted for joining the thermocouples to the specimen.
4. The thermocouple was change from a Chrome/Alummel type to Platinum/Platinum-13%Rhodium, to give higher peak temperature capability.
5. The gas cooling arrangement was changed to give greater control and more effective cooling.
6. The temperature and displacement measurements were recorded on microcomputer.

4.3.3.1 Vacuum Chamber Design.

To ensure that specimens were not subject to oxidation or decarburiation on heating, testing was conducted in an inert atmosphere. The initial chamber used with the equipment, was not suitable for this application and a vacuum chamber was therefore designed and built.

The chamber was manufactured from 6mm stainless steel plate, with extra plates welded in positions were components were to be fitted. The dilatometer specimen was situated axially in the chamber, within the water cooled copper induction coil. It rested on a bottom fixed silica probe and an upper silica probe transferred changes in specimen length to the displacement transducer, fig. 4.70a.

The induction heating coil leads entered the chamber through the rear wall, from which it was isolated using polypropylene inserts, fig. 4.70b. A water cooled copper plate, fixed to the rear chamber wall using high temperature

adhesive, was used to prevent the metal adjacent to the induction coil from being heated.

The displacement transducer was contained within a sealed sheath to prevent vacuum leaks, fig. 4.70c. The transducer could be moved vertically, to allow zeroing prior to each test and a top clamp plate was used to provide a vacuum seal, by tightening onto an O-ring in a 45 degree slot. Sealed thermocouple terminals were provided in the chamber wall and a three way junction was used as a vacuum outlet to the vacuum pump, inlet for the inert gas atmosphere and an outlet for the quenching gas, fig. 4.70d.

The cooling gas entered the chamber via the bottom silica probe. This directed the gas through the centre of the hollow specimen and holes ground in the upper silica probe provided an outlet into the chamber. The flow rate was determined using a calibrated flow meter and gas flow was controlled using solenoid valves which opened the inlet and outlet to the chamber simultaneously, fig. 4.70e.

4.3.3.2 Dilatometer Specimen Design.

Initial tests indicated that the cooling rate was ultimately determined by the mass to surface area of the specimen. A hollow cylindrical specimen was therefore designed, fig. 4.70f, to give the highest possible surface area. The outside diameter of the specimen was standardised at 6mm, but the internal diameter could be adjusted to vary the potential cooling rate. The thinner the wall thickness the faster the specimen could be cooled. However it was found that with specimens of 1mm wall thickness or less, temperature control was difficult. To increase the cooling

rate still further, an inert gas was directed through the centre of the specimen.

The cooling rate could therefore be controlled by variation in specimen wall thickness and cooling gas flow rate. Using these parameters a cooling rate range of 2 to 80 °C/sec. could be achieved, which was suitable for reproducing arc weld cooling rates. Slower cooling rates were also possible using a linear programmed controller, but since this was only applicable to rates less than 1 °C/sec., it was not generally used. A number of different cooling gases were also evaluated, including nitrogen, argon and helium. However, although it was found that marginally higher cooling rates were possible with helium, the required range could be achieved with argon and therefore this gas was used.

Introducing cooling gas through the centre of the hollow specimens was an efficient method of cooling, but since this gas directly impinged on the displacement transducer, tests were initiated to ensure no detrimental effects on measurements were produced. The flow rate was varied from 0.14 to 2.8 cubic metres/hr through the specimen and the transducer output was monitored on a chart recorder and microcomputer. It was found that for flow rates less than 2.6 cubic metres/hr, the gas was successfully vented into the chamber and no influence was observed on the transducer output. With higher flow rates an erratic transducer responce was recorded. However flow rates in the range 0 to 2.1 cubic metres/hr were sufficient to produce the required cooling rates.

4.3.3.3 Chamber Atmosphere.

To prevent degradation of the specimen at the high peak temperatures employed, testing was conducted in an inert atmosphere. This was achieved by evacuating the chamber to 0.02torr, followed by back filling with high purity argon-2%hydrogen gas. This procedure was carried out twice prior to each test. The presence of 2% hydrogen in the gas was thought to further reduce the possibility of oxidation. Subsequent examination confirmed that no oxidation occured on the specimens and metallographic sections exhibited no evidence of surface decarburisation, fig. 4.71.

4.3.3.4 Temperature Distribution In Dilatometer Specimens.

To accurately determine transformation temperatures using dilatometry, it was necessary to ensure that the whole of the specimen was subjected to the same thermal cycle and no excessive temperature gradients existed along its length. The existence of a temperature gradient, would have resulted in regions remote from the thermocouple, transforming at a different stage. The volume changes produced by this remote transformation would however be "picked up" by the displacement transducer and associated with the higher temperature being measured by the thermocouple. Therefore an artificially high transformation temperature would be recorded.

To determine whether the temperature distribution was uniform along the dilatometer specimen, a number of thermocouples were spot welded at 3mm intervals, on each side of the specimen, fig. 4.72a. The specimen was heated to 1350 °C and the resultant thermal cycles recorded on the

Maxsym minicomputer. This computer had upto 16 channels available for analog input and the thermal cycles were recorded using 12 of these channels. The fast recording speed of the computer (2000 samples per second), meant that although a data point was read successively from each thermocouple, effectively all the thermocouples were monitored simultaneously and therefore no displacement in thermal cycle was produced. Examination of the thermal cycles produced suggested that a uniform temperature was achieved along the specimen length, fig. 4.72b. Similar tests were also conducted to ensure that uniform temperature was achieved through the thickness of the specimen. Thermocouples were spot welded to the inner and outer surfaces and heated to 1350°C as before. The thermal cycle recorded on the computer, again indicated that no temperature difference was apparent between the inner and outer surfaces.

4.3.4 MEASUREMENT OF VOLUME CHANGE DURING TRANSFORMATION.

When a steel transforms from austenite to ferrite there is an associated increase in volume, as the crystal structure changes from face centred cubic to body centred cubic. By monitoring the length and temperature of the specimen on cooling, the temperature at which transformation occurs can be determined.

The specimen length was monotored using an LVDT linear displacement transducer, type D5/100A. A D-8 creep monitor was used to provide a power supply too and amplify the output from the transducer. A meter within this equipment also provide a visual indication of the transducer position.

The dilatometer specimen was positioned within the induction coil on a bottom fixed silica tube. The change in specimen length, which occured during the thermal cycle, was transmitted to the transducer armature via the upper silica tube, fig. 4.73a. The accuracy of the transducer could be increased by altering the displacement range on the creep monitor, although the most sensitive range of 0.254 mm full scale, was generally adopted. The output from the transducer was recorded via the creep monitor, on a Commodore microcomputer.

The specimen temperature was recorded using platinum/rhodium "R type" thermocouples. Two thermocouples were employed, one was used for temperature control, while the second was connected to the computer for temperature measurement. The thermocouples were microspot welded onto the side of the specimen at the mid point, fig. 4.73b. To produce a direct visual record of the thermal cycle, the temperature was also monitored on a chart recorder.

The temperature and displacement were transmitted to the microcomputer via an analog to digital converter. The two channels used, were configured to accept data in the range ±20mV for the thermocouple and ±1V for the transducer, giving a recording accuracy of 1.4 °C and 0.1μm respectively. The recording software was similar to that used in the arc melting tests , described in section 4.1.4.3. However for dilatation, the program was modified to accept data on two channels. The channel used to record the temperature was also calibrated in a similar manner to that described in section 4.1.4.3. In general a sampling rate and number

recorded, of 15 per second and 2000 respectively, was sufficient for most of the cooling rates employed, although at high rates 20 samples per second was used. The specimen displacment and temperature were also recorded directly onto an X-Y plotter during testing.

4.3.5 COMPOSITION AND MANUFACTURE OF MATERIALS.

The dilatometer specimens were machined from the central region of 60gm arc melted buttons, fig. 4.74, produced in the same batches as the corresponding "as-deposited" alloys, with each button being analysed to ensure it conformed to the required composition. The reheated base alloy, together with the low and high V, Ti, Nb and Al series were again denoted A to I, but prefixed with D, to differentiate from their corresponding "as-deposited" alloys. Since the reheated and "as-deposited" alloys were produced from the same batches, the compositions of the corresponding series were identical and are shown in table 9. This therefore allows a direct comparison between microstructural development in the "as-deposited" and reheated simulated weld metal.

4.3.6 TEST PROCEDURE.

A dilatomter specimen was degreased and the control and temperature monitoring thermocouples microspot welded onto the side. The specimen was then placed within the induction heating coil, on the lower fixed silica tube and the upper silica tube, was inserted between the specimen and transducer armature. The transducer position was adjusted to give a zero reading on the creep monitor, while increasing the sensitivity of the displacement range to 0.254 mm full scale. Once the transducer had been set and thermocouples

connected to the appropriate terminals, the top plate was tightened and the chamber door closed, to seal the vacuum chamber. If gas cooling was required, the flow rate was set prior to testing, by adjusting the flow meter. The solenoid valves were then closed and the chamber evacuated to 0.02 torr, followed by back-filling with argon-2%hydrogen gas. Once the required atmosphere had been achieved the specimen was heated to 1350 °C. The induction heating was then switched off and if gas cooling was required, the solenoid valves were opened simultaneously, followed by starting the computer to monitor temperature and displacement. It was essential to ensure that the computer was not started before the induction heating source was stopped, to prevent damage to the A-D converter by HF pick-up. For each CCT diagram, 12-15 tests were conducted, with specimens cooled in the range 2 to 60 °C/sec.

4.3.7 ANALYSIS OF DILATATION DATA.

A flow chart showing the route used to analyse the temperature and displacement data is shown in fig. 4.75. The program used to record the data saved the digital equivalents of the temperature and displacement as a single file. The initial processing step was therefore to separate the data and to save as individual sequential files. The data was then smoothed using the software described in section 4.1.4.4 and the temperature, in digital form converted to degrees centigrade, together with cold junction compensation.

To determine the transformation temperatures, a plot of temperature against displacement was produced, on a Hewlet

Packard graph plotter. An example of a dilatation curve, for the base alloy, is shown in fig. 4.76. The transformation region was replotted on a larger scale to enhance the determination of the transformation points and tangents to the point of inversion at a and b, indicated the transformation start and finish respectively.

Analysis of the dilatometer curves produced for each series, indicated that the transformation temperatures were depressed by microalloy additions in the reheated material, but were higher than their respective "as-deposited" alloys, tables 27 to 33. Unfortunately due to problems associated with saving the data for the low V alloy (series DB) on the computer disc, the results for this material were lost. However results were produced indicating the effect of high V additions.

4.3.8 QUANTITATIVE METALLOGRAPHY OF REHEATED SPECIMENS.

Quantitative metallographic examination of the dilatometer specimens from each series, was conducted in the same way to that described for the as-deposited alloys, section 4.1.5. The dilatometer specimens were sectioned through the transverse central axis, adjacent to the thermocouple positions and prepared using standard techniques. Point counting was again carried out from representative photomicrographs, using 1000 determinations for each specimen. The type and proportions of ferrite constituents produced in the reheated alloys were significantly influenced by microalloy additions and cooling rate and the results for series DA to DI are indicated in tables 27 to 34. The ferrite constituents formed in the

microalloyed materials are directly compared with the base alloy in figs. 4.77 to 4.80. Representative photomicrographs showing the microstructures formed in each series at cooling rates of 4 and 12°C/sec. are shown in figs. 4.81 to 4.88.

The microphase contents were also determined for alloys cooled at 7°C/sec and indicated that microalloy additions increased the proportions present, table 35 and figs. 4.89 to 4.92. Examination of the microstructures for each series, figs. 4.81 to 4.88, also revealed that microalloy additions and increased cooling rate, refined the ferrite grain size. A similar prior austenite grain size, of 80μm, was observed in each of the alloys at slow cooling rates, except for the high Ti and Nb alloys, were a marginal decrease to 70μm was noted. A marginal refinement of approximately 10μm, was also observed with increased cooling rates.

4.3.9 HARDNESS DETERMINATIONS.

Because of the relatively thin wall thickness of some of the dilatometer specimens cooled at fast rates, hardness determinations on all the specimens were conducted using a micro-hardness tester, with a 1 Kg load. To ensure that a comparison in hardness could be made with the as-deposited alloys, some of the latter were retested using the micro-hardness tester and some of the larger dilatometer specimens checked using the Vickers hardness tester. A maximum difference of 3 Vickers points was apparent. The hardness results for each series are shown in table 27 to 33 and figs. 4.93 to 4.96.

4.3.10 CONSTRUCTION OF CCT DIAGRAMS FOR REHEATED WELD METAL.

The transformation and quantitative metallographic data

were used to construct CCT diagrams showing the effect of low and high microalloy concentrations, on the transformation and development of ferritic constituents in the simulated reheated weld metal. The CCT diagrams were constructed in a similar manner to that described for the "as-deposited" alloys, section 4.1.7. CCT diagrams for the microalloyed materials are compared directly with the base alloy in figs. 4.97 to 4.100. Composite CCT diagrams were again produced, in which information on the types and proportions of ferrite constituents and corresponding hardness values, are also indicated, figs. 4.101 to 4.107.

CHAPTER 5 - DISCUSSION.

CHAPTER 5. DISCUSSION.

The mechanical properties of weld metal are determined primarily by the microstructure(18), microphase content(20) and the inclusion population(74). It is well established that the optimum strength and toughness are achieved by weld metal with a high proportion of fine grained AF. A low inclusion population is also important for improved weld toughness and there is an increasing trend to reduce the oxygen content of weld metal, to achieve this.

The development of the ferritic microstructure is a complex process, dependent on composition, cooling rate and prior austenite grain size, which are in turn related to the welding consumables and thermal cycle. There are a wide variety of arc welding processes from high heat input submerged arc to low heat input tungsten inert gas, giving cooling rates in the range from 1 to 60 °C/sec. Many structural weld are also produced using multi-run techniques, producing both as-deposited and reheated weld metal.

Microalloying elements may enter the weld pool via the welding wire or flux eg. Ti and Al, or by dilution from the parent plate eg. Nb and V. It has been shown that these elements can significantly effect the mechanical properties of the weld metal, by influencing the microstructure (75,80,90). However detailed information relating microalloy composition, cooling rate and microstructure is not available, particularly for low oxygen content conditions.

In the current work continuous cooling transformation

(CCT) diagrams have been constucted to show the influence of the microalloying elements V, Nb, Ti and Al (at low and high concentrations) and cooling rate, on ferritic weld metal transformation, under low oxygen conditions. These diagrams have been produced using thermal analysis and dilatation data, together with quantitative metallography, from techniques developed to simulate as-deposited and reheated weld metal.

5.1 ASSESSMENT OF THE TECHNIQUE USED FOR SIMULATING AS-DEPOSITED WELD METAL.

CCT diagrams have been constructed indicating the effects of microalloying elements and cooling rate, on the microstructures formed in ferritic weld metal, using a simulative arc welding technique. The technique reproduces the solidification conditions and ferrite microstructures formed in as-deposited weld metal, overcoming the problems associated with testing real weld metal and the limitations of the reheating methods used by previous workers (8,12).

Comparison of the microstructures produced in real and simulated "as-deposited" weld metal produced using identical cooling rates ie. 4°C/sec., revealed that similar microstructures were produced in each. The prior austenite grain size was marginally coarser in the simulated material, although the type and proportions ferrite constituents, which consisted of PF, FSP and LF constituents, were in good agreement, fig. 4.5. This suggested that the technique represented a useful simulative approach to determining the effect of changes in composition and cooling rate, under low oxygen conditions.

The base composition was a C, Mn, Si steel and the microalloying elements V, Ti, Nb and Al were added individually, to isolate their effects. The compositions were chosen to reflect typical levels found in microalloyed steel weld metal. The nominal compositions for each series are shown in table 9. From this table it can be seen that the base elements C, Mn and Si remained consistent in each series, with the carbon equivalent varying by less than 0.03 for the V, Ti and Nb series, with the only change in analysis being that of the required variation in microalloy concentration. However in the Al series the carbon content was found to be 0.02% higher than the base alloy, although the difference between the low and high Al series were negligible. This difference in the carbon content, in the Al series, may influence transformation and therefore some care may be required when comparing these alloys, with the base composition. There is however some evidence to suggest that a difference in the carbon content greater than 0.04%wt, is required to show any significant influence on microstructure, (93). Dispite this slight variation in carbon, when compared to the base alloy, the major alloying elements within the Al series remained consistent and therefore the effect of Al could still be isolated.

In the V, Nb and Ti series the oxygen concentrations were less than 10ppm and marginally higher in the Al series at 20ppm, well within the low oxygen content regime proposed by Abson(46) and even low enough to be completely soluble in Fe at room temperature. With these low oxygen contents

it can be assumed that oxide formation would be very limited, if any. This view was confirmed by extensive metallography in which no obvious oxide inclusions were apparent. Calculations also suggested that with the oxygen concentrations present, should limited oxide formation occur, there would be no significant removal of alloying elements from solution, table 36. Therefore the nucleation of ferrite on oxide inclusions, can be ruled out as a significant mechanism in the austenite decomposition processes observed.

Although the technique proved to be successful in simulating weld microstructures and producing consistent compositions, for isolating the effects of microalloying elements under low oxygen conditions, limitation were found when attempts were made to increase the oxygen levels. Addition of oxygen to the button via the purging gas or by using material containing higher oxygen contents, dramatically affected the composition of the material. Under these high oxygen content conditions, the carbon content in particular appeared to be influenced by the arcing time. In general the longer the arcing time the lower the carbon content produced in the button. This would probably reflect the removal of carbon from the weld pool by the formation of carbon monoxide bubbles, the reactions being:

$$2Fe+O \rightarrow 2FeO$$

$$FeO+C = Fe+CO.$$

The Si and Mn contents did not appear to be affected excessively and a limited number of specimens were produced with similar Si and Mn contents, but with carbon contents of

0.05%wt and 300 ppm of oxygen.

It is conventional to determine the cooling rate for a particular temperature range, which is usually taken as 800 to 500°C, because most of the transformation is said to occur within these limits. Using this criterion the arc melting technique adequately covered the arc welding cooling rate range. However when considering low oxygen content material it was clear that some transformations were not completed until well below 500°C, particularly at the faster cooling rates. It may have therefore been more appropriate to extend the temperature range for calculating the cooling rate to 300°C. The reasons for lower transformation temperatures will be discussed later.

It is also important to note that the cooling rates are effectively the average taken over this 800 to 500°C temperature range. During the major part of the transformation process the cooling rates may be considerably slower, as a result of the large evolution of latent heat. Taking for example the cooling curve for the base alloy with a cooling rate of 6°C/sec.(ΔT800-500), fig. 4.10, during transformation the actual cooling rate was less than 1 °C/sec. This slower effective cooling rate could influence the diffusion controlled processes and possibly promote precipitation, during transformation.

The cooling rate range of the arc melting technique employed ie. 2 to 60°C/sec. was limited compared to the reheating techniques used by other workers. The CCT diagrams produced using simulative reheating methods(8,12), usually cover cooling rates from 0.1 to 1000°C/sec. However only a

limited number of the tests used to construct these diagrams are relevant to arc welding. Therefore although the CCT diagrams produced in the current work only cover cooling rates in the range 2 to 60 °C/sec., this was appropriate for the arc welding processes and since more cooling curves were produced within this range, a more accurate assessment of microstructural development was possible.

5.1.1 THE INFLUENCE OF MICROALLOYING ELEMENTS AND COOLING RATE ON THE PRIOR AUSTENITE GRAIN SIZE OF SIMULATED AS-DEPOSITED WELD METAL.

The prior austenite grain size of as-deposited weld metal significantly affects the type and proportions of ferrite constituents, formed during transformation(3). Since the high nucleation energy of the grain boundaries favour heterogeneous nucleation, a finer prior austenite grain size and corresponding greater area available for nucleation, generally promotes PF (47). Increased transformation temperatures are also associated with finer prior austenite grain size and high proportions of PF(100).

The prior austenite grain size may be influenced by a number of factors, including:-

1. HAZ grain size.
2. Solidification structure.
3. The type and proportion of second phase particles.
4. Elements in solution.
5. The thermal cycle.

The initial solidification structure of low alloy steel weld metal may be either delta ferrite or austenite, depending on the composition. The phase diagram for the Fe-C

system indicates that alloys with carbon levels less than 0.5%wt solidify as delta ferrite, although this may be displaced to higher concentrations due to the high cooling rates associated with welding (22). It has been suggested that delta ferrite may nucleate heterogeneously on oxide, nitride or carbonitride particles, present within the molten pool, due to close lattice matching(29). The austenite which subsequently forms from this delta ferrite would be refined in comparison to alloys which solidified directly as austenite. However some workers(32,33) refute this heterogeneous nucleation mechanism, suggesting that most particles would be dissolved by the high temperatures of the weld pool. Widgery(4) also suggested that austenite could nucleate on delta ferrite boundaries ahead of the epitaxial growth front and the grain size would therefore not be influenced by the HAZ grain size.

Second phase particles and elements in solution may also influence the prior austenite grain size on subsequent cooling after solidification. Cochrane(35) found that weld metal with high oxygen content and corresponding inclusion population, had a refined grain size, when compared to low oxygen content weld metal. Second phase particles may pin the boundaries preventing migration and grain growth. It has also been suggested that elements in solution eg. Nb may also influence grain growth, by segregating to the prior austenite grain boundaries and preventing migration due to a "drag" mechanism(22).

Grain growth would also be influenced by the thermal cycle experienced by the weld metal. Weld metal with slow

cooling rates, would spend a much longer period of time above the grain coarsening temperature, than material with higher cooling rates. Therefore the period in which grain growth could occur would be greater and coarser grains would develop. This cannot normally be proved in the real weld metal because the heat input used to control the cooling rate, would also influence the HAZ grain size. Therefore whether grain refinement had occurred due to the thermal cycle experienced by the weld metal or the corresponding effect on HAZ grain size, could not be distinguished.

Examination of the simulated "as-deposited" alloys produced in the current work, revealed that in each case columnar prior austenite grains were formed, consistent with that observed in real weld metal. Grain size measurements were taken in the transverse direction, representing the shortest diffusional distance, fig. 4.14.

Considering the base alloy (series A), which contained no microalloying additions, the prior austenite grain size decreased gradually from 1.0mm at cooling rates <7°C/sec., to 0.5mm at rates greater than 40°C/sec., fig. 4.15a. The slower rates would equate to those found in SAW metal, while the faster rates would be more characteristic of TIG welding. The grain sizes observed would appear to be coarser than the characteristic grain size reported for weld metal ie.2-4ASTM(250-90μm). However this reported range would be for material of considerably higher oxygen content. The coarser grains observed in the low oxygen simulated "as-deposited" weld metal may therefore be consistent with Cochranes(37) observations that a coarser grain size was

produced in low oxygen weld metal, due to the absence of grain boundary pinning.

The refinement of the prior austenite grain size, with increasing cooling rate would be consistent with a reduced time period above the grain coarsening temperature, during which grain boundary migration could occur. This refinement with increasing cooling rate would reflect a similar trend to that found in real weld metal. Therefore the simulating technique used and the CCT diagrams produced, which reflect this refinement are more applicable to real as-deposited weld metal, than the CCT diagrams produced using reheating methods, in which a constant prior austenite grain size is used.

The effect of low and high microalloy additions on the prior austenite grain size are shown in figs. 4.15a to d. Since a degree of scatter is inevitable when determining grain size, upper and lower bounds are plotted on these graphs, to indicate any significant changes. From these graphs it can clearly be seen that the addition of V or Al, even at the higher concentrations examined, did not significantly influence the prior austenite grain size compared to the base alloy. With low additionsof Ti and Nb the grain sizes were also similar to those observed in the base alloy, ranging from 1.0mm at slow cooling rates to 0.5mm at the faster rates.

However the presence of high concentrations of Ti and Nb produced extensive grain refinement. The addition of 0.05%wt Nb to the alloy, resulted in a refinement in grain size to 0.5mm at cooling rates less than 7°C/sec. and 0.38mm at

rates greater than 40°C/sec., a refinement of 50% and 25% respectively, when compared to the base alloy. Addition of 0.06%wt Ti produced an even greater reduction in the grain size than seen in the Nb alloy. At slow cooling rates a grain size of 0.2mm was observed with no exentive refinement occurring with faster rates, a reduction of 80% and 50% compared to the base alloy. These changes were significantly greater than the scatter associated with grain size measurement and therefore can only be accounted for by the presence of these microalloying elements.

This grain refinement observed in the high Ti and Nb alloys may be accounted for by two mechanisms:-

1. Heterogeneous nucleation within the weld pool.
2. Pinning of grain boundaries during cooling.

Considering firstly the grain refinement observed with high Nb concentration. Nishio (29) suggested that carbides, nitride and carbonitrides of Nb were stable within the weld pool and could influence solidification, producing grain refinement via heterogeneous nucleation of delta ferrite. However austenite grain growth diagrams proposed by Easterling (22), suggested that for NbC particles complete dissolution would occur at approximately 1250°C, with heating rates less than 300°C/sec. The stability of NbCN and NbN particles were marginally higher than for NbC and therefore dissolution temperature would be higher. However with temperatures in the molten pool in excess of 1500°C, it is difficult to envisage these Nb type particles surviving. Thus heterogeneous nucleation, producing grain refinement in these alloys would not appear to be feasible.

Discounting grain refinement during solidification, in the high Nb alloy, would suggest that grain boundary migration during subsequent cooling must have been inhibited. This could occur due to pinning by second phase particles or due to "drag", as a result of segregation of Nb to the prior austenite boundaries. NbC precipitation occurs at approximately 900°C, although a specific cooling rate range is normally required for this process. Cooling rates in excess of 1 °C/sec.(ΔT1000-700 °C) are to fast for precipitation to occur, while with rates slower than 30 °C/min., precipitation could take place, but grain refinement may be limited due to particle coarsening. The cooling curves for the alloys studied, indicated that cooling rates, prior to transformation, were in excess of 30 °C/sec.(Δ T1000-700 °C) and therefore precipitation of Nb carbide/nitride particles was unlikely to occur.

Some workers (63) have suggested that oxide inclusions present in the material may act as sites for nucleation of precipitates and therefore formation could take place at the faster cooling rates present in weld metal. However this mechanism would not be applicable in the current work due to the low oxygen contents present. Therefore the most likely mechanism, to account for the grain refinement observed in the high Nb alloy, would appear to be that proposed by Easterling(22) for similar effects observed in the HAZ. This mechanism involves the segregation of Nb to the prior austenite grain boundaries, were it effectively inhibits migration as a result of a "drag" effect. This effect of Nb in producing grain refinement in "as-deposited" weld metal,

was consistent with work reported by Nishio(31), although the Nb content of 0.053%wt in the current work was higher than 0.03%wt used by Nishio. It is interesting to note that no refinement was observed with 0.02%wt Nb additions, suggesting that the concentration must reach a critical level for this to occur.

Unlike Nb, Ti is not reported to segregate significantly to the prior austenite grain boundaries. Which would suggest that the extensive grain refinement observed with additions of 0.06%wt Ti could not be attributed to the "drag" mechanism proposed for the Nb alloy. However calculations of Ti particle dissolution temperatures particularly for nitrides and carbo-nitrides(22), suggest that these particles may survive the high temperatures present in the molten material. These particles therefore could act as potent sites for the nucleation of delta ferrite, in a similar manner to that proposed by Ohashi(28) and Nishio(29). Calculation of the carbon equivalent for the 0.06% Ti alloy indicated a value of 0.382, which would suggest that the alloy would solidify as delta ferrite and therefore heterogeneous nucleation on second phase particles could occur. Since the oxygen content of the material was low, the refinement observed could not be attributed to titanium oxide inclusions, confirming that the refinement in the prior austenite was most likely to have occurred as a result of heterogeneous nucleation of delta ferrite, on titanium nitride/carbide particles. The presence of these second phase particles would also inhibit subsequent grain boundary migration during cooling.

The absence of austenite grain refinement in the V and Al alloys, would obviously indicate that the conditions required for refinement, were not present in these alloys. Since V and Al carbides, nitrides or carbonitrides have low stability and segregation to the austenite grain boundaries does not readily occur, this may be expected.

5.1.2 TRANSFORMATION OF LOW OXYGEN CONTENT "AS-DEPOSITED" WELD METAL.

5.1.2.1 Transformation Temperatures.

The effect of microalloying elements on the position of the CCT diagrams can be directly compared in figs. 4.44 to 4.47. As a general statement it can be said that the additions of the microalloying elements to the simulated "as-deposited" weld metal, depressed the transformation temperatures and displaced the phase fields of the CCT diagrams to longer times. These effects have been categorised using two parameters of the CCT diagrams:-

1. The transformation start temperature, (Ts).
2. The critical cooling rate, (Rc).

To ensure that Ts. was compared at similar cooling rates for each series, schematic cooling curves corresponding to fixed rates, were superimposed onto each CCT diagram, fig. 5.1. The cooling rates were determined for the commonly used 800 to 500 °C range, but since the Ts temperature would be influenced by the cooling rate prior to transformation, rates are also shown for the range 1500 to 600 °C. The cooling rates of these schematic cooling curves corresponded to 9, 14, 27, 32 and 43 °C/sec.(ΔT800-500 °C). However because these curves did not account for arrests due to

transformation, these rates would be higher than the real cooling rates measured. The effect of microalloying additions and cooling rate on the Ts. temperatures are indicated in figs. 5.2a to 5.2d.

The Ts. temperatures for all the alloys examined were influenced by the cooling rate. Increased cooling rate depressed Ts., although there was also a slight tendency to lower temperatures at very slow rates. This depression in Ts., with increased cooling rate is consistent with CCT diagrams produced for wrought steels and also with diagrams said to be applicable to as-deposited weld metal, produced using reheating techniques(12). The effect of cooling rates may be explained in terms of diffusion controlled nucleation. Transformation requires ferrite to nucleate and grow to a critical size, before the new phase is stable. This initial growth is diffusion controlled and is therefore dependent on the cooling rate. As the cooling rate increases, it becomes progressively more difficult for the new phase(embryo) to attain this critical size. Under these circumstances, further undercooling is required for smaller critical size embryos to become stable and grow, which in turn depresses the transformation temperature.

Since PF is the first phase to transform from austenite, it has been suggested that the Ts. temperature is determined by this process. Christensen(48) indicated that increased prior austenite grain size, reduced the proportion of PF and therefore reduced the transformation temperature. Inegaki(47) suggested that this was due to a reduced grain boundary area available for PF nucleation. Therefore factors

that affect prior austenite grain size may subsequently influence the Ts. temperature. This effect has been confirmed by some workers (60), although it has also been shown that material of completely different microstructure may have similar transformation temperatures(50). Therefore, although the prior austenite grain size is clearly significant, other factors which influence the growth of PF must also be considered.

Low concentrations of V and Ti depressed the Ts. temperature, although increases in concentration did not produce a further significant depression, figs. 5.2a and 5.2b. The most notable difference appeared to occur at intermediate cooling rates, ie.14-27 °C/sec.(ΔT800-500 °C), with only moderate disparities, compared to the base alloy, at slower and faster rates. During this intermediate cooling rate regime, the Ts. temperatures were depressed by upto 30 °C, for both the V and Ti microalloyed materials. In each case, the lower transformation temperatures coincided with a significant reduction in the proportion of PF, observed in the microstructures. This effect would be consistent with the proposal by Christensen(48), that the Ts temperature was influenced by PF nucleation and growth.

With higher V concentrations, the proportion of PF was marginally higher than for the low V alloy, although it was still significantly lower than the base alloy, which would account for the depressed transformation temperatures, when compared with the base alloy. In the high Ti alloy, a refinement in the prior austenite grain size resulted in an increase in the proportion of PF to 30%, compared with 20%

in the base alloy, at slower cooling rates, in agreement with the mechanism proposed by Inegaki(47). However the transformation temperatures were still depressed in comparison to the base alloy, suggesting that the addition of Ti was influencing the nucleation and growth of PF. This effect will be discussed fully in section 5.1.4, later.

With low Nb concentrations Ts. temperatures were similar to the base alloy at cooling rates <4°C/sec., although at higher rates they were consistently depressed by 20 to 30 °C., fig 5.2c. However with high Nb additions, although Ts. was depressed in comparison to the low Nb alloy at slow and fast cooling rates, higher temperatures were found at intermediate rates. This affect may again be related to refinement in the prior austenite grain size, observed in the high Nb alloy. Only marginal differences were observed in the proportions of PF in the low and high Nb alloy at these intermediate cooling rates. However the finer prior austenite grain size may have produce ferrite nucleation at a higher temperature, but subsequent growth may have been inhibited by the presence of Nb. The reduction in Ts. of the Nb alloys, in comparison to the base alloy, was consistent with the reduction in the proportion of grain boundary nucleated phases observed.

In the Al alloyed materials the transformation temperatures were markedly reduced in comparison to the base alloy, fig. 5.2d. Ts. temperatures were depressed by 12 to 42 °C in the low microalloy buttons for cooling rates up to 27 °C/sec.(ΔT800-500) and 65 °C at faster rates. With higher additions, reductions of 30 to 70 °C were observed at slow

and intermediate rates and 70 °C at the faster rates. These large reductions in the transformation temperatures again coincided with marked reduction in the proportion of PF in these alloy.

The reduction in transformation temperature with the addition of microalloying elements and the correlation with lower PF formation, would suggest that these elements were influencing the nucleation and growth of this phase. This effect indicates an increase in the degree of undercooling required for transformation and would be consistent with the higher hardenability produced by these microalloying elements. The importance of hardenability in transformation is further demostrated in the low carbon (0.05%wt) alloy, fig. 5.2e, in which the Ts. temperatures were increased by upto 60 °C, compared to the base alloy, which contained 0.15%wt carbon. This would again be consistent with the lower hardenability, produced as a result of the lower carbon content.

The transformation start temperatures determined in the current work were generally lower than those quoted by other workers. For example Harrison(9) quoted temperatures in the range 625 to 700 °C, for as-deposited weld metal, simulated using a reheating technique. However these lower transformation temperatures would be consistent with the lower oxygen content and resultant coarser prior astenite grain size of the alloys, which favoured lower PF formation, compared to those produced by Harrison et al. Limited work in which oxygen content of weld metal was reduced to low concentrations, indicated a corresponding reduction in

transformation temperatures to levels compatible to those found in the present work.

5.1.2.2 Critical Cooling Rates.

In the current context, the term "critical cooling rate" was taken to mean the rate below which AF was formed, rather than the rate above which martensitic transformation occurs. This definition was chosen because of the desirable properties attributable to the presence of AF in weld metal and therefore the requirements to ensure that cooling rates associated with the weld, were below this rate.

In the base alloy an Rc. of 40 °C/sec.(ΔT800-500 °C) was determined, fig. 5.3. The addition of microalloying elements, decreased Rc., indicating that slower rates were required for AF formation. The most significant change appeared to occur with the addition of low microalloy concentrations, fig. 5.3. Low concentrations of V, Ti, and Nb decreased the Rc. values by approximately 15 to 12 °C/sec., while higher concentrations produced a further 5 °C/sec. reduction, for the Ti and Nb alloys respectively. Additions of Al drastically reduced Rc. by 24 and 27 °C/sec., for the low and high concentrations respectively.

The reduction in Rc. values for the microalloyed materials corresponded with a general movement of the CCT diagrams to slower cooling rates and was indicative of retardation in the ferrite nucleation and growth processes. This movement to slower cooling rates is consistent with effects found in wrought materials and most of the CCT diagrams produced for as-deposited weld metal by the simulative reheating. An exception to this was a CCT diagram

by Harrison(16) which suggested that 0.02%wt Nb moved the CCT diagram to higher cooling rates. However the author suggested that this effect could have been due to adverse changes in the concentrations of other elements, which could have reduced hardenability. The dramatic effect of reduced hardenability on transformation kinetics is apparent in the CCT diagram produced for the low carbon content alloy, fig. 4.57, in which no Rc. value was apparent, because AF was formed even at the fastest cooling rates produced.

Cooling rate data for real as-deposited weld metal, is limited due to the difficulty involved in measurement. Work by Glover et al(10) showed that for a single pass bead on plate weldment, produced by SA welding, heat input from 0.74 to 10kJ/min. produced cooling rates from 68 to 3°C/sec.(Δ T800-500°C). No plate dimensions were given and the range of cooling rates was greater than normally found in SA welding processes. However they do indicate the effect of small changes in heat input on the weld cooling rate. For example a change in heat input from 2.4 to 1.3kJ/min., produced changes in the cooling rate from 21 to 41°C/sec. Applying this to the current work, would suggest that the heat input should be controlled accurately to ensure that the weld cooling rate is suitable for the optimum amount of AF to form. This would appear to be of particular importance with microalloyed weld metal, were heat inputs, which may have been suitable for plain C, Mn, Si welds, may produce low temperature transformation products as a result of the lower Rc. rates.

5.1.2.3 The Type And Proportions Of Ferrite Constituents.

Composite CCT diagrams showing the effect of each microalloying element on the position of the phase fields, together with prior austeninte grain size, the type and proportion of ferrite constituents and hardness, are shown in figs. 4.48 to 4.56. The effect of lower carbon content has also been indicated using a similar CCT diagram, fig. 4.57. The influence of microalloying elements on the ferrite constituents formed will be discussed with respect to specific cooling rate regimes classified as low, intermediate and fast rates. These classifications are defined as:

1. Low- less than 10 °C/sec.
2. Intermediate- 10 to 25 °C/sec.
3. High- greater than 25 °C/sec.

5.1.2.3a Base Alloy.

In the base alloy, at low cooling rates, high proportions of PF (22%) and FSP (26%) structures were formed, with AF comprising 50% of the microstructure, fig. 4.17. However further increases in cooling rate produced a marked reduction in PF and FSP formation to 12% and 3% respectively, fig. 4.21. The reduction in these grain boundary nucleated phases coincided with a large increase in AF content to 84%. At cooling rates approaching 18 °C/sec LF formation increased sharply and although PF and FSP constituents continued to decrease, there was also a corresponding fall in AF content. With increasing cooling rates above 20 °C/sec LF dominated the microstructure.

5.1.2.3b Vanadium.

Low V concentrations (0.027%wt) significantly reduced the proportions of PF and FSP structures formed, in comparison to the base alloy, fig. 4.17. At cooling rates below 10 °C/sec., only 7% PF and 4% FSP were observed, compared to 22% and 26% respectively, in the base alloy. The proportions of these grain boundary nucleated phases, decreased even further as the cooling rate increased, fig. 4.22. The reduction in PF and FSP, as a result of the V addition, coincided with a large increase in the proportion of AF. This effect was particularly notable at cooling rates below 12 °C/sec., with AF contents of 84% compared to 50% in the base alloy. However above 15 °C/sec. LF formation also increased sharply, which produced a corresponding fall in AF content. Above 16 °C /sec. the microstructure consisted of 60% LF, with no AF formation above the critical cooling rate of 18 °C/sec..

The proportions of PF and FSP were again reduced, by high V concentrations (0.088%wt), compared to the base alloy, fig. 4.17, but were marginally higher than in the low V alloy. This again coincided with increased AF formation at cooling rates lower than 10 °C/sec., with 71% observed as opposed to 50% in the base alloy. However there was also a marked increase in LF, which occurred at even lower cooling rates than in the low V alloy and consequently inhibited AF formation, fig. 4.23. The microstructure consisted of 60% LF at a cooling rate of 15 °C/sec., with no AF formation above 17 °C/sec.

The addition of V to the simulated low oxygen "as-

deposited" weld metal, even at low concentrations, would appear to have a profound influence on microstructural transformation. Of particular note was the affect of V in inhibiting PF and FSP nucleation and growth, which enhanced AF formation at slow cooling rates. However increased cooling rates and higher V levels promoted LF, which inhibited AF formation. Applying this to the typical cooling rate range for the SA welding process ie. 3 to 18 °C/sec, V additions would promote AF with high heat input or preheat, giving slow cooling rates. But with low heat input or thin plates, producing faster cooling rates, LF structures would be favoured. The increase in AF content observed was in good agreement with work carried out on SA weld metal by Kirkwood and Garland (80), using a basic flux and heat input of 3.3 kJ/mm. These conditions would give relatively low oxygen content conditions and a cooling rate of ≈3 °C/sec. and it was found that an addition of 0.032%wt V increased AF content from 47 to 73%.

5.1.2.3c Titanium.

At slow cooling rates (<6 °C/sec), low Ti concentrations marginally reduced the proportions of PF formed, but significantly inhibited FSP structures, reducing the proportions to <14%, compared to 26% in the base alloy, fig. 4.18. This decrease in the FSP content, coincided with an increase in AF, of 11%. With faster cooling rates the proportions of PF and FSP fell sharply compared to the base alloy, such that at 10 °C/sec. 85% AF was formed. However although the proportions of PF and FSP continued to fall with further increases in cooling rate, there was also a

corresponding rise in LF content, which prevented higher AF formation, fig. 4.24. Above 16 °C/sec. the microstructures consisted of 60% LF and no AF was observed at cooling rates higher than 18 °C/sec.

The proportion of PF increased sharply in the high Ti alloy at slow cooling rates, ie.30%, compared to 22% in the base and low Ti alloys, although FSP proportions were comparable with the latter, fig. 4.18. This increase in PF would be consistent with the refined prior austenite grain size observed in this alloy, increasing the grain boundary area available for PF nucleation. There was also a marked increase in LF formation even at the slowest cooling rates studied. The consequence of this increase in PF and LF, was a significant reduction in AF content to 35%, at cooling rates <10 °C/sec. Although the proportions of PF decreased at faster cooling rates, fig. 4.25, it still remained relatively high until close to the critical cooling rate at 14 °C/sec. This together with further increases in LF meant that AF formation was limited. Above 13 °C/sec. no AF was observed and the microstructures consisted primarily of LF, with the proportion of FC increasing at the faster cooling rates studied.

Therefore the effect of Ti on transformation appeared to depend critically on the concentrations present. AF formation was promoted with low Ti concentrations, at slow cooling rates, due to a reduction in FSP structures. However with high Ti concentrations there was a marked fall in AF, due to promotion of PF and LF structures. Applying this to SA welding, high heat input would favour AF microstructures,

if the weld metal contained 0.02%wt Ti, but the use of a similar heat input for 0.06%wt Ti weld metal eg. as a result of a higher Ti content in the plate, would form predominantly PF and LF structures.

The reported effects of Ti on weld metal microstructures are conflicting. Snyder(91) and early work by Widgery(52) suggested that Ti additions increase PF formation, particularly at high concentrations eg. 0.13%wt(91), which is consistent with the current work, although there was no mention of austenite grain refinement. Other workers (30,63,92) have noted increased AF and reduced PF with Ti additions. Using highly basic fluxes, which produced relatively low oxygen weld metal (<200ppm) and welding conditions giving cooling rates from 3 to 6 °C/sec., North et al(63) found that Ti contents up to 0.035%wt promoted AF formation, although no proportions were given. This again would be in good agreement with the current work.

5.1.2.3d Niobium.

Low Nb concentrations reduced the proportions of PF and FSP formed at slow cooling rates, by 5% and 15% respectively, which resulted in a higher AF content in the microstructures, ie.68% compared to 50% in the base alloy, fig. 4.19. Above 13 °C/sec. the proportion of grain boundary nucleated phases observed, fell sharply to <10%, although a corresponding increase in LF formation prevented a significant increase in AF, when compared with the base alloy. At cooling rates greater than 16 °C/sec., the microstructures consisted of 60% LF, with no AF formed above ~ 22 °C/sec., fig. 4.26.

The addition of 0.05%wt Nb to the simulated "as-deposited" weld metal, marginally increased the proportions of PF and FSP compared to the base alloy, but were significantly higher than in the low Nb alloy, fig. 4.19. Unlike the reduction in FSP seen previously in the high Ti alloy, at slow cooling rates, in this alloy the FSP content remained high ie.20% and therefore the proportions of AF were similar to that observed in the base alloy. Increased cooling rate again inhibited the formation of PF and FSP, with the proportions falling to <10% in total at 10 °C/sec. However above 6 °C/sec. there was also a large increase in the amount of LF formed, which produced a considerable reduction in AF, fig. 4.27. The microstructures consisted of 60% LF at a cooling rate of 16 °C/sec. and no AF formed above 20 °C/sec.

Therefore at slow cooling rates, low Nb concentrations inhibited PF and FSP, promoting an AF microstructure, but not to the same extent as seen with V and Ti additions. High concentrations of Nb inhibited AF, favouring PF and FSP at slow cooling rates and LF at higher rates. This increase in grain boundary nucleated phases at slow cooling rates, would again be consistent with the refinement in prior austenite grain size, observed in the high Nb alloy. Applying this to SA welding, with high heat input welding of plate of low Nb content, AF may be promoted. However a similar heat input applied to plate with a high Nb content, particularly if a high dilution technique were used eg. single pass weld, would produce a microstructure containing high proportions of PF and FSP, with lower AF contents. Low heat input

processes would generally favour the formation of LF microstructures, with very low AF content.

The reported effects of Nb on weld metal microstructures are again conflicting, with some workers(75,76,77) observing increases in FSP, while others(74,79) noted higher AF contents. In a review by Dolby(78), it was stated that Nb inhibited PF formation. Levine and Hill(75) found that 0.02%wt Nb additions to SA weld metal, produced using a basic flux and heat input of 2.4kJ/mm (10°C/sec.) promoted AF, which would be consistent with the present work. The reduction in PF observed with low Nb contents, was also in good agreement with Dolby(78). The refinement in prior austenite grain size and subsequent increase in PF and FSP in the high Nb alloy may be a characteristic of the low oxygen conditions. Previous studies have been directed towards weld metal of high oxygen content, which would favour a finer grain size and therefore addition of Nb may not produce further refinement.

5.1.2.3e Aluminium.

Low Al concentrations (0.024%wt) markedly reduced the proportions of PF and FSP phases formed at slow cooling rates, in comparison to the base alloy, fig. 4.20. This produced a marginal increase in AF to 60%, compared to 50% in the base alloy, the formation of AF being limited by the presence of 10% LF, even at these slow cooling rates. With increased cooling rate, although PF and FSP were reduced further, there was also a substantial increase in LF, which resulted in an overall decrease in AF formation, fig. 4.28, eg.50% compared to 80% in the base alloy at 15°C/sec. At

cooling rates of 16 °C/sec., the microstructures consisted of 60% LF, with no AF formation occurring above 17 °C/sec.

The effect of high Al concentrations (0.063%wt) on the formation of ferritic constituents, was substantial even compared to the low Al alloy, fig. 4.20. At slow cooling rates the proportions of PF and FSP were reduced to <20% in total, but there was also a marked increase in LF formation eg.30% at 4 °C/sec. This resulted in a sharp fall in AF content to <40%, compared with 60% and 50% in the low Al and base alloys respectively. With higher cooling rates LF proportions continued to increase, fig. 4.28. At a cooling rate of 13 °C/sec., the microstructure consisted of 60% LF and 36% AF, compared to AF contents of 83% and 56% in the base and low Al alloys respectively. No AF formed above the critical cooling rate of 14 °C/sec.

Therefore the general effect of Al additions, was to inhibit PF and FSP formation, while promoting LF. With low Al additions AF increased marginally at slow cooling rates, although at higher cooling rates and particularly with high Al concentration, increased LF formation inhibited AF. Therefore SA welding, of even low Al content plate at relatively high heat input, would favour microstructures with a high LF content.

Previous work studying the effect of Al on weld metal transformations, has generally considered the influence of oxide inclusion type, under relatively high oxygen content conditions. It has been suggested that Al oxide inclusions may nucleate AF(57). However in the low oxygen conditions studied in the current work Al oxide inclusions would not

form. The increases in LF formation observed in the current work would be consistent with results of investigations by Terashima and Hart(100), on SA weld metal using basic fluxes (<200ppm-oxygen content) and heat input of 4.4kJ/mm (≈5.5 °C/sec). They noted that Al additions of 0.038%wt promoted LF microstructures.

5.1.2.3f Carbon.

The reduction in C content significantly influenced the microstructures formed. At low cooling rates PF contents were 10% higher than in the base alloy, although FSP structures were reduced slightly and similar proportions of AF were formed, fig. 4.60. However PF,FSP and AF phases were observed throughout the cooling rate range studied, even at the highest rates ie.50 °C/sec., although the proportion of PF did fall to <10%, fig. 4.61. Significant amounts of LF ie.10%, only formed above 27 °C/sec., which increased to 20% at 50 °C/sec. This was compared with the base alloy, in which LF dominated the microstructures at cooling rates above 20 °C/sec. Therefore in SA welding of low C plate, although the weldability would be good, the microstructures would contain high proportions of PF and FSP phases, even with low heat input conditions.

Previously, it has been difficult to isolate the effect of C on weld metal microstructures, because changes in concentration were also associated with changes in other alloying elements(27). However Harrison(50) has recently suggested that increased C content may promote AF at the expense of PF and FSP, which would be consistent with the present work, for cooling rates in the range 7 to 16 °C/sec.

5.1.2.4 Microphases.

It has been suggested that the microphases present in weld metal are an important factor in determining weld metal toughness(18). The proportions of microphases determined for each microalloy addition, at a cooling rate of 7°C/sec., were compared with the base alloy. The effect of reduced carbon content was also examined.

The addition of each type of microalloy element, even at low concentrations, produced an increase in the microphase content, compared to the base alloy, fig 4.30 to 4.33. The microphases formed were predominantly of the dark etching type, characteristic of those describes as carbides, by Kirkwood(80). With high microalloy concentrations, particularly in the Ti,Nb and Al alloys, there was a further increase in microphase content and also an apparently higher proportion of light etching microphases, possibly of martensite(80). In these high microalloy materials, the microphases were also more lath like, with reduced average spacing between the phases. In all cases this second type of microphase became dominant with increased cooling rate. Reduced carbon content significantly reduced the volume fraction of microphases observed, fig. 4.62.

This effect of increased microphase content, has been noted previously for Nb and V additions to weld metal(80). Although there does not appear to be any available information on the influence of Ti or Al on microphase formation, it would be expected that since these elements increase hardenability, they would also favour increased microphase formation. The increased microphase content with

higher cooling rates, is consistent with work reported by Glover et al(10), of higher microphase contents with reduced heat input, in SA weld metal.

5.1.2.5 Ferrite Grain Size.

It is well established that ferrite grain size influences toughness, which by virtue of its fine grain size, is the reason for the requirement of high AF content in weld metal microstructures. The influence of low and high microalloy additions on AF grain size is shown in representative photomicrographs, figs. 4.35 to 4.38, for a cooling rate of approximately 4 °C/sec, in comparison to the base alloy.

Measurements of AF grain size, table 20 and fig. 5.4 revealed that the additions of each of the microalloying elements studied, even at low concentrations appeared to refine grain size. The average AF grain size determined for the base alloy was 30μm. Low concentrations of V and Nb reduced this grain size to 20μm, while Ti and Al were even more effective, with grain sizes of 14μm produced. Higher additions of these microalloying elements refined the grain size by a further 4μm in each case. With lower carbon contents the AF grain size coarsened to 41μm. The general grain size of the ferrite constituents were also refined by increased cooling rates, which can be seen by comparison of the photomicrographs shown for each series, figs. 4.21 to 4.29. The influence of Nb, V and C in refining the ferritic microstructure are consistent with previous reported effects of these alloying elements,(68,75).

5.1.3 THE INFLUENCE OF MICROALLOYING ELEMENTS AND COOLING RATE ON HARDNESS.

The hardness of a material is a useful parameter in characterising microstructures and may also give an indication of toughness ie. high hardness generally equates with high strength and low toughness, although this is not always the case. Vickers hardness tests were therefore carried to determine the effect of microalloy elements and cooling rate on hardness. In all cases the hardness increased with faster cooling rates, although the magnitude of this increase appeared to relate to the type of microalloy element present.

Considering the base alloy, fig 4.39, at rates below 10 °C/sec., the hardness was relativley constant at about 200 Hv. This generally equated to a cooling rate regime were the microstructure remained consistent, the proportions being approximately 22% PF, 28% FSP and 48% AF. Above this cooling rate the hardness increased to 210 Hv, with a corresponding increase in the proportions of AF and a sharp reduction in grain boundary nucleated phases. With further increases in cooling rate above 20 °C/sec., the hardness increased sharply to 250 Hv at 30 °C/sec, which could be related to a higher proportion of LF formed in the microstructures. With still higher cooling rates the hardness increased to 278 Hv at 50 °C/sec. Again this increases could be related to a gradual increase in FC phases within the LF dominated microstructure. Therefore the increase in hardness with cooling rate could be explained in terms of the change in the type and proportions of constituents present in the

microstructure, with high proportions of PF and FSP structures producing the lowest hardness and LF/FC structures giving the highest.

The trend of increasing hardness with higher cooling rate is again repeated with the addition of microalloying elements. However considering the often dramatic effects on the type and proportions of ferrite constituents produced by these microalloying additions, it might be expected that the hardnesses would have been similarly affected, but this was often not the case.

With V additions, at slow cooling rates the hardness was marginally higher, ie.212 Hv fig. 4.39, than the base alloy, which reflected the higher proportions of AF. As the cooling rate increased above 10 °C/sec. the hardness rose sharply in comparison to the base alloy which, could again be explained by a significant increase in LF constituents in the microstructures. Above 15 °C/sec.. the high V alloy possessed a higher hardness, which continued to increase at a higher rate than the low V alloy, this coincided with higher LF contents and increasing FC in the microstructures. A similar trend was observed with the low and high Al alloys, fig.4.42, although at cooling rates below 30 °C/sec. the hardnesses were lower than the V alloys, even though higher LF contents were found. This apparent contradiction would suggest that factors other than the major ferrite constituents may also be significant. This may relate to the proportion and types of microphases present, the relative grain size of the constituents or even the dislocation density. With the V alloys, although LF contents were lower

than the Al alloys, the grain size was significantly refined and the proportions of microphases appeared to be higher and also of the blocky lath martensite type. This could account for the higher hardnesses noted. Above 30 °C/sec. higher hardnesses were found in the Al alloys, reflecting the significant increase in FC phases.

High Ti additions produced the most significant increase in hardness for cooling rates < 10 °C/sec., ie 220 Hv compared to 200 Hv in the base alloy, fig 4.40. This was not truely reflected in the major microstructural constituents, in which PF formed a large proportion, although LF was also observed. However again there was a large increase in the microphase content and refinement in intragranular microstructure, which would account for the higher hardness. With low Ti additions, fig. 4.40, at slow cooling rates, although AF content was higher, the hardness was only marginally higher ie.3 Hv, however since there was no obvious influence on the microphase content, this might be expected. As cooling rates increased above 13 °C/sec. a sharp rise in hardness coincided with a significant rise in the proportions of LF found in the microstructures. At still faster cooling rates the hardness values appeared to plateau at approximately 300 and 284 Hv (50 °C/sec.) for the high and low Ti alloys, compared to 270 Hv for the base alloy, reflecting the higher proportions of FC constituents in each alloy. The lower hardnesses of the Ti alloys at these fast cooling rates compared to the V and Al alloys would also be consistent with the lower proportions of FC constituents observed.

The effect of Nb additions on hardness, fig. 4.41, follow a similar trend to that seen in the Ti alloys. With high Nb concentrations, although the proportions of PF and FSP were high, the hardness increased by 20 Hv compared to the base alloy. However, unlike the low Ti alloy, the alloy with low Nb concentrations showed an increase in hardness of 10 Hv. These increases in hardness again coincide with higher microphase contents and refined structures, particularly in the high Nb alloy. The hardness again increased at faster cooling rates as the proportion of LF in the microstructures increased, although this did not appear to be as significant as with the other microalloys. This may reflect the fact that AF was formed up to higher cooling rates and also the proportion of FC aggregate did not increase significantly.

Therefore the effect of microalloy elements on hardness can not always be explained in terms of the gross microstructure, but the type and proportion of microphases and grain refinement must be considered, particularly below the critical cooling rate for the alloy. With high additions of Ti and Nb, although higher proportions of PF and FSP were formed in the microstructures, compared to the low concentration of these alloys and similar amounts compared to the base alloy, the increase in the proportion of microphases and general refinement of the structure was sufficient to produced an overall increases in hardness. Similar increases in hardness have been reported for SA weld metal with 0.07 and 0.11 %wt Nb and V additions respectively at slow cooling rates ie. 5.5 °C/sec.(79)

5.1.4 MECHANISMS OF FERRITIC NUCLEATION AND GROWTH IN LOW OXYGEN CONTENT MICROALLOYED AS-DEPOSITED WELD METAL.

It has been shown that microalloying elements significantly affect ferritic transformation, influencing the types and proportions of ferrite constituents present in the microstructures and also the microphase content. However from examination of the relative effects of microalloying elements and cooling rate on the microstructural constituents produced, it is also possible to differentiate some of the mechanisms operating.

To review the conditions studied, the arc melted buttons were in the "as-deposited" state, with oxygen contents of approximately 10 ppm. and cooling rates in the range 3 to 60 °C/sec. The low oxygen contents were particularly significant, since under these conditions oxide inclusions population would be very low, if any, with any elements not in solution, present as carbide/nitride particles. Therefore mechanisms associated with nucleation on oxide inclusions may be discounted, although similar heterogeneous nucleation involving the other particles, can not be ruled out. The microalloying elements were also added individually at two levels of concentration, with no significant change in the other elements present. Therefore the effects on microstructure, could be directly attributable to the change in the microalloying element.

5.1.4.1 Grain boundary nucleated phases.

Mechanisms proposed to account for the effect of composition on PF and FSP formation have included refined prior austenite grain size(60), nucleation on oxide

inclusions at the austenite grain boundaries(35) and inhibition of PF growth, due to grain boundary drag by solute elements(22) or interphase precipitation(50). In the current work the mechanism associated with nucleation of PF on oxide inclusions can be dismissed, because of the low oxygen contents present.

Increased cooling rate in all cases reduced the proportions of PF and FSP observed in the microstuctures. Considering the base alloy in which no microalloying elements were present, this effect may be explained in terms of undercooling and diffusion of solute elements. At slow cooling rates, transformation temperatures were approximately 606°C, which was high for the "as-deposited" alloys studied. Nucleation and growth of PF would occur from the prior austenite boundaries behind a planar front, with solute elements redistributed ahead of this growth front, in a similar manner to that described by Rasanen and Tenkula(36). At these relatively slow cooling rates, some solute diffusion would occur into the austenite grain. However the cooling rates were obviously not slow enough to allow extensive PF growth, which would suggest that sufficient solute "build up" had occurred to produce a solute barrier, inhibiting further planar growth. Only separate ferrite needles would break though this solute barrier, resulting in formation of FSP structures. The FSP structures would then grow until undercooling was sufficient for the formation of AF or lower temperature transformation products.

With a faster cooling rate the transformation start

temperature was reduced. This was consistent with classical nucleation theory, in that a reduced time was available for diffusion, which therefore inhibited growth of the new phase. Therefore a higher degree of undercooling was required before PF could nucleate and grow. The faster cooling rates would also increase segregation at the PF growth front, as a result of reduced diffusion rate. This increased solute barrier would inhibit PF growth. The combination of lower transformation temperature and inhibited growth, would account for the reduction in the proportions of PF, observed at faster cooling rates. The reduction in FSP, at these faster cooling rates, would also suggest that undercooling was sufficient to allow intragranular AF nucleation, which inhibited FSP by a competetive growth process. Further rise in cooling rate would increase the degree of undercooling within the austenite grain, accounting for the higher proportions of LF and FC phases observed.

The addition of low concentrations of microalloying elements, in all cases, reduced the proportions of PF and FSP observed in the microstructures, with V and Al additions being particularly effective. In the V, Ti and Nb alloys there was a corresponding increase in the proportions of AF, although in the Al alloy, AF was inhibited by LF formation. With these low microalloy concentrations, the prior austenite grain size was similar to that observed in the base alloy and therefore any influence due to the grain boundary area available for nucleation, can be ruled out. Transformation temperatures were depressed, suggesting that

the microalloying elements increased the hardenability, which would be consistent with the effect of these elements in solution and in itself would reduce PF formation. However this reduction in the proportions of PF and FSP would also indicate that microalloying elements were inhibiting the growth of these phases and/or promoting AF formation, which would limit the growth of grain boundary phases by a competitive growth process.

This effect on PF formation could be consistent with the mechanisms proposed by Easterling(22) for a similar process observed in the HAZ, in which Nb and V segregation to the austenite-ferrite interface, in solution or as carbide or carbonitride precipitates(64), suppressed the growth of PF. This mechanism could equally well apply to Ti and Al, since they also readily form second phase particles. Examination of the cooling curves, also indicated that during transformation the latent heat evolved was sufficient to reduce the cooling rates significantly, to less than 1 °C/sec., which would be sufficient to favour precipitation of microalloy second phase particles. However the presence of these microalloying elements in solution, would also increase the the hardenability within the solute barrier ahead of the PF growth front, which would increase the effectiveness of this barrier in inhibiting PF growth and therefore could also account for the reduction in PF.

The presence of high levels of Ti and Nb further complicated the transformation process by refining the prior austenite grain size. The greater area available for PF nucleation was reflected in the microstructures, by a

significant increase in the proportion of this phase at slow cooling rates, compared to the alloys with low microalloy concentrations. The higher proportion of PF observed in the Ti alloy was consistent with the finer austenite grain size, compared to the Nb alloy. However the lower transformation temperatures found in these alloys, in comparison to the base alloy, would also indicate that the higher hardenability produced by the microalloying additions were still inhibiting grain boundary nucleation. But the increased grain boundary area available for nucleation offset this effect and therefore the proportions of PF increased.

5.1.4.2 Acicular Ferrite Formation.

A number of mechanisms have been proposed to account for AF formation, with heterogeneous nucleation on oxide inclusions being widely reported as an important factor. Ricks(13) suggested that oxide inclusions could act as a substrate for AF nucleation, with titanium and aluminium oxides being particularly associated with nucleation of this phase(58). But Barrite(60) has also pointed out that the population of inclusions present in weld metal was insufficient to account for the number of AF grains present and it was suggested that initial nucleation on oxide inclusions, was followed by sympathetic nucleation of further AF. However this may also indicate that inclusion site nucleation does not fully account for AF formation. Harrison(64) indicated that AF could nucleate on the dislocaion sub-structure, produced by differential thermal contraction between inclusions and the austenite matrix.

Changes in local chemistry around inclusions and the resultant reduction in hardenability could also be significant (56). It is further suggested by Abson(46), that under low oxygen content conditions AF formation would not occur, due to the absence of inclusions to act as nucleation sites. However, although experimental data for low oxygen content conditions is limited (8,63), AF formation was observed in this work. In the latter case the mechanism proposed suggested nucleation on titanium or vanadium nitride particles.

Of particular note in the current work was that, although the oxygen contents were to low for oxide inclusions to be present, AF was still formed, even in the base alloy. This would suggest that, AF formation does occur in low oxygen content conditions in the absence of a suitable oxide inclusion population, in contrast to Absons(46) suggestion. Harrisons(64) proposal that AF nucleated on the dislocation sub-structure associated with oxide inclusions, would also not explain the AF formation in the present work. However a general dislocation structure and vacancy clusters would still be present in the austenite and could provide sites for AF nucleation. Since AF formed in the base alloy it can also be assumed that microalloy particles are not a pre-requisite for nucleation. Therefore it can be suggested that AF can form, when a suitable combination of cooling rate and chemistry are achieved to inhibit PF and FSP formation, without increasing the hardenability to such an extent that LF is formed.

The addition of low concentrations of V, Ti and Nb did

increase the proportion of AF observed in the microstructures, within a specific cooling rate regime. From this it might be suggested that second phase particles associated with these elements provide sites for nucleation of AF, in a similar manner to that proposed by North et al.(63). This would infer that either these particles survive in the molten metal or precipitate during the cooling process. If cooling rates, prior to transformation, were less than 1 °C/sec. precipitation of Nb or Ti particles may occur in the austenite and since the transformation temperatures were low ie. 600 °C, V may also have precipitated in the austenite if the conditions were suitable. However it is well established that precipitation only occurs at these relatively slow cooling rates and would be inhibited by fast cooling rates present during welding and in the current work, prior to transformation. The mechanism proposed by North(63) to account for nitride particles in the weld metal ie. precipitation on oxide inclusions, would again not be feasible in the current work due to the low oxygen contents. Therefore it is unlikely that precipitation prior to transformation could have occurred and subsequently influenced AF formation.

Thermodynamic considerations indicate that Ti carbide/nitride particles are very stable at high temperatures and may survive in the molten metal(33). This was confirmed by evidence of austenite grain refinement with high Ti additions, although not with low concentrations. Therefore these Ti compound particles may have been present in the austenite and heterogeneous nucleation of AF cannot

be ruled out. As discussed in section 5.1.1, Nb and particularly V carbide/nitride particles are more likely to dissolve during the heating cycle, although it has been suggested that niobium carbonitride particles may survive, due to the fast heating and cooling rates associated with welding(33). Therefore it was unlikely that second phase particles associated with these latter elements, were present in the austenite prior to transformation, to influence AF formation by heterogeneous nucleation. However for each of these microalloying elements, increased AF content coincided with reduced proportion of PF and FSP phases. It may therefore be suggested that these elements inhibit growth of the grain boundary nucleated phases, allowing the interiors of the austenite grains to undercool sufficiently, to activate intragranular nucleation sites for AF formation.

With Al additions and high concentrations of V, although PF and FSP phases were still inhibited, there was an overall reduction in the proportions of AF. This reduction in AF was accompanied by a corresponding increase in the proportion of LF. This would indicate that while the microalloying elements were inhibiting nucleation and growth of grain boundary phases, there was also sufficient concentration remaining in solution in the austenite to increase hardenability. This increased hardenability within the grain, inhibited transformation from austenite to AF, thereby allowing undercooling to increase to such an extent that LF formation occurred.

High additions of Ti and Nb further complicate the

transformation process by refining the prior austenite grain size. This increased the proportion of grain boundary phases observed, as discussed in section 5.1.4.1. However the proportions of LF also increased, which resulted in a decrease in AF formation. This effect must reflect a significant increase in hardenability within the austenite grains, due to the higher microalloy content in solution, which was possibly supplemented by further element redistributed from PF. With higher hardenability, greater undercooling would be required for transformation to occur and therefore LF would be promoted.

It was also found that lower carbon content significantly influenced the microstructures, raising transformation temperatures and increasing the proportions of grain boundary nucleated constituents and AF, even at the fastest cooling rates studied, while reducing LF constituents to very low levels. This again would be consistent with the effect of reduced carbon content, decreasing the hardenability of the alloy and could also reflect a reduced solute barrier ahead of the PF planar growth front. This effect of carbon content on transformation, may also be used to explain some of the observed effects of changes in flux type, on the microstructures formed in SA weld metal. With a change from basic to acidic fluxes it is well documented that microstructures are dominated by PF and FSP constituents. It has been suggested by Cochrane et al (40), that the higher oxygen content associated with acidic fluxes increase the inclusion population, particularly at the prior austenite grain boundaries, which further enhances

heterogeneous nucleation of PF at these sites. However it is also well known that welds deposited under acidic fluxes, tend to have lower carbon contents. Therefore although inclusions may play a part, the reduced carbon content could also account for the observed microstructural changes.

5.1.4.3 Low Temperature Transformation Products.

The low temperature transformation products LF and FC were promoted by increased cooling rate and higher microalloy concentrations. This again would be consistent with higher hardenability and increased undercooling, inhibiting PF,FSP and AF formation. During cooling at slow rates transformation starts at the prior austenite grain boundaries and as the temperature decreases FSP growth occurs. However further reduction in temperature would allow transformation to start intragranularly, with AF formation. The relative amounts of these phases present in the final microstructure would depend on the competitive growth process. As discussed in section 5.1.4.1, increased cooling rate reduces the growth of the grain boundary phases, which initially favours higher AF contents. However at faster cooling rates, undercooling within the austenite grains would increase to a level at which LF formation could occur, before the AF reaction had gone to completion. This increase in undercooling with higher cooling rates would account for the increase in LF formation. Even higher degrees of undercooling would favour FC formations, which would again be consistent with the higher proportions of this phase observed in the microstuctures at higher cooling rates.

The addition of microalloying elements particularly at

high concentrations increased the proportions of LF, with large amounts observed even at slow cooling rates. This effect can again be explained by the microalloying elements increasing the hardenability of the austenite. This increased hardenability would inhibit transformation to AF, preventing completion of the AF reaction at slow cooling rates. Therefore regions which had not transformed to AF would undercool further and in turn transform to LF. The AF reaction would again be inhibited by faster cooling rates, accounting for the higher proportion of LF observed. A higher hardenability would also be consistent with the increased FC formation, observed in these alloys at the faster cooling rates.

5.1.4.4 Microphases And Ferrite Grain Size.

Microphases are formed during the final stage of transformation and therefore the austenite is rich in solute elements redistributed from the ferrite. These regions therefore have a high hardenability and transform to carbides or M-A constituents, depending on the cooling rate and local composition. The microphase content observed in the alloys studied, increased at higher cooling rates and also with additions of microalloying elements, particularly at high concentrations. This again would be consistent with higher hardenability and greater degree of undercooling produced by these conditions. In a similar way to that used to explain the effects of cooling rate on the major microstructural constituents, higher cooling rates would increase the degree of undercooling occurring before the ferrite reaction had gone to completion. Therefore more

austenite would remain untransformed when undercooling had reached a suitable level for the microphases to form, therefore the proportions would increase. High microalloy concentrations increased the proportions of microphases observed and also favoured the lath martensite type. This again would be consistent with the microalloying elements increasing hardenability and favouring lower temperature transformation.

The refinement in ferrite grain size observed with increasing cooling rate and also microalloying additions, is further evidence of the higher hardenability and increased undercooling, produced by these variables. As the level of undercooling in the austenite increases, the number of sites available for nucleation would also increase. Therefore, for example, more grains of AF would form and grow to mutual impingement, which effectively refinesthe grain size. Obviously the formation of lower temperature transformation products, produced as a result of undercooling, also effectively refines the grain size of phases formed at higher temperatures by competing for space within the structure. The higher hardenability produced by additions of microalloying elements, also allow increased undercooling, which would account for the refined ferrite grain size observed.

5.1.5 THE POTENTIAL INFLUENCE OF MICROALLOYING ELEMENTS ON THE TOUGHNESS OF LOW OXYGEN AS-DEPOSITED WELD METAL.

Although no direct testing was undertaken to determine the influence of the microalloying elements on mechanical properties, some general comments can be made. The toughness of weld metal is determined by the type and proportion of ferrite constituents, microphases, ferrite grain size and the inclusion population. The influence of microalloying elements may therefore be discussed in terms of the effect on these parameters. It will be assumed that weld metal microstructures containing a high proportion of AF, are required for an optimum combination of strength and toughness(71).

Due to poor interfacial bonding between certain inclusions and the matrix, microcracks can nucleate and an easy fracture path is provided, reducing material toughness. Also relative to impact fracture, inclusions may decrease the upper shelf and transition temperature. There is an increasing demand from fabricators to be able to produce lower oxygen content weld metal, with a corresponding low inclusion population. This has prompted the development of basic fluxes. Therefore weld metal produced with similar oxygen contents to those of the arc melted buttons studied in the present work, would be expected to have a high toughness. However, as already discussed, the effect of these low oxygen contents on microstructural features other than inclusions, must also be considered.

At cooling rates, below 10 °C/sec., in the base alloy containing no microalloying elements, high proportions of PF

and FSP structures were observed, with less than 50% AF present. However with higher cooling rates the AF content increased to >85%. This increase in the proportion of AF, together with the refined grain size observed at these faster rates, would favour relatively high toughness. But further increases in cooling rates substantially raised the proportions of LF observed. From this it may be inferred that the welding parameters used which influence cooling rate, ie.heat input, plate size, pre-heat etc., must be optimised to produce high toughness, with too slow or too fast cooling rates having a deleterious effect on weld toughness.

Low concentrations of V, Ti and Nb reduced the proportions of PF and FSP, formed in the microstructure at slow cooling rates (<10 °C/sec.). This resulted in an increase in the proportions of AF and also a refinement in the ferrite grain size. This improved microstructure would favour increased toughness, although the higher proportions of microphases also observed, may prevent the full potential from being realised. This increase in AF content was particularly noticable with low concentrations of V and would be consistant with workers(83,84,85) who reported increases in toughness at concentrations less than 0.04%wt. With Ti and Nb additions the increase in AF contents were smaller and would more likely be outweighed, by the corresponding increases noted in the microphase contents. Therefore with these alloys, the cooling rate would have a critical influence on the toughness, with higher rates favouring higher M-A content, which would eventually

outweigh the beneficial microstructural changes. This may account for the apparent contradiction in the effect on toughness, reported with additions of these microalloying elements. With the addition of low concentrations of Al, although the proportions of AF increased there was also a substantially higher proportion of LF observed in the microstuctures, even at slow cooling rates. This, together with the increased microphase content observed, would be deleterious to weld toughness and would also be consistent with observations by Hannerz(84), of reduced toughness in SA weld metal produced with basic fluxes.

High concentrations of microalloying elements reduced the proportions of AF, throughout the cooling rate range. In all cases the microalloying elements favoured higher proportions of LF, FC and microphases and the refinement in prior austenite grain size in the Ti and Nb alloys, also promoted PF and FSP phases at slower cooling rates. Therefore high microalloy concentrations would generally be particularly detrimental to toughness. This would be consistent with most of the work reporting the detrimental influence of high levels of these microalloying elements on weld metal toughness.

5.2 THE INFLUENCE OF OXYGEN CONTENT ON AS-DEPOSITED WELD METAL MICROSTRUCTURE.

A number of tests were conducted using the arc melting technique to determine the effect of higher oxygen content on the as-deposited microstructures. The prior austenite grain size was refined to 90μm with an increase in oxygen content to 300ppm, compared to 800μm in the low oxygen

alloy, fig. 4.58. This effect would be consistent with oxide inclusions pinning the prior austenite grain boundaries preventing growth, as proposed by a number of workers(35,60,61), although in contrast with Harrison(50), who suggested that oxygen content did not influence austenite grain size.

The increased grain boundary area available for nucleation, subsequently raised the proportions of PF observed in the microstructures to 52%, compared with 28% in the low oxygen alloy, at similar cooling rates, fig. 4.58, although the FSP content were marginally reduced. This reduction in FSP may be accounted for by reduced solute "build up" at the PF planar growth front, due to the reduced carbon content and a general reduction in alloying, as a result of manganese and silicon being present in oxide inclusions rather than in solution. In fact although the reduction in prior austenite grain size was obviously a major factor in promoting PF and increasing transformation temperature, the reduction in hardenability of the material, as a result of the lower alloy concentration, could also contribute to this effect.

The increase in grain boundary nucleation, reduced the amount of material remaining for transformation within the grains and therefore there was a corresponding reduction in the proportion of intragranular nucleation, with AF reduced by 20% compared to series J. There was no evidence of increased intragranular nucleation on inclusions, which might be expected since the inclusions would be of the manganese silicate type, rather than those said to be

normally associated with AF formation ie. titanium or aluminium based (64).

5.3 SIMULATED REHEATED WELD METAL.

In many commercial fabrications, up to 90% of the weld metal may be reheated, due to the multi-run weld techniques employed. The microstructures produced will therefore be influenced by these subsequently imposed weld thermal cycles. The thermal cycle experienced is dependent on the proximity of the material, to the heat source of the following weld runs. The closer the material is to the heat source, the higher the peak temperature experienced and corresponding effect on prior austenite grain size and segregation of alloying elements.

It has been shown in the previous sections that microalloying elements significantly influence the microstructures formed in "as-deposited" weld metal. It might be expected that similar effects may be observed on the transformation processes in reheated weld metal. However a systematic study of the influence of changes in these variables, on the ferritic microstructural develpoment in reheated weld metal, has previously received little attention.

The specimens used were machined from the arc melted buttons and were therefore of identical composition, consisting of a base C, Mn, Si alloy with low and high concentrations of V, Ti, Nb, Al and low oxygen contents, table 9. Allowing a direct comparison to be made between the reheated and "as-deposited" alloys. As with the "as-deposited" material, for the V, Ti and Nb series the only

significant differences in compositions were those of the microalloy elements, although with the Al series the carbon contents were again marginally higher than the base alloy. This therefore allowed the effects of these microalloying additions, on the reheated microstructures, to be isolated without ambiguity.

The thermal cycle used was that associated with the coarse grained region of reheated weld metal, adjacent to the final weld run. The peak temperature determined for this region was 1350°C. Simulated specimens subjected to a similar thermal cycle, were found to have comparible microstructures to this region. Suggesting that the technique used was a useful approach for simulating reheated weld metal.

In the following section the influence of microalloying elements on reheated materials will be discussed in terms of the effects on prior austenite grains size, the position of the CCT diagrams, types and proportions of ferrite constituents and microphases and also hardness. A comparison will also be made between these effects and those observed in the "as-deposited" alloys.

5.3.1 THE INFLUENCE OF MICROALLOYING ELEMENTS AND COOLING RATE ON THE MICROSTRUCTURE AND TRANSFORMATION KINETICS OF REHEATED WELD METAL.

5.3.1.1 Reheated Prior Austenite grain Size.

The prior austenite grains produced on reheating were equi-axed and significantly finer than those observed in the "as-deposited" material. This refinement in prior austenite grain size was consistent with observation in real weld metal, by Evans(69) and Rodrigues(49) There were no

significant differences in prior austenite grain sizes between the base and low microalloy reheated material, ie. 80μm, although some refinement was again observed with high additions of Ti and Nb. However the refinement observed with these elements was marginal compared to that seen in the corresponding "as-deposited" alloys. Since the prior austenite grain sizes were generally consistent, except for the marginal effects observed with Ti and Nb, it may be suggested that the microalloy elements have no obvious influence on the grain coarsening process in reheated material.

The fineness of the reheated austenite grain size, compared to that observed in the "as-deposited" alloys, would be indicative of the number of sites avaialable for austenite nucleation and the differences in peak temperatures involved. In the reheated material a large number of austenite nucleation sites were available at ferrite boundaries. Therefore extensive nucleation would take place, with the austenite grains growing to mutual impingement on heating. For grain growth to occur, boundary migration has to take place and grains with more sides begin to "swallow" grains with less sides (22). Temperature is the driving force for this process, but because of the fast heating and relatively fast cooling rates employed, the time period above the grain coarsening temperature would be limited, thus preventing extensive growth. With "as-deposited" materials the number of nucleation sites available for austenite formation were more limited and therefore impedence of boundary migration by mutual

impingement, would be less likely to occur. This, together with the higher peak temperatures, would provide a much greater driving force for grain growth and account for the coarser austenite grain size observed in the "as-deposited" alloys, compared to the reheated materials. Because of the inherent finer grain size of the reheated alloys, mechanisms influencing grain growth would also be less apparent. This may explain the marginal influence observed for high Ti and Nb concentrations on the reheated grain size, when compared to significant effects produced by these elements in the "as-deposited" material.

In a similar manner to that seen in the "as-deposited" material the grain size was also refined with increasing cooling rate, although the effect was again marginal in the reheated alloys. However this would again reflect the limited time period for grain coarsening as the cooling rates increased.

5.3.1.2 The Position Of The Reheated CCT Diagrams.

The influence of microalloying additions on the transformation of the reheated alloys, together with the type and proportions of ferrite constituents and hardness, are shown in the composite CCT diagrams, figs. 4.101 to 4.108. The CCT diagrams are directly compared with the reheated base alloy in figs. 4.97 to 4.100. Generally the addition of microalloying elements depressed transformation temperatures, but the effect on the positions of the phase fields in relation to the cooling rates were less clear.

To directly compare the influence of the microalloying additions on the transformation start temperature, schematic

cooling curves corresponding to cooling rates between 3.7 and 44 °C/sec. (ΔT800-500 °C) were superimposed onto each of the CCT diagrams, in a similar manner to that described for "as-deposited" alloys in section 5.1.2. the transformation start temperatures for each of the reheated alloys at these cooling rates are shown in fig. 5.5.

Considering the base alloy (series DA), the transformation start tempertatures were consistently higher than those determined for the "as-deposited" material of similar composition (series A), fig.5.2, eg. 671 and 605 °C at a cooling rate of 6.1 °C/sec. respectively. This would be consistent with the finer prior austenite grain size of the reheated alloy, increasing the grain boundary area available for PF nucleation and growth, therfore raising transformation temperatures. This mechanism was confirmed by the the substantial increase in PF constituents observed in this alloy compared to the "as-deposited" alloy, fig.4.81.

Comparing transformation temperatures in the reheated microalloyed materials, fig. 5.5, with there respective "as-deposited" alloys, fig. 5.2, for cooling rates <20 °C/sec., it can be seen that the start temperatures were approximately 20 °C higher. The reheated alloys had a significantly finer prior austenite grain size and much higher PF contents, particularly in the low microlloyed materials, which would again be consistent with the higher transformation temperatures determined.

In the reheated alloys, even with low microalloy additions, there was a substantial decrease in the transformation start temperature(Ts.), when compared to the

reheated base alloy, fig. 5.5a to d. Although there were some differences between individual microalloy elements, at various cooling rates, in general, the Ts. temperatures were depressed by upto 55 °C. In all the reheated alloys, containing low microalloy concentrations, with the exception of Nb, there was a sigificant reduction in PF formation compared to the base alloy, which may account for the lower transformation temperatures. However, with higher concentrations of the microalloying elements, although in most cases there was a further reduction in PF formation, the transformation temperatures were relatively similar to those found in the low microalloy materials. For this reason high proportions of PF were not always indicative of higher transformation temperatures. The exception to this was with the high Ti alloy, in which the Ts. tempertature was depressed by a further 15 °C, which was again consistent with a sharp reduction in the proportions of grain boundary nucleated phases. These effects would confirm that the presence of these microalloying elements, were influencing the nucleation and grow of PF, in a similar manner to that seen in the "as-deposited" materials.

Generally low microalloying concentrations did not significantly influence the critical cooling rates for PF and FSP formation, although the rate for AF was reduced, fig. 5.6. This reduction in the critical cooling rate for AF formation depended on the microalloying element, with Ti being particularly effective, reducing the rate to less than 18 °C/sec., compared to 35 °C/sec in the base alloy. With higher concentrations of microalloying elements, the

critical cooling rates for PF,FSP and AF formation were also reduced, fig. 5.6, with the influence on the grain boundary nucleated phases being most significant. The addition of high Ti concentrations again appeared to be most potent, in reducing the critical rate for PF and FSP formation.

Comparision of the relative position of the reheated CCT diagrams with those produced for the "as-deposited" material, indicated that the critical cooling rates for PF and FSP formation, were usually significantly lower in the latter. This again would be consistent with the finer prior austenite grain size of the reheated alloys, favouring grain boundary nucleation and growth and therefore moving the CCT diagrams to faster times.

5.3.1.3 The Type And Proportion Of Ferrite Constituents And Microphases.

The influence of microalloying elements on the type and proportion of ferrite constituents formed in the reheated alloys, with increasing cooling rate are shown in figs. 4.77 to 4.80 and in representative photomicrographs, figs. 4.81 to 4.88. Comparing these diagrams with those for their respective "as-deposited" alloys, figs. 4.44 to 4.47 indicates the effects of the reheating process on the microstructures produced.

In the reheated base alloy (series DA), it was found that the reheating process considerably increased the proportion of PF, fig. 4.77, compared to that observed in the equivalent "as-deposited" alloy, fig. 4.17. This may be demonstrated by comparing the PF content at 5°C/sec, which were 44% and 21% for the reheated and "as-deposited" alloys

respectively. These considerably higher PF contents were formed for cooling rates up to 28 °C/sec., decreasing above this rate until no PF formation occurred above 35 °C/sec.. In the "as-deposited" alloy PF formation ceased above 28 °C/sec. For cooling rates above 8 °C/sec. the proportion of FSP constituents was also considerably higher, ie. 25% and 10%, for the reheated and "as-deposited" alloys respectively. This increase in the nucleation and growth of grain boundary nucleated phases, reflected the significant refinement in the prior austenite grain size. The proposed mechanism is that described previously for the "as-deposited" alloys, in that increased grain boundary area favours higher PF nucleation. This increase in PF on reheating has been noted by some workers(69), although others(49) have observed higher FSP contents. An increase in the formation of grain boundary phases was observed in all the reheated alloys, compared to their respective "as-deposited" equivalents and reflected a refinement in the prior austenite grain size in all cases.

Additions of microalloying elements, in the reheated materials, revealed that low and high concentrations produced a significant reduction in the proportion of PF, when compared with the base alloy. Low V,Ti and Al additions, generally reduced the PF contents by upto 23%, fig. 4.77, 4.78 and 4.80, with Ti being most effective. With low Nb concentration there was a marginal reduction in PF contents at slow cooling rates, but above 14 °C/sec. the proportions fell to approximately 6%, compared to 34% in the base alloy, fig. 4.79. Higher concentrations of each of the

microalloying elements reduced the proportions of PF still further. High additions of Ti appeared to be particularly potent in reducing the PF content, which was reduced to <10% above 5°C/sec. and was not formed at cooling rates greater than 16°C/sec. With other microalloying elements the reductions were less dramatic, compared with low concentrations. These effects would appear to confirm the observation made in the "as-deposited" alloys, that microalloying elements significantly retard the nucleation and growth of PF, even though the prior austenite grain size was considerably finer.

The influence of microalloying additions on the formation of FSP constituents appeared to depend on the elements and concentrations involved. With low V, Ti and Nb levels the proportions of FSP were increased, particularly at slow cooling rates, although with Al there did not appear to be any significant effect. With higher concentrations of Al and particularly Ti, the FSP contents were markedly reduced, compared to the base alloy, with <13% being observed in the Ti alloy at 5°C/sec., compared to 29% in the base alloy. Additions of high concentrations of V and Nb did not significantly influence the FSP contents, at slower cooling rates, although the proportions were reduced at faster rates.

However it must be noted that no increase in the proportions of FSP were observed with low concentrations of these microalloying elements, in the "as-deposited" alloys, which at first site might seem anomalous. But this effect may be explained in terms of the influence of the finer

austenite grain size, on the redistribution of solute elements and the higher transformation temperatures present, in the reheated alloys. The finer prior austenite grain size of the reheated alloys favoured significantly higher PF development, compared to the "as-deposited" alloys, with consequently higher solute redistribution. Therefore a solute barrier would develop more readily in the reheated alloys, encouraging FSP structures to form, by the mechanism proposed by Rasenen(36), section 5.1.4. Also in the reheated alloys the transformation temperatures were higher and therefore once FSP stuctures had formed, a greater time period would be available for growth, before the grain interiors had undercooled sufficiently for intragranular nucleation to occur. Thus a combination of greater redistribution of solute elements and higher transformation temperatures, would account for the increased proportions of FSP structures, observed in the low microalloyed reheated materials. The reduction in FSP, with higher microalloy concentrations, would suggest that intragranular nucleation and growth processes were inhibiting FSP growth.

Intragranular nucleation and growth processes were also significantly influenced by microalloying addition in the reheated alloys. In general the proportions of AF were reduced by low and high concentrations of all the microalloying elements studied, with <16% observed at slow cooling rates compared to 21 % in the base alloy. However the most significant reduction in AF content was that produced by the reheating process itself. Comparing any of the reheated alloys with their respective "as-deposited"

equivalent, revealed that AF contents were reduced by 50-60%, particularly in some of the low microalloyed materials.

Low and high concentrations of microalloying elements, also significantly increased the proportions of LF observed in the reheated alloys, even at the slower cooling rates studied. For example with low microalloy concentrations, 17 to 25% LF was observed at a cooling rate of 10 °C/sec., compared to <2% in the base alloy, with contents increasing sharply above this rate. With higher microalloy concentrations the LF contents increased still further, particularly in the Ti alloy, were 67% LF was formed at 10 °C/sec. The proportions of LF were generally significantly higher than those observed in the "as-deposited" alloys, at the slower cooling rates. However in the reheated alloys, the critical cooling rates for PF and FSP, were much higher than those observed in the "as-deposited" alloys and therefore these phases were formed at significantly higher cooling rates. These higher PF and FSP contents in the reheated alloys, restricted intragranular LF formation at these higher cooling rates and therefore the proportions of LF were reduced in comparison to the "as-deposited" alloys.

Increasing the cooling rates generally had the effect of reducing the proportions of PF, FSP and AF phases, while increasing the amount of LF and FC constituents, observed in the microstructures. This would be consistent with the higher degrees of undercooling present, with increasing cooling rate favouring lower temperature transformations products, in a similar way to that seen in the "as-deposited" alloys.

The influence of microalloying elements on the proportions of microphases in the reheated alloys, are shown in figs. 4.89 to 4.92. In the base alloy the microphases colonies were large. With microalloy additions, although the proportions of microphases appeared to be greater, particularly with the higher microalloy contents, the colony size was much smaller. This difference in the microphase colony size would probably reflect the variation in ferrite grain size between the alloys.

5.3.2 HARDNESS OF SIMULATED REHEATED WELD METAL.

The hardness values determined for the base and low microalloyed simulated reheated weld metal, figs 4.93 to 4.96, were lower than their corresponding "as-deposited" alloys, figs. 4.39 to 4.42., reflecting the significant increase in the proportion of PF and FSP phases formed, particularly at slower cooling rates. With high microalloy content and increased cooling rate the hardness increased, which in a similar manner to the "as-deposited" alloys, was associated with higher LF and FC contents.

5.3.3 TOUGHNESS OF REHEATED WELD METAL.

With similar arguements to those used when discussing the "as-deposited" alloys, the influence of microalloying elements, cooling rate and the reheating process itself, on the potential toughness may be inferred from the microstructures observed. The absence of an oxide inclusion population, would again suggest that the reheated material was likely to exhibit good toughness. However assumming that a high proportion of AF was again beneficial, it would appear that the microstructures produced in the reheated

weld metal, would in general be detrimental to weld toughness. In all cases, including the base alloy, the proportions of AF were markedly reduced, as a result of significant increases in the proportions of PF,FSP and LF phases, compared to the "as-deposited" alloys. Suggesting that the reheating process in itself would be detrimental to toughness.

Additions of microalloying elements appeared to aggravate this problem by reducing the proportions of AF still further, while increasing the formation of LF phases. However in practice other factors must also be considered when assessing the effect of reheating on the properties of weld metal. Generally the use of multi-run techniques would reduce the residual stresses present in the weld metal, which would be beneficial to the weld properties.

5.4 DEVELOPMENT OF FERRITIC WELD MICROSTRUCTURE UNDER LOW OXYGEN CONDITIONS.

In the previous sections it has been shown that the composition (in terms of the microalloy concentration), cooling rate and prior austenite grain size significantly affect the development of the ferrite microstructure in both "as-deposited" and reheated weld metal. It is clear that the mechanisms involved are complex and interactive. However in general the effects observed can be explained using a similar model to that described by Harrison(50). In this model it is suggested that composition, cooling rate and austenite grain size may be related to the microstructural development, in terms of their influence on undercooling. The vector diagram proposed by Harrison is shown in

fig. 2.11. In the following section a general model describing the effect of these parameters on microstructural development will be proposed, with examples from the previous sections used to substantiate this.

5.4.1 THE INFLUENCE OF PRIOR AUSTENITE GRAIN SIZE.

Schematic diagrams showing microstructural development in a plain carbon steel weld metal with coarse and fine austenite grains sizes, cooled at similar rates are shown in fig. 5.7. The austenite grain size directly affects the grain boundary area available for PF nucleation and therefore a larger proportion of PF would be expected in the finer austenite grained alloy. On continuous cooling, transformation would initially begin with the nucleation of PF at the austenite grain boundaries. In the alloy with the finer grain size transformation starts at a higher temperature and a high proportion of PF would be formed. FSP needles develop when the solute barrier ahead of the ferrite growth front reaches a critical level to prevent further PF growth. This level would depend on the concentration and type of alloying elements within the barrier and their influence on hardenability. In the coarse grained austenite alloy, a lower initial transformation temperature, together with less redistribution of solute elements would suggest that FSP formation would also occur at a lower temperature, compared to the finer grained alloy. On further cooling FSP growth would take place, until the grain interiors had undercooled sufficiently for intragranular nucleation.

In the fine grained austenite alloy, redistribution of

alloying elements within the austenite would be significant, increasing the hardenability and consequently the undercooling required for intragranular transformation to take place. The lower alloy redistribution in the coarse grained material would suggest that a lower degree of undercooling would be necessary for intragranular transformation and therefore this may occur at an earlier stage in the transformation process, compared to the fine grained material. The consequence of the higher transformation temperature and greater hardenability within the austenite, in the fine grained alloy, is that the period for FSP growth is significantly longer, compared to the coarse grained alloy and therefore the proportion formed would be much higher.

Intragranular microstructural development, would also be influenced by the effective difference required in undercooling, between the fine and coarse grained alloys. On further cooling the higher intragranular transformation temperature of the coarse grained alloy would favour AF formation, while the higher degree of undercooling required by the fine grained alloy may promote the lower temperature transformation products, LF and FC. The proportion of LF formed would depend upon the hardenability and cooling rate. Therefore in general for weld metal of similar composition, a cooling rate that favoured high proportions of AF in a coarse austenite grained material, would in a fined grained material cooled at an identical rate, form PF,FSP and possibly LF dominated microstructures.

Evidence for the operation of this proposed mechanism,

accounting for the effect of prior austenite grain size, can be seen by a comparison between the microstructurse formed in the "as-deposited" and reheated base alloys, figs. 4.17 and 4.77. For example, at a cooling rate corresponding to 10 °C/sec., the coarser grain size of the "as-deposited" alloy produced a transformation temperature of 600 °C and a microstructure of 14,10 and 76% PF,FSP and AF respectively. While in the reheated alloy of identical composition and cooling rate, but with a significantly finer austenite grain size, the transformation temperature was 660 °C and the microstructure formed consisted of 35,28 and 33% PF,FSP and AF respectively. At this cooling rate it would appear that intragranular undercooling was not sufficient to form LF in either of the alloys.

5.4.2 THE INFLUENCE OF COOLING RATE.

The influence of cooling rate on microstructural development in weld metal, of identical composition and prior austenite grain size is shown schematically in fig. 5.8. The cooling rate directly influences the diffusional processes within the alloy and consequently the nucleation and growth processes, as described previously. Faster cooling rates depress the transformation temperatures, increasing the degree of undercooling.

On transformation redistribution of alloying elements would occur ahead of the PF growth front as described in the previous section, but the extent of the solute barrier would be influenced by the cooling rate. At slow cooling rates these solute elements would diffuse away from the PF growth front and therefore solute "build-up" would be limited and

PF may continue to grow. However as the cooling rate increases the diffusion rate would be reduced and the solute concentration at the PF growth front would increase, eventually reaching a critical level of hardenability to inhibit PF growth. The faster the cooling rate the quicker the solute barrier would develop, to inhibit PF growth. Therefore a combination of reduced transformation temperature and growth, would limit PF formation, as the cooling rate increased.

The proportion of FSP formed would depend on the time period available for growth, prior to intragranular nucleation. If FSP forms at a sufficiently high transformation temperature, a long time period may be available, before the grain interiors had undercooled sufficiently for intragranular nucleation to occur. Under these circumstances a high proportion of FSP may form. However with low transformation temperatures, only a small further degree of undercooling may be required for intragranular nucleation and therefore FSP growth would also be limited. Increased cooling rate, would increase the degree of undercooling required for intragranular nucleation, but it would also increase the rate at which this was achieved. Therefore the reduced formation temperature for FSP, together with the higher intragranular nucleation, with increasing cooling rate would generally reduce FSP formation, while increasing the formation of AF or LF and FC phases. The increased degree of undercooling, required with increasing cooling rate, would also favour higher proportions of LF and FC aggregate phases, as opposed

to AF. Therefore in general slow cooling rates would favour PF and FSP phases, while with increasing rates the proportions of grain boundary nucleated phases would be reduced, in favour of AF and at faster rates LF/FC structures.

The influence of cooling rate on the microstructures formed in the "as-deposited" base alloy, fig. 4.17,can be used as an example to show the application of this mechanism to the alloys studied. For cooling rates upto 7°C/sec. the microstructures consisted of 21,27 and 50% PF,FSP and AF. With increasing cooling rate eg.13°C/sec. the proportions of PF and FSP were reduced to 14% and 7% respectively, while the AF content increased to 78%. With still higher cooling rates eg. 25°C/sec. the proportions of PF,FSP and AF were reduced to less than 23% in total, whereas LF formation increased to 66%. This development in the ferritic microstructure, from high proportions of PF/FSP phases at slow cooling rates and microstructures dominated by AF at intermediate rates, to LF microstructures at fast cooling rates, would be consistent with the proposed mechanism.

5.4.3 MICROALLOYING ELEMENTS.

When considering transformation in microalloyed steel weld metal, the basic mechanisms proposed for the effects of prior austenite grain size and cooling rate would still apply, but would be further influenced by the microalloy element present and its concentration. The presence of microalloying elements in the "as-deposited" and reheated alloys have been found to influence:-

1. The prior austenite grain size.
2. The transformation temperatures.
3. The hardenability of the alloys.
4. The nucleation and growth of grain boundary nucleated phases.
5. The nucleation and growth of intragranular nucleated phases.

The effects of the microalloying elements on microstructural development were complex and depended on the type and concentrations present.

The influence of microalloying elements on microstructural development is shown schematicaly in fig. 5.9. In all cases, the microalloying element is the only compositional variable and the oxygen contents are low and therefore ferrite nucleation on oxides would not be significant. Comparing microalloyed weld metal, with similar material of identical prior austenite grain size and cooling rate, the influence on microstructural development may again be explained in terms of the effect on undercooling. As before transformation would initially start at the prior austenite grain boundaries with the formation of PF. But since the presence of the microalloy element would increase the hardenability of the alloy, greater undercooling would be required and the transformation temperature in the microalloyed weld metal, would be depressed.

Redistribution of alloying elements would result in the formation of a solute barrier, which would eventually inhibit further PF growth. However the presence of microalloy elements in this solute barrier, would increase

the effective hardenability locally and therefore increase the undercooling required for further PF growth. This would inhibit PF growth at an earlier stage in the transformation process and promote the formation of FSP. Therefore a combination of a lower transformation temperature and limited growth period, prior to the formation of FSP, would reduced the proportion of PF formed in the microalloyed weld metal.

The transformation temperature would also influence the proportion of FSP formed. The higher transformation temperature of the plain carbon material, would give a longer time period for FSP growth, before the grain interiors had undercooled sufficiently for transformation to occur and therefore FSP development could be extensive. With the microalloyed weld metal, the grain interiors would require a higher degree of undercooling before transformation, due to the higher hardenability. But as a consequence of the already low transformation temperature, the formation of intragranular phases may occur with relatively little further undercooling. Therefore FSP growth would be inhibited by impingement with these intragranular phases.

A further consequence of the reduced PF and FSP growth, in the microalloyed material, is that the microstucture would be dominated by intragranular transformation products. The proportion of AF,LF and FC phases formed would depend on the hardenability. However with the presence of the microalloy element and the resulting higher hardenability, there would be an increased tendency to form lower

temperature transformation products. From this it would follow that a cooling rate which produced high proportions of PF and FSP structures, in plain carbon steel weld metal, would, in microalloyed materials form microstructures with lower proportions of grain boundary phases and consequently dominated by intragranular nucleated constituents.

Higher concentrations of microalloying elements within the alloy would further increase the hardenability and consequently the levels of undercooling prior to transformation. However if only small concentrations are required to inhibit grain boundary nucleation, reducing PF and FSP formation to low levels, further increase in concentration may have little effect on the transformation temperature and proportions of these phases. But the higher microalloy concentration would influence intragranular nucleation, by increasing the hardenability of the austenite. The degree of undercooling prior to intragranular transformation would increase. Therfore a high microalloy concentration, would promote the lower temperature transformation products, LF and FC phases.

With increases in the cooling rate, the trend for reduced PF and FSP formation will be compounded by the higher hardenability of the microalloyed materials. The reduced transformation temperature and inhibition of PF and FSP growth, with higher cooling rates would favour even higher proportions of intragranular nucleation and growth. However the increased hardenability of the microalloyed weld metal, would also favour higher degrees of intragranular undercooling and therefore the proportions of LF and FC

phases would be increased and would also form at lower cooling rates.

Examination of the microstructures formed in the "as-deposited" V microalloyed weld metal series, fig. 4.17, can be used to show the application of this mechanism. For a cooling rate corresponding to 5°C/sec. in the plain carbon base alloy, 21,27 and 50% PF,FSP and AF were formed. However with low and high microalloy concentrations, the proportions of grain boundary nucleated phases were reduced to less than 20% in total, with the majority of the microstructure consisting of AF. With higher cooling rates the proportions of PF and FSP structures continued to decrease, but the AF constituent was also reduced as a result of LF and FC formation. The cooling rate at which LF formed, was also reduced with higher V concentrations, which would also be consistent with the proposed mechanism.

Refinement in the prior austenite grain size in microalloyed weld metal would further influence, subsequent microstructural development. Finer prior austenite grain size would increase the proportions of PF and raise the transformation temperature, as discussed in section 5.3.1.1. However with the presence of microalloying elements, the hardenability in the solute barrier ahead of the PF growth front would be higher and therefore growth of this constituent would be inhibited at an earlier stage, compared to a similar alloy containing no microalloy elements. The intragranular hardenability would also be greater in the microalloyed material, resulting in a higher degree of undercooling prior to transformation. Therefore if the

transformation temperature is relatively high, the inhibition of PF formation in the microalloyed weld metal, would give a longer time period for FSP growth, prior to intragranular transformation and therefore the proportion of this phase would be increased. However with lower transformation temperatures the period for FSP growth would be limited, resulting in a microstructure dominated by intragranular nucleation. This would infer that the influence of microalloying elements on the transformation start temperature, was an important factor in subsequent microstructural development. The higher intragranular hardenability of the finer grained microalloyed materials, would also favour the formation of higher proportions of LF and FC phases, in the microstructure.

A comparison of the effects of Ti and Nb concentration in the reheated weld metal can be used as an example of the operation of this mechanism. In the low concentration Ti and Nb alloys, figs. 4.78 and 4.79, although the transformation temperatures were reduced in comparison to the base alloy, the proportion of FSP increased, while PF formation reduced. This would suggest that the transformation tempertature was sufficiently high to allow significant FSP growth, prior to intragranular nucleation. However with increased Ti concentration, the further depression of transformation temperature inhibited PF and FSP formation, favouring intragranular nucleation and growth. Since the high microalloy concentration also increased the hardenability, the microstructures were dominated by low temperature transformation products.

With high Nb concentration no further reduction in transformation temperature occurred and the FSP content increased to 46%, while PF formation continued to decrease. Therefore in this case the high transformation temperature, together with the greater degree of intragranular undercooling, required as a result of the higher hardenability, would favour longer growth periods for the FSP phase and account for the higher proportions observed.

5.5 FUTURE WORK.

It is clear that the composition of as-deposited and reheated weld metal significantly influences the microstructures formed. However a wide range of materials are used in welded construction and information on the resultant effects of different compositions on microstructural development is required. Further CCT diagrams showing the influence of major alloying elements eg. Mn, Mo or combinations of elements eg. Ti+B, Nb+V would therefore be of great interest.

High proportions of acicular ferrite were observed in the as-deposited alloys, although the oxygen contents were to low for significant oxide inclusion formation. A recent model proposed to account for acicular ferrite formation, suggested that this phase nucleated on oxide inclusions. However this mechanism would clearly not account for the acicular ferrite observed in the current work. Therefore in view of the potential beneficial effects imparted by a high acicular ferrite content and low inclusion population, further study is required to fully understand the nature of

this phase.

The prior austenite grain size significantly influences transformation in as-deposited weld metal. The factors which affect this grain size, in terms of solidification and subsequent grain coarsening on cooling, are not clear and require further research.

Continued research is required to relate the mechanical properties of weld metal to the microstructure. This should include full information on the type and proportions of ferrite constituents and microphases, prior austenite and ferrite grain size and inclusion population.

CHAPTER 6 - CONCLUSIONS.

CHAPTER 6 - CONCLUSIONS.

1. Simulative techniques have been used to study microstructural development in as-deposited and reheated low carbon microalloyed steel weld metal, with oxygen content less than 20ppm.

2. CCT diagrams have been produced isolating the effects of low and high concentrations of the microalloying elements V(0.03,0.09%wt), Ti(0.01,0.06%wt), Nb(0.02,0.05%wt) and Al(0.02,0.06%wt), on as-deposited and reheated weld metal microstructures under low oxygen content conditions. The concentrations studied are shown in brackets.

3. All the microalloying elements studied depressed the transformation start (Ts.) temperatures. The degree to which this occurred depended on the microalloy type and concentration and cooling rate. For as-deposited steels, V, Ti and Nb additions depressed the Ts. temperature by up to 30°C and Al by up to 40°C. For reheated steels the Ts. temperatures were depressed by up to 70°C. Ts temperatures were higher in the reheated weld metal compared to the as-deposited weld metal.

4. In the as-deposited and reheated weld metal microalloying additions moved the positions of the phase fields on the CCT diagrams to longer times. The degree to which this occurred depended on the microalloy type and concentration.

5. As-deposited weld metal:

5.1 Low microalloy concentrations suppressed the formation of primary ferrite and ferrite side plate structures at cooling rates less that 15°C/sec, with acicular ferrite proportions increasing by upto 35%. Promotion of acicular ferrite is thought to occur due to segregation of microalloying elements to the primary ferrite boundary inhibiting growth, allowing undercooling within the austenite grains to reach levels at which acicular ferrite formation could occur. At higher cooling rates lath ferrite formation increased.

5.2 High Ti and Nb concentrations refined the prior austenite grain size by 80% and 50% respectively. The increased grain boundary area promoted primary ferrite. In the Ti alloy the refinement was thought to be due to heterogeneous nucleation of delta ferrite on Ti carbide/nitride particles. In the Nb alloy, it is proposed that segregation to the austenite boundaries, produces refinement as a result of grain boundary drag.

5.3 High microalloy concentrations increased the proportions of lath ferrite. This probably

reflects an increase in hardenability, which allows undercooling to reach a sufficient level for lath ferrite formation.

5.4 Acicular ferrite was observed in all the alloys at cooling less than 15°C/sec., with up to 80% observed at specific cooling rates, even in the base alloy. This would suggest that an oxide inclusion population is not a pre-requisite for acicular ferrite nucleation and growth. It is therefore proposed that acicular ferrite will form when growth of primary ferrite and ferrite side plate structures are inhibited, and providing the undercooling is not sufficient for lath ferrite to form.

5.5 Increased cooling rate refined the prior austenite grain size and promoted lath ferrite and ferrite carbide aggregate structures. Faster rates also refined the ferrite lath size.

5.6 A reduction in carbon content to 0.05%wt, increased the transformation temperatures by up to 70°C., compared with the base alloy (0.15%wt% carbon). The proportion of primary ferrite and ferrite side plates were increased as a result of lower hardenability. Lath ferrite was limited even at cooling rates of 50°C/sec.

5.7 An increase in oxygen content to 300ppm, refined the prior austenite grain size and promoted primary ferrite. This was consistent with oxide pinning of the grain boundaries.

6. Reheated weld metal.

6.1 The prior austenite grain size was significantly finer and equi-axed compared to the as-deposited alloys. This increased the proportions of primary ferrite for the base and low microalloy reheated weld metal compared with their respective as-deposited alloys.

6.2 High microalloy additions inhibited primary ferrite formation and promoted lath ferrite constituents.

6.3 In all the reheated alloys acicular ferrite was limited, due to primary ferrite and ferrite side plate formation at slow cooling rates and lath ferrite at faster rates.

7. Microalloy additions increased the microphase content, refined the ferrite structure and increased the hardness of both as-deposited and reheated alloys. These effects would be consistent with increased hardenability produced by the microalloying elements. The hardness values determined could be related to the microstructures.

TABLES.

Table 1. Typical Compositions of Low and High Microalloyed Steel Weld Metal, Selected for Investigation

Microalloy Type	Composition % wt.							
	C	Mn	Si	V	Ti	Nb	Al	Fe
Low Vanadium	0.15	1.5	0.25	0.02	-	-	-	Bal
High Vanadium	"	"	"	0.08	-	-	-	"
Low Titanium	"	"	"	-	0.01	-	-	"
High Titanium	"	"	"	-	0.06	-	-	"
Low Niobium	"		"	-	-	0.01	-	"
High Niobium	"	"	"	-	-	0.05	-	"
Low Aluminium	"	"	"	-	-	-	0.01	"
High Aluminium	"	"	"	-	-	-	0.06	"

Table 2. Composition of Simulated And Real As-Deposited RQT-500 Steel Weld Metal, After Arc Melting.

Material	Composition % Wt.																
	C	Si	Mn	P	S	Ni	Cr	Mo	Al	Cu	Nb	V	Co	Sn	O_2	N_2	Fe
As received	0.15	0.34	1.44	0.011	0.025	0.06	0.08	0.02	0.004	0.080	0.060	0.030	0.02	0.008	0.015	0.005	Bal
Real	0.13	0.32	1.40	0.01	0.010	0.06	0.07	0.02	0.001	0.075	0.058	0.028	0.02	0.006	0.005	0.003	Bal
Simulated	0.13	0.30	1.42	0.010	0.010	0.05	0.08	0.02	0.001	0.080	0.057	0.028	0.02	0.005	0.004	0.003	Bal

Table 3. The Type And Proportion of Ferrite Constituents Observed In The Simulated And Real As-Deposited RQT-500 Steel Weld Metal, Cooled At 4°C/Sec.

		% of Ferrite Constituents*				
Material	Test I.D.	PF	FSP	AF	LF	FC
Real	R1	32	20	9	34	5
Weld	R2	30	24	6	37	3
Metal	R3	34	21	7	33	5
Simulated	S1	30	19	10	33	4
Weld	S2	34	23	9	31	3
Metal	S3	29	24	9	35	3

*Abbreviation Key:

PF = Primary Ferrite.
FSP = Ferrite Side Plates.
AF = Acicular Ferrite.
LF = Lath Ferrite.
FC = Ferrite Carbide Aggregate.

Table 4. Chemical Analysis of the Hoganas ASC-100 Iron Powder Used for Producing the Experimental Alloys.

Composition % wt															
Fe	C	Si	Mn	P	S	Ni	Cr	Mo	Al	Cu	Nb	V	Ti	Co	Sn
99.99	<0.001	0.002	<0.001	<0.001	<0.001	<0.001	<0.001	<0.001	<0.001	<0.001	<0.001	<0.001	<0.001	<0.001	<0.001

Table 5. Composition of Arc Melted Buttons Produced To Determine The Reproducibility Of The Required Microalloyed Steel Weld Metal Compositions.

Test Identification	Composition % Wt.									
	C	Mn	Si	V	Ti	Nb	Al	O_2	Fe	CE*
Base	0.151	1.52	0.24	-	-	-	-	< 0.001	Bal	0.404
V.1	0.153	1.49	0.26	0.023	-	-	-	< 0.001	Bal	0.403
V.2	0.149	1.48	0.22	0.084	-	-	-	< 0.001	Bal	0.401
Ti.1	0.148	1.51	0.25	-	0.022	-	-	< 0.001	Bal	0.400
Ti.2	0.150	1.49	0.23	-	0.061	-	-	< 0.001	Bal	0.393
Nb.1	0.149	1.48	0.28	-	-	0.014	-	< 0.001	Bal	0.396
Nb.2	0.152	1.52	0.26	-	-	0.054	-	< 0.001	Bal	0.399
Al.1	0.155	1.51	0.25	-	-	-	0.023	0.0011	Bal	0.405
Al.2	0.156	1.51	0.26	-	-	-	0.064	0.0013	Bal	0.408

* CE - Carbon Equivalent.

Table 6. The Influence of Purging Gas Flow Rate on the Composition of the Arc Melted Buttons

Gas Flow Rate m^3/hr	Composition % Wt				
	C	Mn	Si	O_2	Fe
2.55	0.149	1.51	0.26	0.001	Bal
1.40	0.148	1.52	0.24	0.001	"
1.00	0.151	1.48	0.27	0.001	"
0.60	0.148	0.48	0.24	0.001	"
0.40	0.152	1.49	0.25	0.001	"
0.20	0.148	1.51	0.24	0.0015	"
0.10	0.121	1.47	0.23	0.0040	"

Table 7. The Influence of Arc Melted Button Size on Composition (Purging Gas Flow Rate 0.80 m^3/hr)Gas Flow

Button Size (gms)	Composition % Wt				
	C	Mn	Si	O_2	Fe
60	0.147	1.53	0.23	0.001	Bal
30	0.149	1.51	0.25	0.001	"
15	0.152	1.54	0.27	0.001	"
5	0.148	1.49	0.24	0.001	"

Table 8. The Effect of Arcing Time on Arc Melted Button Composition

Arcing Time (Sec)	Composition % Wt				
	C	Mn	Si	O_2	Fe
1	0.149	1.50	0.23	0.001	Bal
5	0.148	1.47	0.28	0.001	"
15	0.148	1.49	0.24	0.001	"
30	0.152	1.53	0.27	0.001	"

Table 9. Composition And Identification of Simulated As-Deposited Weld Metal, Used To Construct CCT Diagrams. Showing The Effect of Low And High Microalloy Concentrations on Transformation in Ferritic Steel Weld Metal

Series Identification	Composition % Wt.										
	C	Mn	Si	V	Ti	Nb	Al	O_2	N_2	Fe	CE*
A	0.153 ±0.002	1.52 ±0.01	0.24 ±0.01	-	-	-	-	<0.001	0.0030	Bal.	0.406
B	0.155 ±0.003	1.49 ±0.02	0.25 ±0.02	0.027 ±0.002	-	-	-	<0.001	0.0035	Bal.	0.403
C	0.151 ±0.002	1.50 ±0.01	0.25 ±0.01	0.088 ±0.002	-	-	-	<0.001	0.0038	Bal.	0.401
D	0.149 ±0.003	1.46 ±0.01	0.24 ±0.02	-	0.020 ±0.001	-	-	<0.001	0.0038	Bal.	0.394
E	0.145 ±0.002	1.42 ±0.01	0.24 ±0.02	-	0.063 ±0.002	-	-	<0.001	0.0040	Bal.	0.382
F	0.149 ±0.003	1.44 ±0.01	0.24 ±0.01	-	-	0.021 ±0.001	-	<0.001	0.0037	Bal.	0.389
G	0.148 ±0.004	1.46 ±0.01	0.25 ±0.02	-	-	0.053 ±0.002	-	<0.001	0.0038	Bal.	0.391
H	0.174 ±0.003	1.51 ±0.02	0.25 ±0.01	-	-	-	0.024 ±0.002	0.002	0.0039	Bal.	0.426
I	0.178 ±0.004	1.52 ±0.02	0.25 ±0.02	-	-	-	0.063 ±0.002	0.0023	0.0040	Bal.	0.431

Table 10. Thermal Analysis, Quantitative Metallographic and Hardness Test Results, For the base alloy (Series A) Simulated As-Deposited Weld Metal, with Low Oxygen Content.

Series Identification	Cooling Rate $^{o}C/sec(\Delta T800-500)$	Transformation Temperatures ^{o}C		Prior Austenite Grain Size mm	% of Microstructural Constituents*						Hardness Hv20
		Ts	Tf		PF	FSP	AF	LF	FC	P	
A6	4.0	595	504	0.93	14	13	70	-	-	3	200
A3	4.6	593	504	0.89	12	14	71	-	-	3	201
A7	5.2	604	503	0.73	21	27	50	-	-	2	197
A11	6.0	612	507	0.69	23	26	51	-	-	-	201
A8	6.7	609	505	0.68	19	20	58	-	-	5	210
A1	7.0	608	504	0.67	20	15	60	-	-	2	214
A9	9.3	600	485	0.68	13	10	69	-	-	2	212
A10	10.7	597	460	0.60	10	4	84	3	-	-	210
A12	12.0	604	462	0.55	12	7	77	2	-	2	212
A2	12.6	600	446	0.61	7	4	83	5	-	-	210
A19	14.0	565	440	0.59	10	5	72	10	-	-	213
A14	19.6	559	430	0.62	11	3	35	50	1	-	221
A20	22.1	554	421	0.60	10	3	22	62	3	-	239
A17	24.9	553	417	0.63	7	3	19	63	-	-	246
A4	26.1	542	418	0.64	3	4	6	76	11	-	247
A13	27.6	548	401	0.61	5	3	8	74	10	-	247
A5	28.0	549	395	0.56	-	-	6	80	14	-	245
A18	34.6	522	390	0.49	-	-	4	83	13	-	246
A15	42.3	530	390	0.48	-	-		81	19	-	265
A16	48.8	524	384	0.49	-	-		80	20	-	278

* Abbreviations Key, Table 3.

Table 11. Thermal Analysis, Quantitative Metallographic and Hardness Test Results, For the 0.027% Wt Vanadium (Series B) Simulated As-Deposited Microalloyed Steel Weld, With Low Oxygen Content.

Series Identification	Cooling Rate °C/sec(ΔT800-500)	Transformation Temperatures °C		Prior Austenite Grain Size mm	% of Microstructural Constituents*						Hardness Hv20
		Ts	Tf		PF	FSP	AF	LF	FC	P	
B9	4.2	584	520	1.10	5	3	88	-	-	4	207
B8	5.5	587	521	0.99	6	1	88	-	-	5	208
B10	7.2	586	523	0.89	8	5	82	-	-	5	208
B7	8.0	588	533	0.87	9	5	78	2	-	6	206
B11	9.2	584	522	0.83	6	4	84	-	-	6	210
B6	10.8	580	517	0.83	4	4	88	-	-	4	211
B5	11.8	565	489	0.89	2	2	92	-	-	4	236
B12	14.9	550	460	0.70	2	3	84	11	-	-	239
B15	16.1	541	447	0.70	1	2	60	35	2	-	246
B2	17.3	536	443	0.68	-	-	10	86	4	-	250
B13	21.4	501	422	0.63	-	-	-	90	10	-	254
B14	27.6	496	417	0.62	-	-	-	83	17	-	257
B3	33.8	486	385	0.57	-	-	-	73	27	-	291
B16	39.3	480	365	0.56	-	-	-	68	32	-	305
B17	44.5	480	362	0.54	-	-	-	64	36	-	319
B4	63.0	476	358	0.54	-	-	-	65	35	-	347

*Abbreviations Key, Table 3.

Table 12. Thermal Analysis, Quantitative Metallographic and Hardness Test Results, For the 0.088% Wt Vanadium (Series C) Simulated As-Deposited Microalloyed Steel Weld, With Low Oxygen Content.

Series Identification	Cooling Rate °C/sec(ΔT800-500)	Transformation Temperatures °C		Prior Austenite Grain Size mm	% of Microstructural Constituents*						Hardness Hv20
		Ts	Tf		PF	FSP	AF	LF	FC	P	
C10	3.7	583	505	0.86	13	8	76	-	-	3	212
C9	5.5	580	510	0.85	7	11	79	-	-	3	213
C8	6.1	585	500	0.83	6	5	86	-	-	4	215
C12	8.8	600	500	0.85	14	10	69	5	-	4	225
C13	11.5	601	505	0.87	9	12	57	21	-	1	233
C21	13.4	580	440	0.73	10	8	52	30	-	-	236
C16	16.2	566	439	0.71	9	2	34	49	5	-	241
C15	17.0	568	448	0.64	5	2	10	79	8	-	250
C20	18.2	556	436	0.58	-	-	-	84	16	-	252
C18	19.9	558	432	0.60	-	-	-	83	17	-	249
C1	20.1	554	464	0.57	-	-	-	82	18	-	250
C2	24.0	537	449	0.47	-	-	-	72	28	-	261
C17	29.9	539	413	0.49	-	-	-	67	33	-	261
C7	30.4	525	420	0.50	-	-	-	68	32	-	286
C19	44.9	515	432	0.50	-	-	-	40	60	-	324
C22	50.2	510	430	0.51	-	-	-	38	62	-	331

* Abbreviations Key, Table 3.

Table 13. Thermal Analysis, Quantitative Metallographic and Hardness Test Results, For the 0.020%Wt Titanium (Series D) Simulated As-Deposited Microalloyed Steel Weld, With Low Oxygen Content.

Series Identification	Cooling Rate °C/sec(ΔT800-500)	Transformation Temperatures °C		Prior Austenite Grain Size mm	% of Microstructural Constituents*						Hardness Hv20
		Ts	Tf		PF	FSP	AF	LF	FC	P	
D8	4.1	581	500	1.09	18	16	55	-	-	8	203
D18	5.1	580	500	0.09	13	10	72	-	-	4	201
D2	6.9	583	503	0.09	8	5	83	4	-	-	204
D1	7.5	574	490	0.84	9	4	83	4	-	-	205
D19	8.7	574	486	0.80	7	5	82	6	1	-	210
D20	10.5	576	470	0.77	7	4	80	5	2	-	211
D10	13.9	575	445	0.77	6	9	61	19	5	-	225
D4	14.9	577	483	0.76	5	8	59	22	6	-	230
D14	15.9	577	464	0.78	5	6	54	28	7	-	237
D15	16.7	572	430	0.78	3	4	25	57	11	-	250
D11	17.3	555	432	0.77	-	-	24	63	13	-	252
D6	18.9	548	416	0.76	-	-	-	85	15	-	260
D21	21.2	544	417	0.63	-	-	-	83	17	-	260
D13	24.3	544	419	0.56	-	-	-	80	20	-	272
D12	25.8	543	413	0.54	-	-	-	81	19	-	272
D16	28.8	539	416	0.54	-	-	-	83	17	-	271
D17	32.8	546	394	0.54	-	-	-	81	19	-	277
D22	39.2	530	392	0.56	-	-	-	81	19	-	279
D23	45.1	521	387	0.57	-	-	-	78	22	-	280
D7	56.4	519	372	0.52	-	-	-	73	27	-	286

* Abbreviations Key, Table 3.

Table 14. Thermal Analysis, Quantitative Metallographic and Hardness Test Results, For the 0.063% Wt Titanium (Series E) Simulated As-Deposited Microalloyed Steel Weld, With Low Oxygen Content.

Series Identification	Cooling Rate °C/sec(ΔT800-500)	Transformation Temperatures °C		Prior Austenite Grain Size mm	% of Microstructural Constituents*						Hardness Hv20
		Ts	Tf		PF	FSP	AF	LF	FC	P	
E7	4.1	575	499	0.31	26	20	38	11	-	5	225
E17	5.2	576	500	0.30	24	7	53	9	-	5	220
E2	6.7	585	501	0.31	22	7	57	10	-	1	218
E1	7.1	583	496	0.25	21	6	59	12	1	-	219
E8	8.6	590	499	0.26	22	6	59	11	2	-	218
E3	10.2	595	480	0.23	17	3	64	14	2	-	219
E20	11.4	576	473	0.27	11	6	62	14	3	-	229
E18	12.9	570	450	0.28	11	6	41	41	4	-	240
E19	15.1	555	445	0.25	-	-	-	93	7	-	258
E4	17.4	550	442	0.23	-	-	-	83	17	-	265
E11	19.1	545	423	0.22	-	-	-	95	5	-	265
E14	19.5	541	420	0.18	-	-	-	93	7	-	262
E10	19.9	543	417	0.29	-	-	-	95	5	-	261
E12	21.1	539	419	0.27	-	-	-	85	15	-	268
E5	23.8	540	419	0.24	-	-	-	80	20	-	265
E21	29.1	532	420	0.27	-	-	-	74	26	-	281
E13	32.1	521	420	0.26	-	-	-	75	25	-	306
E16	42.0	520	408	0.20	-	-	-	60	40	-	296
E15	42.9	523	407	0.25	-	-	-	60	40	-	299
E6	48.4	522	396	0.28	-	-	-	61	39	-	

* Abbreviations Key, Table 3.

Table 15. Thermal Analysis, Quantitative Metallographic and Hardness Test Results, For the 0.021% Wt Niobium (Series F) Simulated As-Deposited Microalloyed Steel Weld, With Low Oxygen Content.

Series Identification	Cooling Rate °C/sec(Δ T800-500)	Transformation Temperatures °C		Prior Austenite Grain Size mm	% of Microstructural Constituents*						Hardness Hv20
		Ts	Tf		PF	FSP	AF	LF	FC	P	
F5	4.2	594	523	0.98	13	13	71	–	–	3	207
F18	5.4	590	520	0.92	12	13	72	–	–	3	207
F4	7.1	584	482	0.74	12	13	71	3	–	–	206
F3	8.1	582	471	0.83	10	10	73	2	–	5	203
F10	8.6	587	473	0.87	11	17	65	5	1	1	217
F11	10.5	582	478	0.82	12	19	58	5	1	–	214
F12	11.5	580	452	0.82	10	9	74	4	3	–	221
F19	13.6	573	446	0.80	7	4	72	9	8	–	230
F14	16.1	568	440	0.77	5	2	60	19	12	–	236
F20	17.3	560	432	0.74	3	2	22	60	13	–	245
F7	19.4	554	426	0.67	1	1	18	75	14	–	253
F15	22.2	549	410	0.72	–	–	15	71	14	–	261
F13	22.2	544	419	0.73	–	–	14	73	13	–	262
F21	23.4	530	401	0.70	–	–	–	85	15	–	264
F22	25.9	525	402	0.63	–	–	–	84	16	–	264
F6	30.5	523	390	0.57	–	–	–	83	17	–	268
F16	32.1	520	392	0.62	–	–	–	83	17	–	262
F2	33.6	525	387	0.65	–	–	–	84	16	–	270
F23	39.2	515	385	0.56	–	–	–	73	27	–	292
F17	42.4	510	374	0.48	–	–	–	76	24	–	298

* Abbreviations Key, Table 3.

Table 16. Thermal Analysis, Quantitative Metallographic and Hardness Test Results, For the 0.053% Wt Niobium (Series G) Simulated As-Deposited Microalloyed Steel Weld, With Low Oxygen Content.

Series Identification	Cooling Rate °C/sec(ΔT800-500)	Transformation Temperatures °C		Prior Austenite Grain Size mm	% of Microstructural Constituents*						Hardness Hv20
		Ts	Tf		PF	FSP	AF	LF	FC	P	
G4	3.9	572	502	0.43	19	24	52	-	-	5	213
G25	5.5	580	501	0.47	16	19	57	6	-	2	214
G16	7.0	586	499	0.52	12	17	46	24	-	1	225
G3	7.4	589	495	0.56	11	20	42	26	-	1	224
G2	8.2	583	462	0.54	11	18	43	28	-	-	222
G19	8.4	580	455	0.51	12	12	46	29	1	-	227
G20	8.5	580	455	0.52	13	14	41	30	2	-	231
G21	10.3	582	435	0.50	10	6	50	32	2	-	232
G22	12.1	579	427	0.51	6	3	54	32	5	-	231
G14	14.2	571	425	0.50	1	2	55	36	8	-	230
G13	17.7	552	413	0.50	-	-	40	46	14	-	230
G23	18.4	550	410	0.49	-	-	1	72	16	-	231
G24	19.6	552	411	0.47	-	-	2	78	10	-	230
G6	20.8	554	414	0.46	-	-	-	75	25	-	231
G1	23.1	542	407	0.45	-	-	-	75	25	-	239
G10	24.0	546	408	0.41	-	-	-	77	23	-	245
G15	33.2	535	406	0.44	-	-	-	80	20	-	246
G5	37.5	516	392	0.45	-	-	-	80	20	-	248
G11	39.3	516	396	0.40	-	-	-	82	18	-	260
G12	40.8	501	388	0.40	-	-	-	75	25	-	268

* Abbreviations Key, Table 3.

Table 17. Thermal Analysis, Quantitative Metallographic and Hardness Test Results, For the 0.024% Wt Aluminium (Series H) Simulated As-Deposited Microalloyed Steel Weld, With Low Oxygen Content.

Series Identification	Cooling Rate $^{o}C/sec(\Delta T800-500)$	Transformation Temperatures ^{o}C		Prior Austenite Grain Size mm	% of Microstructural Constituents*						Hardness Hv20
		Ts	Tf		PF	FSP	AF	LF	FC	P	
H2	4.1	592	480	1.10	9	9	61	19	-	1	205
H1	4.2	598	478	1.10	11	10	60	18	-	1	200
H3	5.4	575	466	0.80	4	3	72	18	-	1	204
H4	7.7	563	459	0.84	5	2	78	15	-	-	206
H17	10.5	564	432	0.80	4	4	64	27	1	-	213
H6	12.7	564	426	0.67	3	5	59	31	3	-	213
H5	12.9	561	420	0.69	3	7	49	35	6	-	220
H18	13.7	555	421	0.69	2	4	56	34	4	-	226
H13	14.9	551	424	0.64	1	2	59	33	5	-	227
H19	15.5	550	417	0.65	1	1	21	70	7	-	230
H12	16.1	533	407	0.60	-	-	-	86	14	-	236
H15	16.8	542	392	0.63	-	-	-	85	15	-	235
H14	19.7	560	407	0.63	-	-	-	83	17	-	235
H11	23.8	548	402	0.62	-	-	-	85	15	-	238
H20	27.9	520	390	0.60	-	-	-	86	14	-	254
H9	32.9	502	384	0.56	-	-	-	86	14	-	264
H16	33.5	502	373	0.56	-	-	-	88	12	-	264
H10	36.4	507	380	0.52	-	-	-	86	14	-	274
H21	41.3	495	360	0.51	-	-	-	84	16	-	293
H7	49.3	464	355	0.54	-	-	-	84	16	-	330

* Abbreviations Key, Table 3.

Table 18. Thermal Analysis, Quantitative Metallographic and Hardness Test Results, For the 0.063% Wt Aluminium (Series I) Simulated As-Deposited Microalloyed Steel Weld, With Low Oxygen Content.

Series Identification	Cooling Rate °C/sec(ΔT800-500)	Transformation Temperatures °C		Prior Austenite Grain Size mm	% of Microstructural Constituents*						Hardness Hv20
		Ts	Tf		PF	FSP	AF	LF	FC	P	
I1	4.5	576	480	0.77	8	10	43	30	-	10	204
I2	4.6	574	482	0.79	8	11	42	32		8	205
I21	5.6	563	473	0.76	2	4	58	32		4	207
I3	6.8	560	456	0.72	2	3	51	42	-	1	212
I4	6.8	561	454	0.71	3	4	50	41		2	213
I17	8.1	551	430	0.70	2	6	39	50		3	219
I5	9.7	543	424	0.71	3	6	40	47	-	2	218
I16	10.6	540	415	0.67	1	2	45	57	-	1	221
I18	12.1	538	407	0.65	1	2	43	59	-	1	220
I19	13.1	536	407	0.65	-	-	15	76	9	-	224
I13	15.9	531	393	0.66	-	-	-	88	12	-	225
I15	19.7	516	397	0.60	-	-	-	84	16	-	245
I14	23.0	510	376	0.52	-	-	-	84	16	-	289
I7	30.0	491	369	0.60	-	-	-	89	11	-	289
I6	30.8	496	372	0.53	-	-	-	87	13	-	286
I12	32.5	496	362	0.45	-	-	-	90	10	-	281
I9	34.1	488	356	0.41	-	-	-	91	9	-	303
I11	39.1	459	320	0.40	-	-	-	26	73	-	351
I20	45.6	447	302	0.42	-	-	-	15	85	-	362
I10	51.4	446	300	0.45	-	-	-	3	97	-	374
I8	51.7	434	301	0.42	-		-	4	96	-	373

* Abbreviations Key, Table 3.

Table 19. The Proportion of Microphases Formed in Low Oxygen Content Simulated As-Deposited Weld Metal, Cooled at 7°C/sec. Determined from Micrographs at a Magnification of X1200.

	As-Deposited Alloys								
Series (Microalloy Addition, % wt.)	A (Base Alloy)	B (0.027 V)	C (0.088 V)	D (0.020 Ti)	E (0.063 Ti)	F (0.021 Nb)	G (0.053 Nb)	H (0.024 Al)	I (0.063 Al)
Proportion of Microphases %	12	20	22	18	30	15	16	21	20

Table 20. Acicular Ferrite Grain Size Determined in the Low Oxygen Content Simulated As-Deposited Weld Metal, Cooled at 4°C/sec.

	As-Deposited Alloys								
Series (Microalloy Addition, % wt.)	A (Base Alloy)	B (0.027 V)	C (0.088 V)	D (0.020 Ti)	E (0.063 Ti)	F (0.021 Nb)	G (0.053 Nb)	H (0.024 Al)	I (0.063 Al)
Acicular Ferrite Grain Size, μm.	30	20	17	14	10	19	15	14	9

Table 21. The Influence Of Arcing Time On Button Composition Using An Argon-2% Oxygen Purging Gas.

Arcing Time (sec.)	Composition % Wt.				
	C	Mn	Si	O_2	Fe
2	0.131	1.47	0.23	0.0020	Bal.
5	0.082	1.48	0.25	0.00295	Bal.
7	0.052	1.47	0.22	0.0309	Bal.
10	0.051	1.31	0.21	0.0321	Bal.
12	0.049	0.09	0.18	0.0317	Bal.
15	0.050	0.07	0.16	0.0320	Bal.

Table 22. The Influence of Arc Melted Button Size on Composition Using An Argon-2% Oxygen purging Gas and 5 Second Arcing Time.

Button Size (gms)	Composition % Wt.				
	C	Mn	Si	O_2	Fe
30	0.082	1.48	0.25	0.0295	Bal.
15	0.061	1.47	0.23	0.0302	Bal.
10	0.051	1.46	0.23	0.0310	Bal.
5	0.052	1.34	0.20	0.0325	Bal.

Table 23. The Influence of Mixing Unsintered Buttons With Sintered Buttons, On Composition, In An Attempt To Increase Oxygen Content.

Button Size Mixed (gms)	Composition % Wt.			
	C	Mn	Si	O_2
30 gm Sintered + 5 gm Unsintered	0.081	1.45	0.23	0.0020
20 gm Sintered + 10 gm Unsintered	0.072	1.40	0.23	0.0035
10 gm Sintered + 10 gm Unsintered	0.070	1.41	0.24	0.0041

Table 24. Composition of High Oxygen Content As-Deposited Weld Metal, Produced Using An Argon-2% Oxygen Purging Gas, 30 gm Button and 5 Second Arcing Time.

Specimen Identification	Composition % Wt.				
	C	Mn	Si	O_2	Fe
01	0.053	1.46	0.23	0.0290	Bal.
02	0.050	1.47	0.22	0.0316	Bal.
03	0.049	1.44	0.24	0.0309	Bal.

Table 25. Composition of Low Carbon Simulated As-Deposited Weld Metal.

Series identification	Composition % Wt.						
	C	Mn	Si	O_2	N_2	Fe	CE
J	0.053 ±0.003	1.44 ±0.002	0.24 ±0.002	<0.001	0.0021	Bal.	0.299

Table 26. Thermal Analysis, Quantitative Metallographic and Hardness Test Results, For the 0.05% Wt Carbon (Series J) Simulated As-Deposited Plain Carbon Steel Weld Metal, With Low Oxygen Content.

Series Identification	Cooling Rate °C/sec(ΔT800-500)	Transformation Temperatures °C		Prior Austenite Grain Size mm	% of Microstructural Constituents*						Hardness Hv20
		Ts	Tf		PF	FSP	AF	LF	FC	P	
J1	4.0	673	537	0.72	35	20	45	-	-	-	175
J2	4.1	675	535	0.70	40	17	43	-	-	-	171
J17	5.5	562	520	0.70	30	22	48	-	-	-	177
J3	6.4	659	519	0.69	30	24	47	-	-	-	180
J5	8.0	641	517	0.70	28	18	53	1	-	-	180
J4	9.4	668	513	0.63	25	20	56	1	-	-	179
J18	10.8	644	509	0.60	28	20	52	1	-	-	180
J7	12.4	635	501	0.50	35	15	46	4	-	-	189
J6	15.2	614	490	0.51	25	15	57	3	-	-	193
J8	24.9	618	481	0.52	20	20	56	4	-	-	194
J16	25.1	604	471	0.50	20	20	57	3	-	-	201
J14	25.3	609	489	0.49	22	16	53	9	-	-	194
J13	26.0	608	466	0.47	18	20	54	8	-	-	201
J15	36.9	605	480	0.48	22	20	42	16	-	-	206
J9	38.5	598	471	0.43	16	22	45	17	-	-	203
J12	38.7	596	477	0.46	20	26	37	17	-	-	203
J10	41.7	597	483	0.48	18	20	43	19	-	-	204
J11	46.0	600	477	0.40	13	27	38	17	-	-	204

* Abbreviations Key, Table 3.

Table 27. Dilametric, Quantitative Metallographic and Hardness Test Results, For the Base Alloy (Series DA) Simulated Reheated Plain Carbon Steel Weld Metal, With Low Oxygen Content.

Series Identification	Cooling Rate °C/sec(ΔT800-500)	Transformation Temperatures °C		% of Microstructural Constituents						Hardness Hv 1 Kg
		Ts	Tf	PF	FSP	AF	LF	FC	P	
DA5	2.8	736	650	48	25	21	-	-	6	146
DA11	4.2	685	535	44	29	23	-	-	3	145
DA4	5.3	675	521	42	29	25	-	-	5	143
DA12	7.9	675	520	40	28	27	-	-	5	145
DA2	10.2	670	521	32	28	36	4	-	-	150
DA1	11.5	664	520	35	27	32	5	-	1	156
DA6	11.8	659	524	33	29	33	3	-	2	157
DA8	12.5	652	524	32	33	26	4	-	2	164
DA13	14.2	641	501	34	25	27	14	-	-	180
DA14	19.4	640	480	34	26	20	21	1	-	184
DA10	26.4	637	452	29	36	3	34	8	-	192
DA15	29.5	602	430	17	36	-	34	19	-	199
DA16	32.1	594	425	9	21	-	51	21	-	200
DA3	34.4	556	422	-	-	-	75	25	-	210
DA17	40.8	530	419	-	-	-	70	30	-	220

*Abbreviations Key, Table 3.

Table 28. Dilametric, Quantitative Metallographic and Hardness Test Results, For the 0.027% Wt Vanadium (Series DC) Simulated Reheated Microalloyed Steel Weld Metal, With Low Oxygen Content.

Series Identification	Cooling Rate $^{o}C/sec(\Delta T800-500)$	Transformation Temperatures ^{o}C		% of Microstructural Constituents*						Hardness Hv 1 Kg
		Ts	Tf	PF	FSP	AF	LF	FC	P	
DC1	4.0	632	515	36	26	30	-	-	8	203
DC2	4.1	630	515	32	28	33	-	-	7	206
DC11	5.7	621	500	30	28	30	6	-	6	205
DC3	6.9	605	491	22	26	34	16	-	1	210
DC7	9.9	608	490	22	25	29	21	-	3	211
DC8	12.1	604	468	21	24	25	29	1	-	210
DC9	15.4	599	450	20	24	19	34	3	-	210
DC4	18.4	589	436	19	23	14	44	1	-	215
DC10	21.6	585	434	14	22	11	45	8	-	214
DC12	24.9	885	435	7	19	10	49	14	-	214
DC5	28.4	581	436	5	10	-	62	23	-	217
DC 6	31.6	580	434	1	2	-	74	23	-	224
DC14	34.5	560	433	-	-	-	73	27	-	229

*Abbreviations Key, Table 3.

Table 29. Dilametric, Quantitative Metallographic and Hardness Test Results, For the 0.020% Wt Titanium (Series DD) Simulated Reheated Microalloyed Steel Weld Metal, With Low Oxygen Content.

Series Identification	Cooling Rate °C/sec(ΔT800-500)	Transformation Temperatures °C		% of Microstructural Constituents*						Hardness Hv 1 Kg
		Ts	Tf	PF	FSP	AF	LF	FC	P	
DD3	0.9	650	500	57	17	24	-	-	12	133
DD13	3.9	625	497	22	40	16	10	-	6	192
DD9	5.5	620	498	22	46	17	11	-	4	200
DD8	5.7	621	495	21	46	15	14	1	3	209
DD10	7.1	621	501	22	43	15	15	5	-	207
DD1	8.7	609	490	22	45	14	16	3	-	201
DD2	9.8	607	467	23	45	14	18	-	-	204
DD15	11.9	593	454	19	41	14	21	5	-	206
DD16	15.0	590	448	14	37	7	33	7	-	210
DD6	18.2	581	424	10	28	-	50	11	-	221
DD11	23.8	578	420	7	29	-	55	8	-	231
DD5	25.6	568	419	12	20	-	50	18	-	227
DD12	27.0	568	424	12	15	-	53	20	-	228
DD18	32.5	567	423	10	14	-	42	34	-	240
DD7	37.6	562	424	9	11	-	35	46	-	247
DD20	40.1	550	420	2	7	-	40	51	-	250

*Abbreviations Key, Table 3.

Table 30. Dilametric, Quantitative Metallographic and Hardness Test Results, For the 0.063% Wt Titanium (Series DE) Simulated Reheated Microalloyed Steel Weld Metal, With Low Oxygen Content.

Series Identification	Cooling Rate °C/sec(ΔT800-500)	Transformation Temperatures °C		% of Microstructural Constituents*						Hardness Hv 1 Kg
		Ts	Tf	PF	FSP	AF	LF	FC	P	
DE9	0.65	734	552	58	7	31	-	-	3	203
DE8	2.0	633	490	28	15	44	12	-	1	205
DE15	4.1	609	472	14	14	19	50	2	1	220
DE16	5.5	607	468	10	13	16	56	4	-	221
DE1	6.8	595	467	4	10	13	65	8	-	226
DE10	7.5	587	459	5	13	9	66	7	-	224
DE18	9.8	572	430	4	11	11	67	6	-	225
DE5	11.4	565	423	4	12	9	67	8	-	229
DE20	12.5	562	422	3	11	9	69	8	-	227
DE11	15.2	560	415	1	12	4	72	11	-	225
DE4	15.8	543	405	-	-	-	75	25	-	257
DE12	16.8	541	381	-	-	-	78	22	-	250
DE14	17.3	540	380	-	-	-	74	26	-	260
DE3	18.7	536	384	-	-	-	74	26	-	261
DE21	21.3	528	370	-	-	-	76	24	-	264
DE22	25.2	528	371	-	-	-	76	24	-	263
DE24	28.6	527	362	-	-	-	76	24	-	266
DE2	30.8	530	342	-	-	-	71	29	-	273
DE13	36.4	525	346	-	-	-	78	22	-	278

*Abbreviations Key, Table 3.

Table 31. Dilametric, Quantitative Metallographic and Hardness Test Results, For the 0.021% Wt Niobium (Series DF) Simulated Reheated Microalloyed Steel Weld Metal, With Low Oxygen Content.

Series Identification	Cooling Rate °C/sec(ΔT800-500)	Transformation Temperatures °C		% of Microstructural Constituents*						Hardness Hv 1 Kg
		Ts	Tf	PF	FSP	AF	LF	FC	P	
DF9	4.3	649	524	42	38	17	-	-	3	185
DF13	4.6	647	520	42	40	15	-	-	4	182
DF17	5.9	630	515	38	39	15	14	-	4	185
DF18	7.0	625	510	33	38	15	10	-	4	189
DF14	8.1	620	487	29	37	16	13	-	5	193
DF7	10.8	615	484	23	33	21	19	-	5	191
DF11	11.5	613	480	20	34	21	20	-	4	192
DF2	13.3	609	484	10	29	22	36	5	-	194
DF1	12.8	612	485	20	31	24	22	3	-	192
DF19	15.8	608	480	6	28	17	43	6	-	204
DE21	19.1	608	480	5	23	3	54	15	-	210
DF20	23.1	602	478	5	22	1	51	21	-	212
DF5	27.0	598	479	5	19	1	44	32	-	212
DF12	27.1	601	465	6	17	1	46	31	-	218
DF23	31.3	597	457	5	16	-	47	32	-	218
DF15	36.4	593	443	5	10	-	46	31	-	220
DF6	37.4	582	447	2	8	-	58	32	-	230
DF3	46.8	588	430	2	8	-	57	33	-	236

* Abbreviations Key, Table 3.

Table 32. Dilametric, Quantitative Metallographic and Hardness Test Results, For 0.053% wt. Niobium (Series DG) Simulated Reheated Microalloyed Steel Weld Metal, With Low Oxygen Content.

Series Identification	Cooling Rate °C/sec(Δ T800-500)	Transformation Temperatures °C		% of Microstructural Constituents*						Hardness Hv 1 Kg
		Ts	Tf	PF	FSP	AF	LF	FC	P	
DG6	4.6	623	497	17	47	21	14	-	1	204
DG7	4.6	622	500	16	51	19	13	-	1	206
DG14	5.9	624	493	19	44	21	14	-	2	201
DG16	7.2	623	489	19	41	22	16	-	2	203
DG11	8.9	626	481	19	39	24	16	-	2	201
DG8	10.8	624	479	10	38	23	27	2	-	206
DG1	12.3	622	475	8	33	18	36	5	-	209
DG17	14.1	619	475	7	30	7	58	8	-	208
DG18	16.3	619	470	6	27	4	53	10	-	209
DG3	18.8	616	465	5	23	2	45	25	-	215
DG12	20.9	615	454	5	20	1	53	21	-	217
DG4	25.1	616	451	5	25	1	47	22	-	220
DG10	26.6	609	454	6	23	2	46	24	-	226
DG9	30.8	604	450	5	23	-	40	32	-	235
DG5	34.6	592	451	6	6	-	36	52	-	247
DG2	47.1	557	434	1	2	-	34	63	-	254

* Abbreviations Key, Table 3.

Table 33. Dilametric, Quantitative Metallographic and Hardness Test Results, For the 0.024% Wt Aluminium (Series DH) Simulated Reheated Microalloyed Weld Metal, With Low Oxygen Content.

Series Identification	Cooling Rate $^{o}C/sec(\Delta T800-500)$	Transformation Temperatures ^{o}C		% of Microstructural Constituents*						Hardness Hv 1 Kg
		Ts	Tf	PF	FSP	AF	LF	FC	P	
DH1	4.9	623	493	23	27	20	18	-	12	177
DH2	4.9	622	492	24	25	20	19	-	12	178
DH12	5.8	620	491	23	25	20	22	-	10	183
DH13	7.2	620	492	22	24	19	24	-	11	185
DH3	8.3	617	493	21	26	16	26	-	11	182
DH15	10.9	610	480	21	27	17	25	-	10	180
DH16	13.2	603	475	19	29	15	36	-	11	185
DH4	15.4	602	465	17	31	13	37	1	11	192
DH18	16.9	600	458	17	29	12	34	4	4	192
DH5	18.2	598	448	15	28	1	35	21	-	199
DH17	20.8	591	440	14	24	-	40	22	-	202
DH6	23.5	589	439	12	10	-	53	25	-	201
DH7	29.1	571	420	11	14	-	54	21	-	222
DH8	33.0	562	407	9	11	-	49	31	-	225
DH9	38.0	560	403	7	8	-	49	36	-	230
DH10	45.0	559	400	3	3	-	54	40	-	233

* Abbreviations Key, Table 3.

Table 34. Dilametric, Quantitative Metallographic and Hardness Test Results, For the 0.063% Wt Aluminium (Series DI) Simulated Reheated Microalloyed Steel Weld Metal, With Low Oxygen Content.

Series Identification	Cooling Rate $^{o}C/sec(\Delta T800-500)$	Transformation Temperatures ^{o}C		% of Microstructural Constituents*						Hardness Hv 1 Kg
		Ts	Tf	PF	FSP	AF	LF	FC	P	
DI1	4.1	615	493	19	25	30	12	-	14	198
DI2	4.2	618	506	21	27	27	14	-	11	188
DI3	6.5	612	488	18	33	19	19	-	11	193
DI6	8.7	624	468	14	17	8	43	17	-	194
DI8	10.1	620	442	12	17	5	49	17	-	196
DI10	12.3	602	431	9	18	2	52	19	-	204
DI11	15.2	580	415	6	20	-	53	21	-	220
DI4	17.3	569	405	5	18	-	54	23	-	222
DI13	19.1	568	402	3	11	-	61	25	-	247
DI14	20.9	564	400	1	5	-	67	27	-	258
DI5	24.7	566	399	-	-	-	72	28	-	264
DI15	29.1	563	390	-	-	-	70	30	-	265
DI16	33.6	562	390	-	-	-	67	33	-	264
DI7	36.4	565	393				66	34	-	

* Abbreviations Key, Table 3.

Table 35. The Proportion of microphases formed in Low Oxygen Content Simulated Reheated Weld Metal, cooled at 7°C/sec. Determined from Micrographs at a Magnification of X1200.

Series (Microalloy Addition, % Wt)	DA (Base Alloy)	DC (0.088 V)	DD (0.020 Ti)	DE (0.063 Ti)	DF (0.021 Ti)	DG (0.053 Nb)	DH (0.024 Al)	DI (0.063 Al)
Proportion of Microphases, %	11	19	20	27	15	17	19	30

Table 36. The Proportion of Alloying Elements which may be removed from solution should Oxides form from the Limited Oxygen Content Present in the Experimental Alloys. (Assumed Oxygen Content, 10ppm

Element	Mn	Si	Al	Ti	V	Nb
Type of Oxide	MnO	SiO_2	Al_2O_3	TiO_2	*	*
% Wt of Alloying Element Removed From Solution	0.007	0.002	0.002	0.003	-	-

*Unlikely to form oxides.

APPENDIX 2 - FIGURES.

FIGURES FOR CHAPTER 2.

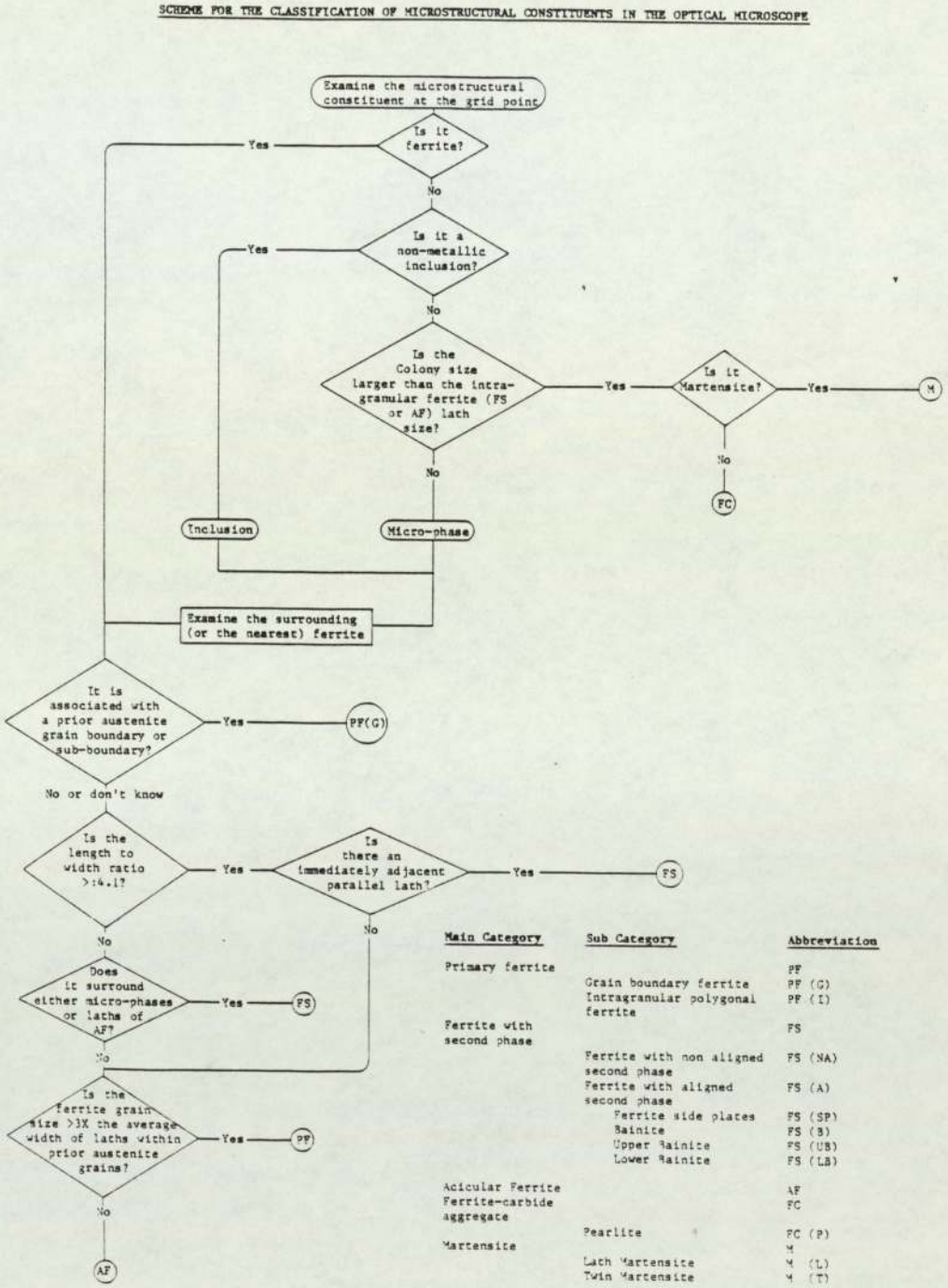

Figure No. 2.1

Flow Chart Of Microstructural Constituents For The Classification Of Ferrite Weld Metal Microstructures, Proposed In The IIW Scheme (6), Using An Optical Microscope.

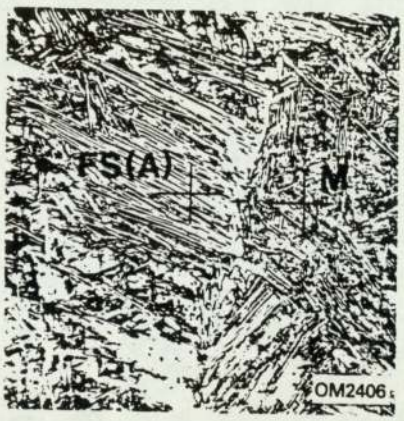

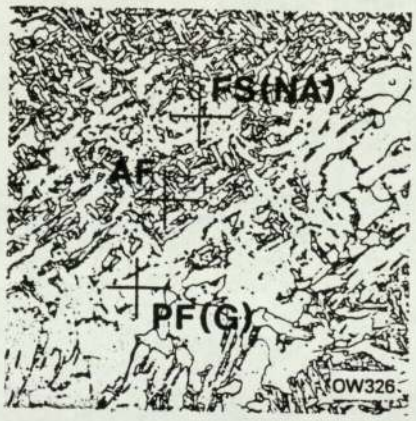

Key

PF	Primary ferrite
PF(G)	Grain boundary ferrite
PF(I)	Intragranular polygonal ferrite
AF	Acicular ferrite
FS(A)	Ferrite with aligned second phase
FS(NA)	Ferrite with non-aligned second phase
FC	Ferrite carbide aggregate (includes pearlite)
M	Martensite

20µm

As-deposited weld microstructures showing the various microstructural constituents.

Figure No. 2.2

IIW Scheme For The Classification Of Microstructural Constituents In Ferritic Steel Weld Metal Using An Optical Microscope (6).

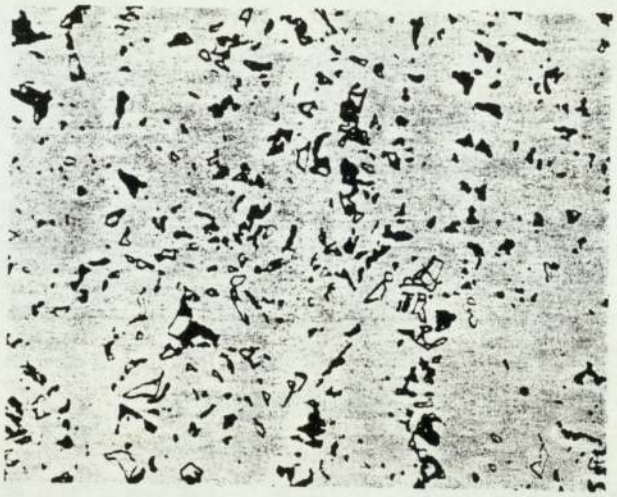

A. Dark Etching Microphase Classified As Carbides.

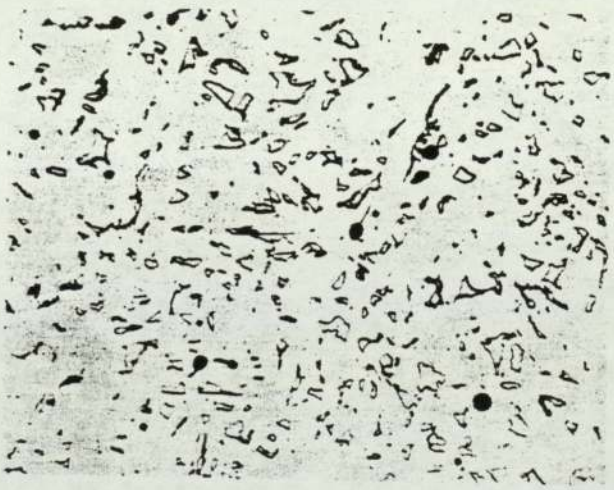

B. Light Etching Microphase Surrounded By Dark Band, Classified As Lath Martensite.

Mag. X2000.
Etchant, Picral.

Figure No. 2.3

Microphase Types Observed In Carbon Steel Weld Metal, (16).

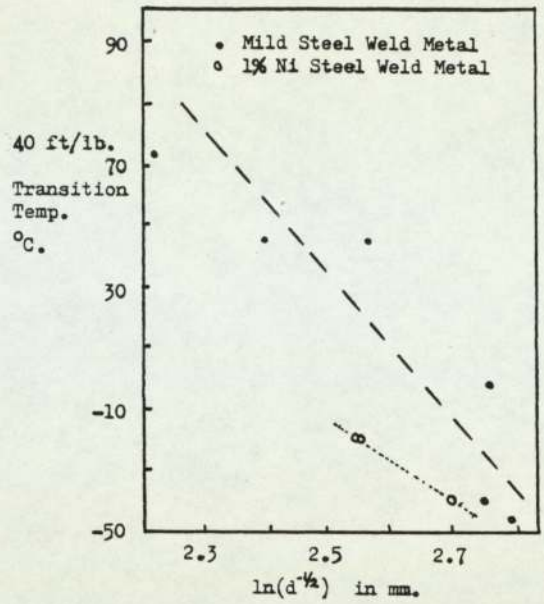

Figure No. 2.4

The Influence Of Ferrite Grainsize On Toughness, (18).

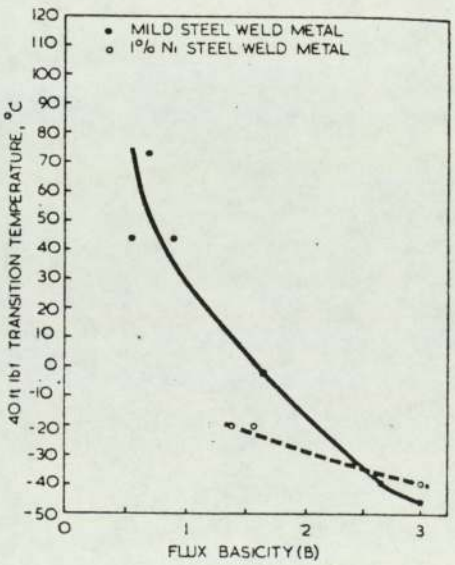

Figure No. 2.5

The Influence Of Flux Basicity On Weld Metal Toughness,(18).

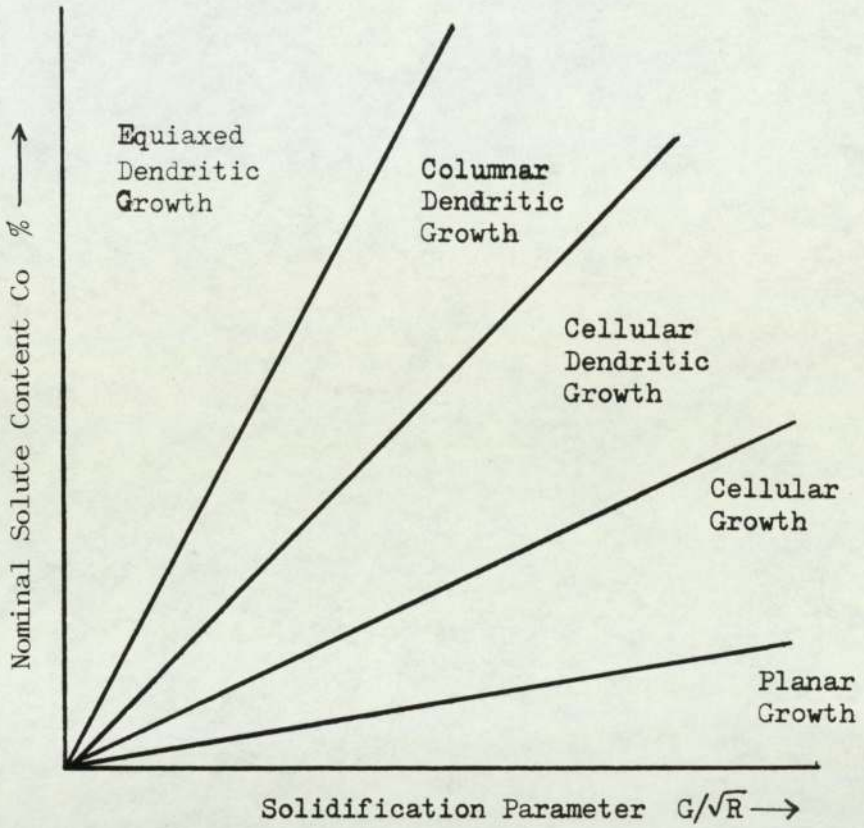

Figure No. 2.6

The Influence Of Composition And Solidification Parameter On The Solidification Structure, (23). G Is The Temperature Gradient And R Is The Growth Rate.

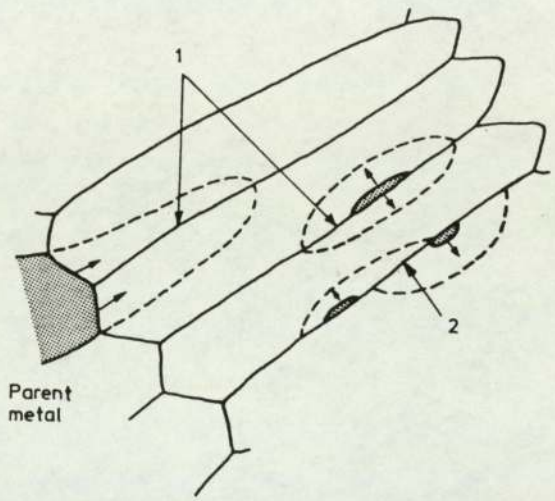

1 Growth of columnar austenite grains from columnar δ ferrite solidification structure showing how δ ferrite boundaries may be either lost (1) or preserved (2)

Figure No. 2.7

Mechanisms For Austenite Grain Development In Weld Metal Which Initially Solidifies As Delta Ferrite, (15).

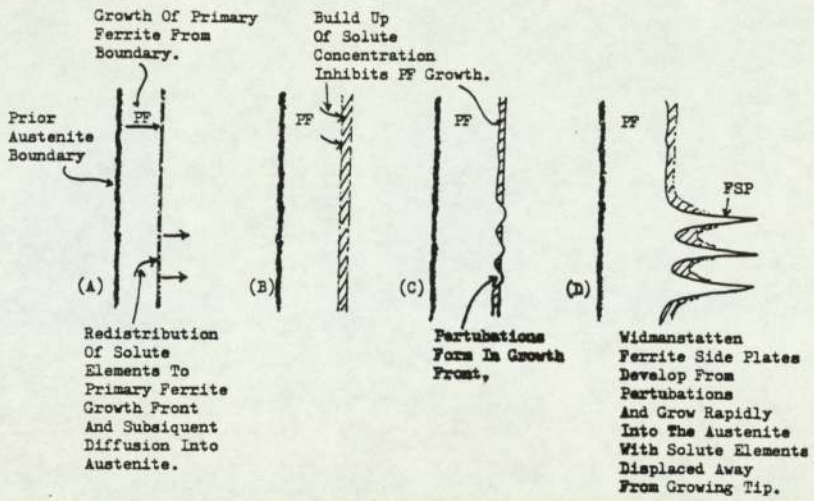

Figure No. 2.8a

Mechanism For The Formation Of Ferrite Side Plate Structures In Weld Metal, Proposed By Rasenen et al (36).

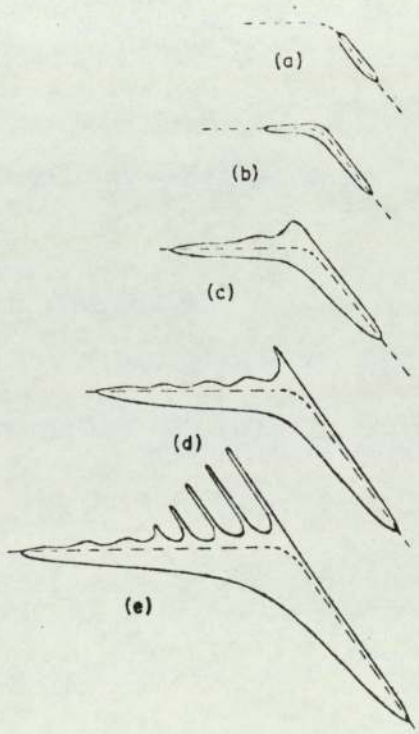

Figure No. 2.8b

Mechanism For The Formation Of Ferrite Side Plate Structures Proposed By Townsend et al (44).

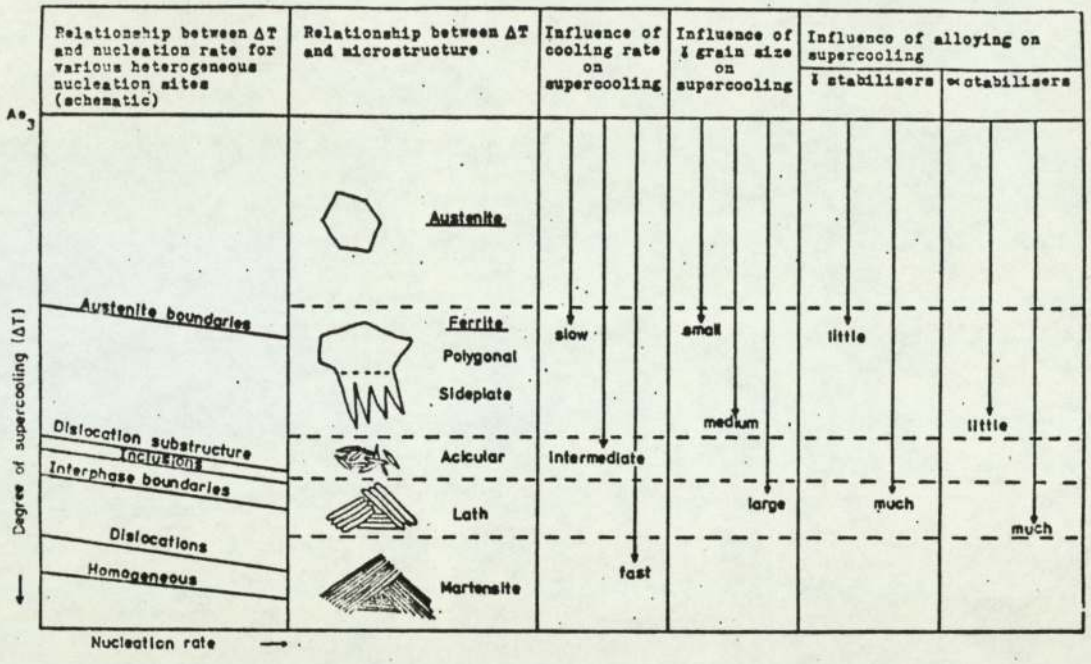

Figure No. 2.9

Schematic Model For Microstructural Development In Weld Metal, Proposed By Harrison (50).

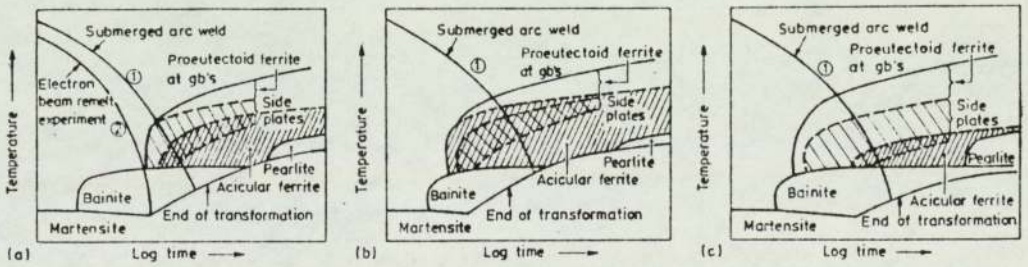

Figure No. 2.10

Schematic CCT Diagrams, Proposed By Abson (46), Indicating The Effect Of Oxygen Content And Corresponding Inclusion Population On Weld Metal Microstructures.

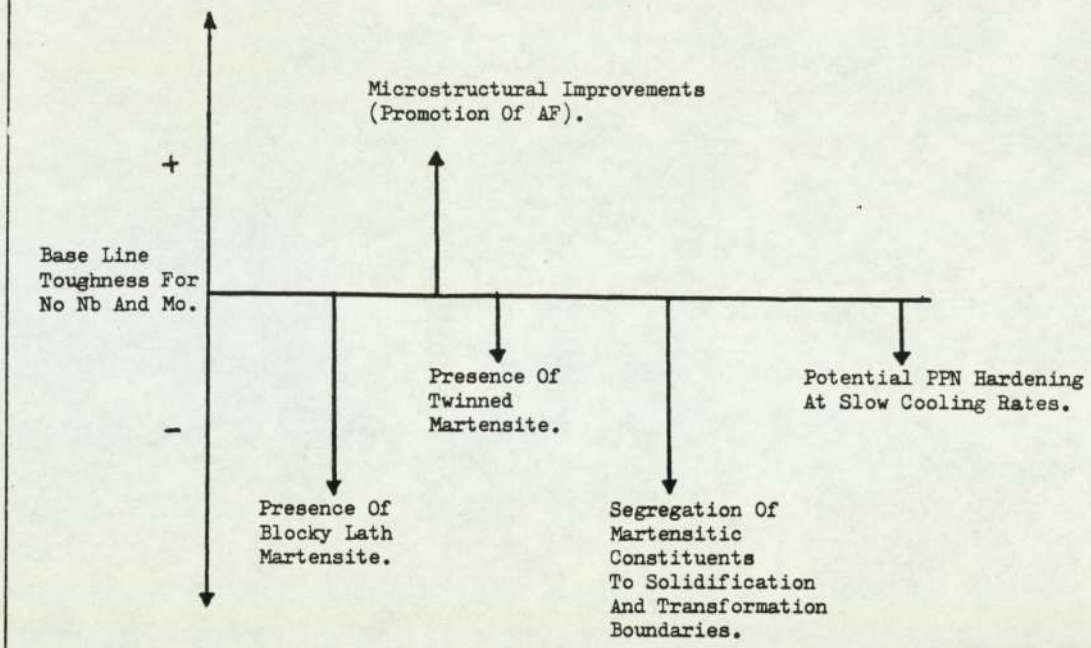

Figure No. 2.11a

Vector Diagram Showing The Influence Of Nb On The Toughness And Microstructure Of Weld Metal, Proposed By Garland (16).

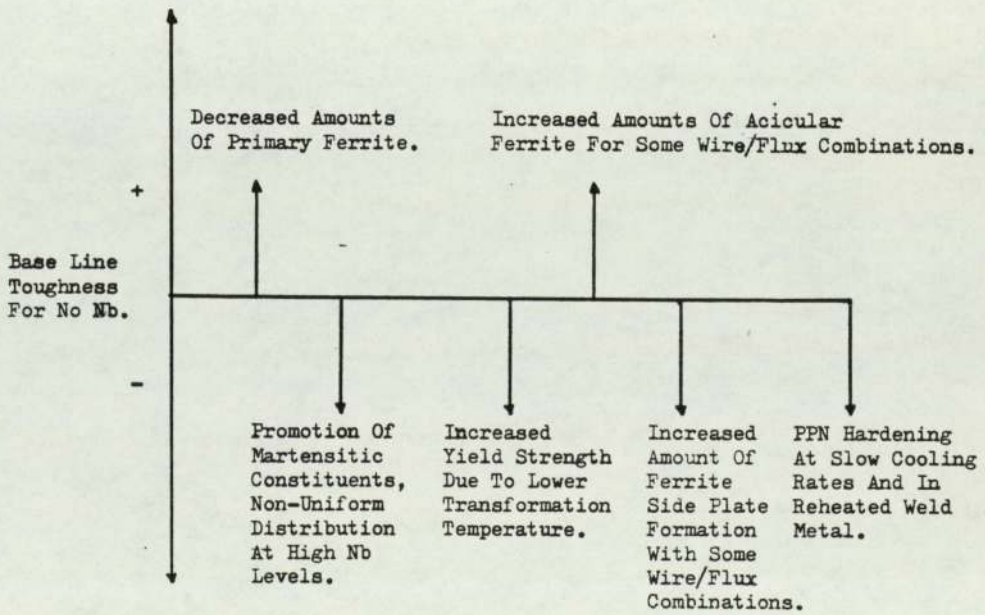

Figure No. 2.11b

Vector Diagram Showing The Influence Of Nb, Modified By Dolby (88).

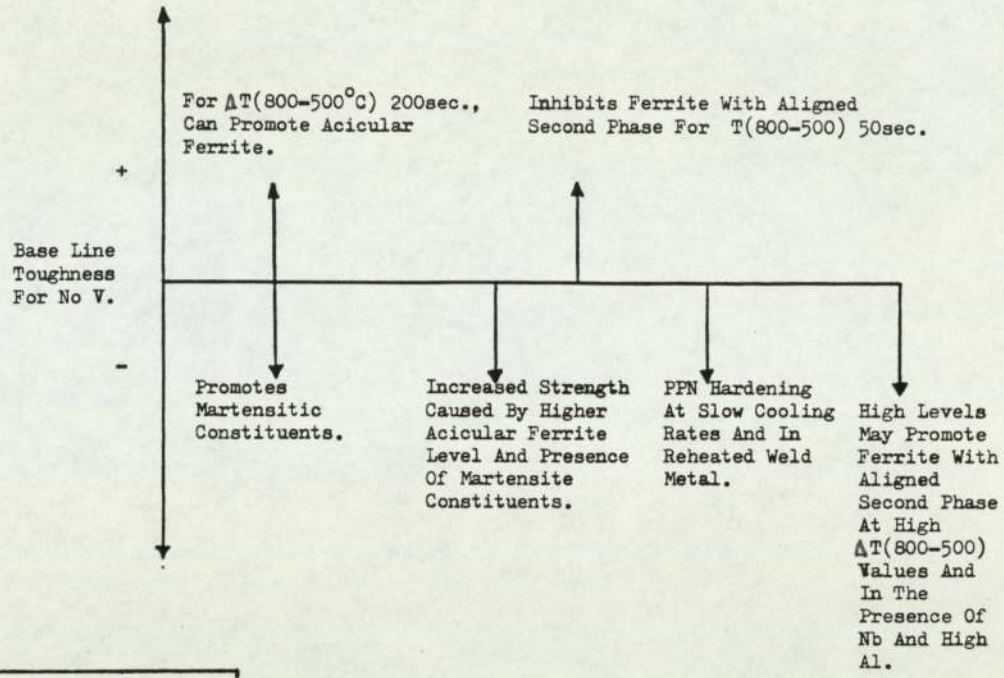

Figure No. 2.12

Vector Diagram Showing The Influence Of V On Toughness And Microstructure In Weld Metal, Proposed By Dolby (88).

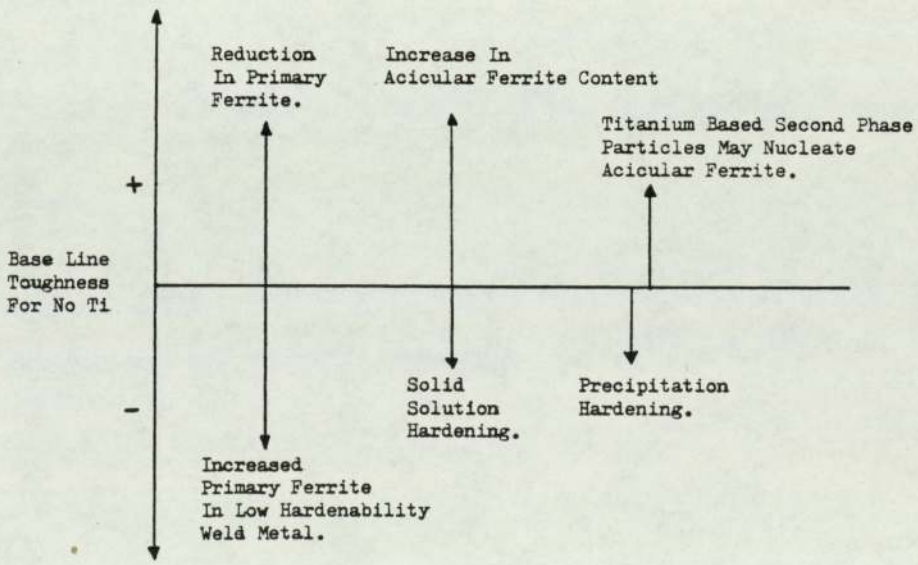

Figure No. 2.13

Vector Diagram Showing The Effect Of Ti On Toughness And Microstructure In Weld Metal.

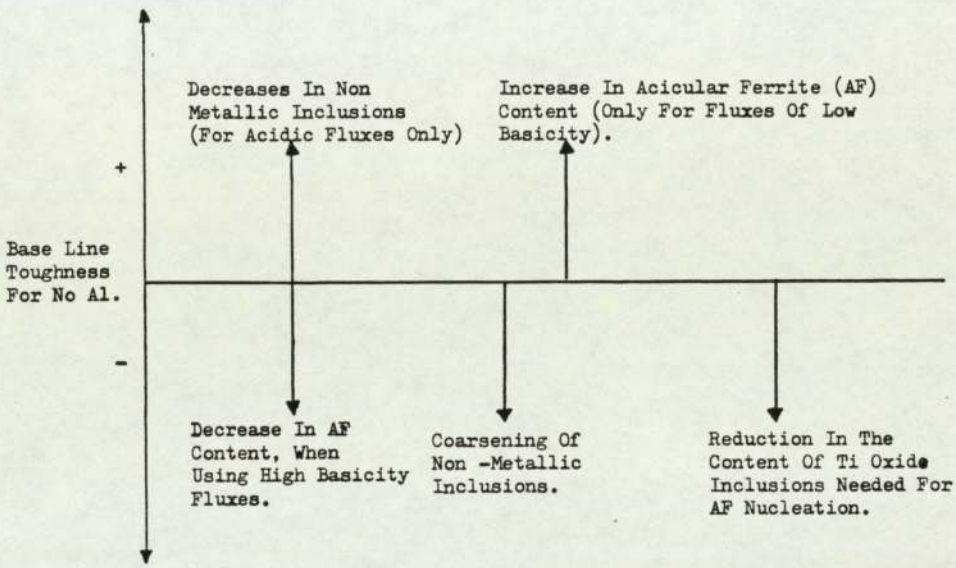

Figure No. 2.14

Vector Diagram Showing The Effects Of Al On Toughness And Microstructure In Weld Metal, Proposed By Hannerz (101).

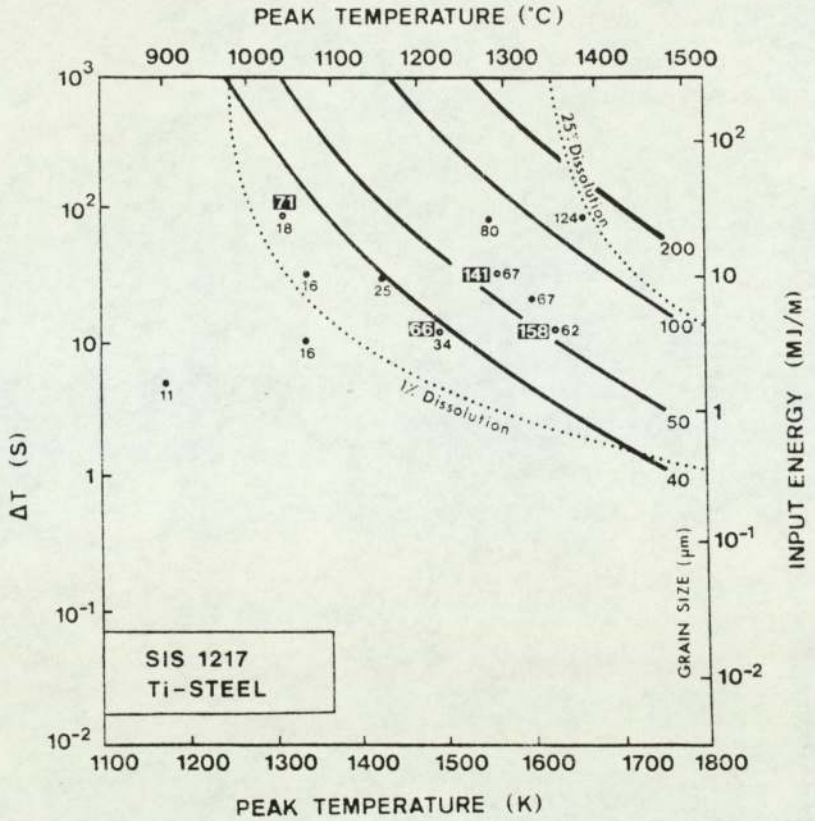

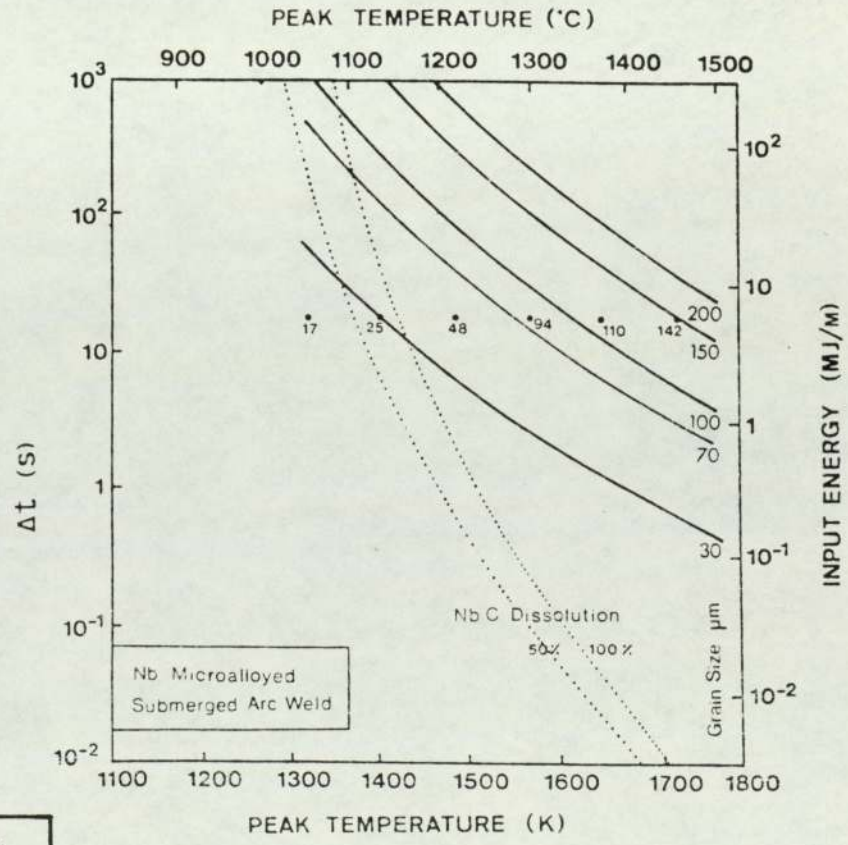

Figure No. 2.15

Grain Growth Diagrams Showing The Influence Of TiN And NbC Second Phase Particles On Austenite Grain Coarsening In The HAZ, Constructed By Easterling et al (22).

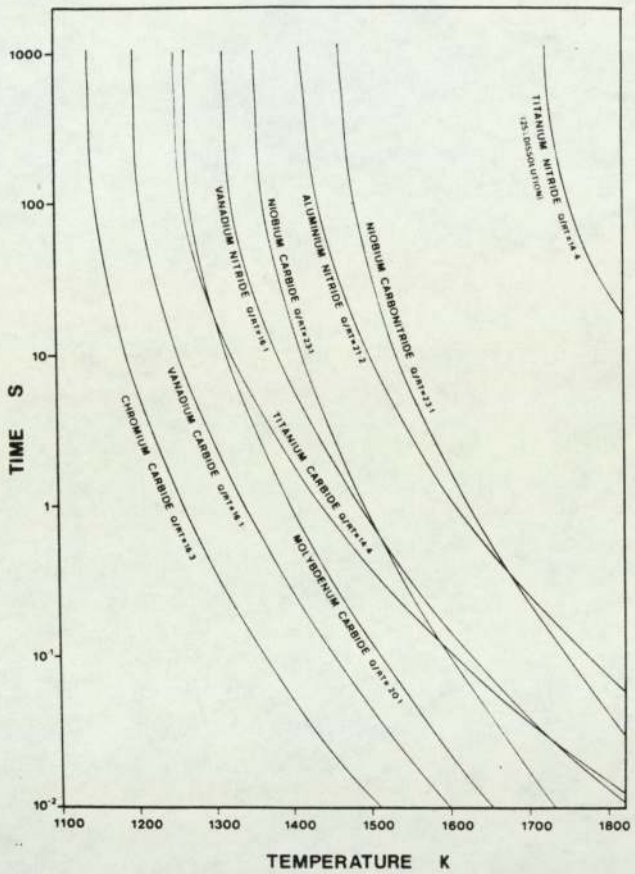

Figure No. 2.16

The Times Of Complete Dissolution Of Various Carbides And Nitrides As A Function Of Temperature, (22).

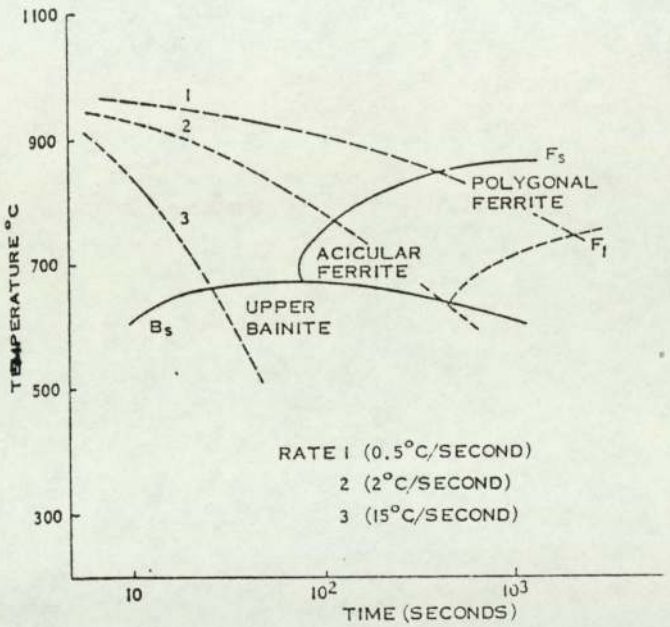

Figure No. 2.17

Schematic CCT Diagram For Weld Metal, Proposed By Glover et al(10)

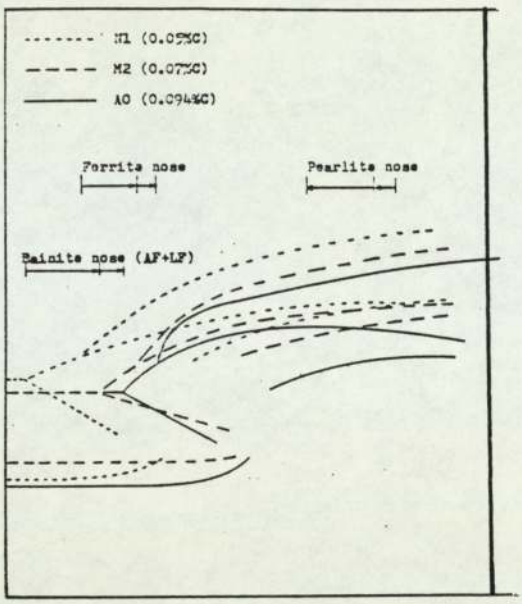

A. Carbon.

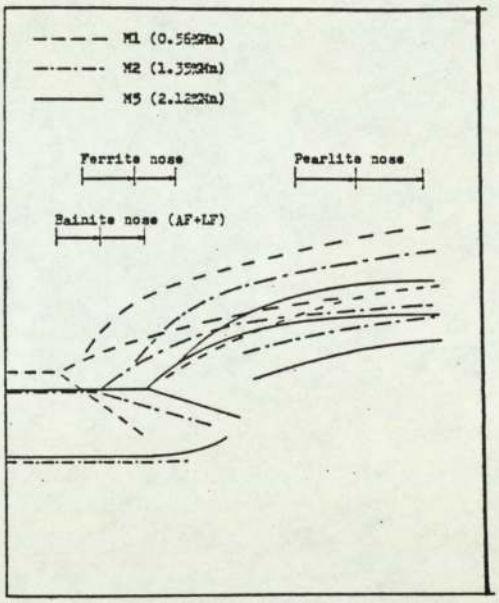

B. Manganese.

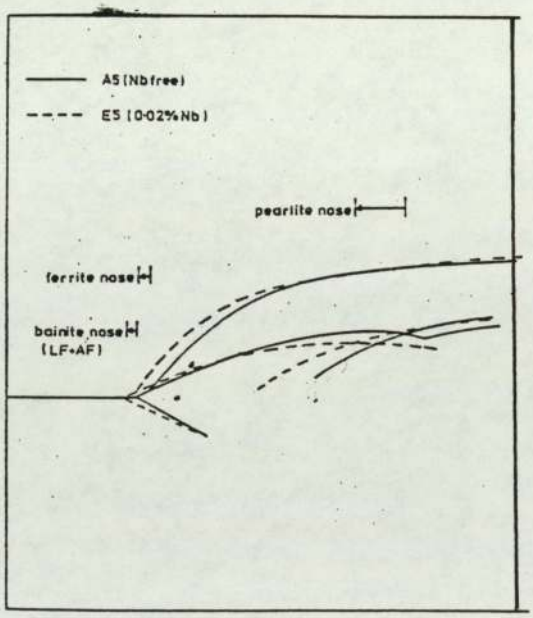

C. 0.02%wt Niobium.

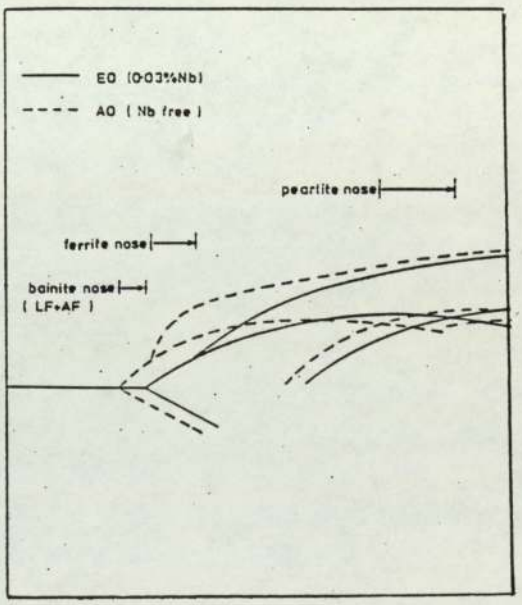

D. 0.03%wt Niobium.

Figure No. 2.18

CCT Diagrams Constructed By Harrison (12) Using A Simulative Reheating Technique, Said To Be Applicable To As-Deposited Weld Metal.

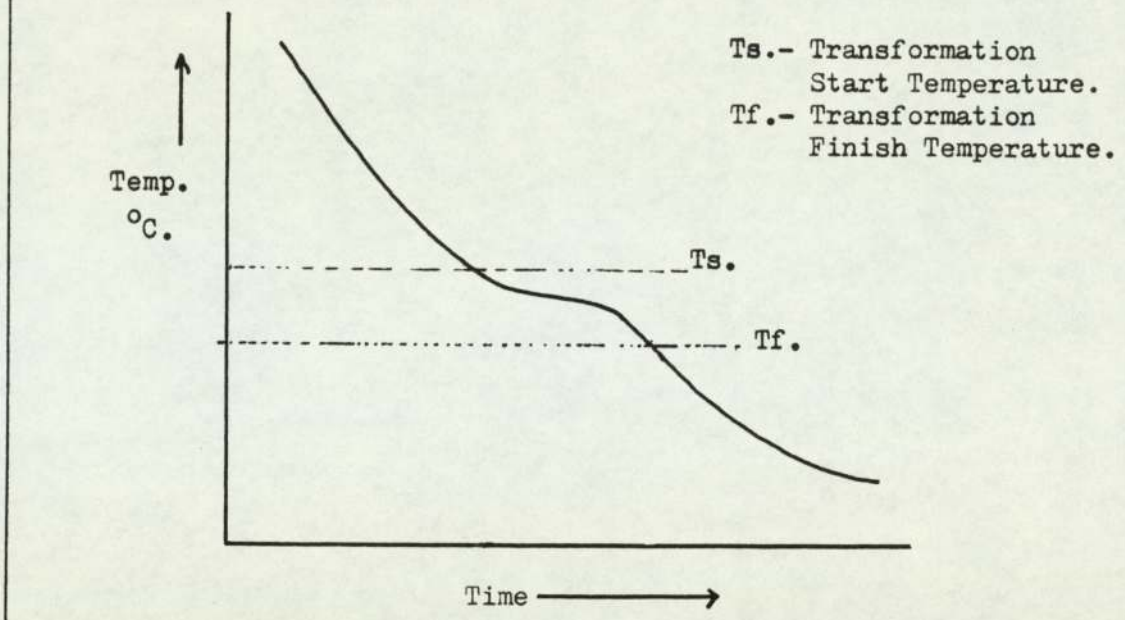

Figure No. 2.19

Schematic Cooling Curve Showing The Arrest In Temperature On Cooling, Corresponding To The Transformation From Austenite To Ferrite.

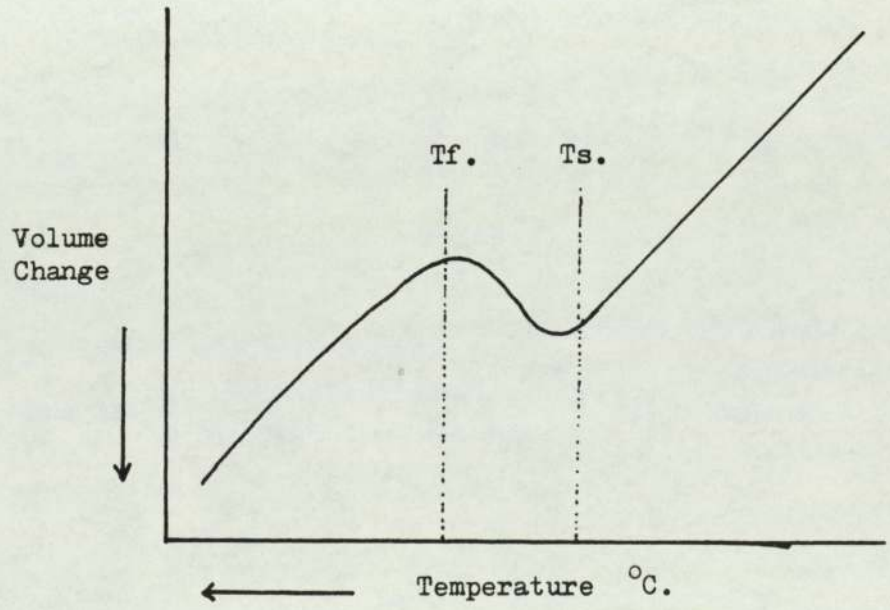

Figure No. 2.20

Schematic Diagram Showing The Change In Volume Associated With The Transformation From Austenite To Ferrite And Determined Using Dilatometry.

FIGURES FOR CHAPTER 3.

A. Primary Ferrite And Ferrite Side Plates.
Mag. X160.

B. Acicular Ferrite.
X350.

C. Lath Ferrite.
X350.

D. Ferrite Carbide Aggregate.
X350.

E. Pearlite.
X160.

Etchant, 2% Nital.

Figure No. 3.1

Representative Photomicrographs Of Ferritic Constituents Identified In The Simulated As-deposited And Reheated Weld Metal.

FIGURES FOR CHAPTER 4.

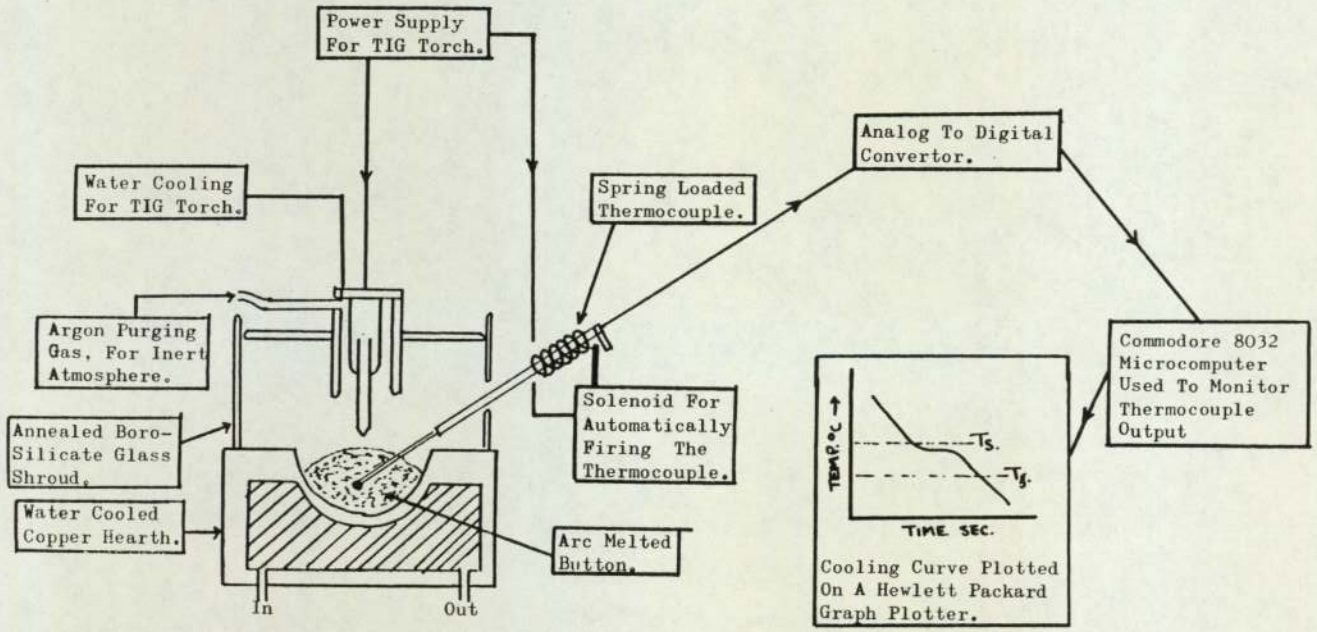

Figure No. 4.1

Schematic Diagram Of Arc Melting Apparatus Used For Simulating As-Deposited Weld Metal.

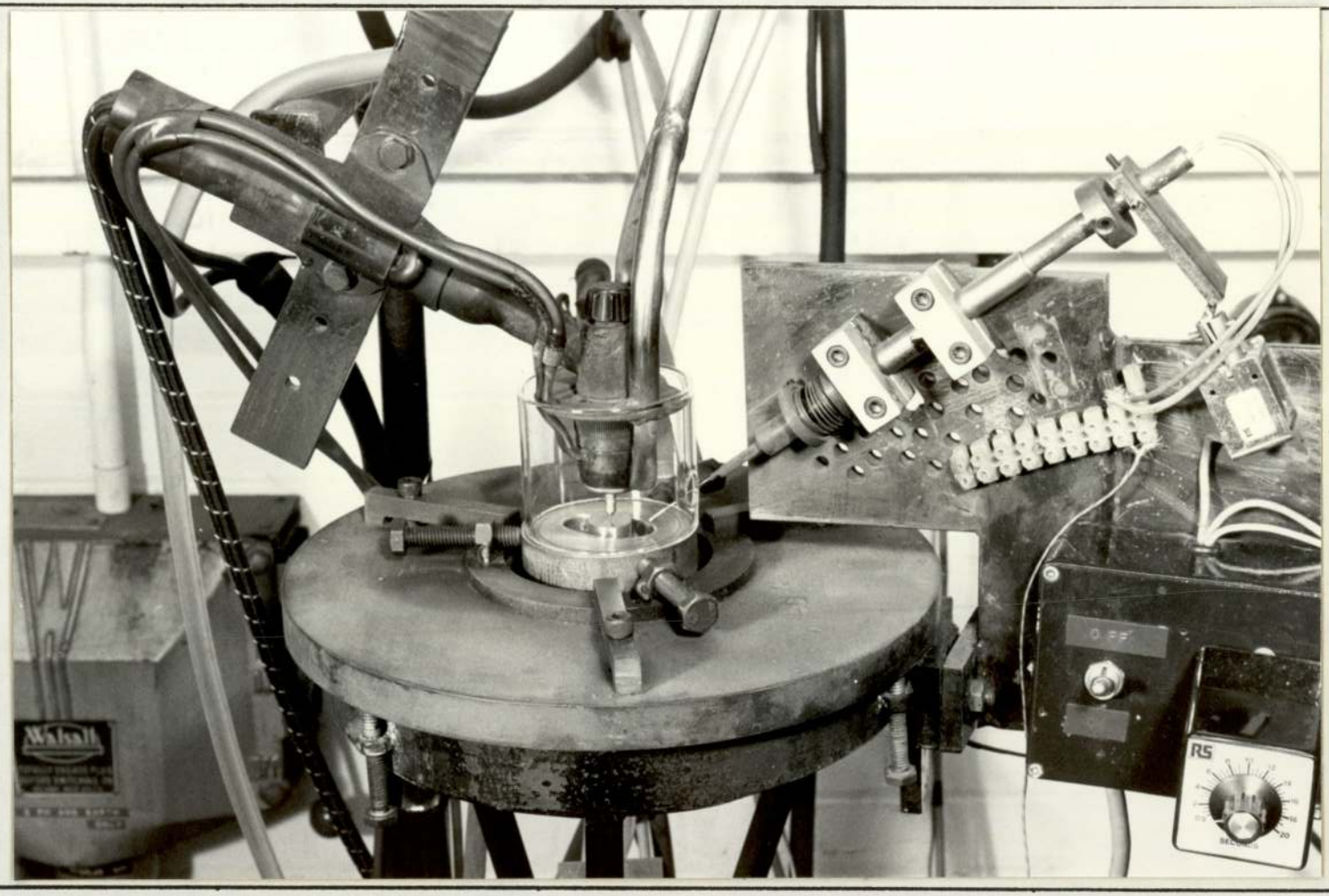

Figure No. 4.2

Photograph Of Arc Melting Apparatus.

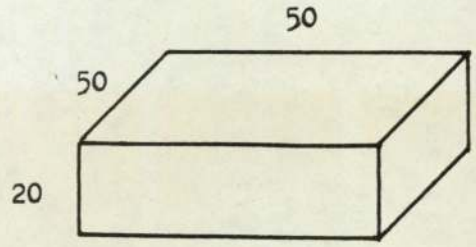

RQT-500 Specimen
Dimensions. (mm).

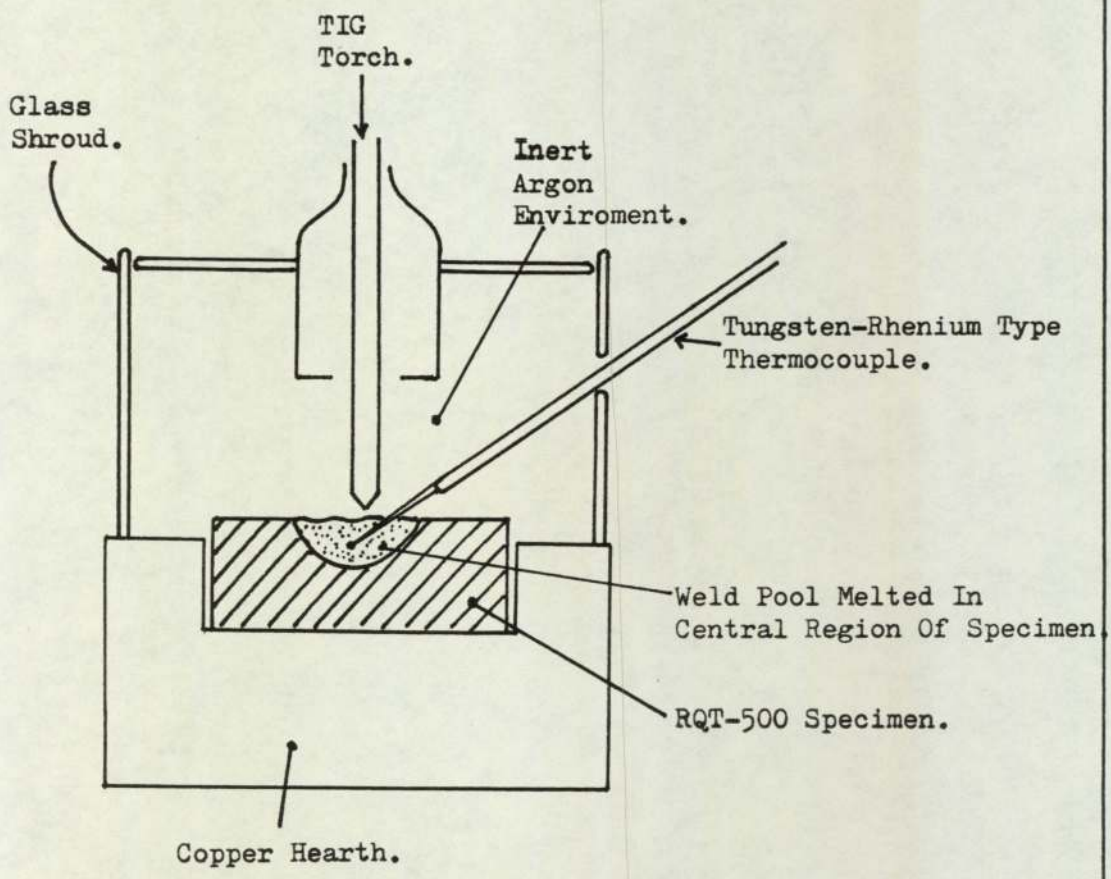

Figure No. 4.3

Test Arrangement For Producing "Real" Weld Metal, For Comparison Of The Ferritic Microstructure Formed With The Simulated As-Deposited Weld Metal Of The Same Material.

A. Real Weld Metal Produced Using A Tungsten Inert Gas Process And Welding Conditions Which Gave A Cooling Rate Of 4°C/sec. ($\Delta T_{800-500°C}$).

B. Simulated As-Deposited Weld Metal, With A Cooling Rate Of 4°C/sec. ($\Delta T_{800-500°C}$).

Mag. X160.
Etchant, 2% Nital.

Figure No. 4.4

Representative Photomicrographs Comparing The Ferrite Microstructures Formed In Real And Simulated As-Deposited RQT-500 Weld Metal.

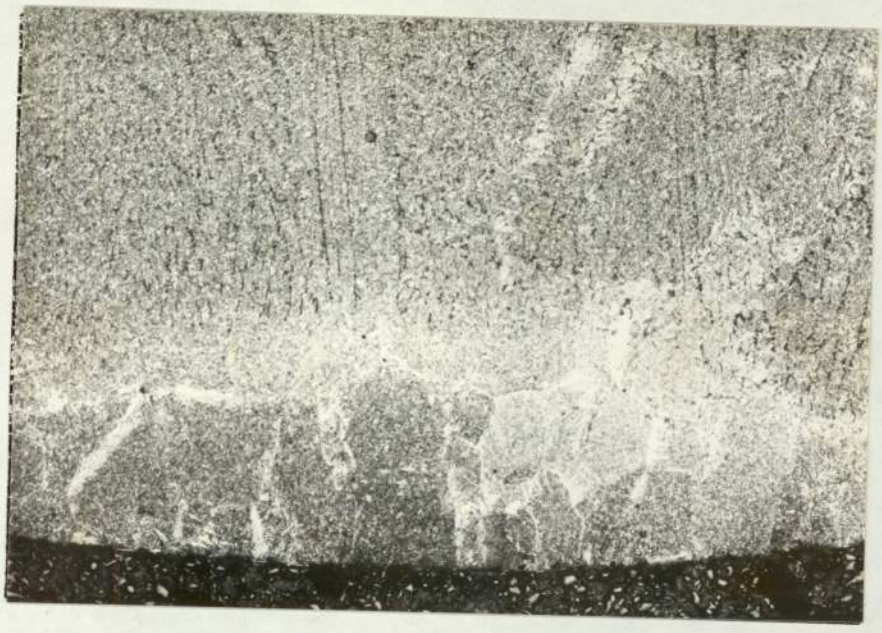

Figure No. 4.5

Photomicrograph Showing The Fine Prior Austenite Grain Size At The Base Of The Arc Melted Buttons From Which Columnar Growth Occurs.

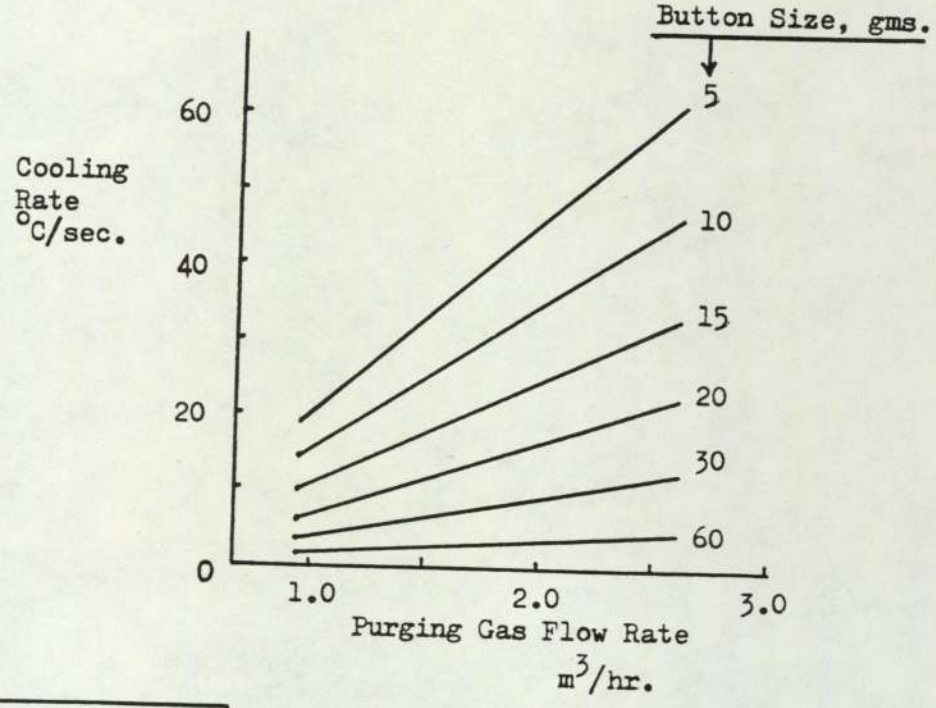

Figure No. 4.6

The Influence Of Button Size And Purging Gas Flow Rate On The Cooling Rate.

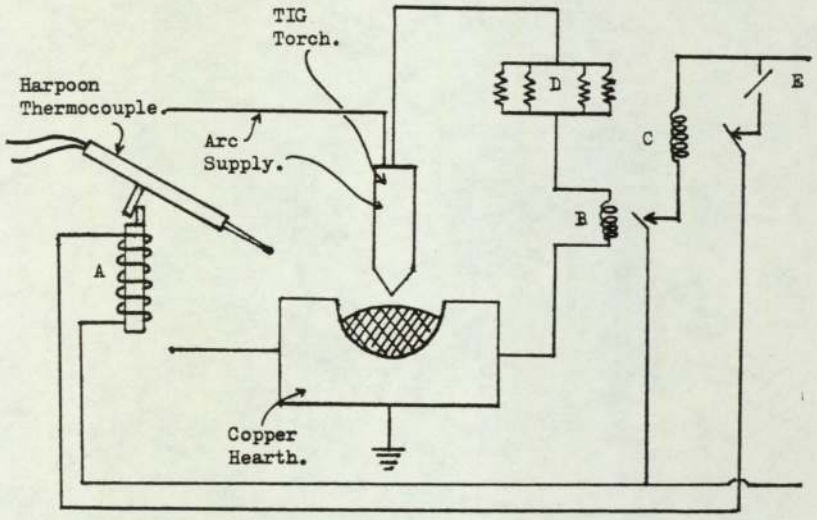

Operation. Solenoid Plunger 'A' Holds Thermocouple In Spring Loaded Position.
Initially Arc Relay 'B' Open And Harpoon Relay 'C' Closed.
When Arc Struck, Arc Relay Energises And Closes.
Restistors 'D' Prevent Damage To Relays.
When Arc Relay Closes, Harpoon Relay Energises And Opens.
Open Harpoon Relay Isolates Solenoid Circuit.
When Solenoid Isolated, Control Switch 'E' Set To 'On'.
Switch Arc Off, De-energises The Arc Relay Which Opens,
This Closes The Harpoon Relay Which Closes, Causing The
Solenoid To Energise, Moving The Plunger Down And Firing
The Thermocouple.

Figure No. 4.7

Harpoon Thermocouple Arrangement For Automatically Firing The Thermocouple Into The Arc Melted Button.

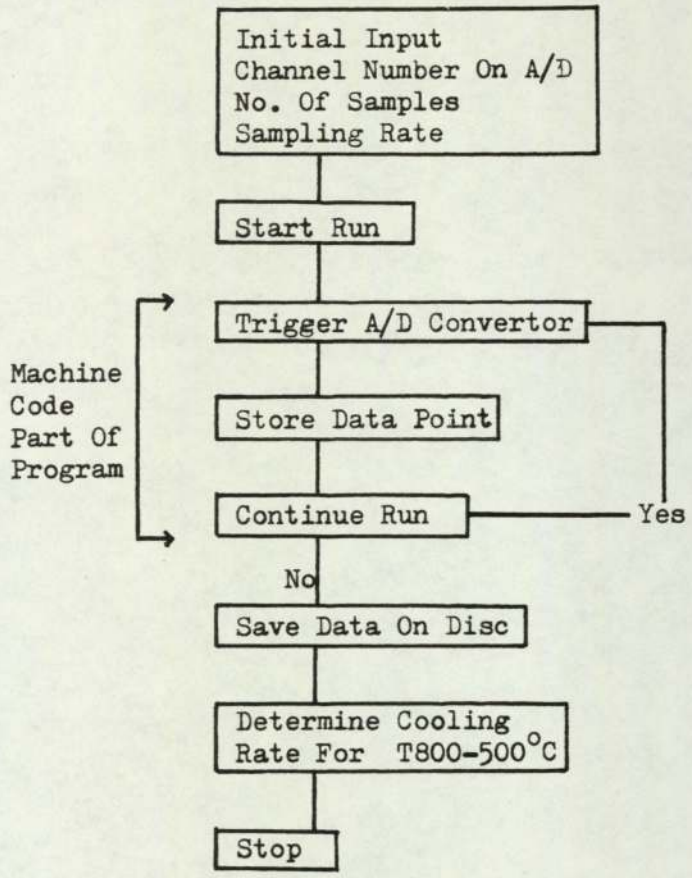

A. Flow Chart For Temperature Recording Program.

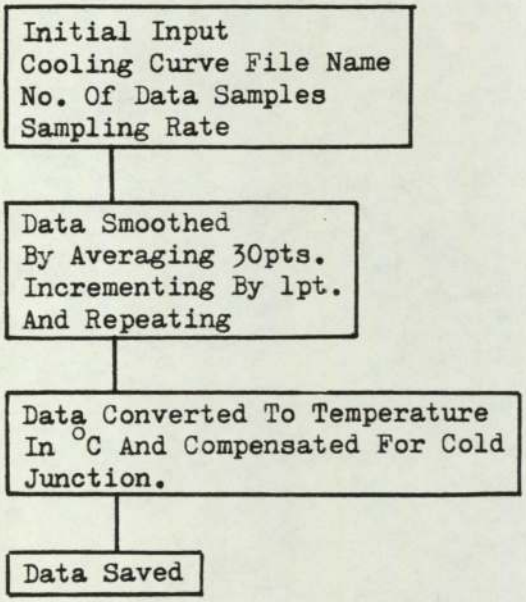

B. Flow Chart For Processing The Temperature Recording.

Figure No. 4.8

Simplified Flow Charts Of Computer Programs Used To Record The Temperature Of The Arc Melted Buttons, On A Commodore Microcomputer Via An A/D Convertor And Subsequently Process This Data.

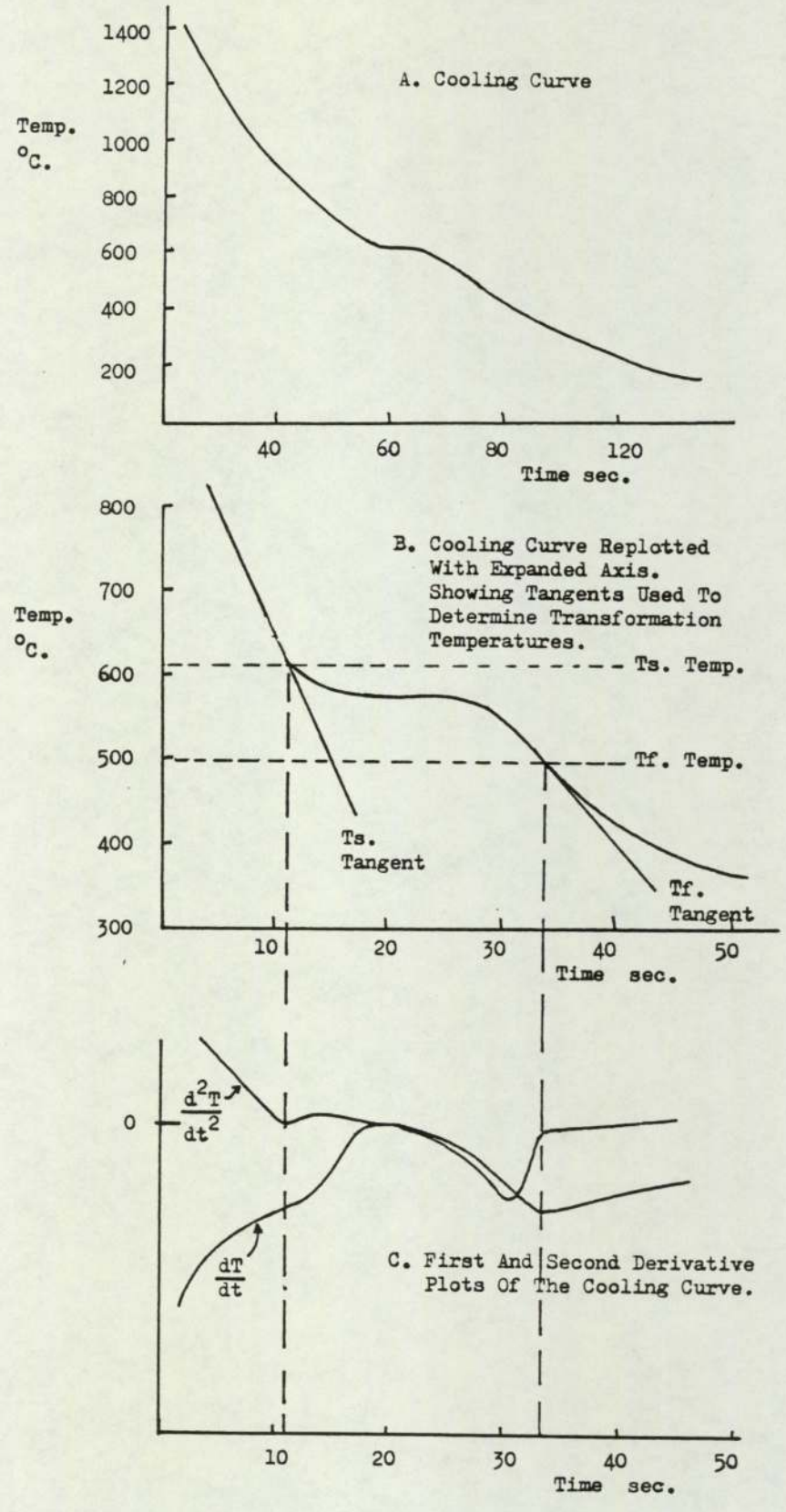

Figure No. 4.9

Determination Of The Transformation Start (Ts) And Finish (Tf) Temperatures, Using The Tangent Method And First And Second Derivative Plots.

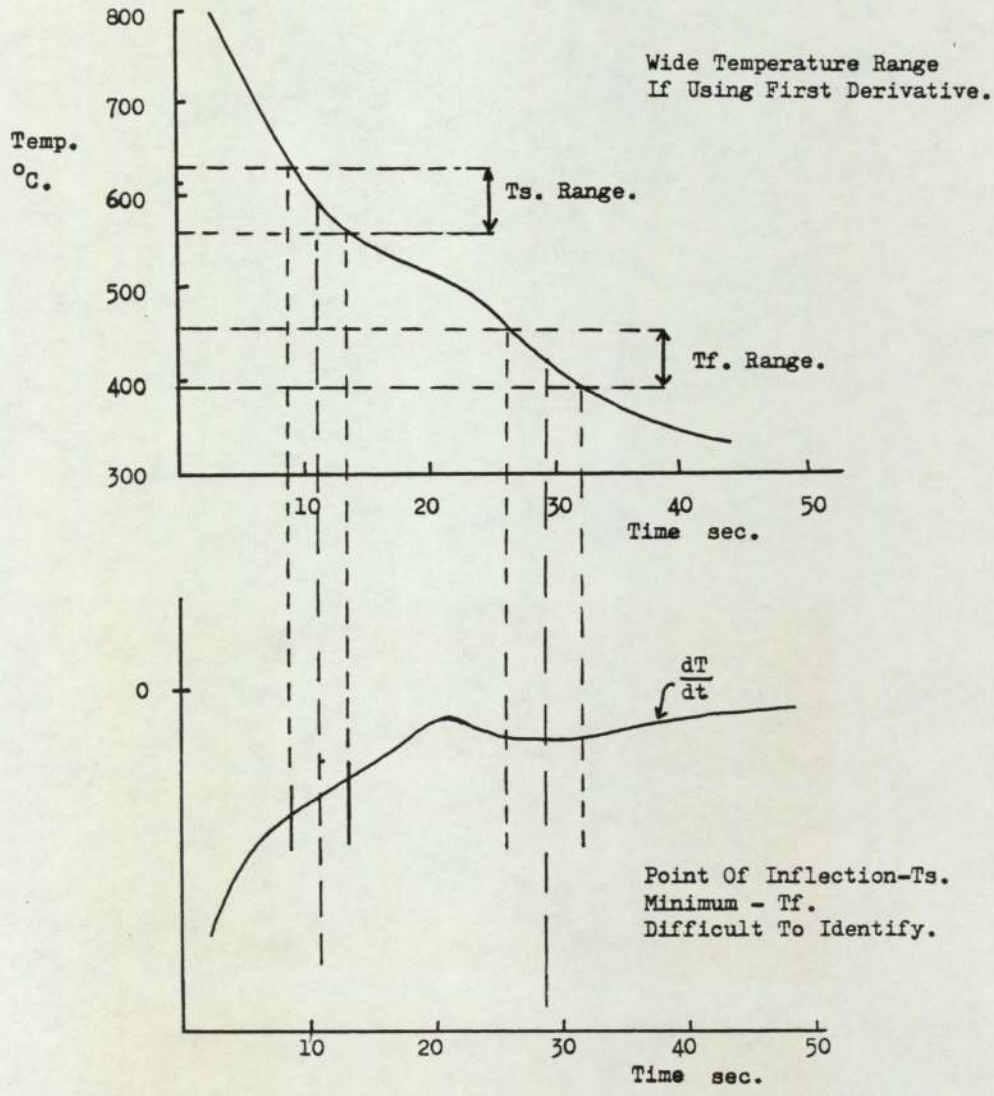

Figure No. 4.10

Diagram Showing The Problem Of A Large Temperature Range Associated With The Determination Of The Transformation Start (Ts) And Finish (Tf) Temperatures, When Using First Derivative Plots For Cooling Curves With Less Significant Arrests.

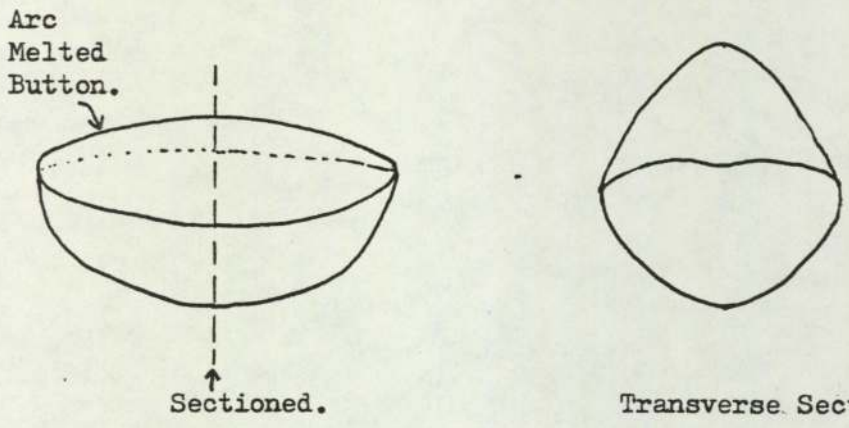

Figure No. 4.11

Sectioning Of The Arc Melted Button For Metallographic Examination.

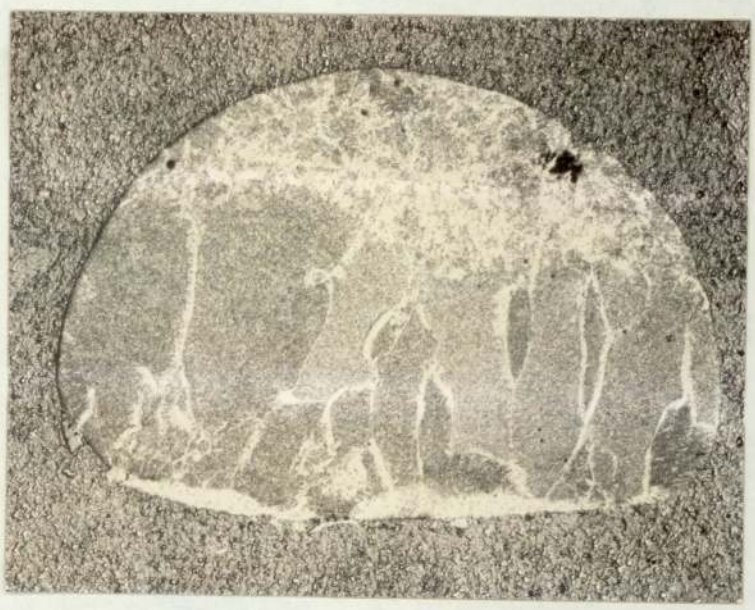

Figure No. 4.12

Macrograph Of A Transverse Section Through The Arc Melted Button, Showing The Prior Austenite Grain Distribution.

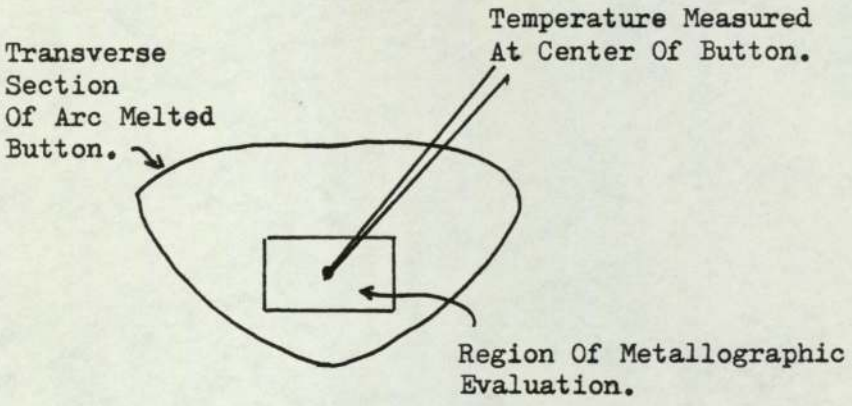

Figure No. 4.13

Central Region Of The Arc Melted Button In Which The Ferritic Microstructural Constituents Were Determined.

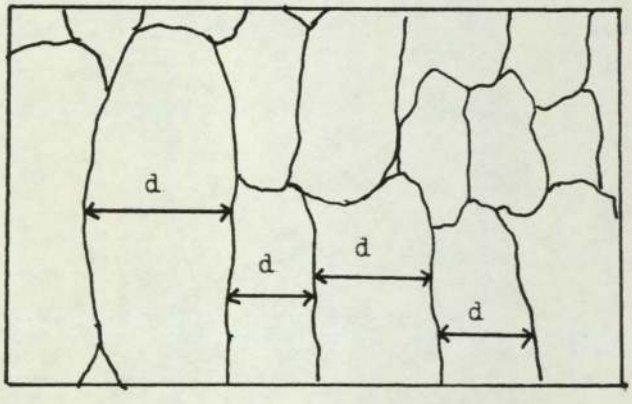

The Prior Austenite Grain Size Was Measured Across The Short Diameter 'd', At The Widest Point. The Average Diameter Was Determined For The Grains Within The Central Region Of The Arc Melted Button.

Figure No. 4.14

Prior Austenite Grain Size Determination In The Arc Melted Button.

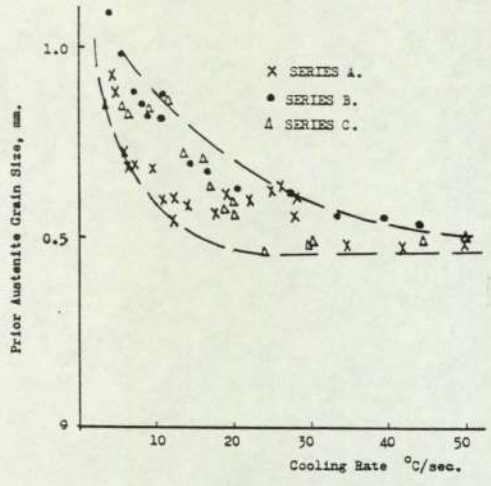

A. 0.027%wt V (Series B)
And 0.088%wt V (Series C).

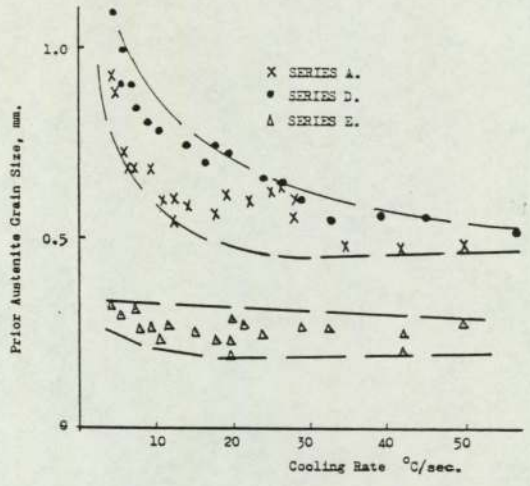

B. 0.020%wt Ti (Series D)
And 0.063%wt Ti (Series E).

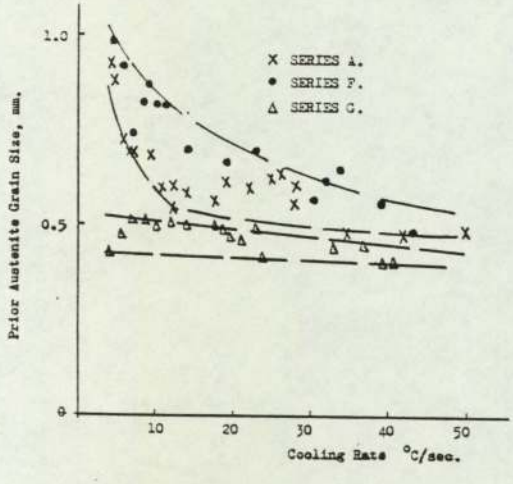

C. 0.021%wt Nb (Series F)
And 0.053%wt Nb (Series G).

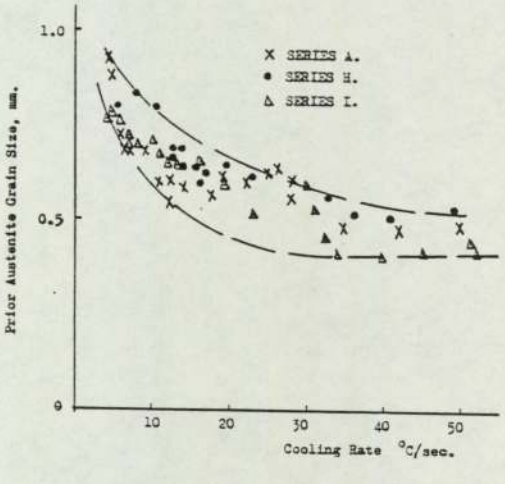

D. 0.024%wt Al (Series H)
And 0.063%wt (Series I).

Figure No. 4.15

The Influence Of Microalloying Additions On The Prior Austenite Grain Size Of Low Oxygen Content Simulated As-Deposited Weld Metal.

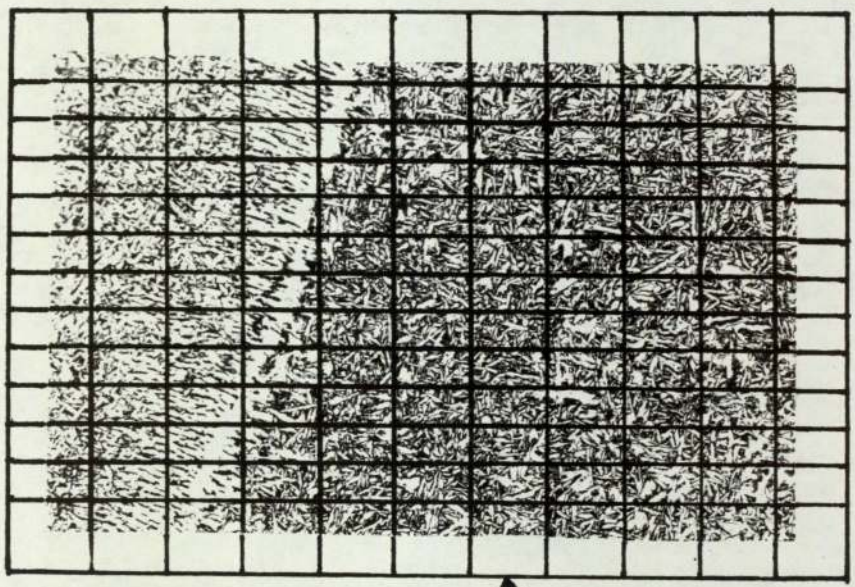

Perspects Grid Placed On
Micrograph And Phase Determined
At Each Intersection.

Figure No. 4.16

Point Counting Technique Used For Quantitative Metallographic Examination Of Specimens.

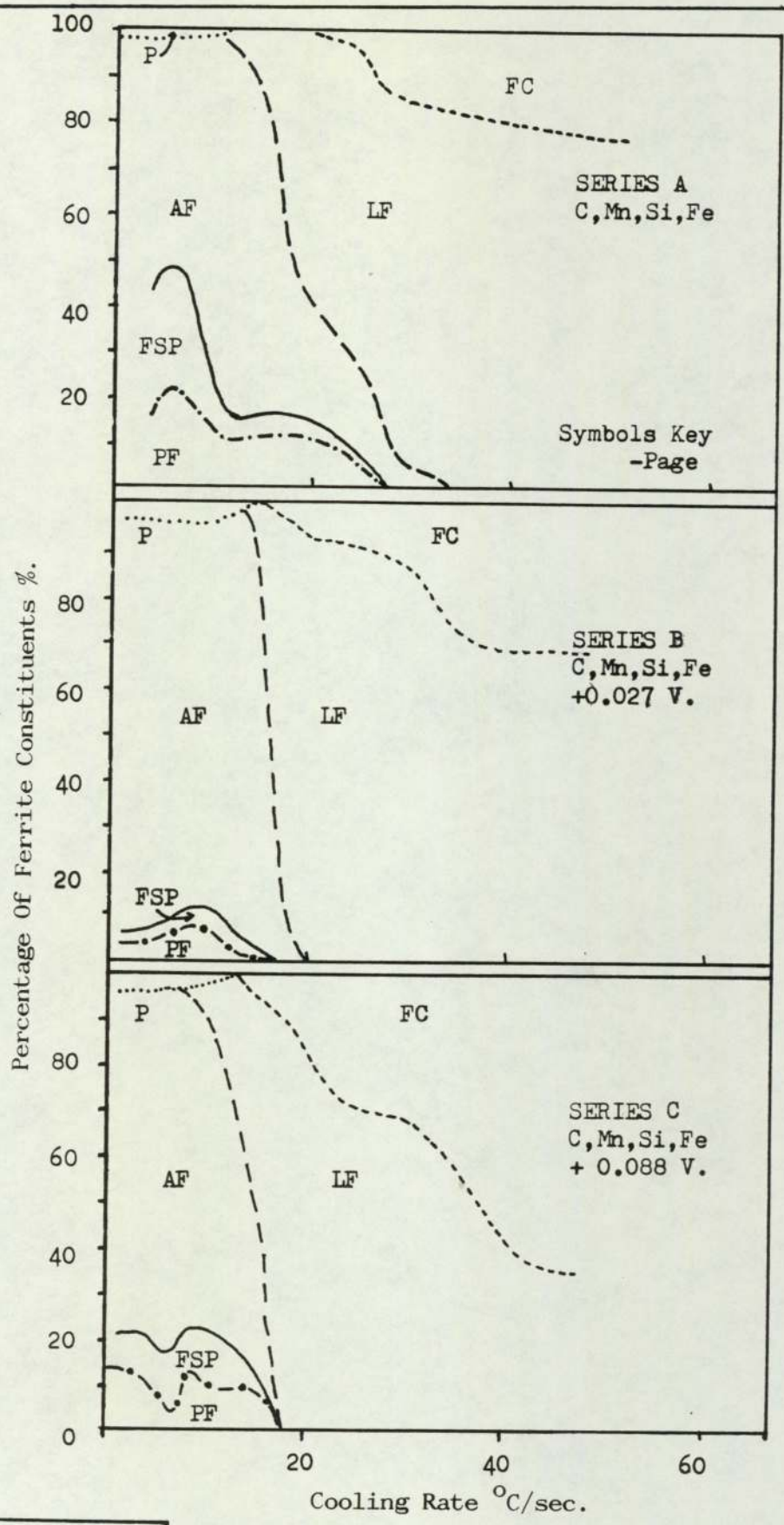

Figure No. 4.17

The Effect Of Increased V Concentration On The Type And Proportions Of Ferrite Constituents Formed In As-Deposited Simulated Weld Metal, With Low Oxygen Content.

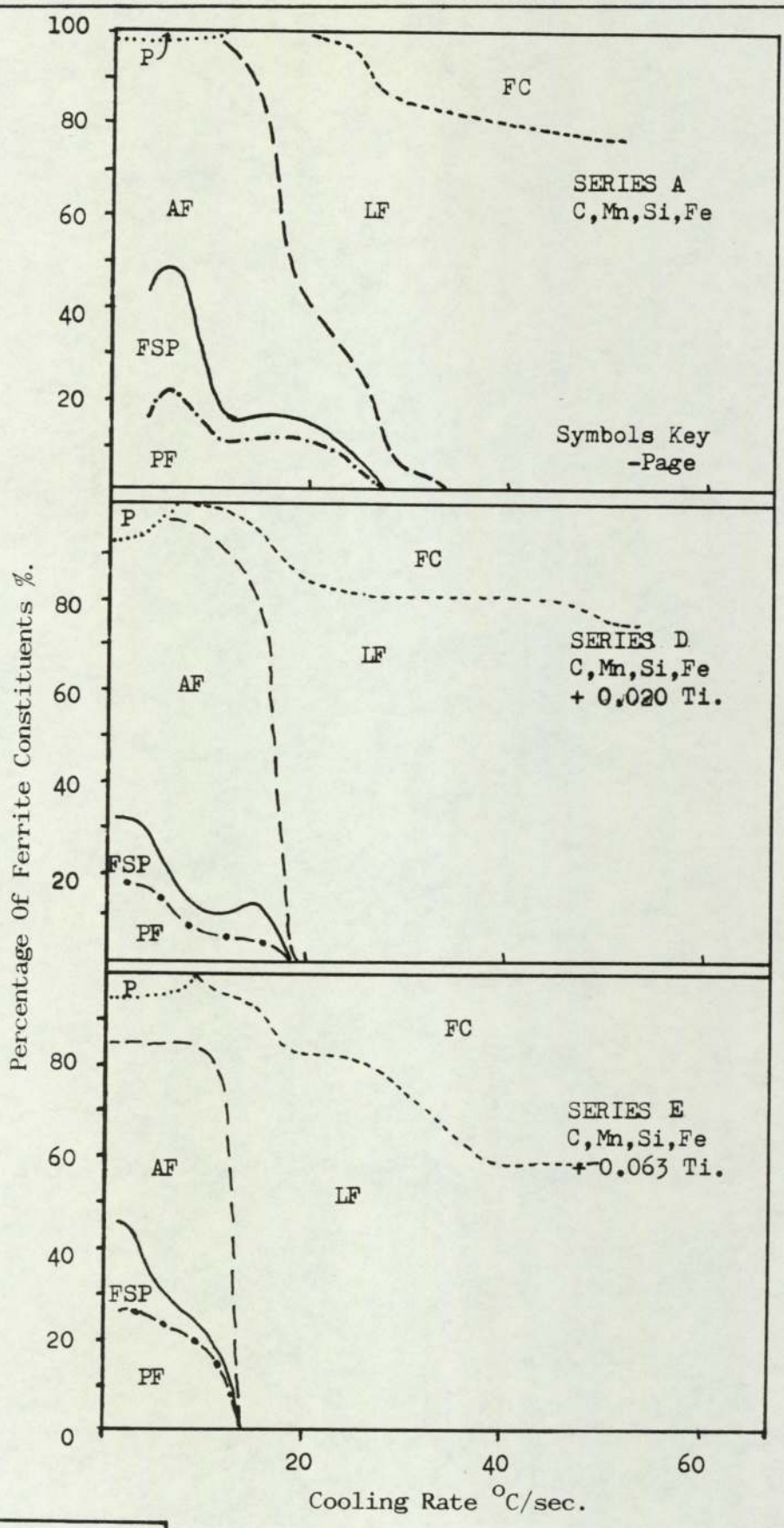

Figure No. 4.18

The Effect Of Increased Ti Concentration On The Type And Proportions Of Ferrite Constituents Formed In As-Deposited Simulated Weld Metal, With Low Oxygen Content.

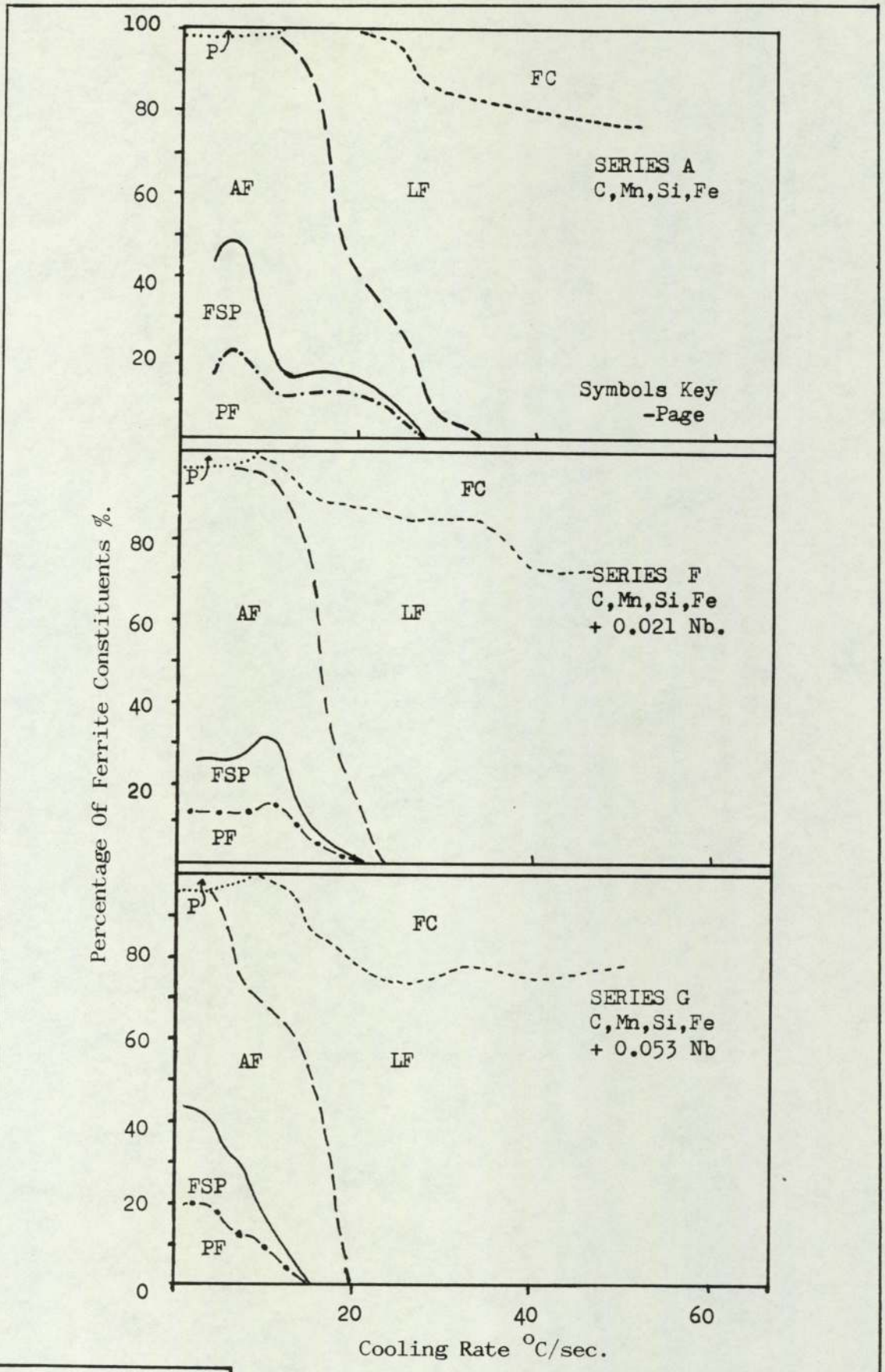

Figure No. 4.19

The Effect Of Increased Nb Concentration On The Type And Proportions Of Ferrite Constituents Formed In As-Deposited Simulated Weld Metal, With Low Oxygen Content.

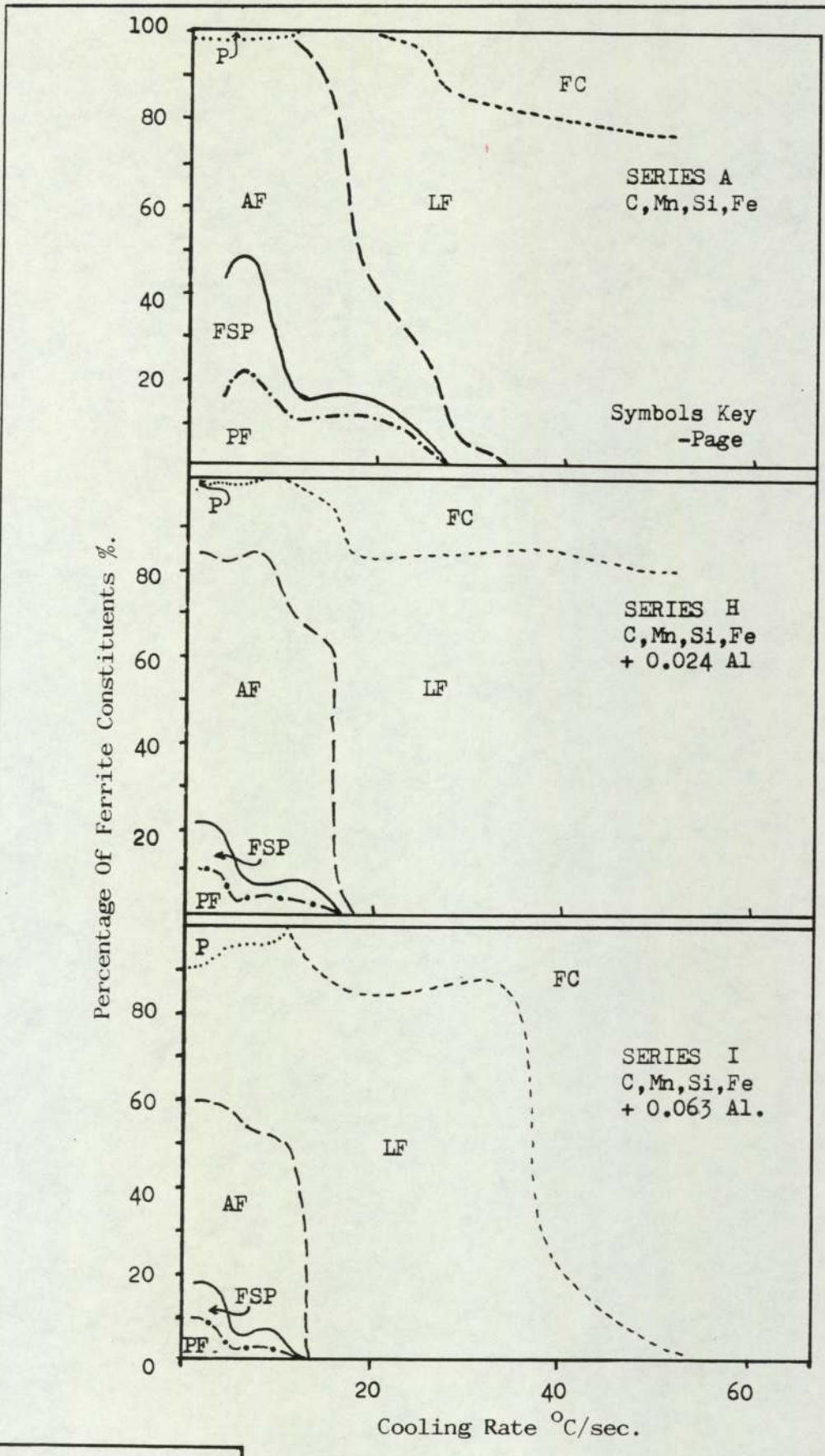

Figure No. 4.20

The Effect Of Increased Al Concentration On The Type And Proportions Of Ferrite Constituents Formed In As-Deposited Simulated Weld Metal, With Low Oxygen Content.

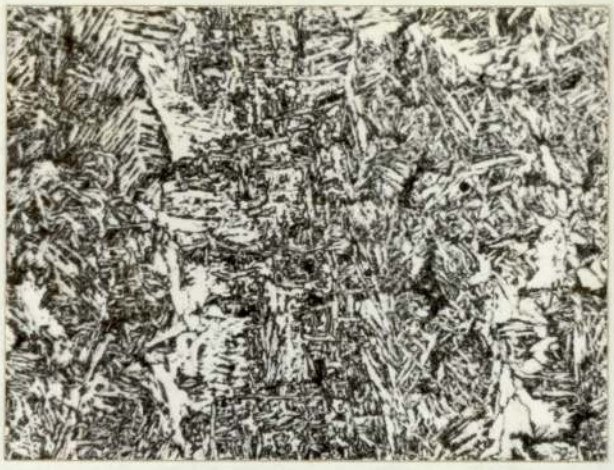

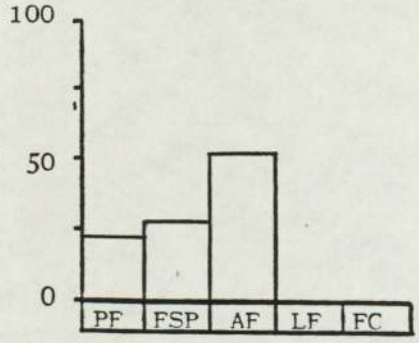

A. Specimen A11.
Cooling Rate(CR),
6.0°C/sec.

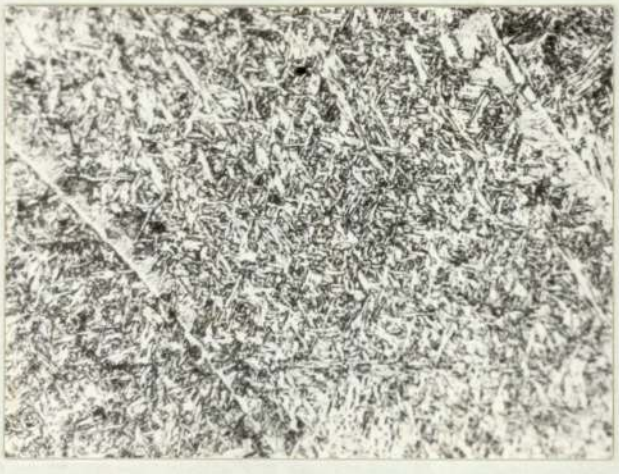

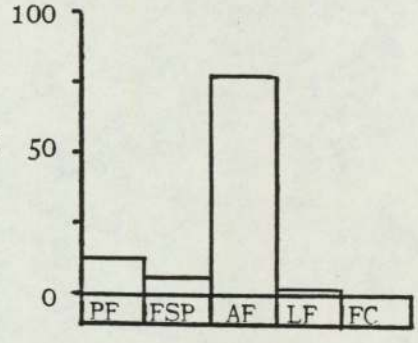

B. Specimen A12.
CR, 12°C/sec.

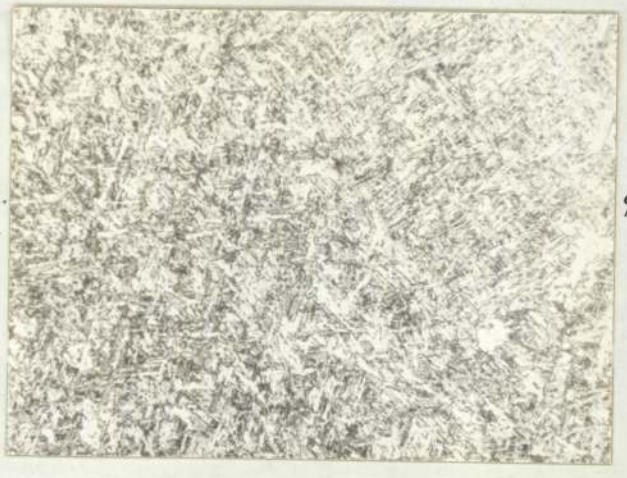

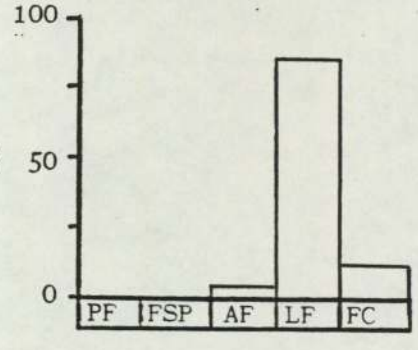

C. Specimen A18.
CR, 34.6°C/sec.

Mag. X160.
Etchant. 2% Nital.

Figure No. 4.21

Representative Photomicrographs Showing The Microstructures Formed In The Plain Carbon Manganese (Series A) Simulated Low Oxygen As-Deposited Weld Metal, With Increasing Cooling Rate.

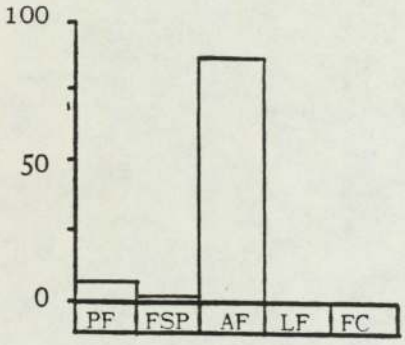

A. Specimen B8.
Cooling Rate(CR),
5.5°C/sec.

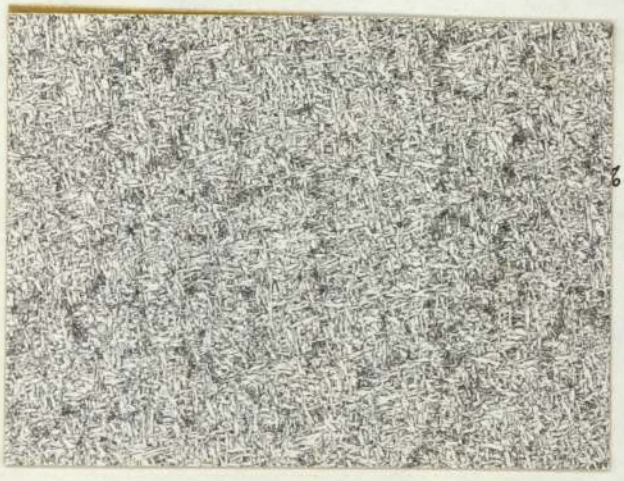

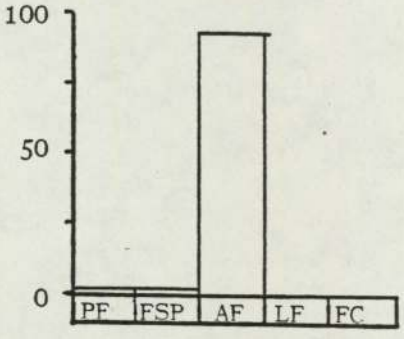

B. Specimen B5.
CR, 11.8°C/sec.

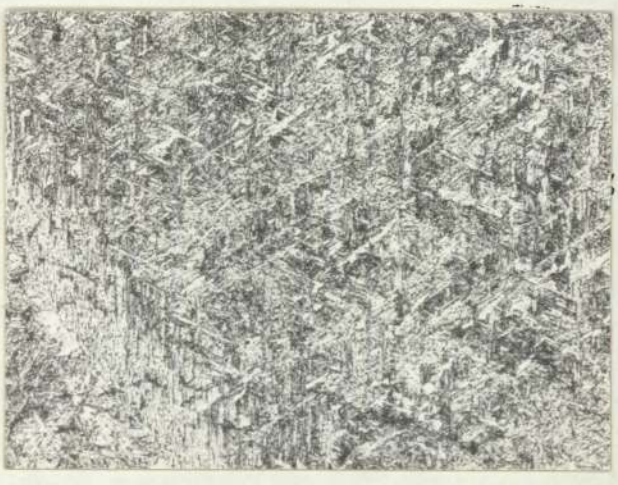

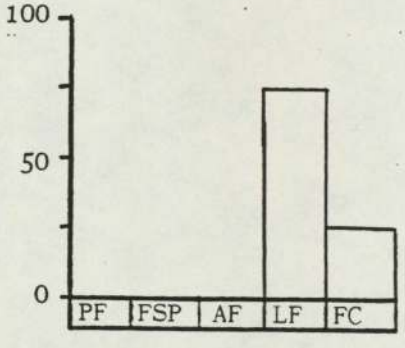

C. Specimen B3.
CR, 33.8°C/sec.

Mag. X160.
Etchant. 2% Nital.

Figure No. 4.22

Representative Photomicrographs Showing The Microstructures Formed In The 0.027%wt V Concentration (SeriesB) Simulated Low Oxygen As-Deposited Weld Metal, With Increasing Cooling Rate.

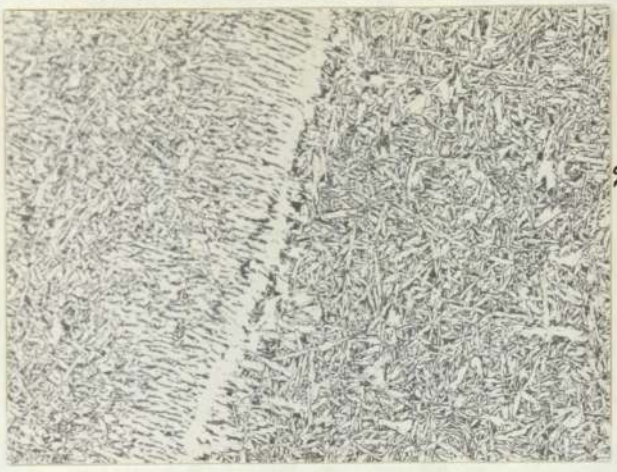

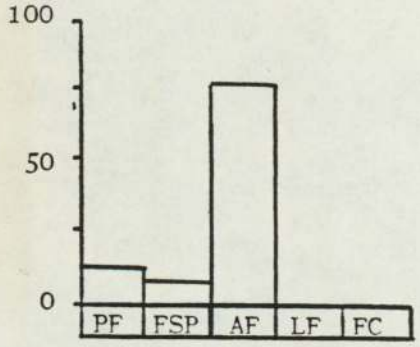

A. Specimen C10.
Cooling Rate(CR),
3.7°C/sec.

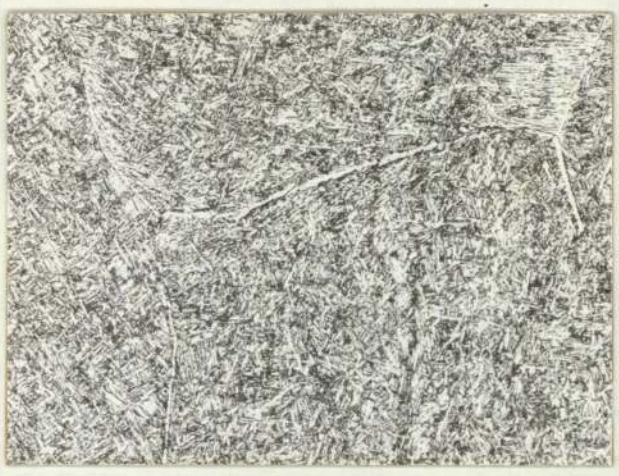

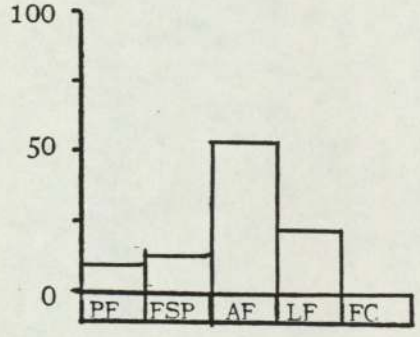

B. Specimen C13.
CR, 11.5°C/sec.

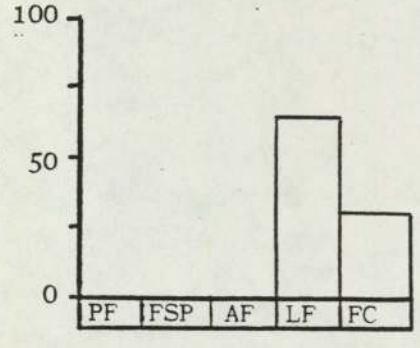

C. Specimen C17.
CR, 29.9°C/sec.

Mag. X160.
Etchant. 2% Nital.

Figure No. 4.23

Representative Photomicrographs Showing The Microstructures Formed In The 0.088%wt V Concentration (Series C) Simulated Low Oxygen As-Deposited Weld Metal, With Increasing Cooling Rate.

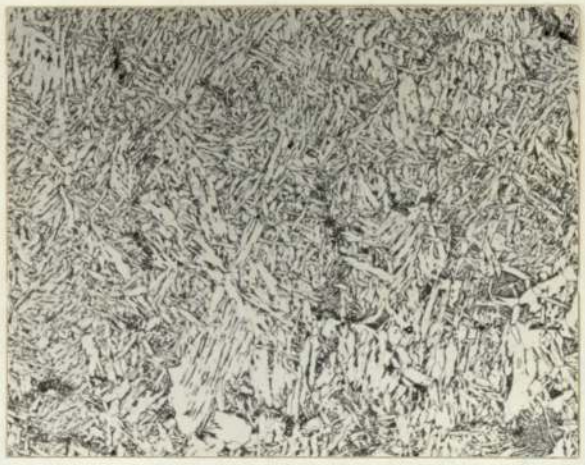

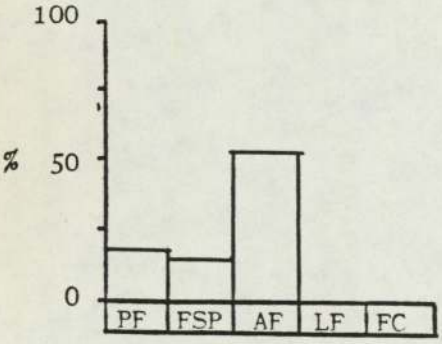

A. Specimen D8.
Cooling Rate(CR),
4.1°C/sec.

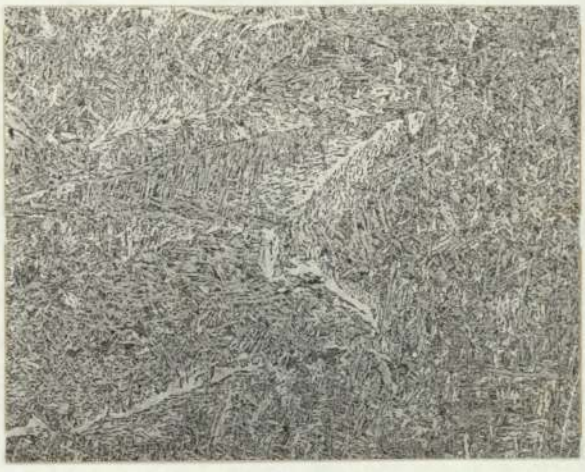

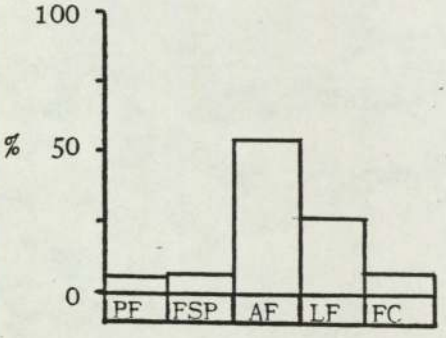

B. Specimen D10.
CR, 13.9°C/sec.

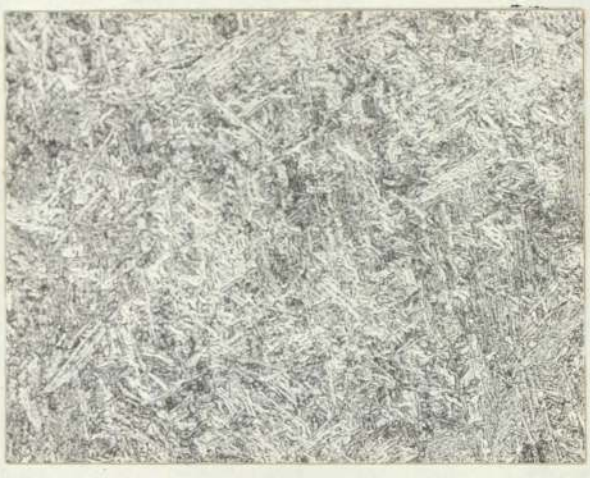

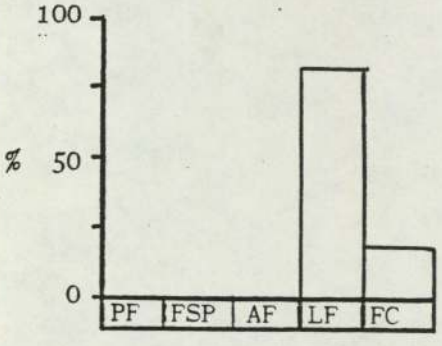

C. Specimen D17.
CR, 32.8°C/sec.

Mag. X160.
Etchant. 2% Nital.

Figure No. 4.24

Representative Photomicrographs Showing The Microstructures Formed In The 0.020%wt Ti Concentration (Series D) Simulated Low Oxygen As-Deposited Weld Metal, With Increasing Cooling Rate.

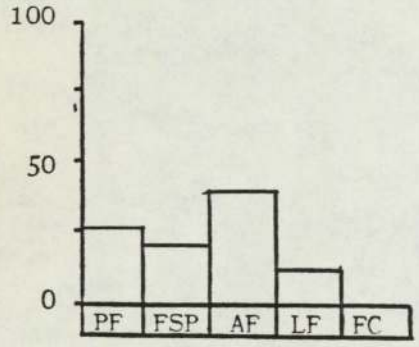

A. Specimen E7.
Cooling Rate(CR),
4.1°C/sec.

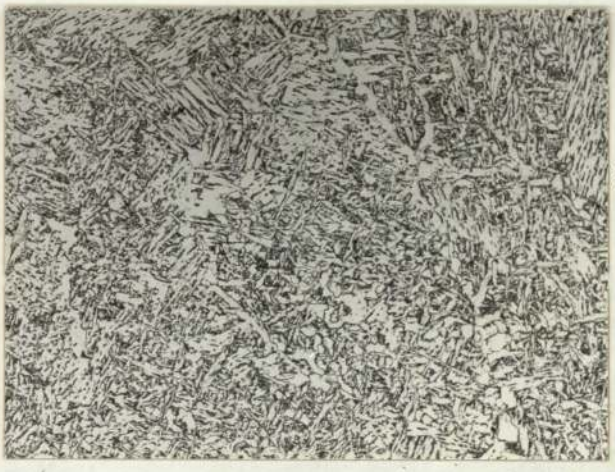

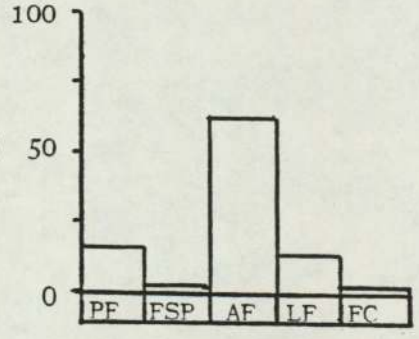

B. Specimen E3.
CR, 10.2°C/sec.

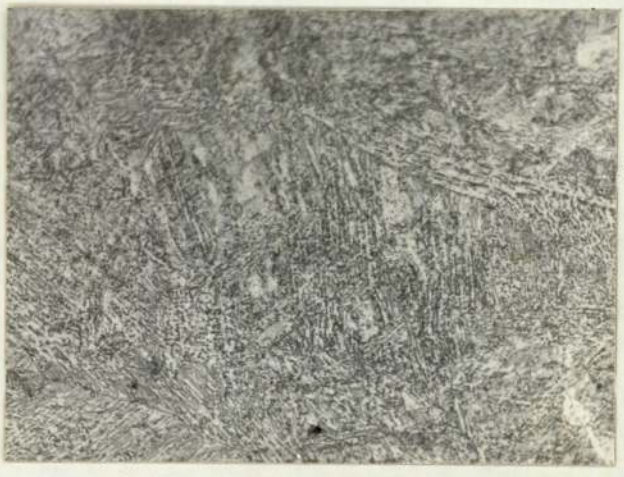

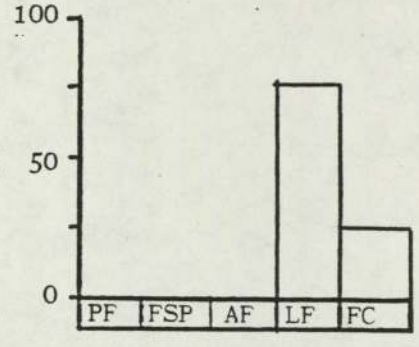

C. Specimen E13.
CR, 32.1°C/sec.

Mag. X160.
Etchant. 2% Nital.

Figure No. 4.25

Representative Photomicrographs Showing The Microstructures Formed In The 0.063%wt Ti Concentration (Series E) Simulated Low Oxygen As-Deposited Weld Metal, With Increasing Cooling Rate.

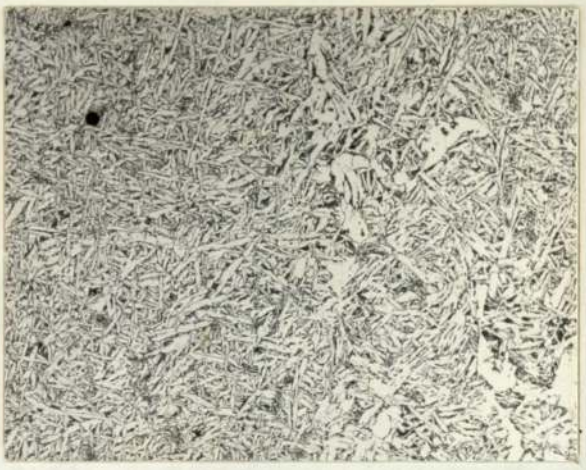

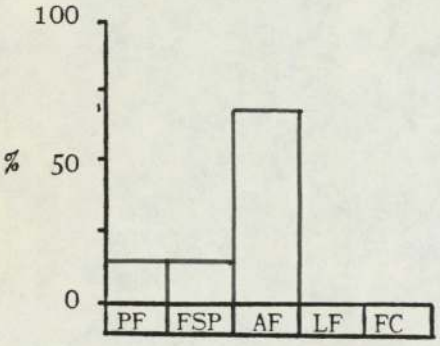

A. Specimen F5.
Cooling Rate(CR),
4.2°C/sec.

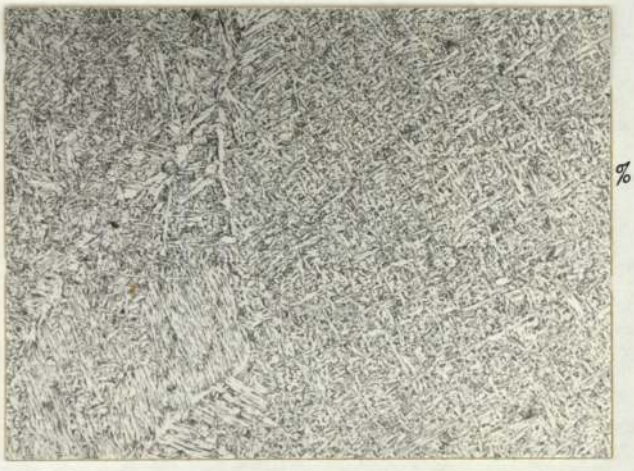

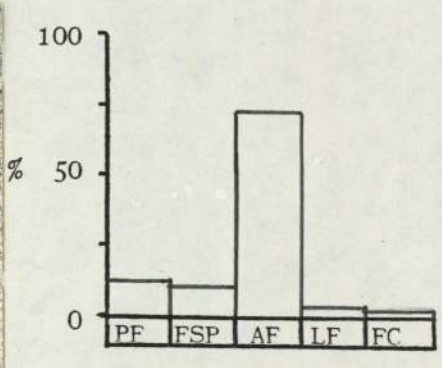

B. Specimen F12.
CR, 11.5°C/sec.

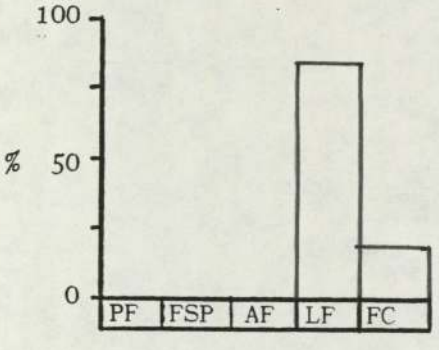

C. Specimen F16.
CR, 32.1 C/sec.

Mag. X160.
Etchant. 2% Nital.

Figure No. 4.26

Representative Photomicrographs Showing The Microstructures Formed In The 0.021%wt Nb Concentration (SeriesF) Simulated Low Oxygen As-Deposited Weld Metal, With Increasing Cooling Rate.

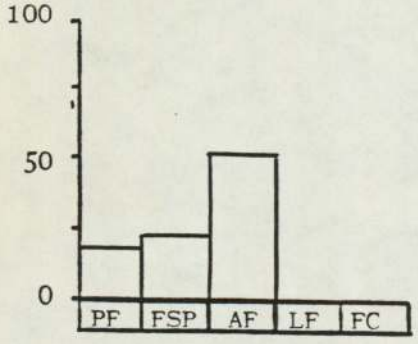

A. Specimen G4.
Cooling Rate(CR),
3.9°C/sec.

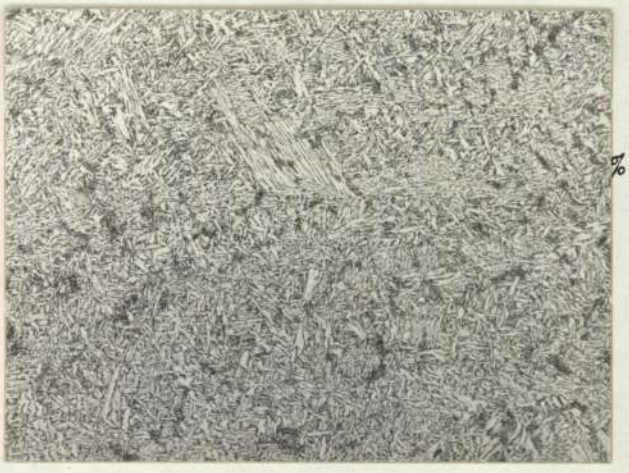

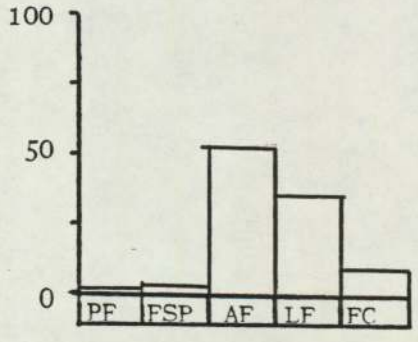

B. Specimen G14.
CR, 14.2°C/sec.

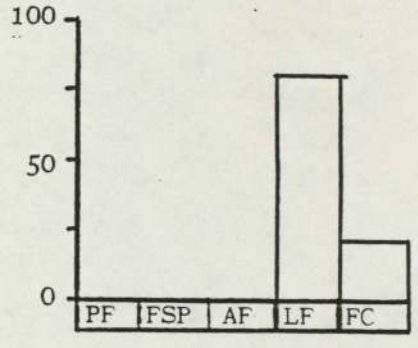

C. Specimen G15.
CR, 33.2°C/sec.

Mag. X160.
Etchant 2% Nital.

Figure No. 4.27

Representative Photomicrographs Showing The Microstructures Formed In The 0.053%wt Nb Concentration (Series G) Simulated Low Oxygen As-Deposited Weld Metal, With Increasing Cooling Rate.

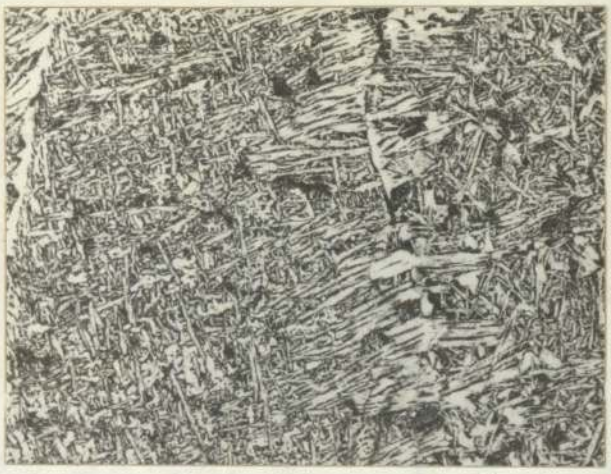

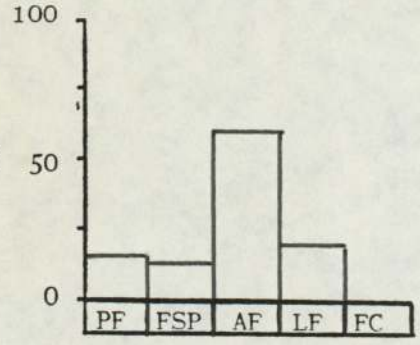

A. Specimen H1.
Cooling Rate(CR),
4.2°C/sec.

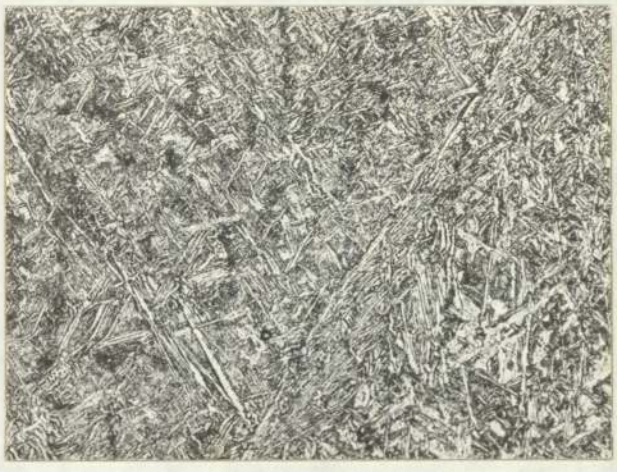

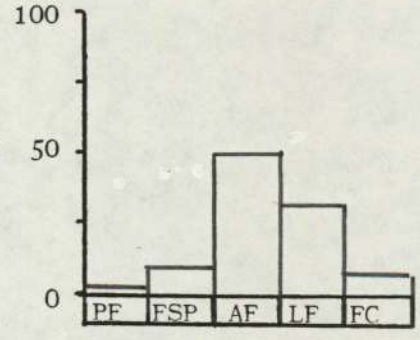

B. Specimen H5.
CR, 12.9°C/sec.

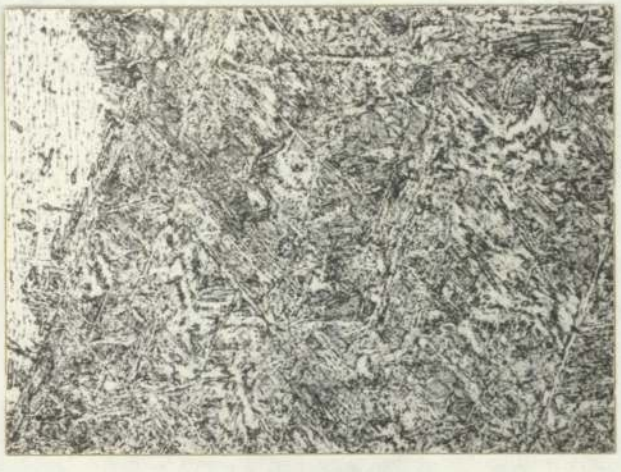

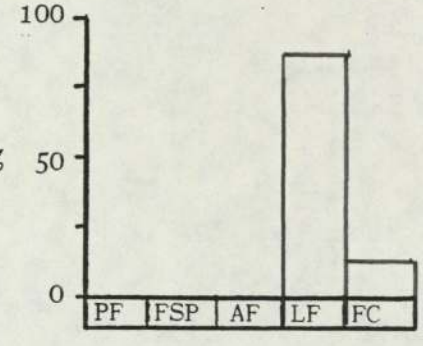

C. Specimen H16.
CR, 33.5°C/sec.

Mag. X160.
Etchant. 2% Nital.

Figure No. 4.28

Representative Photomicrographs Showing The Microstructures Formed In The 0.024%wt Al Concentration (Series H) Simulated Low Oxygen As-Deposited Weld Metal, With Increasing Cooling Rate.

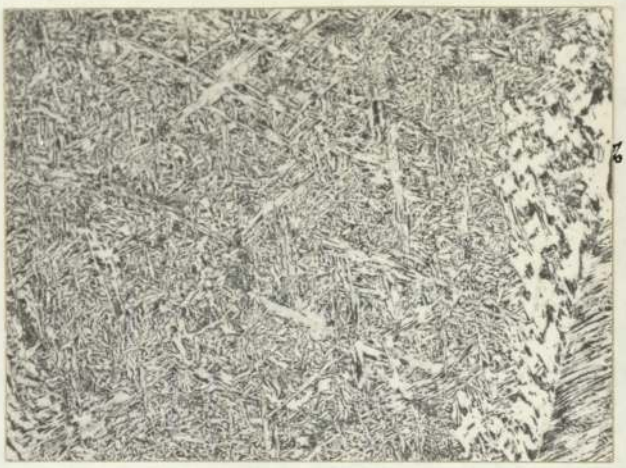

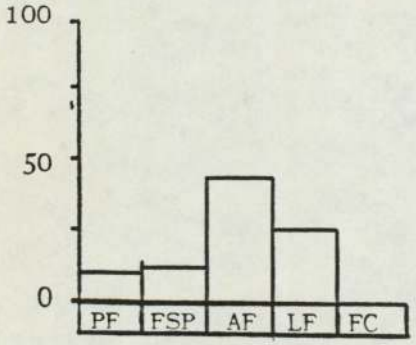

A. Specimen I2.
Cooling Rate(CR),
4.6°C/sec.

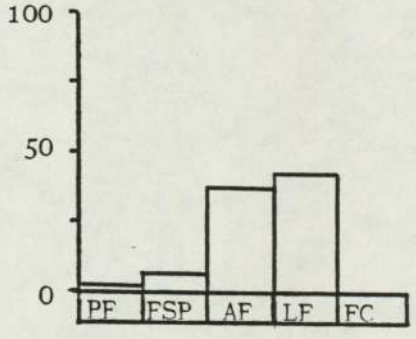

B. Specimen I5.
CR, 9.7°C/sec.

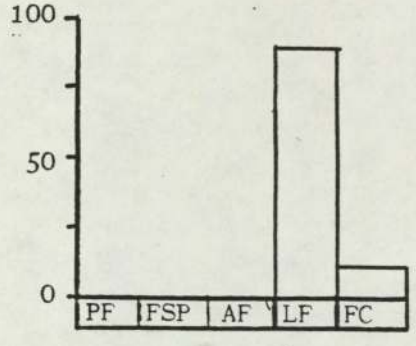

C. Specimen I9.
CR, 34.1°C/sec.

Mag. X160.
Etchant. 2% Nital.

Figure No. 4.29

Representative Photomicrographs Showing The Microstructures Formed In The 0.063%wt Al Concentration (Series I) Simulated Low Oxygen As-Deposited Weld Metal, With Increasing Cooling Rate.

Base Alloy, Series A.
Cooling Rate (CR) 7.0°C/sec.

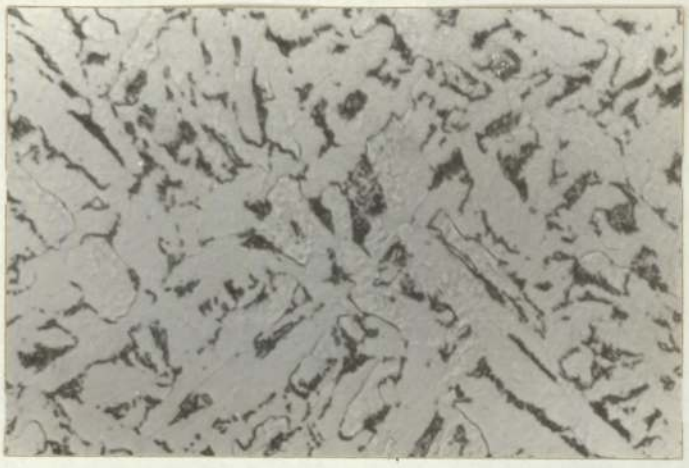

0.027 %wt V, Series B.
CR, 7.2 C/sec.

0.088 %wt V, Series C.
CR, 6.1 C/sec.

Mag. X1200.
Etchant Picral.

Figure No. 4.30

Photomicrographs Showing The Effect Of V Addition On The Microphases Formed In The Simulated As-Deposited Weld Metal.

0.020 %wt Ti, Series D.
Cooling Rate (CR) 6.9°C/sec.

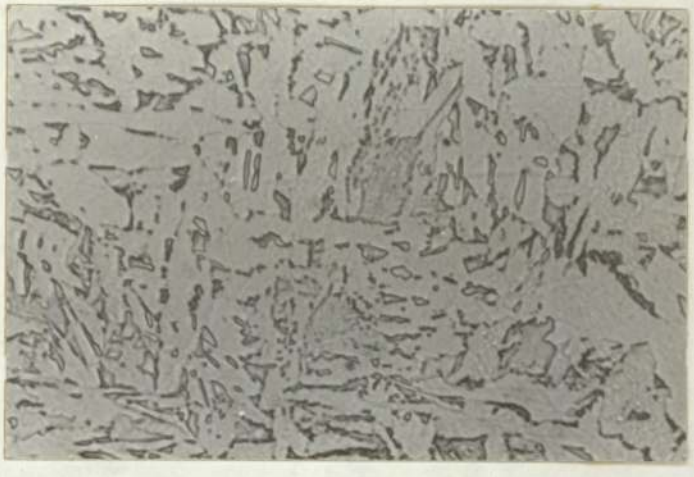

0.063 %wt Ti, Series E.
CR 6.7°C/sec.

SEE FIGURE 4.30 FOR BASE ALLOY.

Mag. X1200.
Etchant, Picral.

Figure No. 4.31

Photomicrographs Showing The Effect Of Ti Addition On The Microphases Formed In The Simulated As-Deposited Weld Metal.

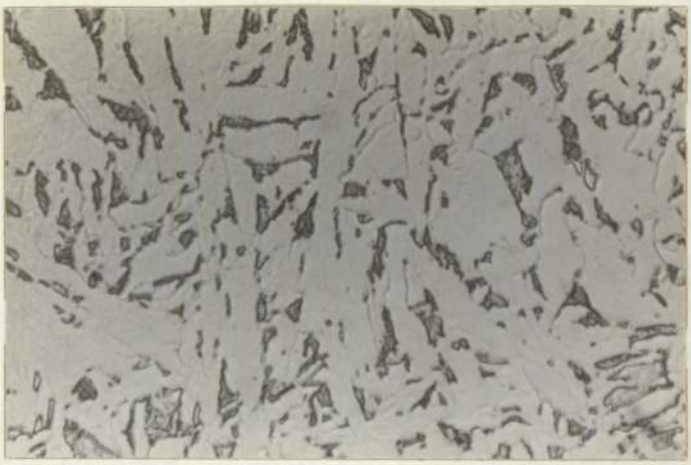

0.021 %wt Nb, Series F.
Cooling Rate (CR) 7.1°C/sec.

0.053 %wt Nb, Series G,
CR, 7.0°C/sec.

SEE FIGURE 4.30 FOR BASE ALLOY.

Mag. X1200.
Etchant, Picral.

Figure No. 4.32

Photomicrographs Showing The Effect Of Nb Addition On The Microphases Formed In The Simulated As-Deposited Weld Metal.

0.024 %wt Al, Series H.
Cooling Rate (CR) 7.7°C/sec.

0.063 %wt Al, Series I.
CR, 6.8°C/sec.

SEE FIGURE 4.30 FOR BASE ALLOY.

Mag. X1200.
Etchant, Picral.

Figure No. 4.33

Photomicrographs Showing The Effect Of Al Addition On The Microphases Formed In The Simulated As-Deposited Weld Metal.

Specimen A1.
Cooling Rate 7.0 °C/sec.
Microphase Content, 12%.

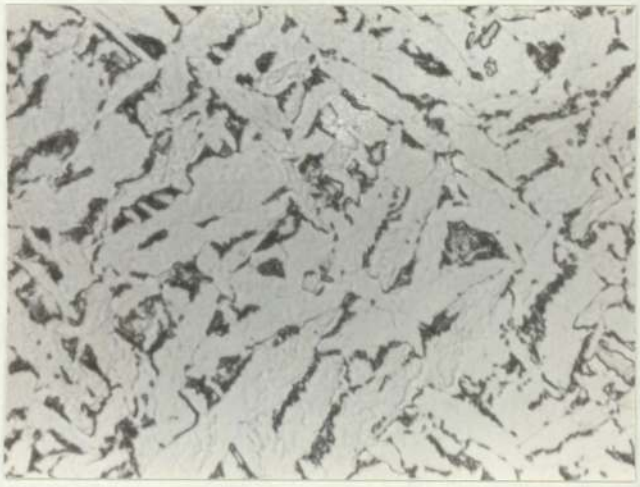

Specimen A10.
Cooling Rate 10.7 °C/sec.
Microphase Content, 18%.

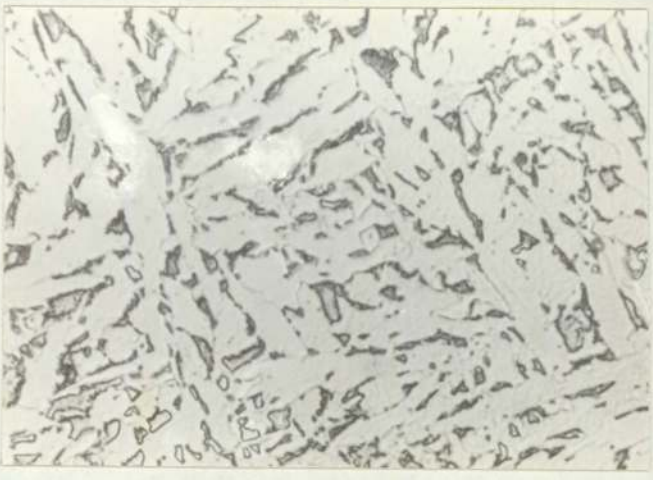

Specimen A19.
Cooling Rate 19.6°C/sec.
Microphase Content, 27%.

Mag. X1200.
Etchant, Picral.

Figure No. 4.34

The Effect Of Cooling Rate On The Microphase Content In Simulated As-Deposited Weld Metal.

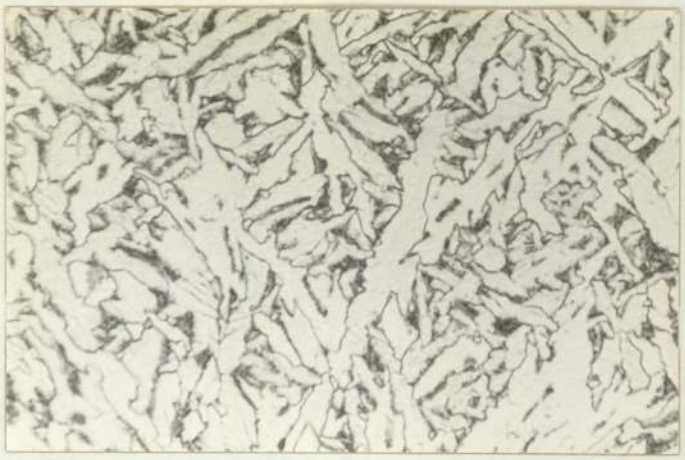

Base Alloy, Series A.
Cooling Rate (CR) 4.6°C/sec.

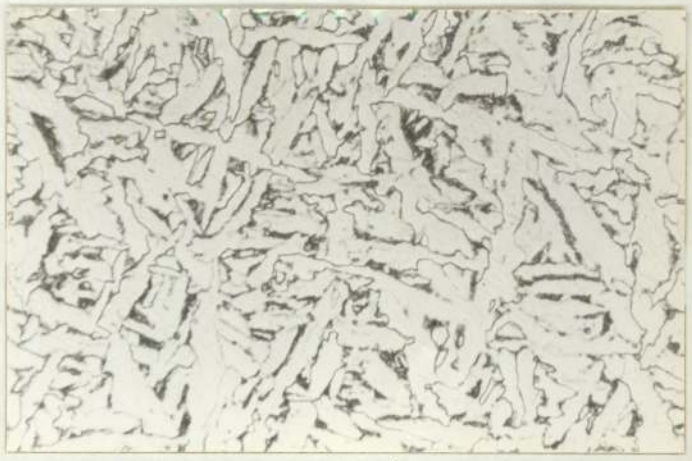

0.027 %wt V, Series B.
CR, 4.2 C/sec.

0.088 %wt V, Series C.
CR, 3.7°C/sec.

Mag, X600.
Etchant 2%Nital.

Figure No. 4.35

Photomicrographs Showing The Effect Of V Addition On The Acicular Ferrite Grain Size, In The Simulated As-Deposited Weld Metal.

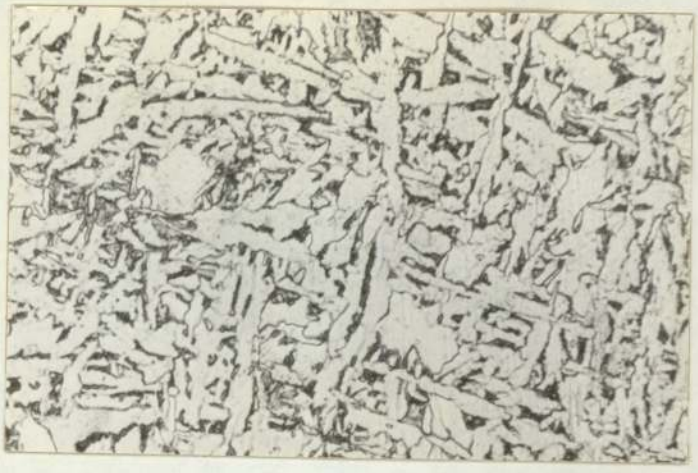

0.020 %wt Ti, Series D.
Cooling Rate (CR) 4.1°C/sec.

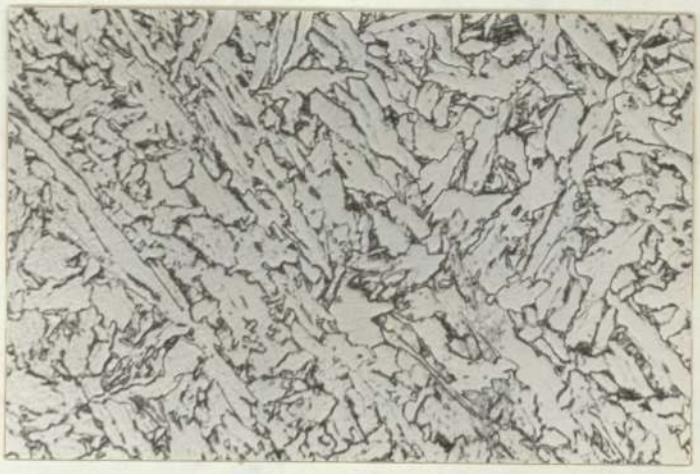

0.063 %wt Ti, Series E.
CR, 4.1°C/sec.

SEE FIGURE 4.35 FOR BASE ALLOY.

Mag. X600.
Etchant 2% Nital.

Figure No. 4.36

Photomicrographs Showing The Effect Of Ti Addition On The Acicular Ferrite Grain Size, In The Simulated As-Deposited Weld Metal.

0.021 %wt Nb, Series F.
Cooling Rate (CR) 4.2°C/sec.

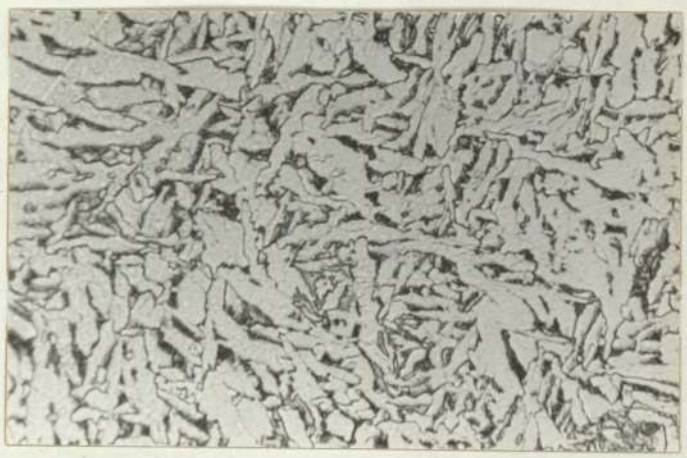

0.053 %wt Nb, Series G.
CR, 3.9°C/sec.

SEE FIGURE 4.35 FOR BASE ALLOY.

Mag. X600.
Etchant 2% Nital.

Figure No. 4.37

Photomicrographs Showing The Effect Of Nb Addition On The Acicular Ferrite Grain Size, In The Simulated As-Deposited Weld Metal.

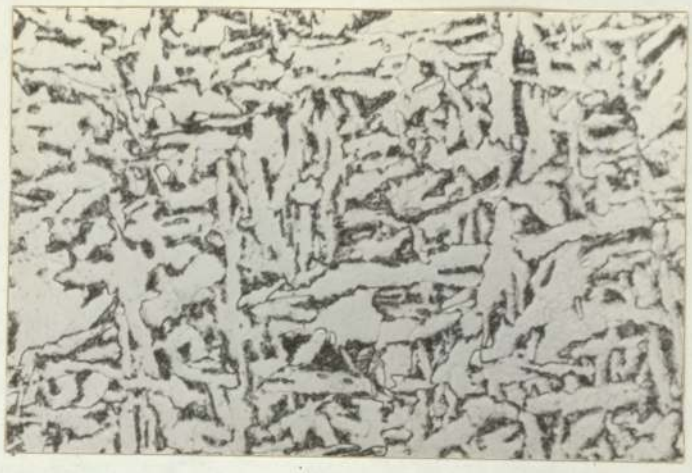

0.024 %wt Al, Series H.
Cooling Rate (CR) 4.1°C/sec.

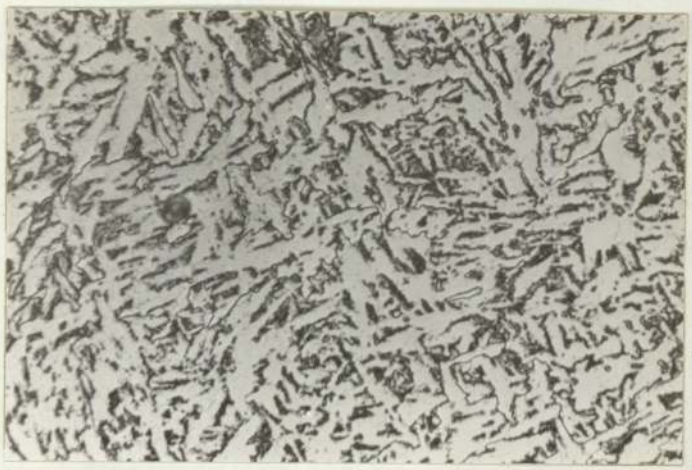

0.063 %wt Al , Series I.
CR, 4.5°C/sec.

SEE FIGURE 4.35 FOR BASE ALLOY.

Mag. X600.
Etchant 2% Nital.

Figure No. 4.38

Photomicrographs Showing The Effect Of Al Addition On The Acicular Ferrite Grain Size, In The Simulated As-Deposited Weld Metal.

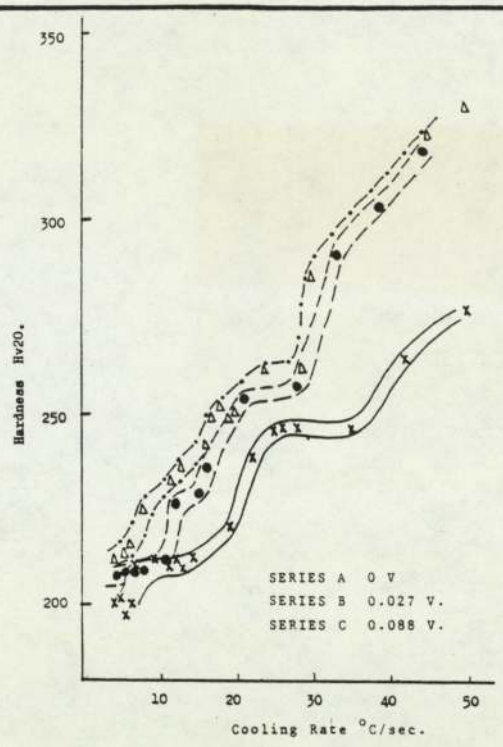

Fig. 4.39 Vanadium Additions.

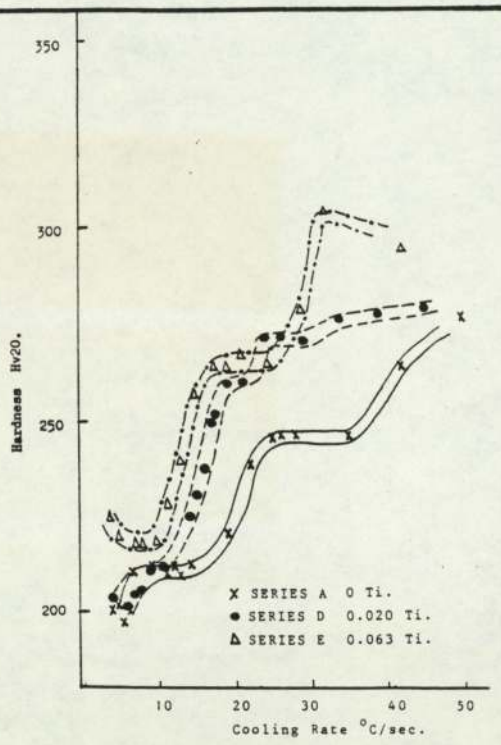

Fig. 4.40 Titanium Additions.

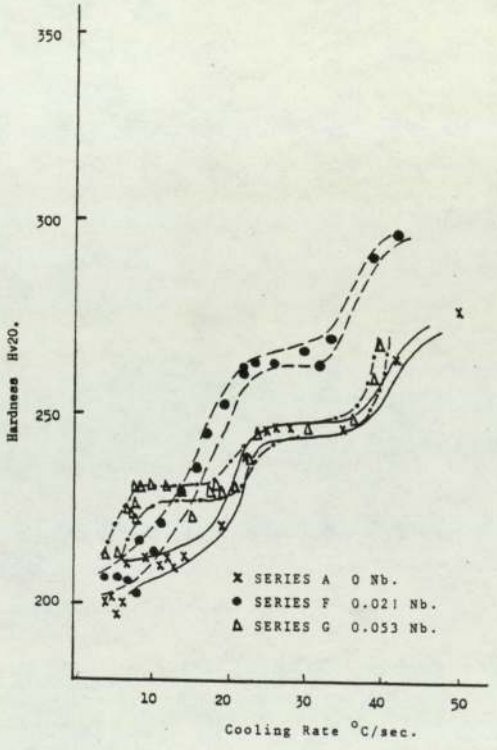

Fig. 4.41 Niobium Additions.

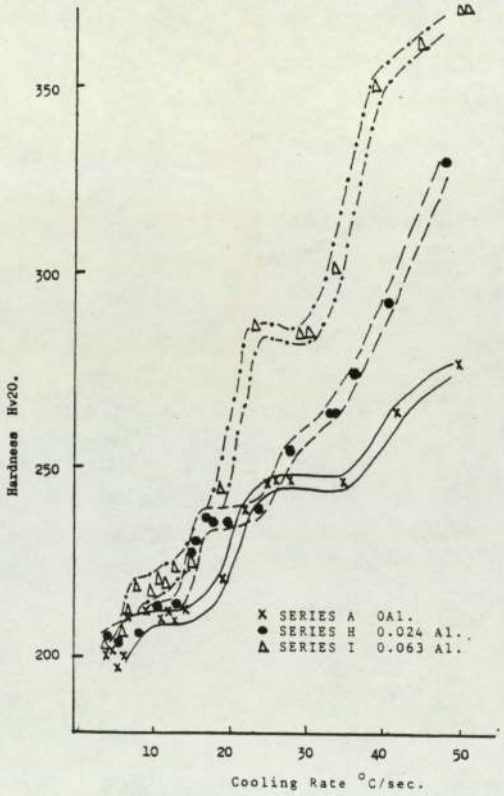

Fig. 4.42 Aluminium Additions.

Figure Nos. 4.39 to 4.42

The Influence Of Microalloy Additions On The Hardness Of Low Oxygen Content Simulated As-Deposited Weld Metal.

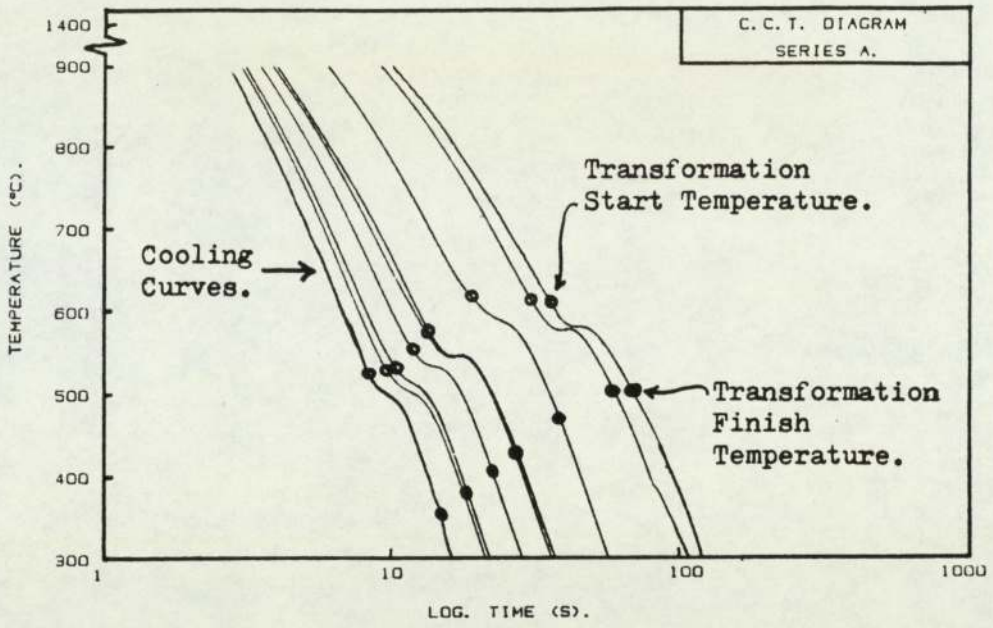

A. Cooling Curves For Alloy Plotted Onto Temperature Log. Time Axis, Using A Computer Plotter And Transformation Start And Finish Temperatures Plotted Onto Each Curve.

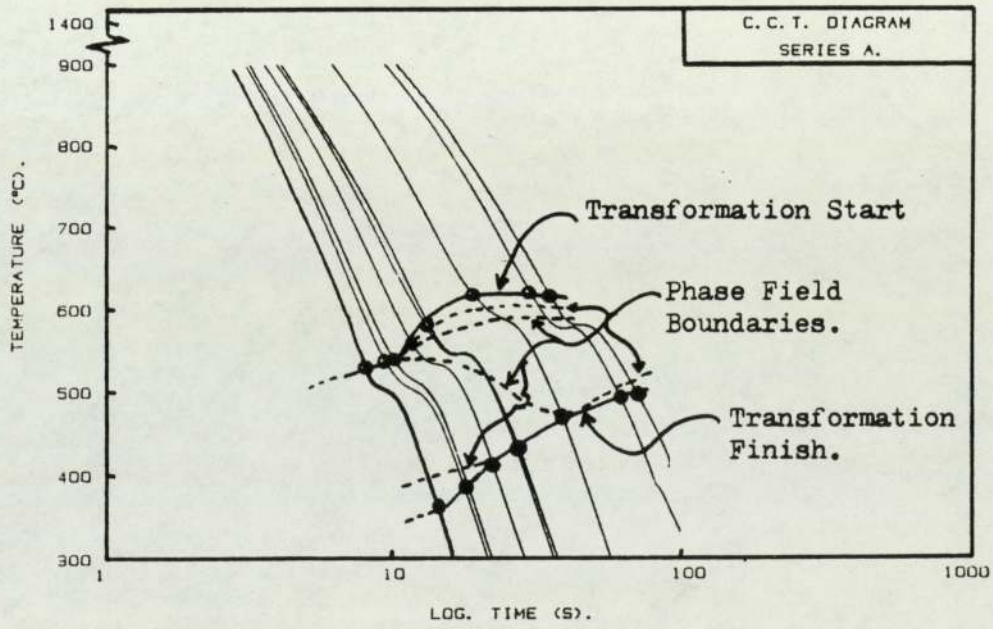

B. Transformation Start And Finish Line Drawn Onto Cooling Curves And Phase Fields Plotted By Dividing The Curves Into The Proportions Determined From Quantitative Metallography.

Figure No. 4.43

Construction Of Continuous Cooling Transformation Diagrams.

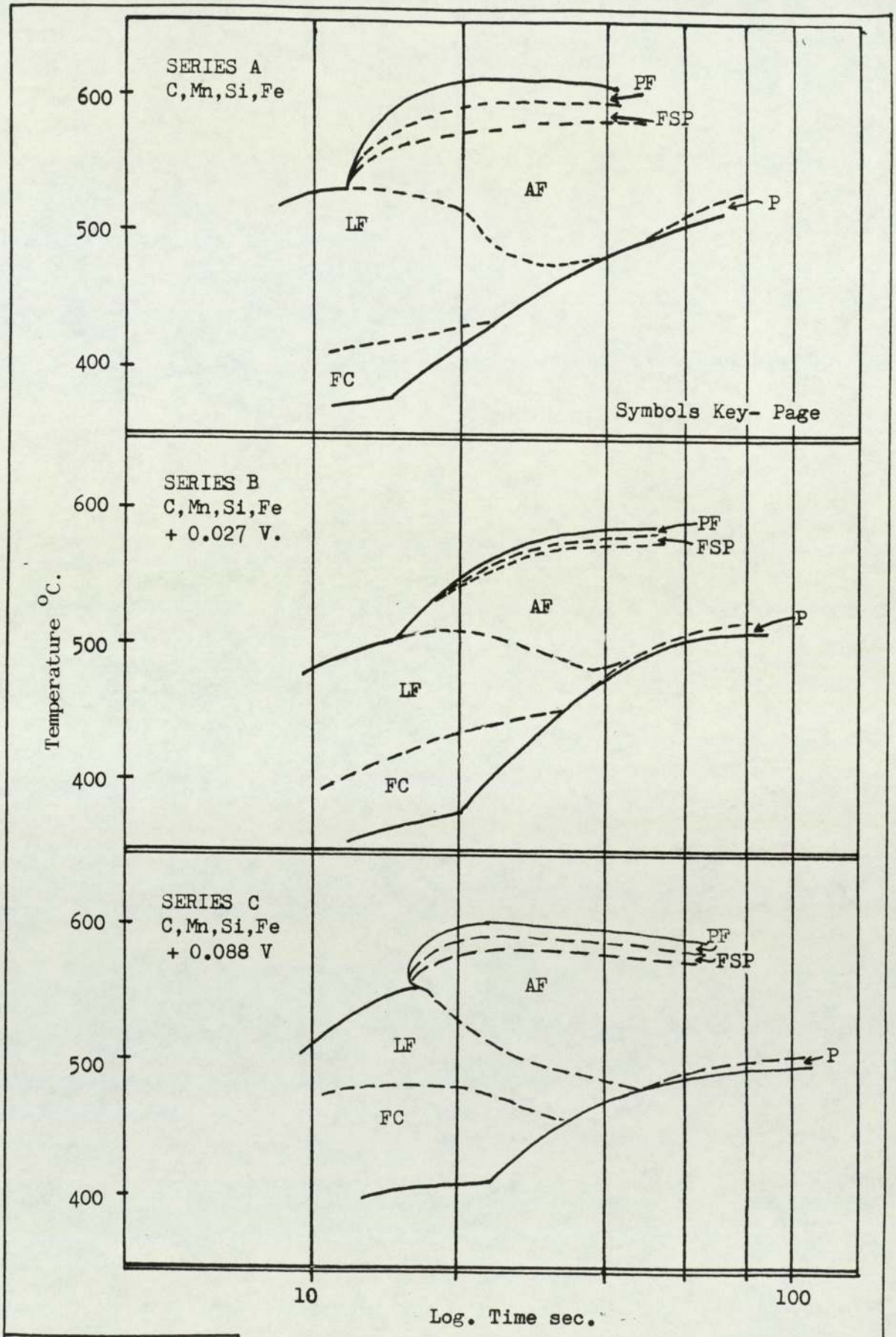

Figure No. 4.44

CCT Diagrams Showing The Effect Of Increased V Concentration On The Transformation Temperatures And Ferrite Constituents Formed In Simulated As-Deposited Weld Metal, With Low Oxygen Content.

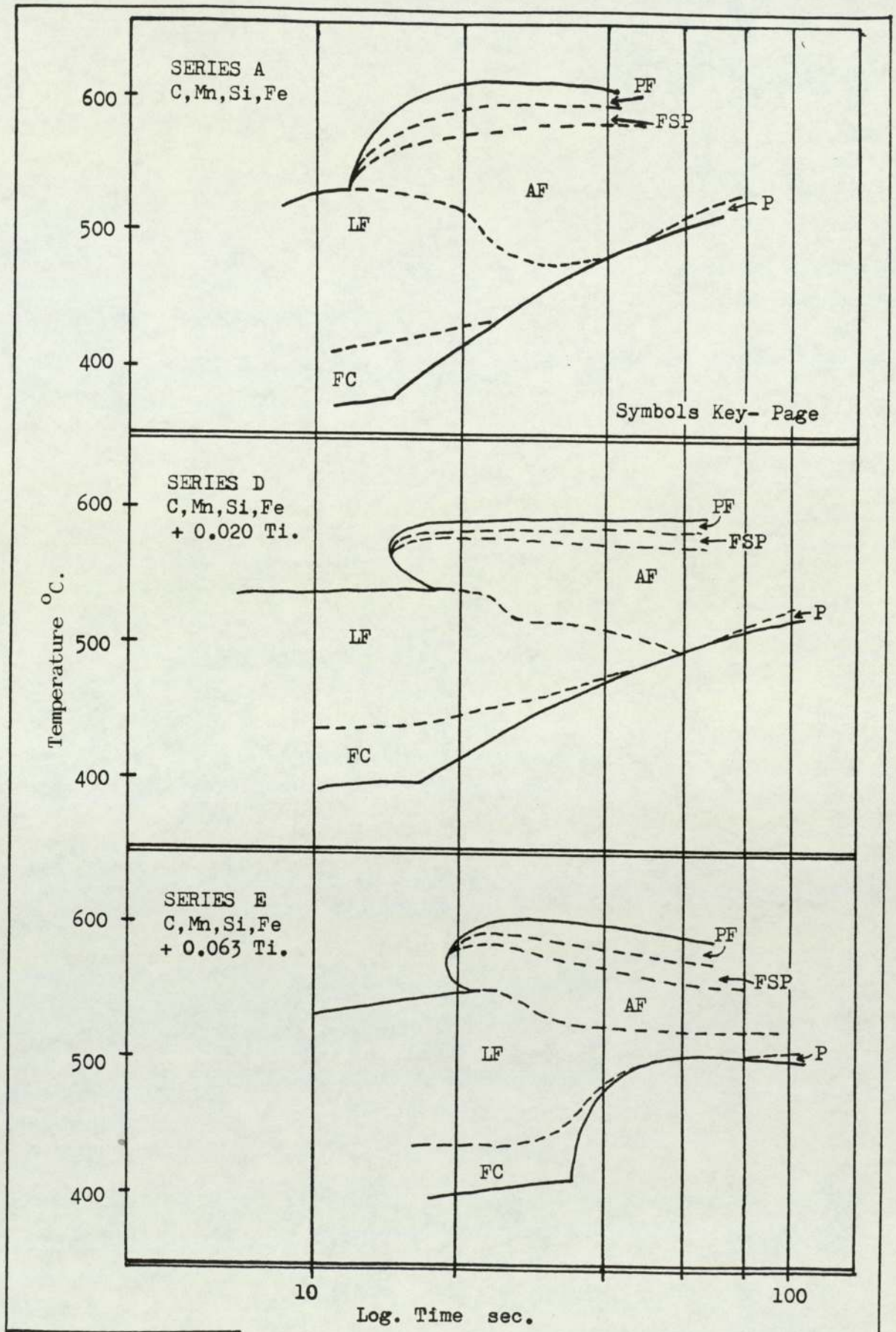

Figure No. 4.45

CCT Diagrams Showing The Effect Of Increased Ti Concentration On The Transformation Temperatures And Ferrite Constituents Formed In Simulated As-Deposited Weld Metal, With Low Oxygen Content.

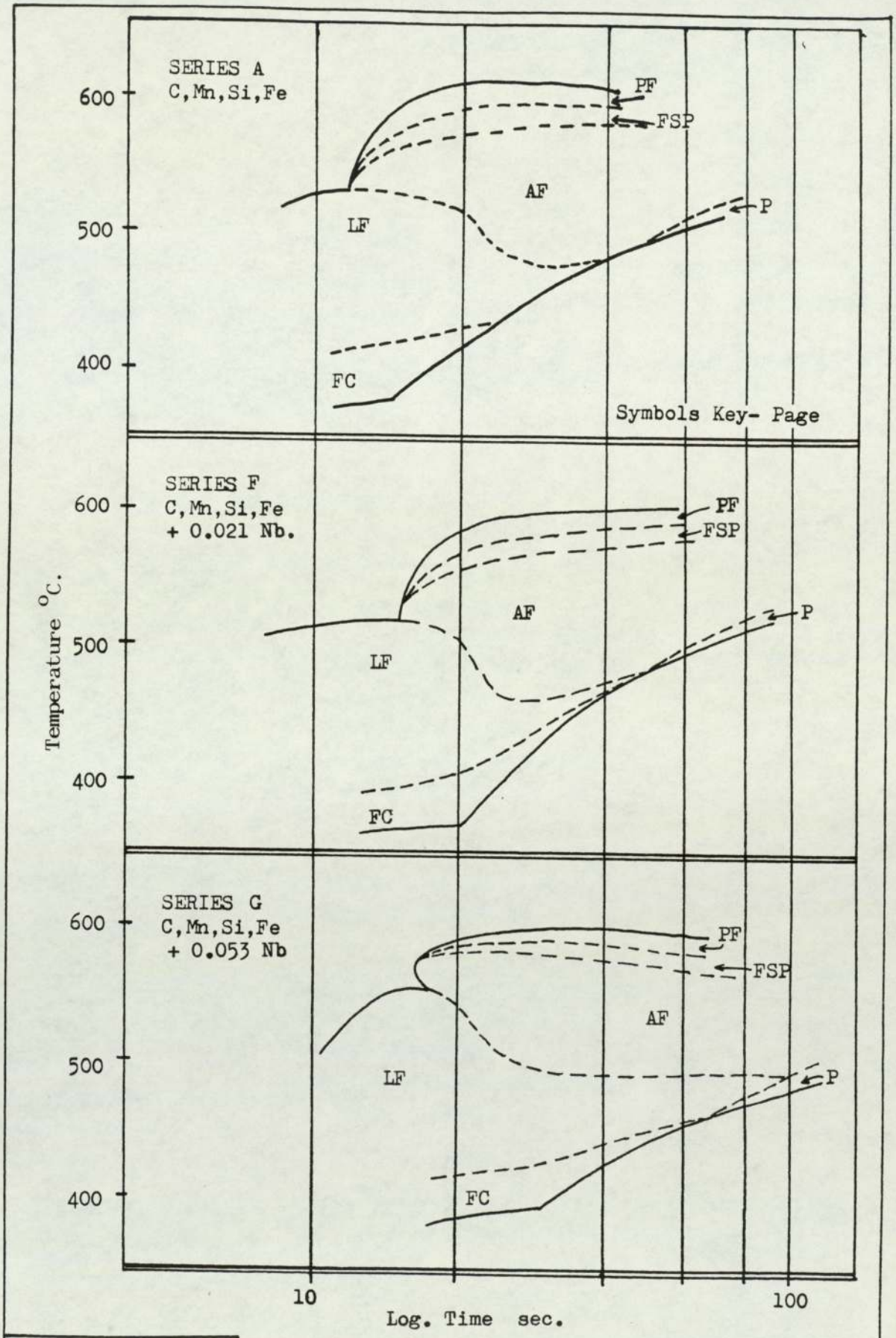

Figure No. 4.46

CCT Diagrams Showing The Effect Of Increased Nb Concentration On The Transformation Temperatures And Ferrite Constituents Formed In Simulated As-Deposited Weld Metal, With Low Oxygen Content.

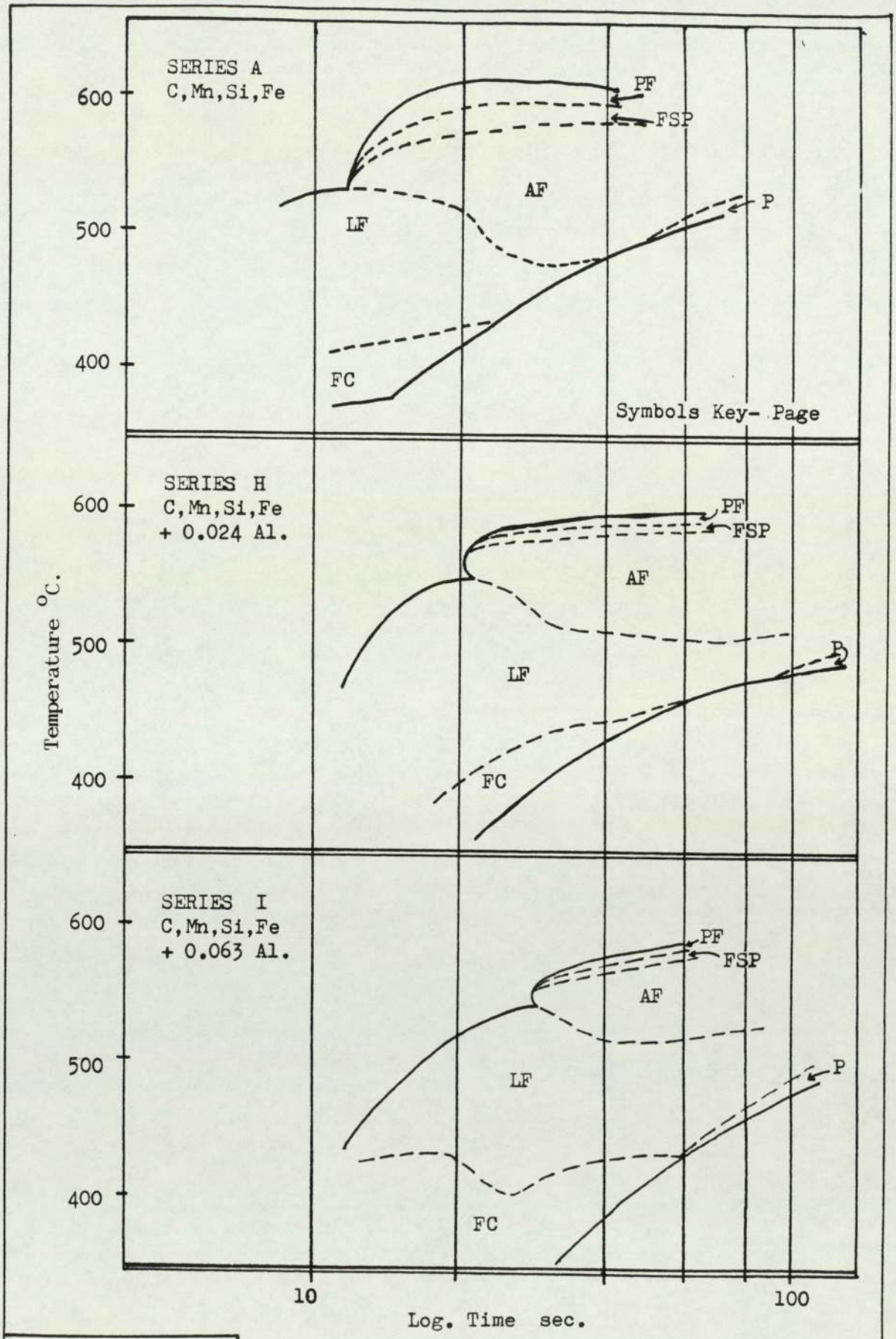

Figure No. 4.47

CCT Diagrams Showing The Effect Of Increased Al Concentration On The Transformation Temperatures And Ferrite Constituents Formed In Simulated As-Deposited Weld Metal, With Low Oxygen Content.

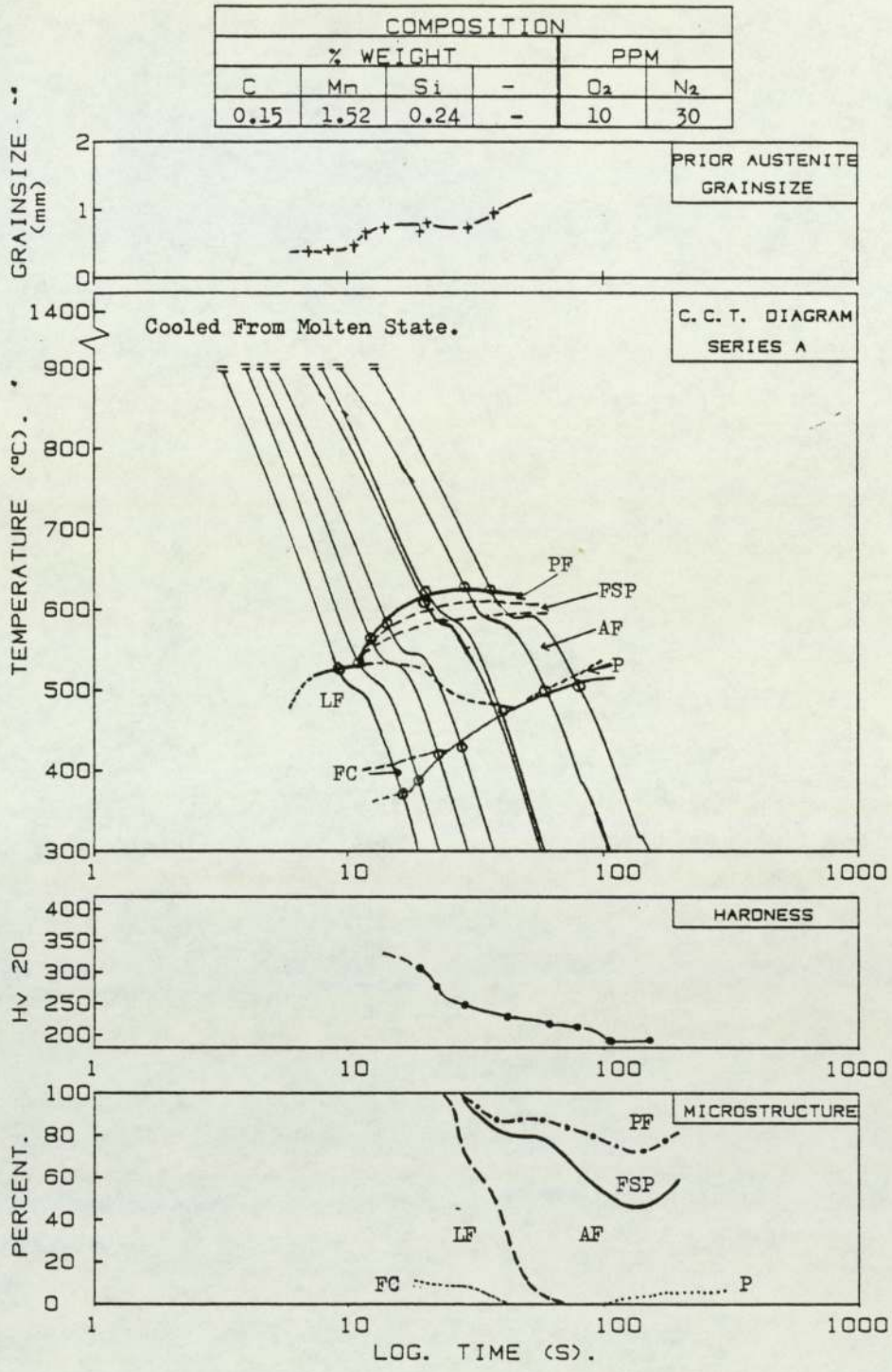

Figure No. 4.48

CCT Diagram For A Plain Carbon Manganese Steel (series A) Simulated As-Deposited Weld Metal, With Low Oxygen Content Showing The Transformation Characteristics, Prior Austenite Grain Size And Hardness.

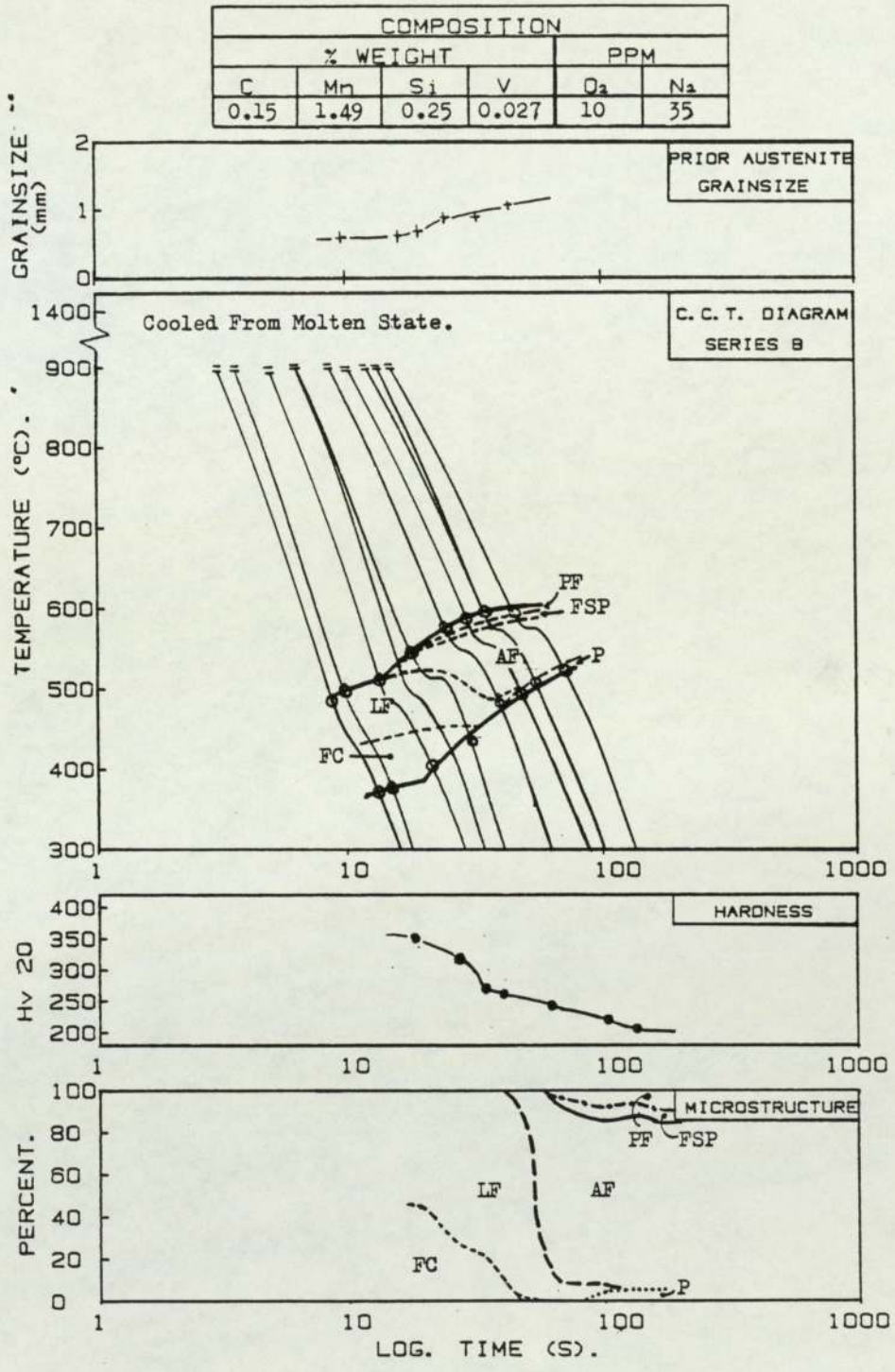

Figure No.4.49

CCT Diagram Showing The Influence Of 0.027 %wt V Concentration On The Transformation Characteristics, Prior Austenite Grain Size And Hardness Of Simulated As-Deposited Steel Weld Metal, With Low Oxygen Content.

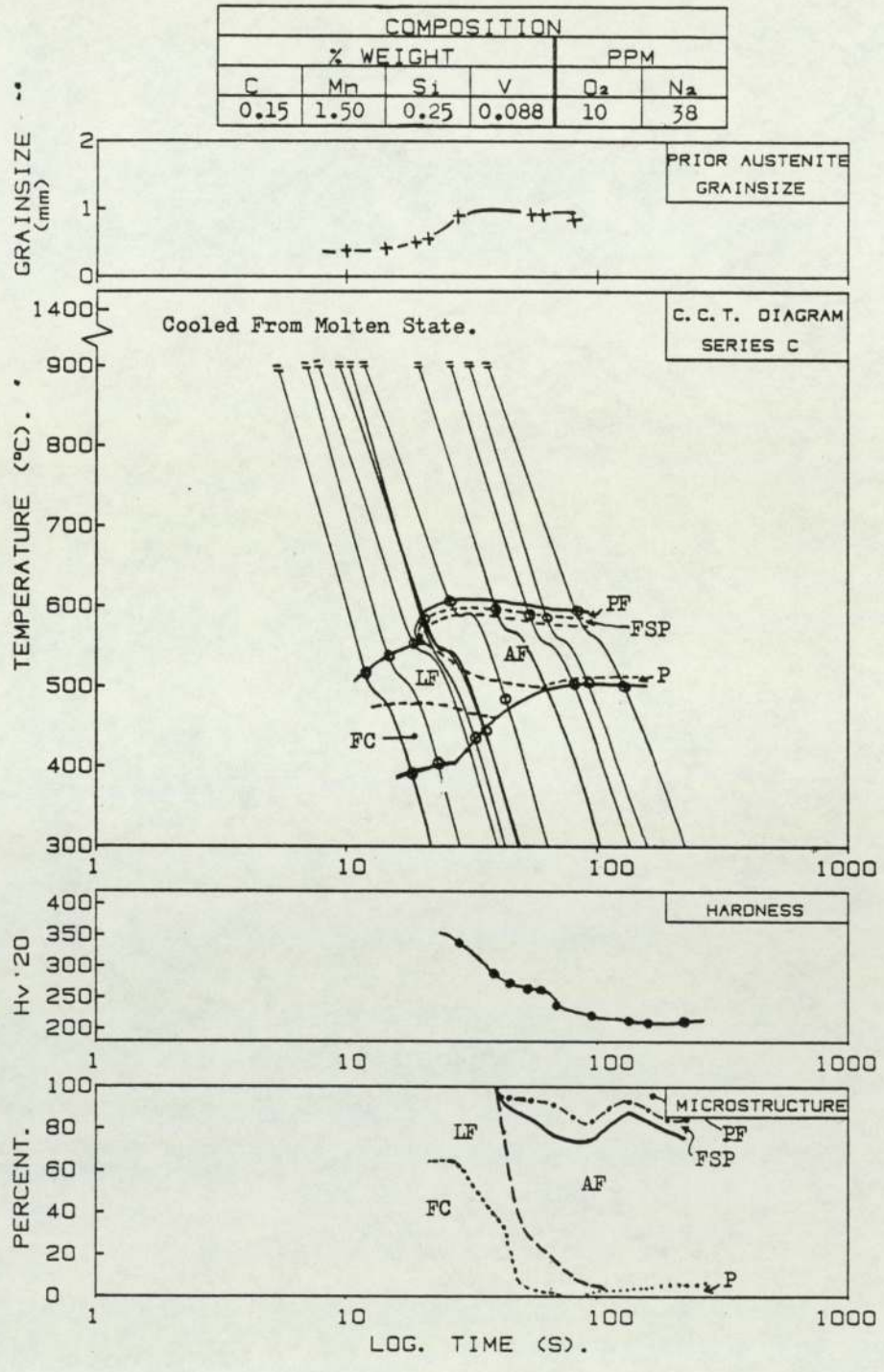

Figure No. 4.50

CCT Diagram Showing The Influence Of 0.088 %wt V Concentration On The Transformation Characteristics, Prior Austenite Grain Size And Hardness Of Simulated As-Deposited Steel Weld Metal, With Low Oxygen Content.

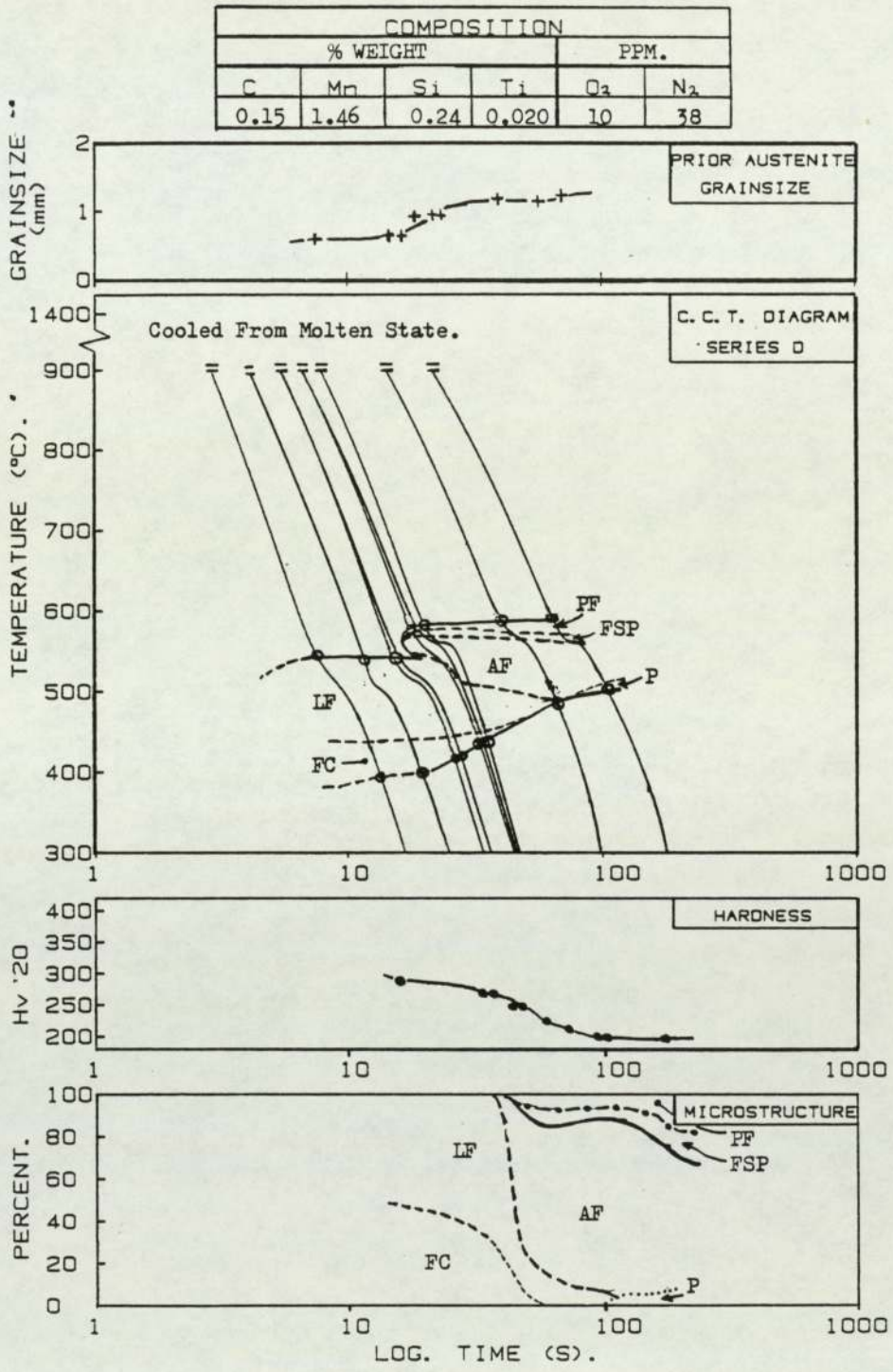

Figure No. 4.51

CCT Diagram Showing The Influence Of 0.020 %wt Ti Concentration On The Transformation Characteristics, Prior Austenite Grain Size And Hardness Of Simulated As-Deposited Steel Weld Metal, With Low Oxygen Content.

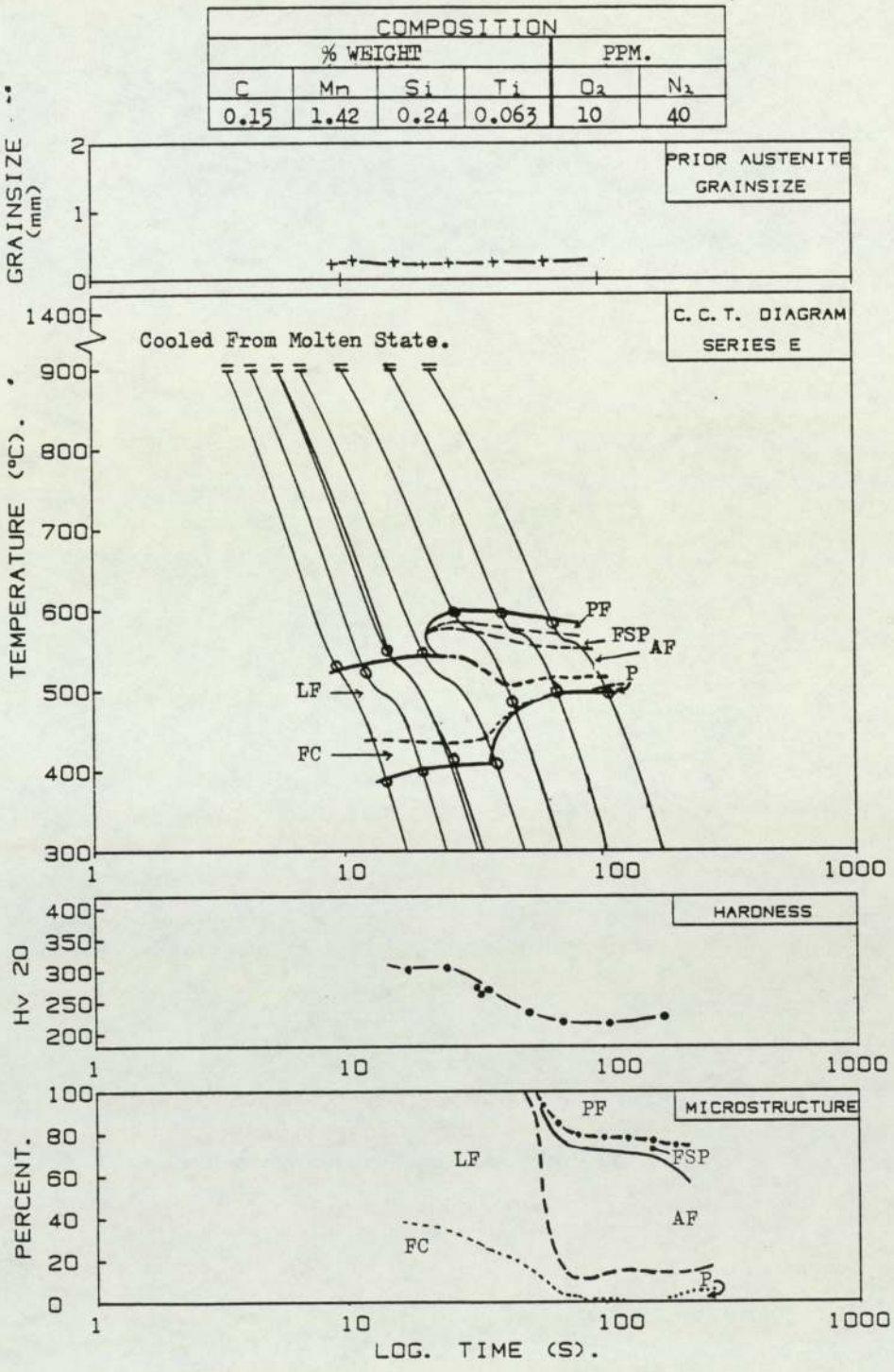

Figure No. 4.52

CCT Diagram Showing The Influence Of 0.063 %wt Ti Concentration On The Transformation Characteristics, Prior Austenite Grain Size And Hardness Of Simulated As-Deposited Steel Weld Metal, With Low Oxygen Content.

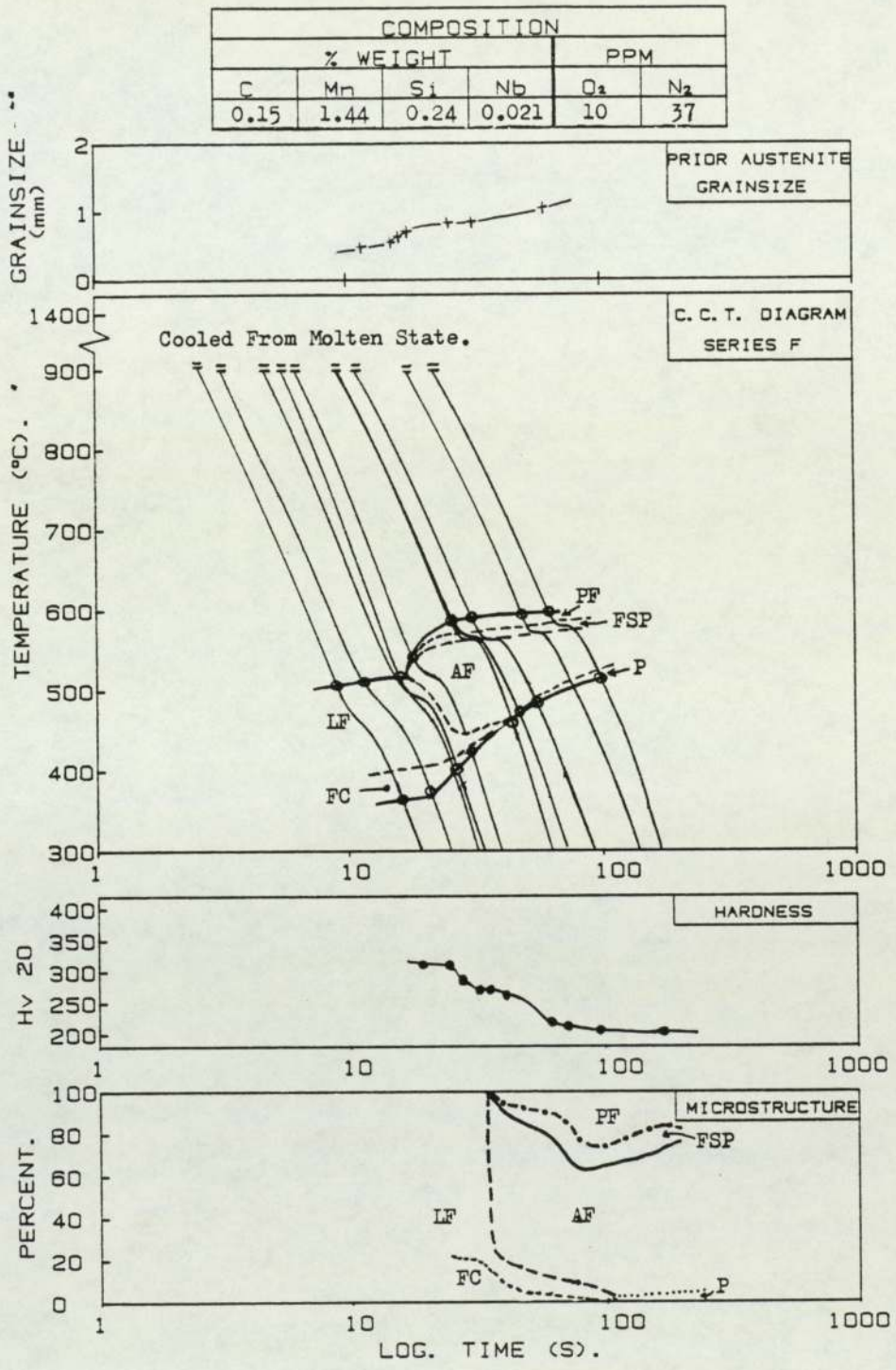

Figure No. 4.53

CCT Diagram Showing The Influence Of 0.021 %wt Nb Concentration On The Transformation Characteristics, Prior Austenite Grain Size And Hardness Of Simulated As-Deposited Steel Weld Metal, With Low Oxygen Content.

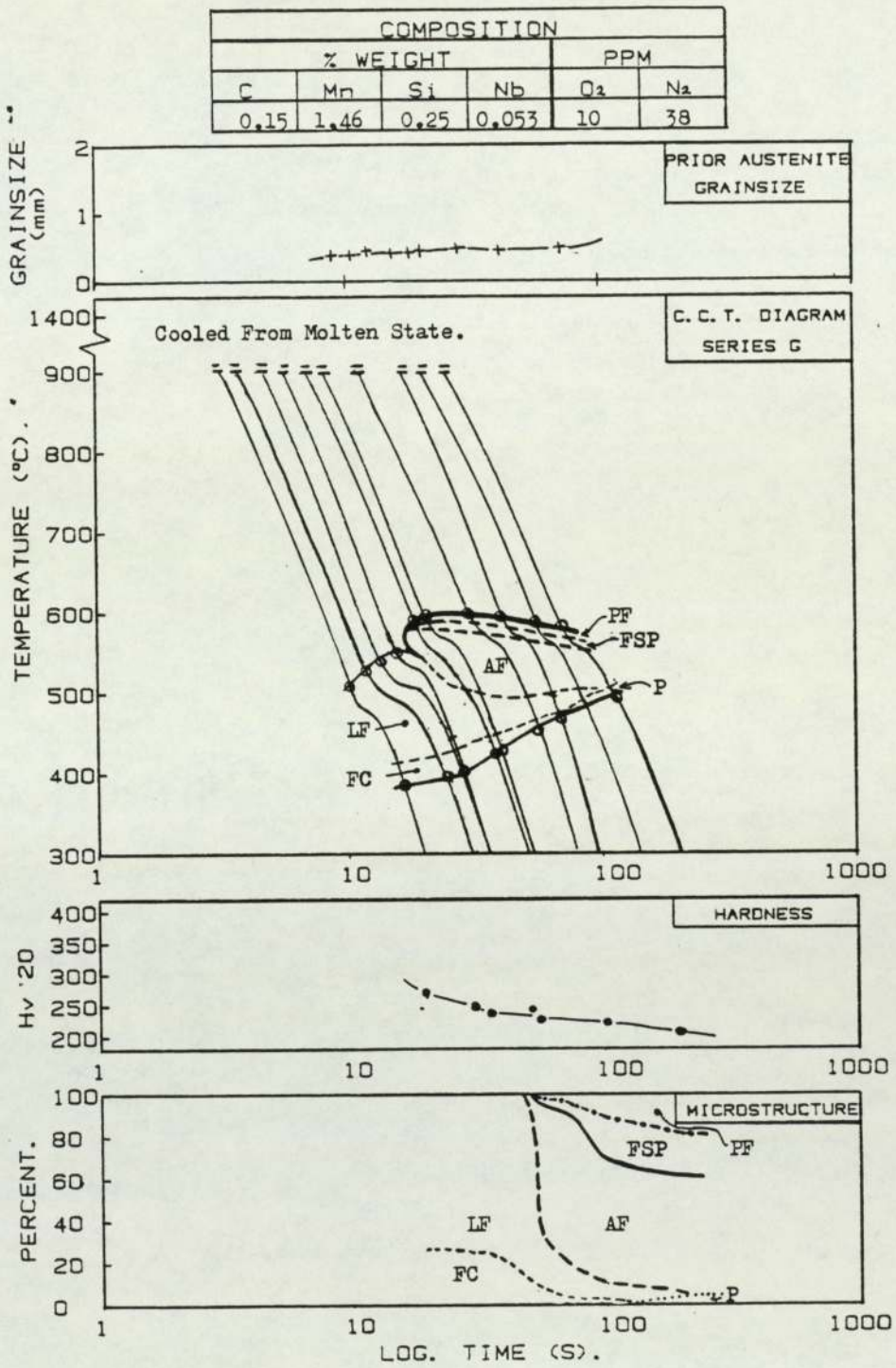

Figure No. 4.54

CCT Diagram Showing The Influence Of 0.053 %wt Nb Concentration On The Transformation Characteristics, Prior Austenite Grain Size And Hardness Of Simulated As-Deposited Steel Weld Metal, With Low Oxygen Content.

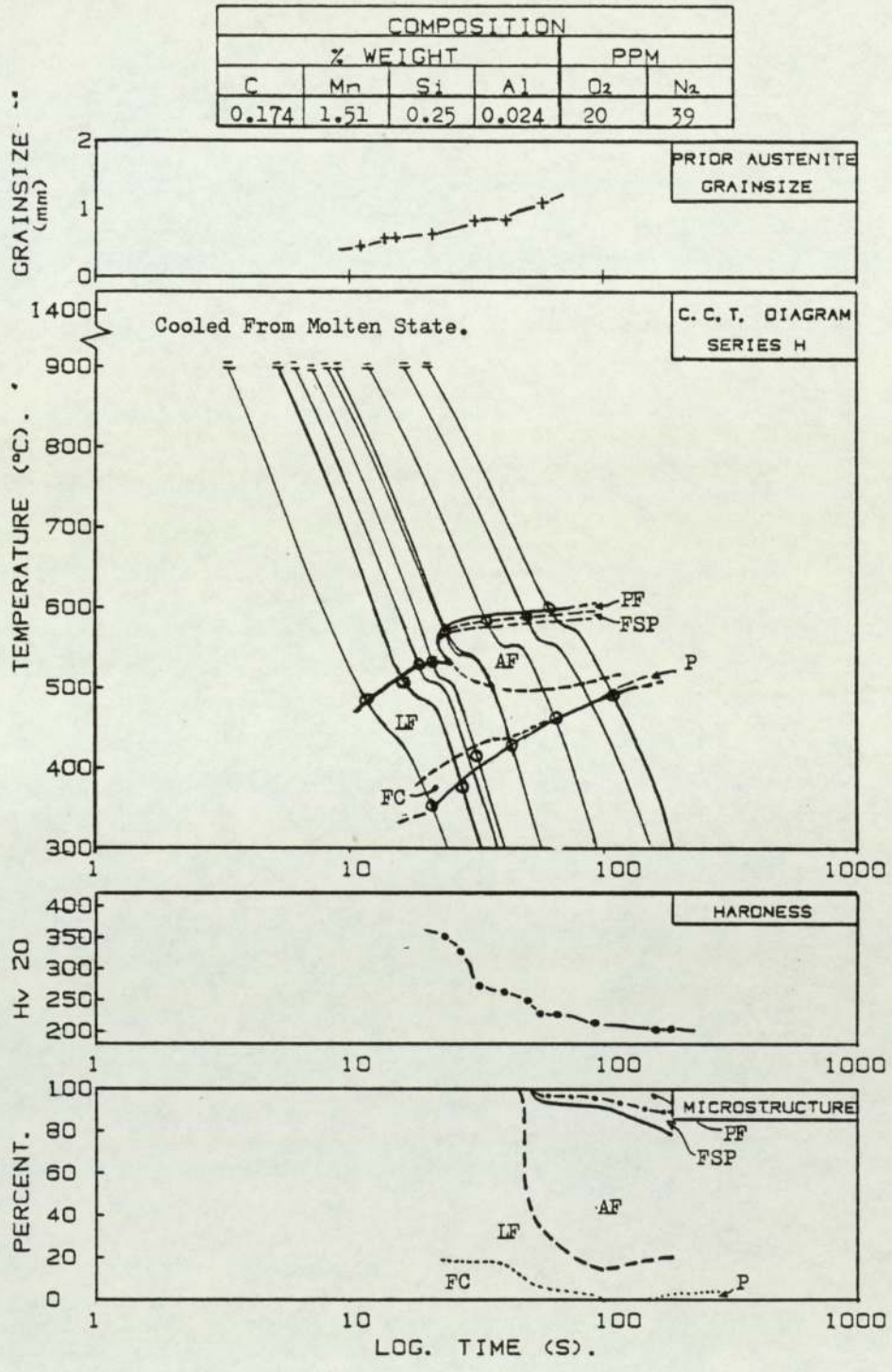

Figure No. 4.55

CCT Diagram Showing The Influence Of 0.024 %wt Al Concentration On The Transformation Characteristics, Prior Austenite Grain Size And Hardness Of Simulated As-Deposited Steel Weld Metal, With Low Oxygen Content.

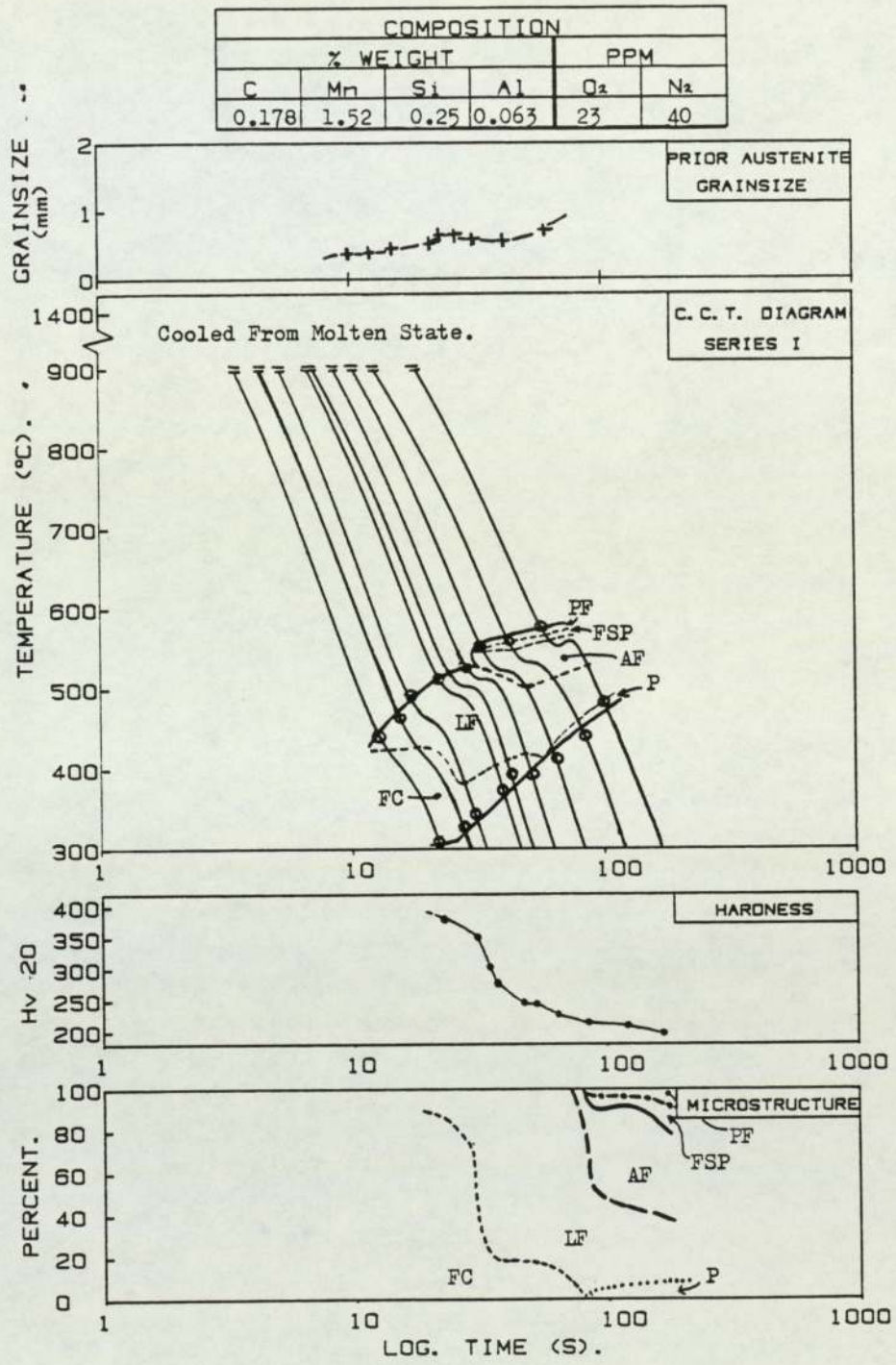

Figure No. 4.56

CCT Diagram Showing The Influence Of 0.063 %wt Al Concentration On The Transformation Characteristics, Prior Austenite Grain Size And Hardness Of Simulated As-Deposited Steel Weld Metal, With Low Oxygen Content.

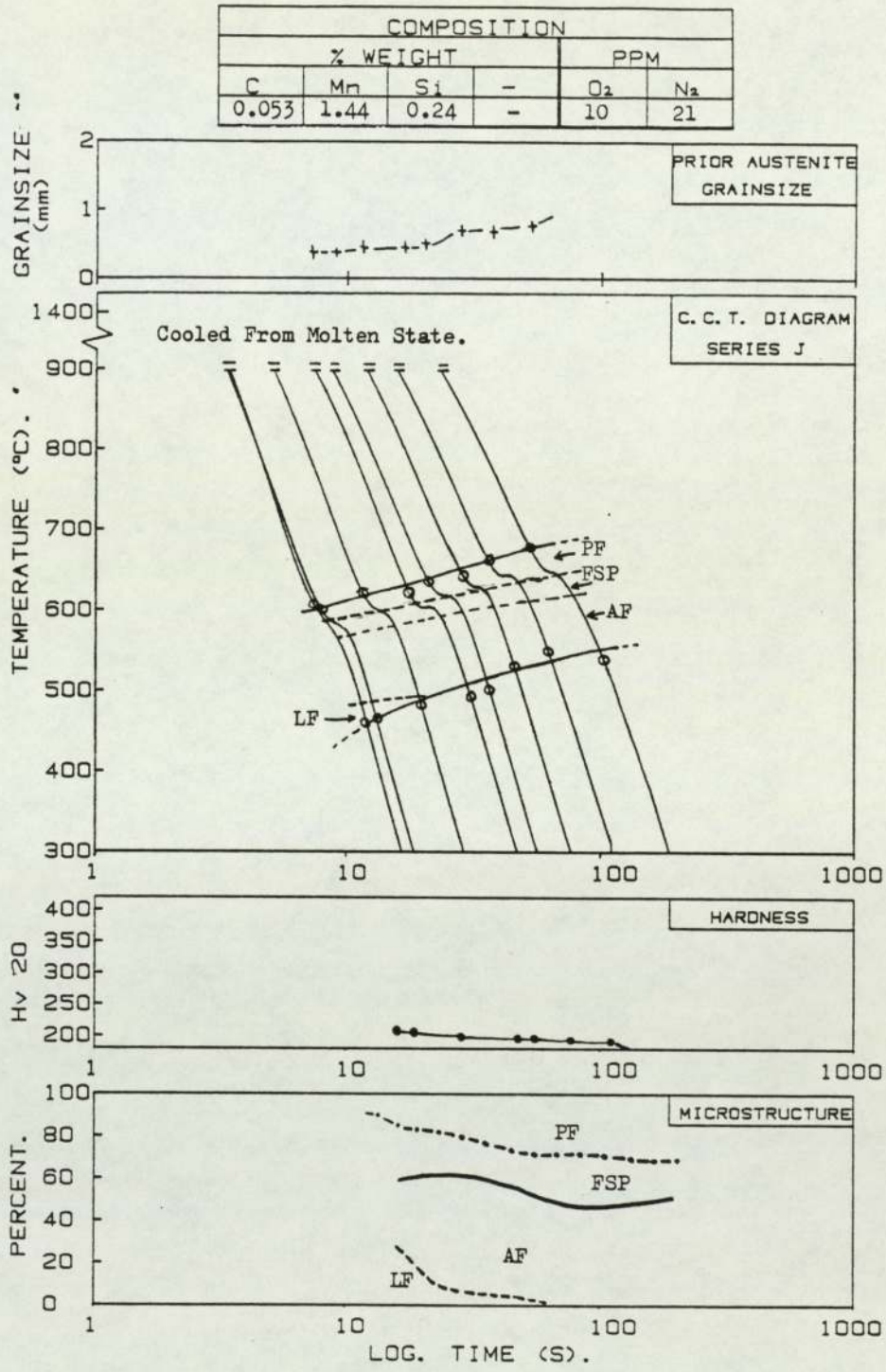

Figure No.4.57

CCT Diagram For The Low Carbon Steel (series J) Simulated As-Deposited Weld Metal With Low Oxygen Content, Showing The Transformation Characteristics, Prior Austenite Grain Size And Hardness.

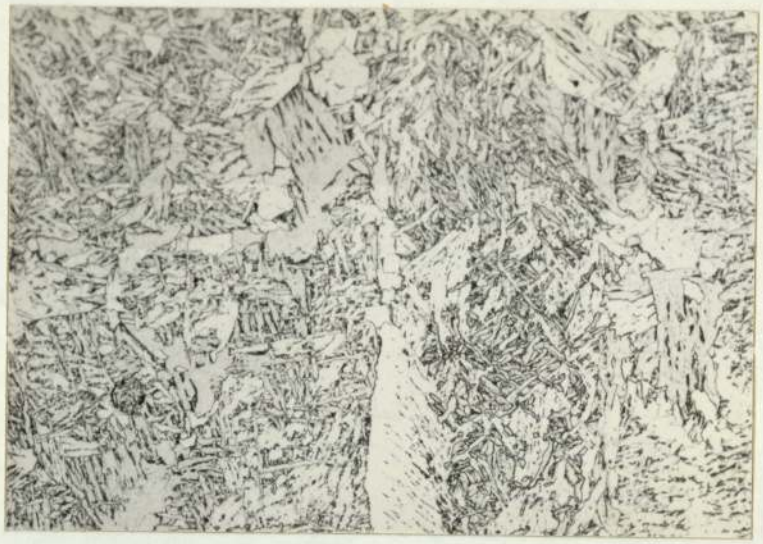

A. Low Oxygen As-Deposited Weld Metal, (Series J).
Cooling Rate 8.0°C/sec.
Oxygen Content 10ppm.

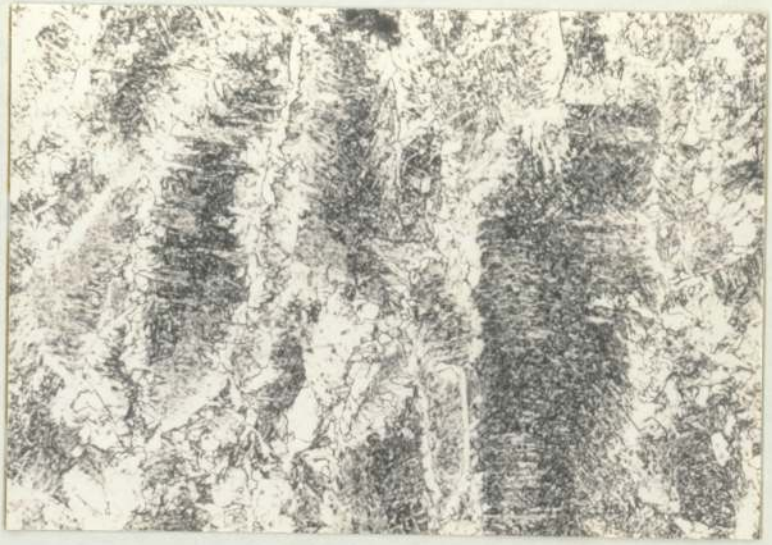

B. High Oxygen Content As-Deposited Weld Metal With Alloy Concentration To Series J.
Cooling Rate 8.0°C/sec.
Oxygen Content 300ppm.

Mag. X160.
Etchant 2% Nital.

Figure No. 4.58

Photomicrographs Comparing The Microstructures Formed In Low And High Oxygen Content Simulated As- Deposited Weld Metal Produced Using Similar Conditions.

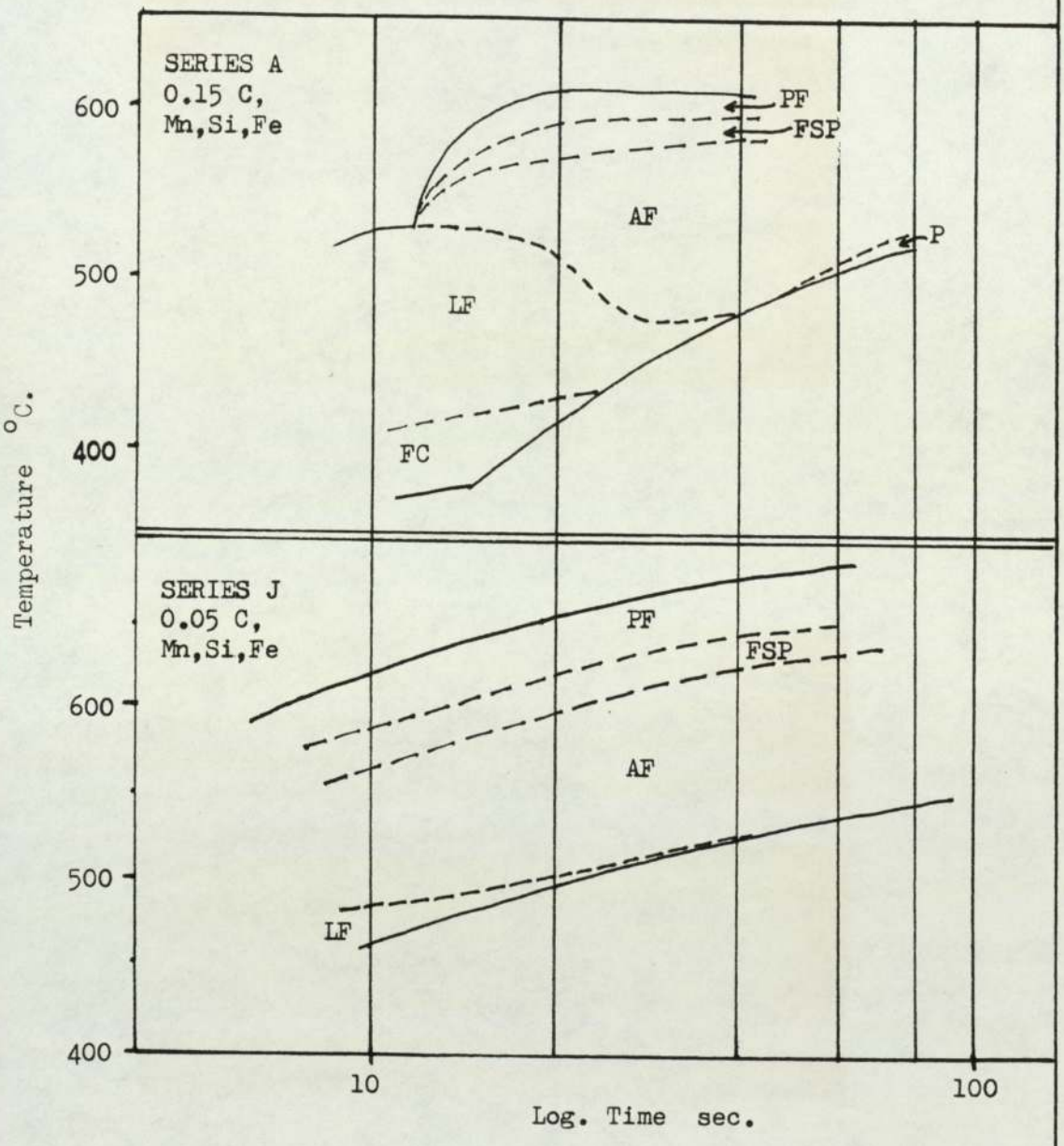

Figure No. 4.59

CCT Diagrams Showing The Effect Of Reduced Carbon Concentration On The Transformation Temperatures And Ferrite Constituents Formed Simulated As-Deposited Weld Metal, With Low Oxygen Content.

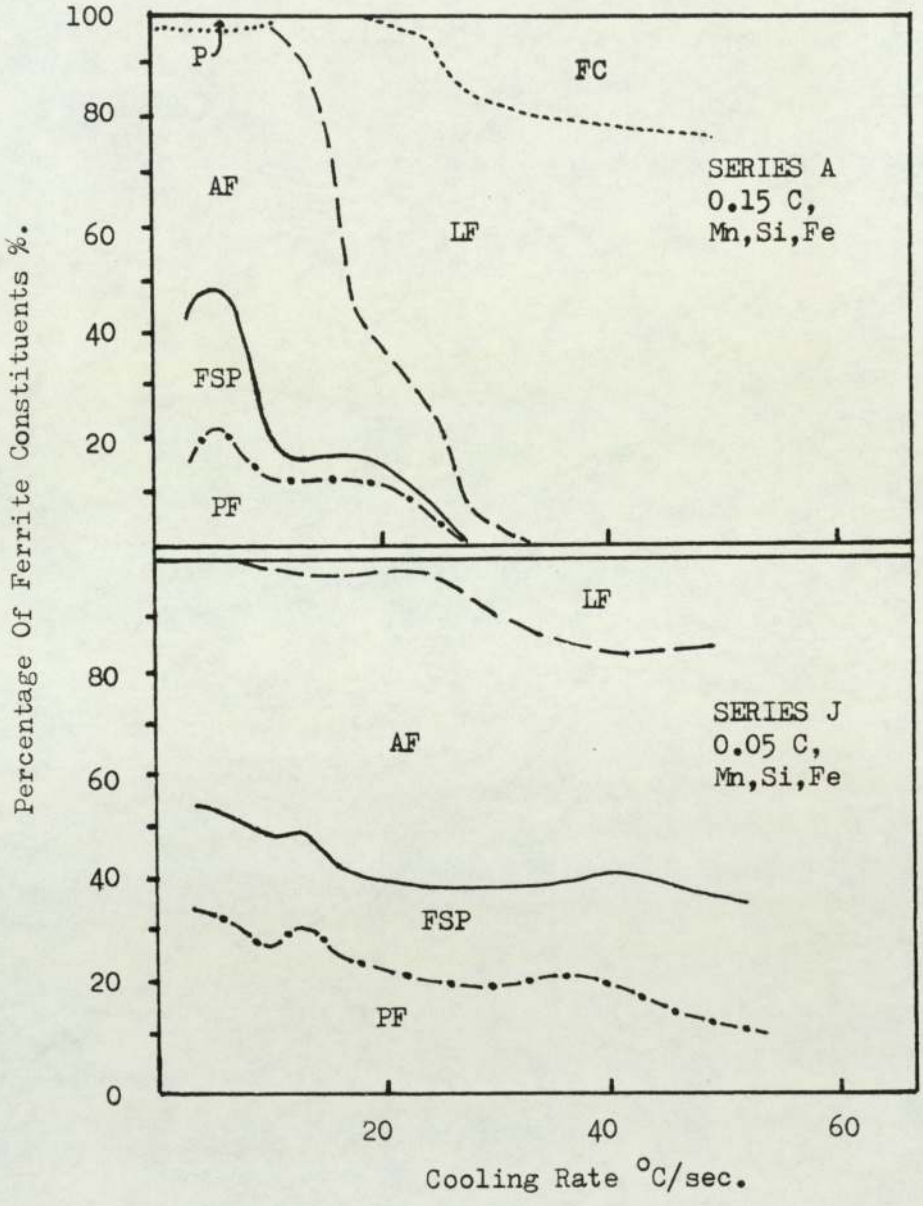

Figure No. 4.60

The Effect Of Reduced Carbon Concentration On The Type And Proportion Of Ferrite Constituents Formed In Simulated As-Deposited Weld Metal, With Low Oxygen Content.

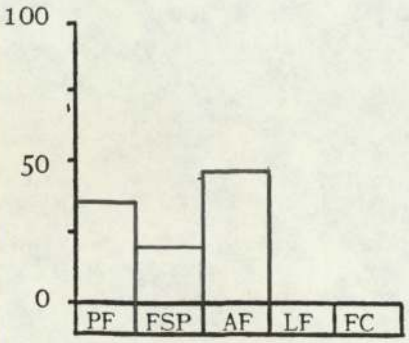

A. Specimen J1.
Cooling Rate(CR),
4.0°C/sec.

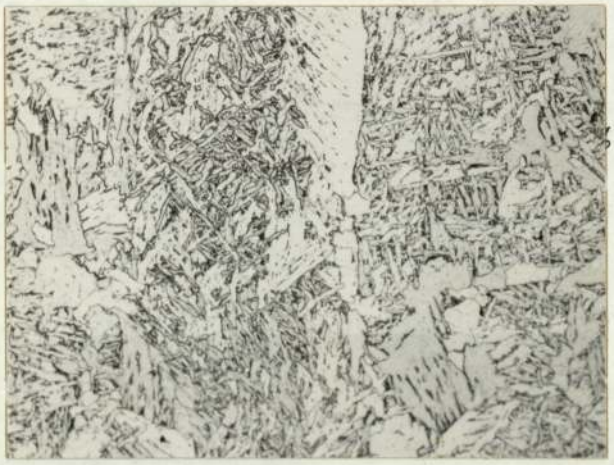

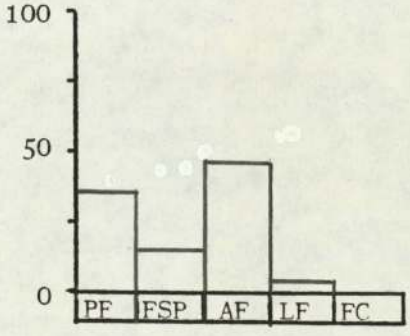

B. Specimen J7.
CR, 8.0°C/sec.

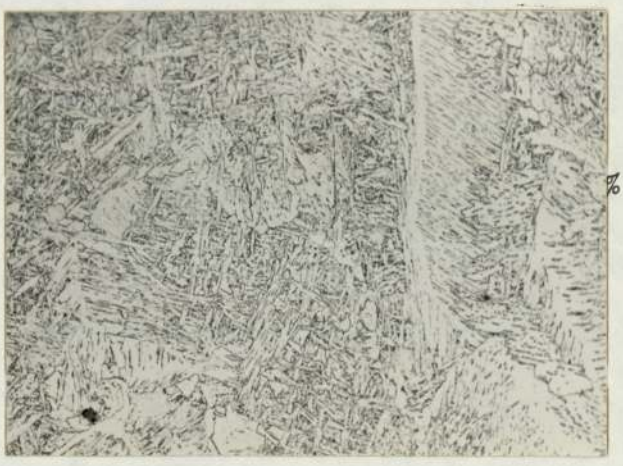

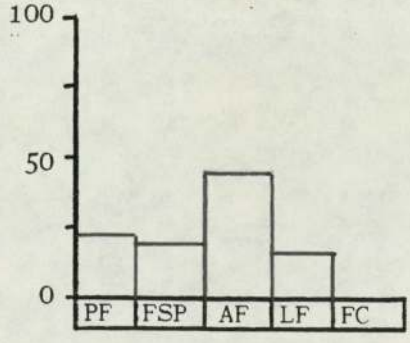

C. Specimen J15.
CR, 36.9 C/sec.

Mag. X160.
Etchant. 2% Nital.

Figure No. 4.61

Representative Photomicrographs Showing The Microstructures Formed In The 0.05%wt C Concentration (SeriesJ) Simulated Low Oxygen As-Deposited Weld Metal, With Increasing Cooling Rate.

A. 0.05%wt Carbon Alloy
Series J.
Cooling Rate 8.0°C/sec.

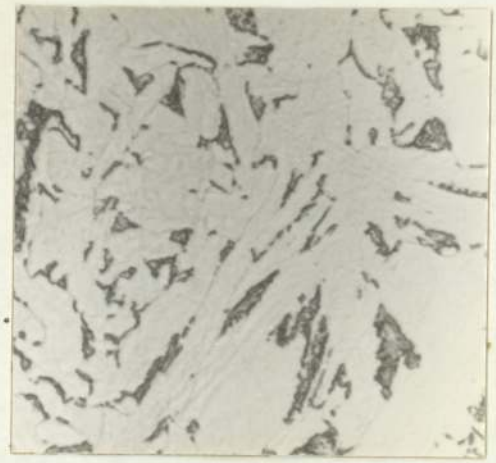

B. 0.15%wt Carbon.
Series A.
Cooling Rate 7.0°C/sec.

Figure No. 4.62

Comparison Of The Microphase Contents In The Low And High Carbon, Low Oxygen Simulated As-Deposited Weld Metal.

A. 0.05%wt Carbon Alloy.
Cooling Rate 4°C/sec.

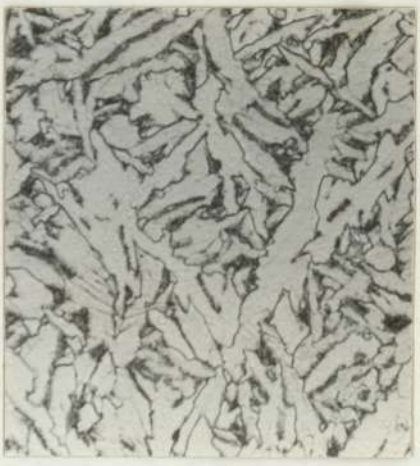

B. 0.15%wt Carbon Alloy.
Cooling Rate 4°C/sec.

Figure No. 4.63

The Influence Reduced Carbon Content On The Acicular Ferrite Grain Size.

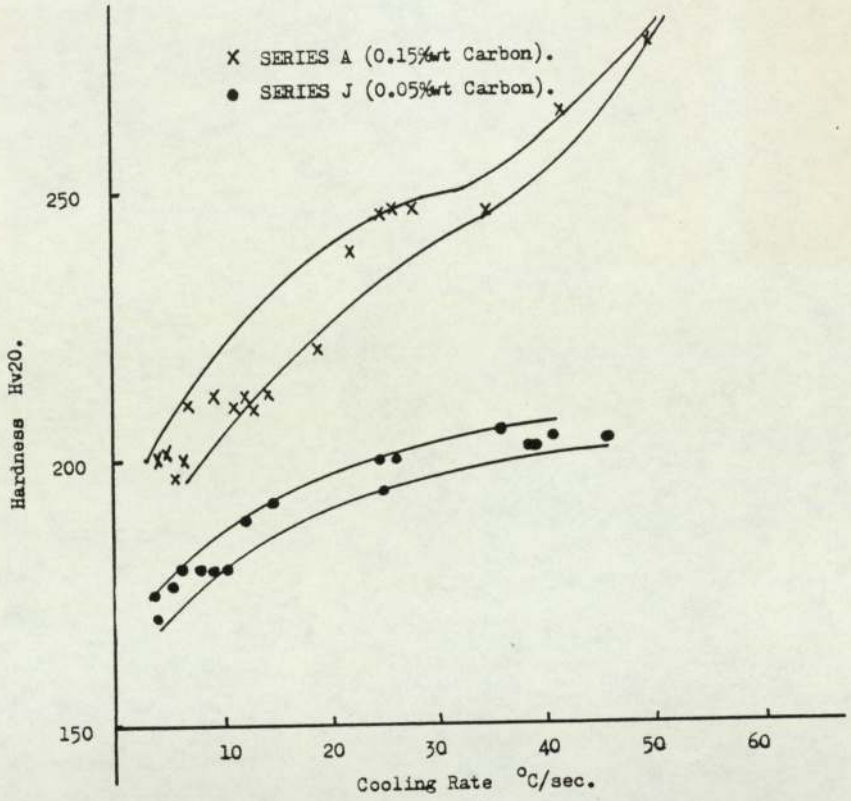

Figure No. 4.64

Comparison Of The Influence Of Low And High Carbon Content And Cooling Rate On The Hardness Of Low Oxygen Simulated As-Deposited Weld Metal.

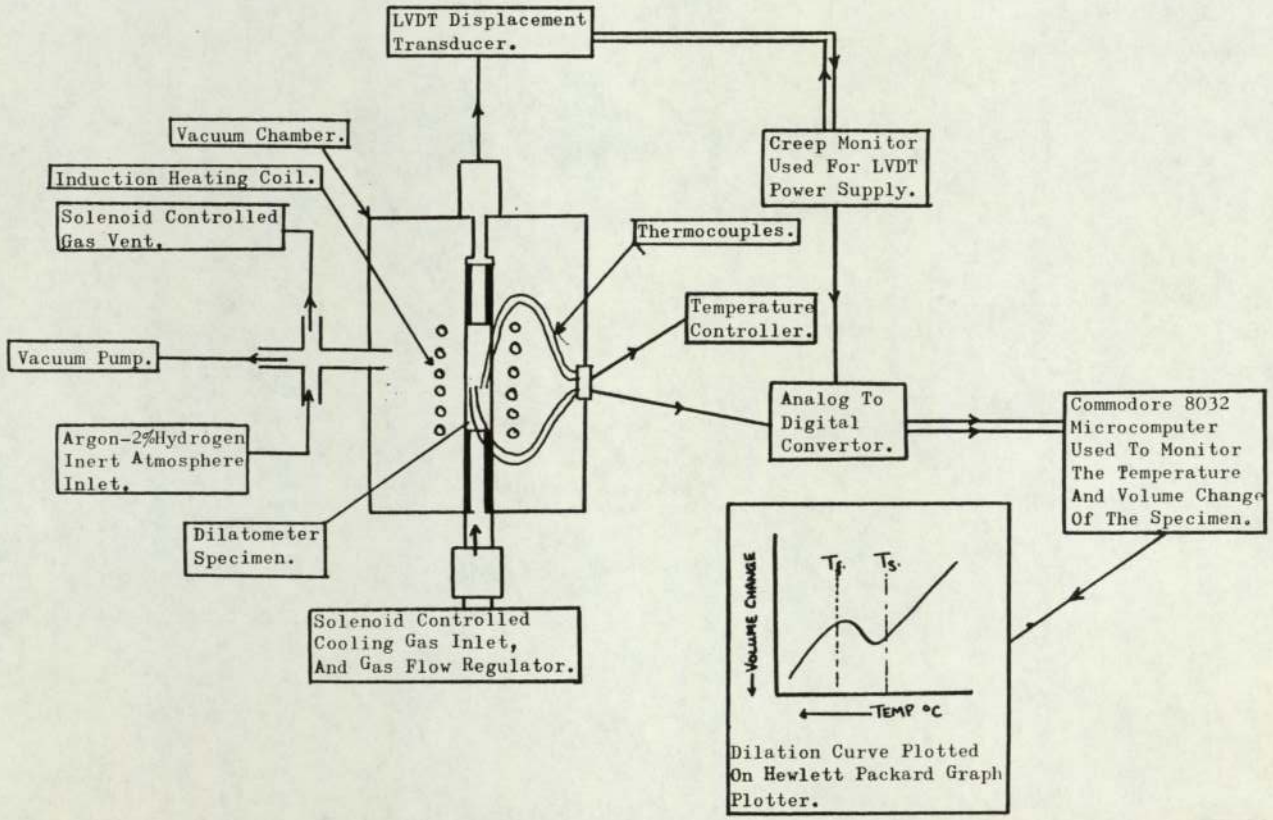

Figure No. 4.65

Schematic Diagram Of The Dilatometer Equipment Used For Simulating The Reheated Weld Metal.

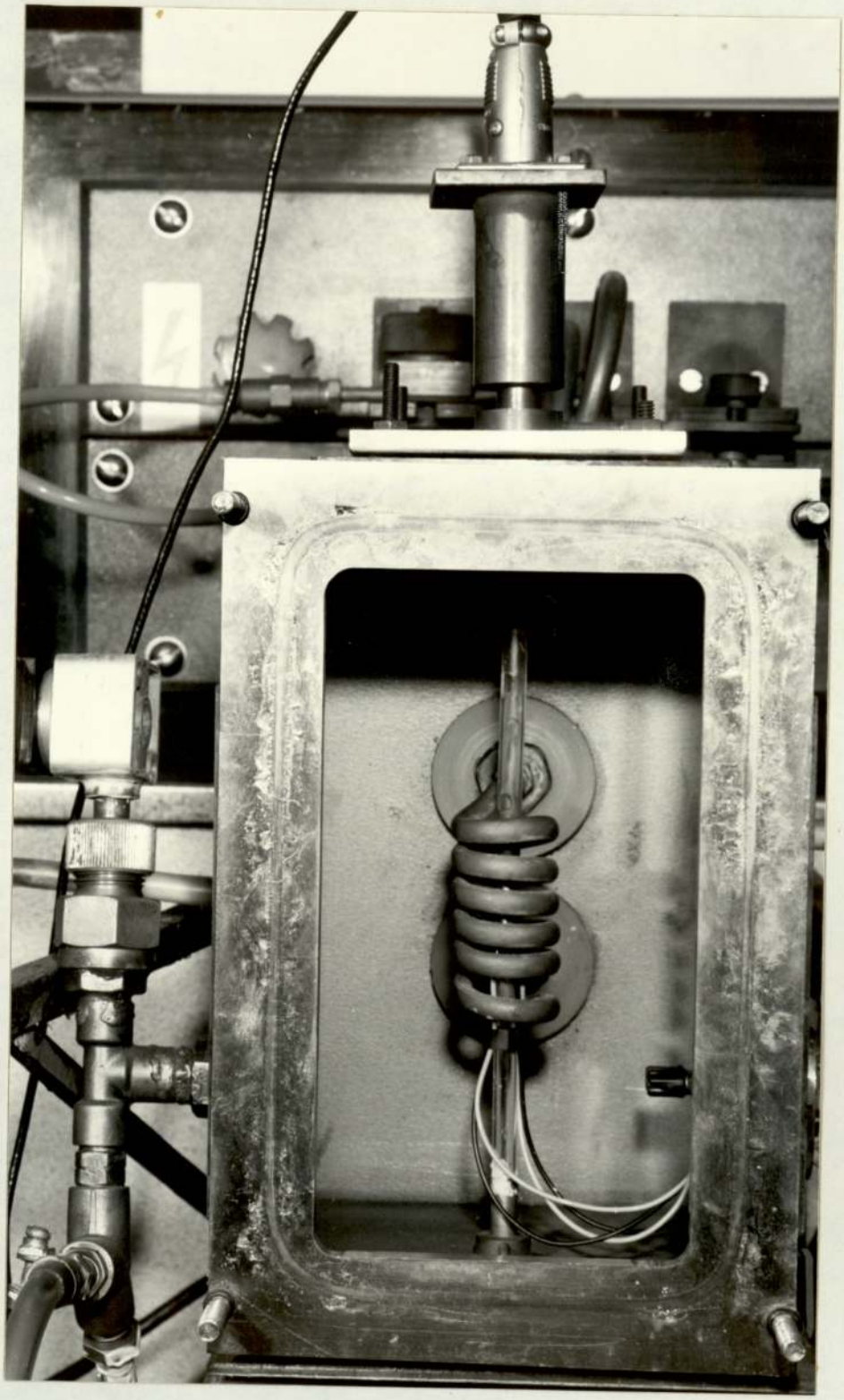

Figure No. 4.66

Photograph Of Dilatometer Chamber.

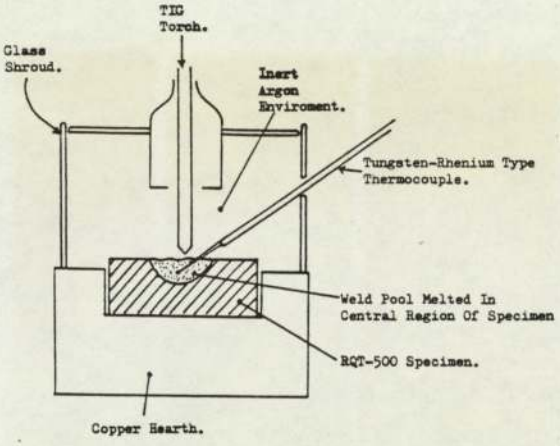

A. Arrangement Of RQT-500 Block In Copper Hearth.

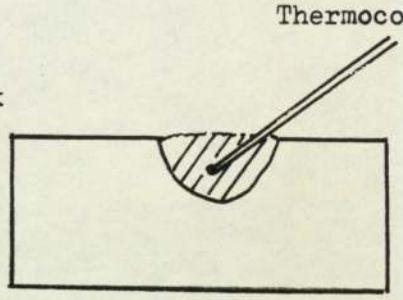

B. First Weld Pool.

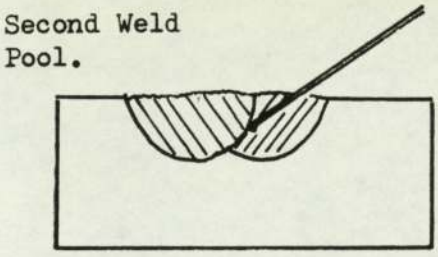

C. Second Weld Pool Adjacent To First. Thermocouple In The Coarse Grained Reheated Weld Metal.

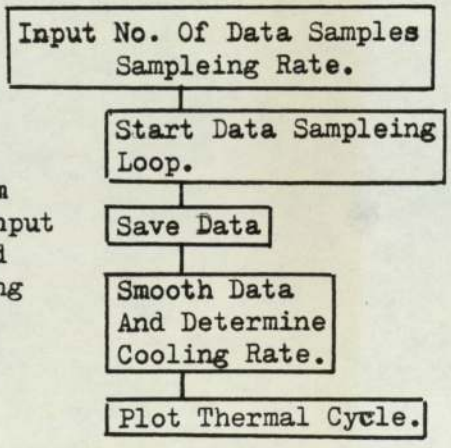

D. Flow Diagram Of Analog Input Program Used For Measuring The Thermal Cycle.

Figure No. 4.67

Technique Used For Measuring The Thermal Cycle Of The Coarse Grained Reheated Weld Metal.

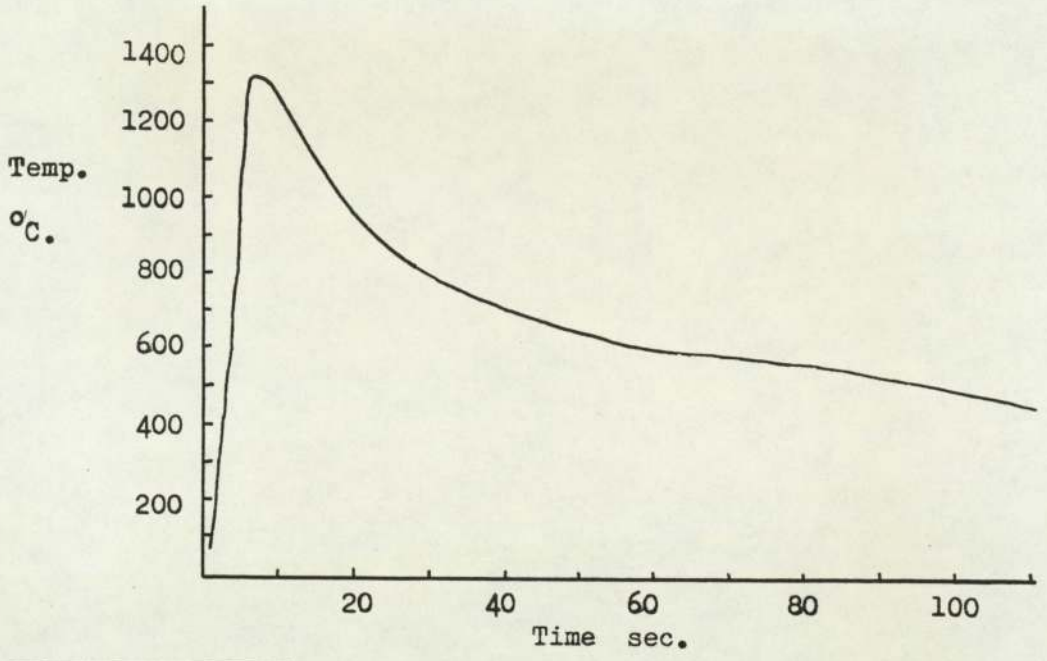

Figure No. 4.68

Thermal Cycle Determined In The Coarse Grained Zone Of The Reheated RQT-500 Steel Weld Metal.

A. Real Reheated Weld Metal
Heating Cycle, 1350°C In 7 S conds.
Cooling Rate, 4°C/sec.

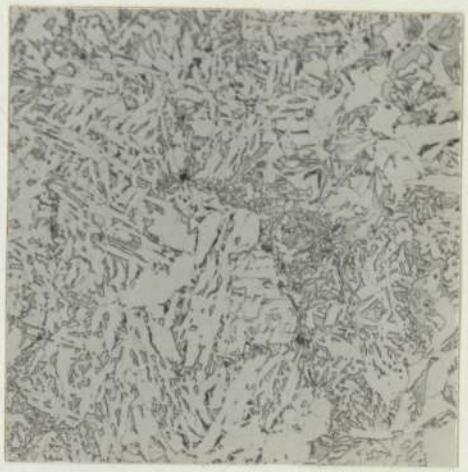

B. Simulated Reheated Weld Metal.
Heating Cycle, 1350 C In 9 Seconds.
Cooling Rate, 4°C/sec.

Figure No. 4.69 Mag. X240 And Etchant 2% Nital.

Comparison Of The Microstructures Formed In The Real And Simulated RQT-500 Reheated Weld Metal.

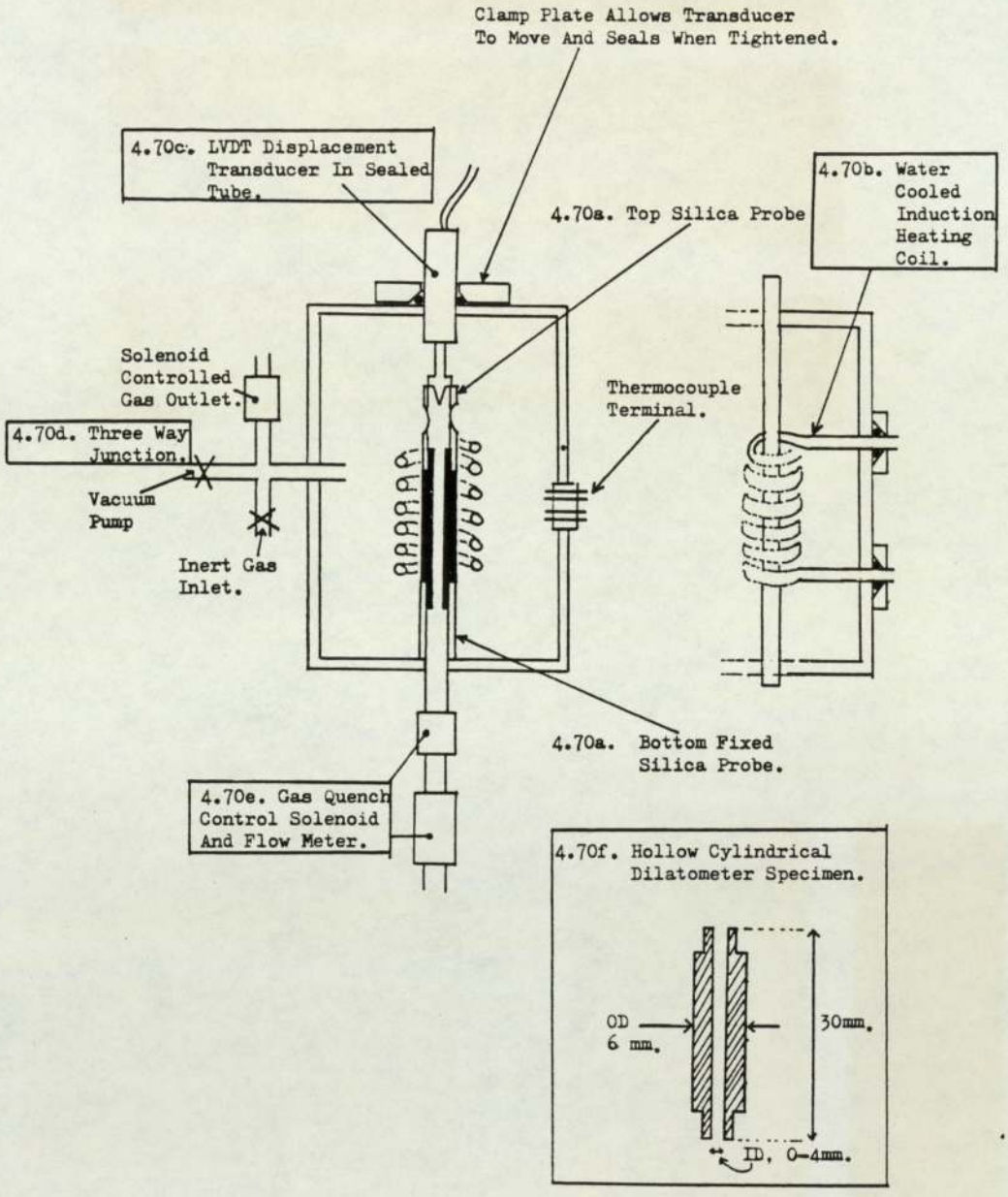

Figure No. 4.70

Arrangement Of Dilatometer Chamber.

Figure No. 4.71

Micrograph Showing Effectiveness Of Chamber Enviroment In Preventing Oxidation And Decarburisation Of The Dilatometer Specimens.

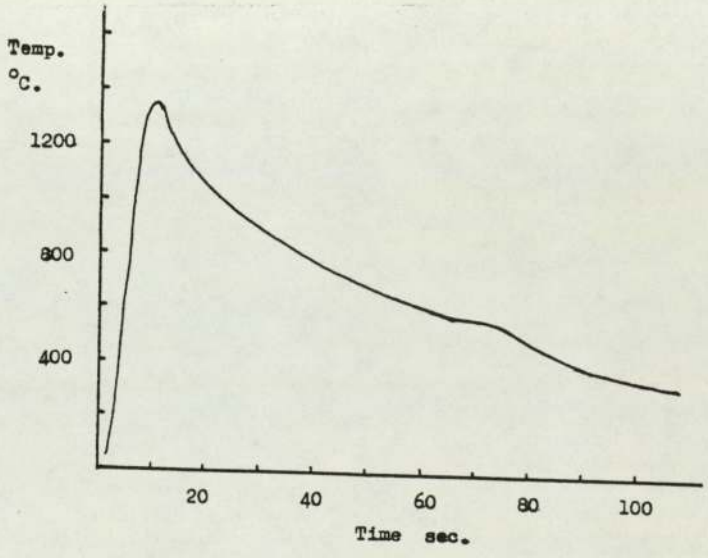

A. Thermocouples Microspot Welded Onto Dilatometer Specimen.

B. Uniform Thermal Cycle Determined In Each Position.

Figure No. 4.72

Measurement Of Temperature Distribution In The Dilatometer Specimen.

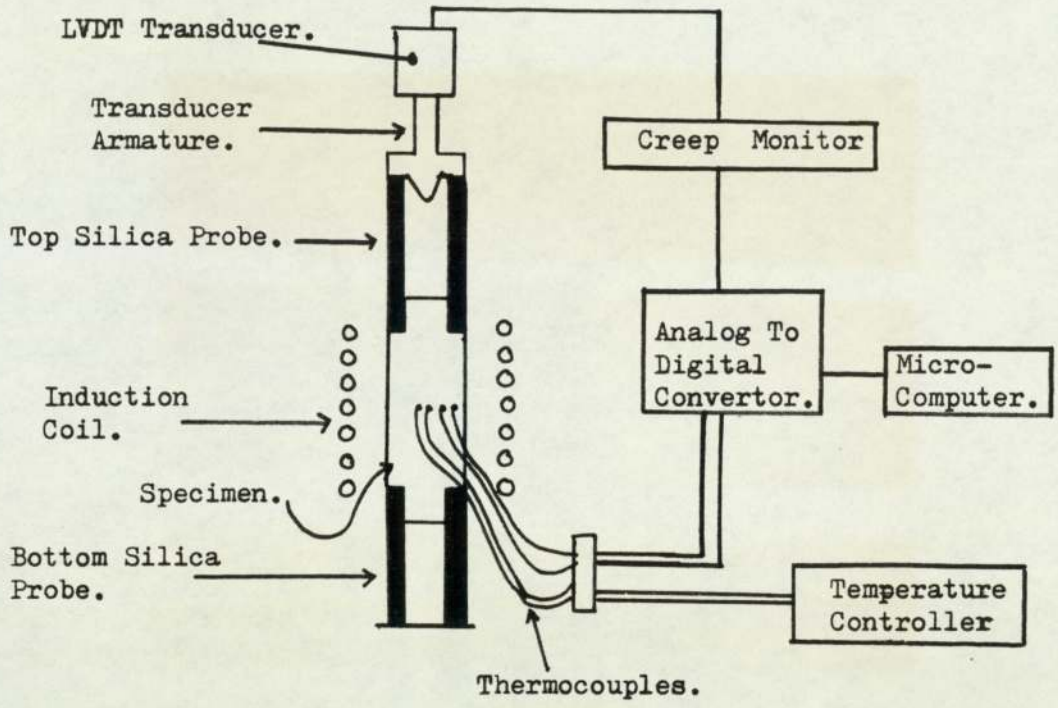

Figure No. 4.73

Measurement Of Volume Change And Temperature Of The Dilatometer Specimen During Cooling, To Determine Transformation Temperatures.

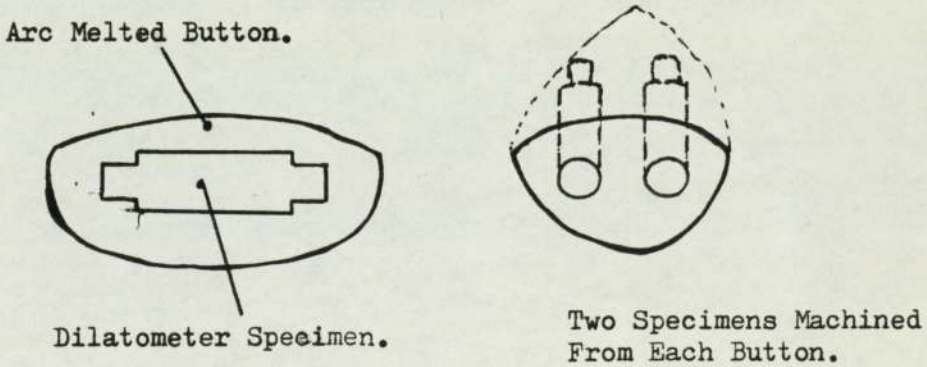

Figure No. 4.74

Machining Of The Dilatometer Specimens From The Arc Melted Buttons.

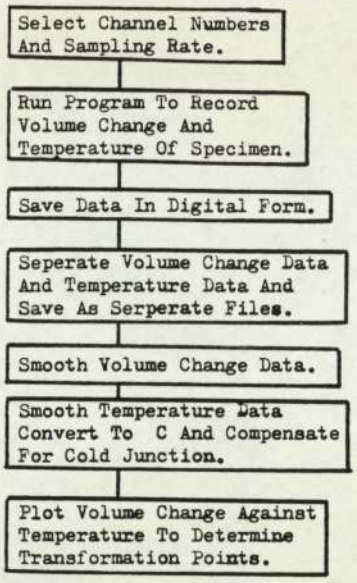

Figure No. 4.75

Flow Chart Showing The Sequence Used To Determine The Transformation Temperatures From Dilatometry, Using Computer Software.

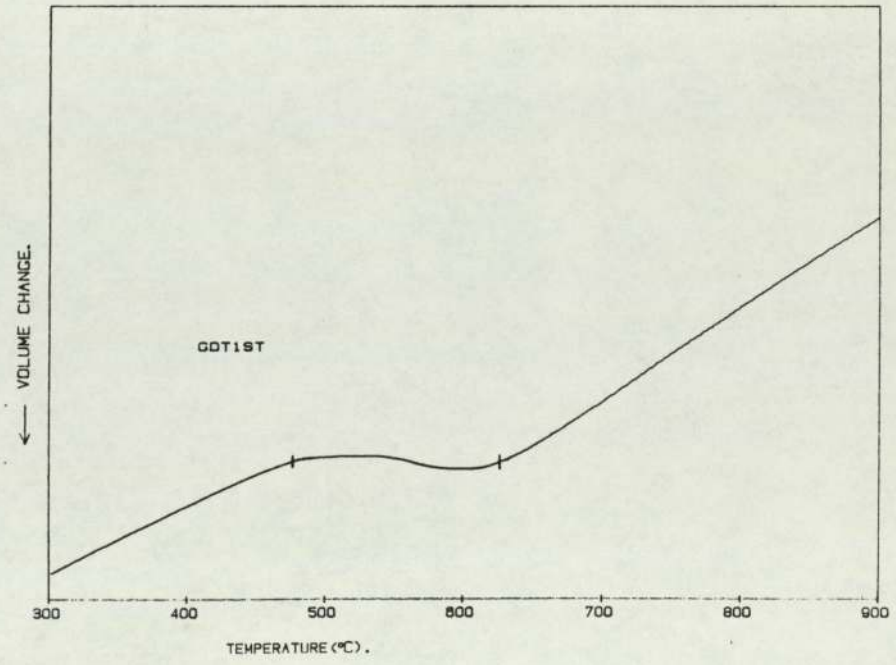

Figure No. 4.76

Example Of Dilatation Curve Produced For The Simulated Reheated Weld Metal.

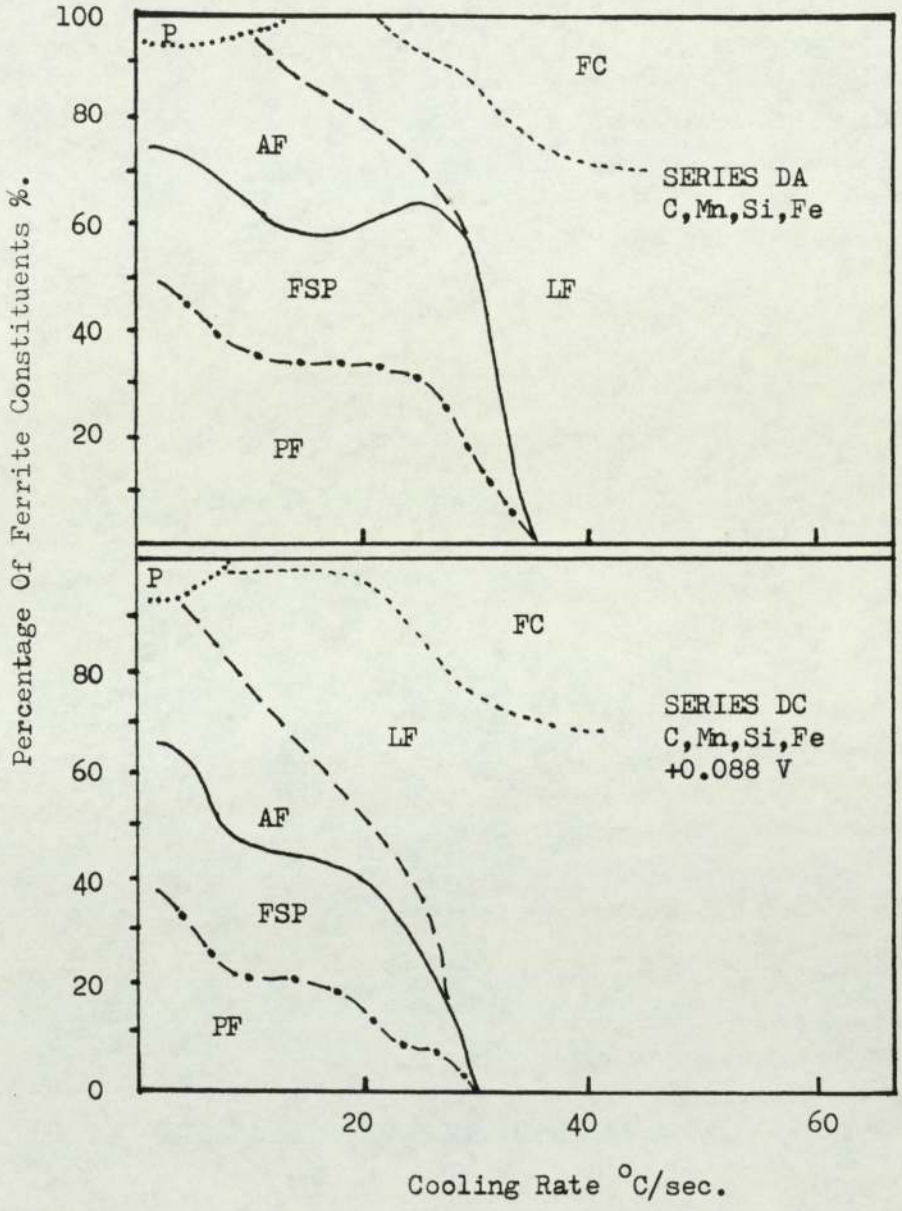

Figure No. 4.77

The Effect Of Increased V Concentration On The Type And Proportions Of Ferrite Constituents Formed In Simulated Reheated Weld Metal, With Low Oxygen Content.

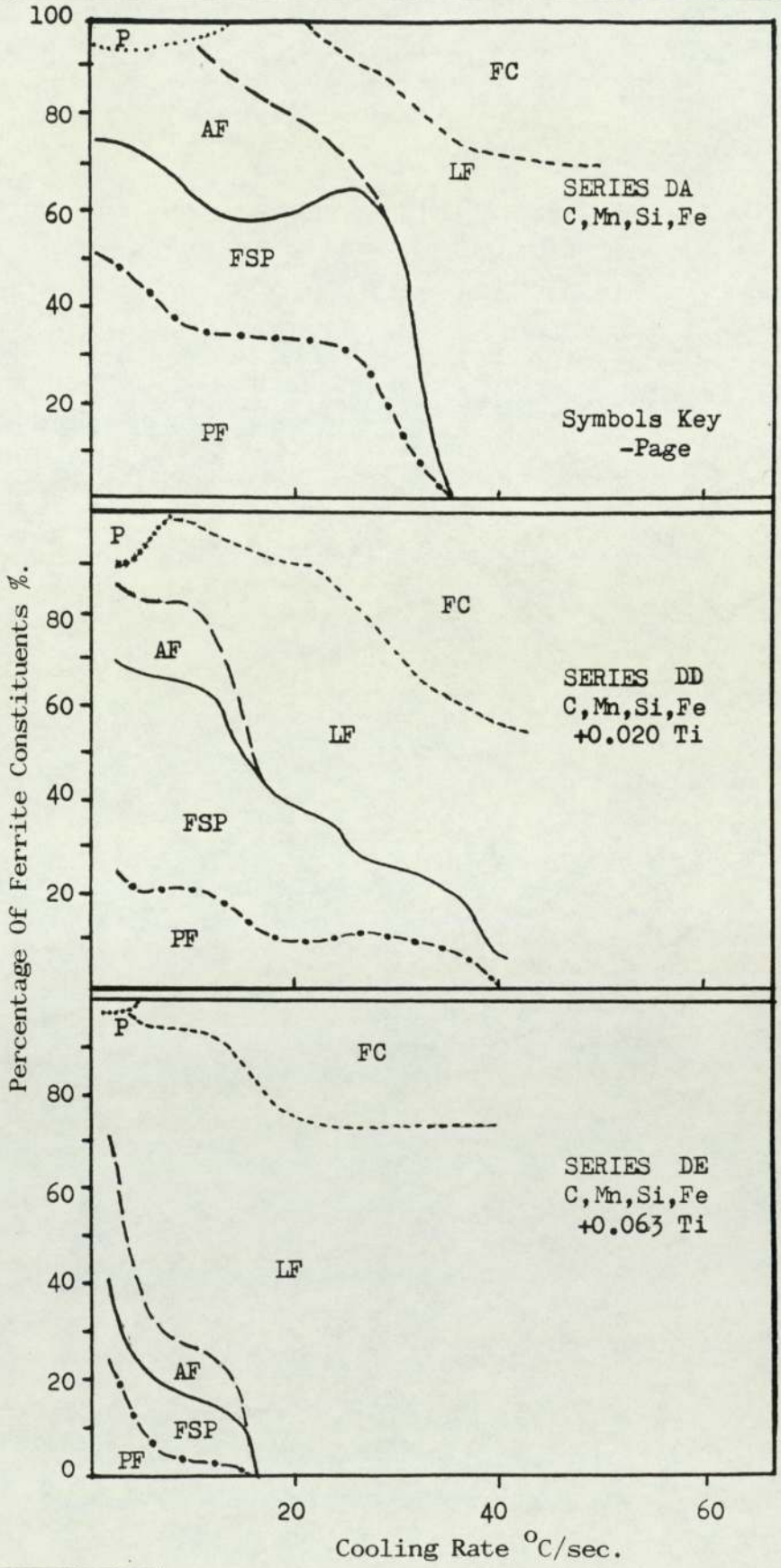

Figure No. 4.78

The Effect Of Increased Ti Concentration On The Type And Proportions Of Ferrite Constituents Formed In Simulated Reheated Weld Metal, With Low Oxygen Content.

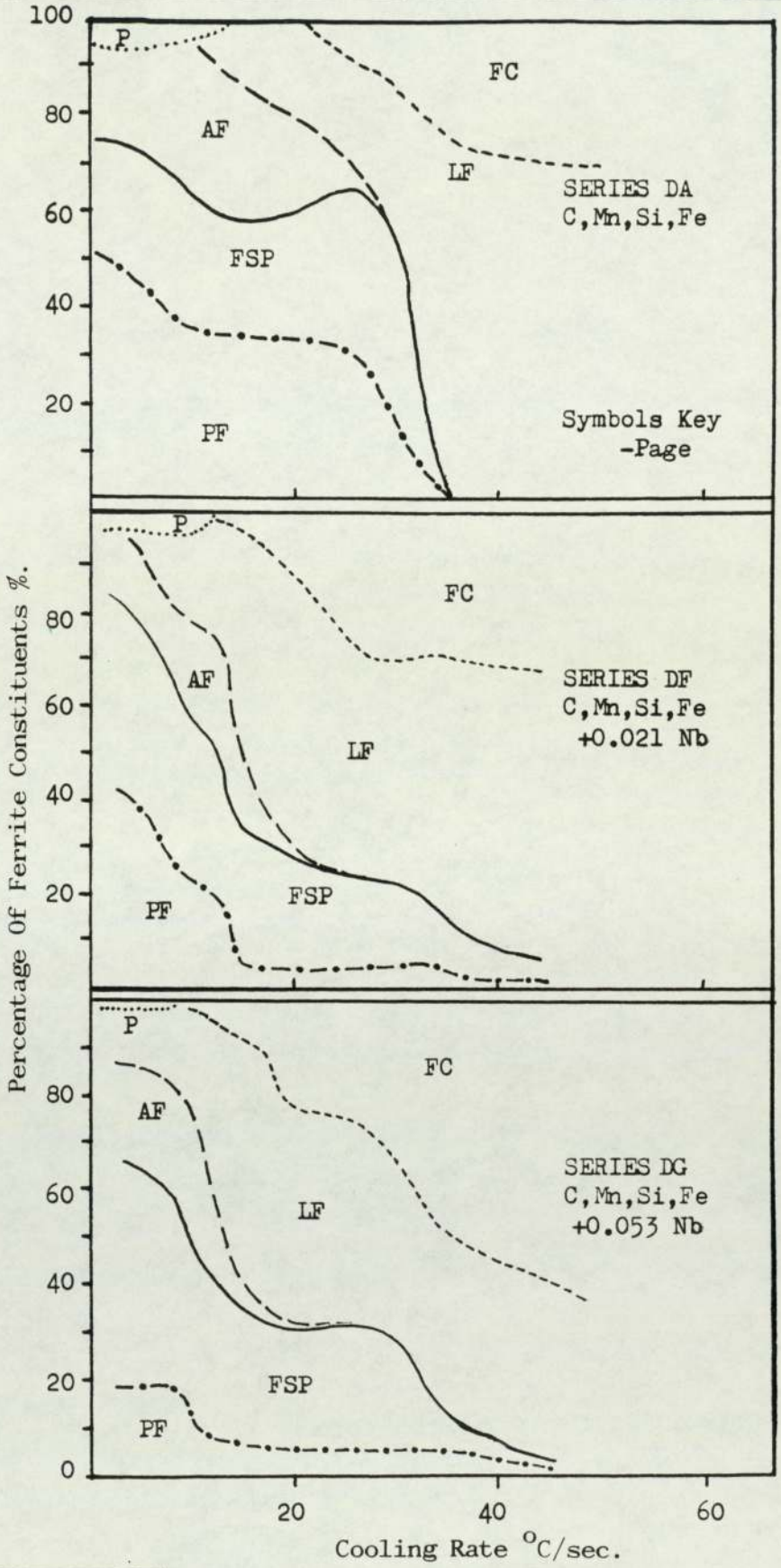

Figure No. 4.79

The Effect Of Increased Nb Concentration On The Type And Proportions Of Ferrite Constituents Formed In Simulated Reheated Weld Metal, With Low Oxygen Content.

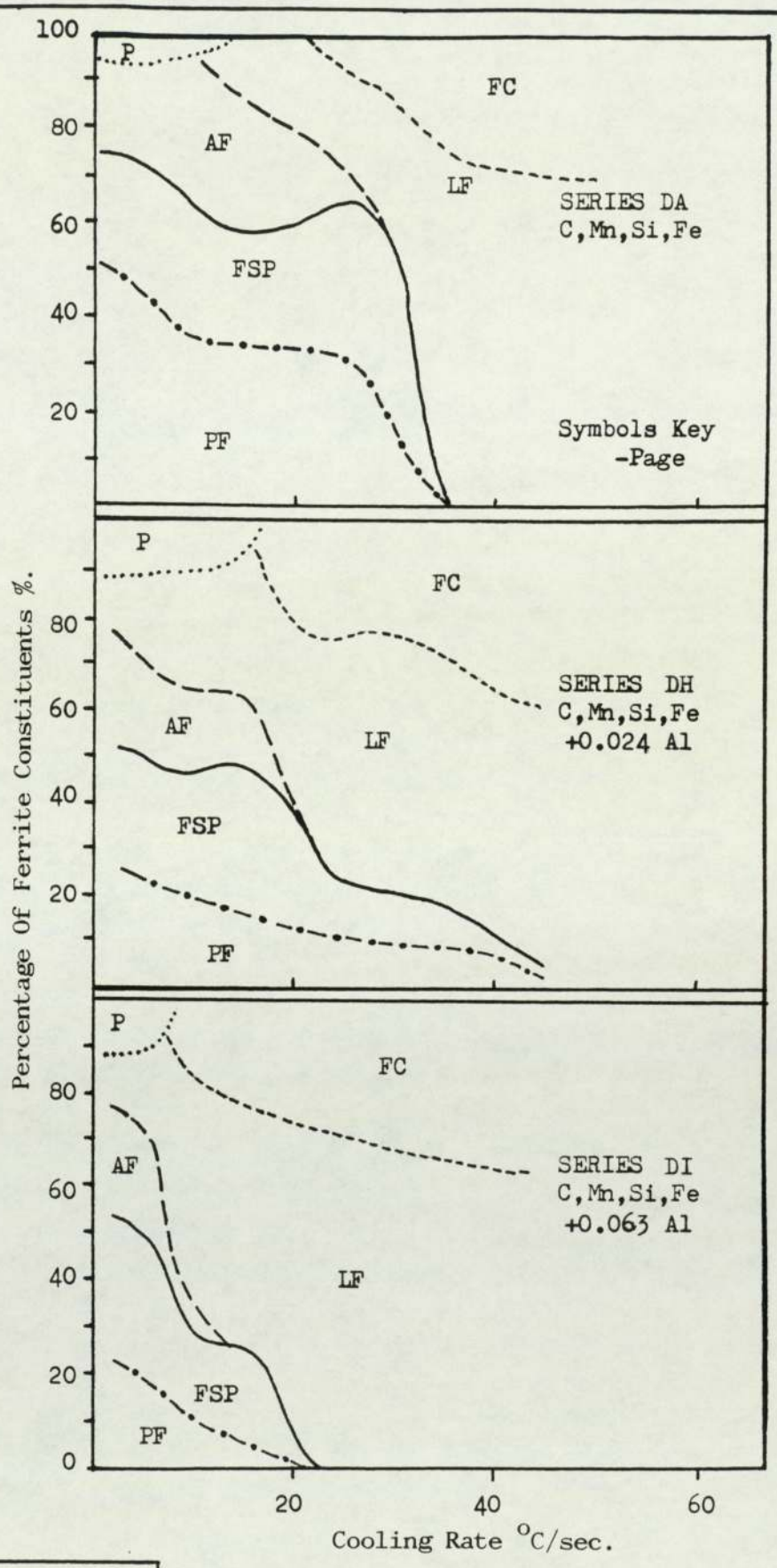

Figure No. 4.80

The Effect Of Increased Al Concentration On The Type And Proportions Of Ferrite Constituents Formed In Simulated Reheated Weld Metal, With Low Oxygen Content.

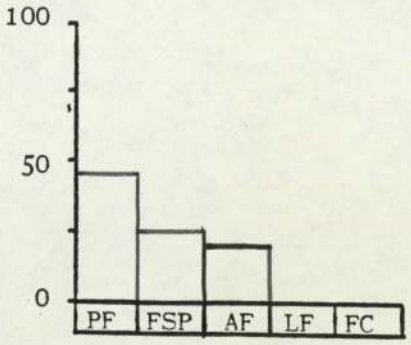

A. Specimen DA4.
Cooling Rate(CR),
4.2°C/sec.

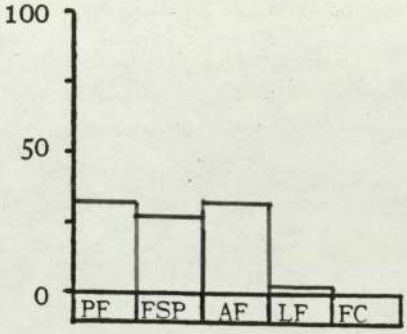

B. Specimen DA8.
CR, 11.8°C/sec.

Mag. X160.
Etchant 2% Nital.

Figure No. 4.81

Representative Photomicrographs Showing The Microstructures Formed In The Reheated Base Alloy (Series DA) Simulated Low Oxygen Reheated Weld Metal, With Increasing Cooling Rate.

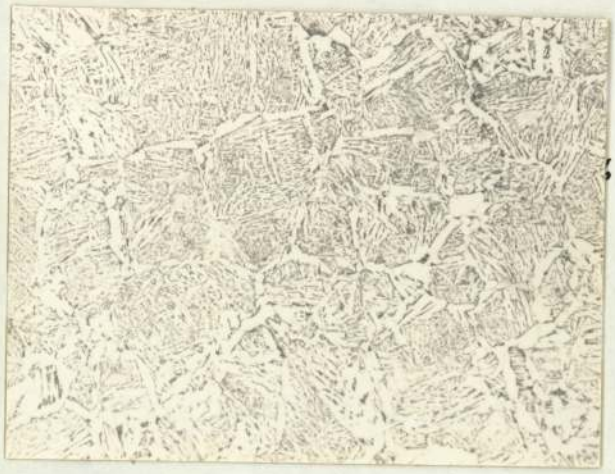

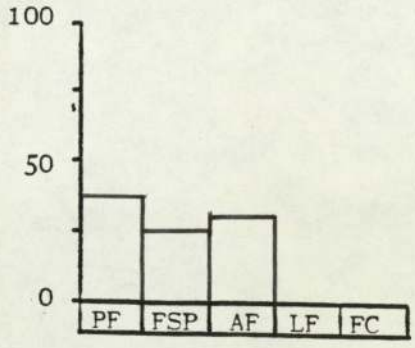

A. Specimen DC2.
Cooling Rate(CR),
4.1°C/sec.

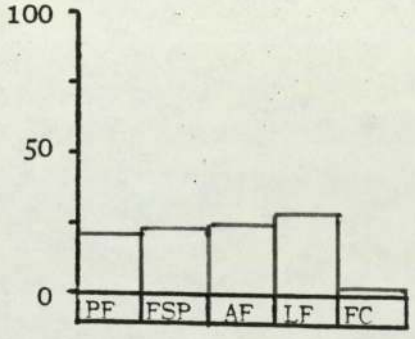

B. Specimen DC8
CR, 12.1°C/sec.

Mag. X160.
Etchant 2% Nital.

Figure No. 4.82

Representative Photomicrographs Showing The Microstructures Formed In The 0.088%wt V Concentration, (Series DV) Simulated Low Oxygen Reheated Weld Metal, With Increasing Cooling Rate.

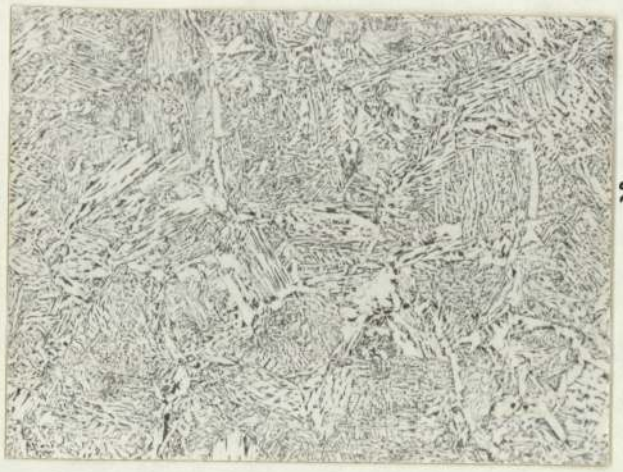

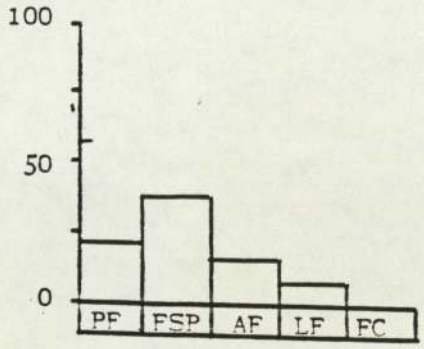

A. Specimen DD13
Cooling Rate(CR),
3.9°C/sec.

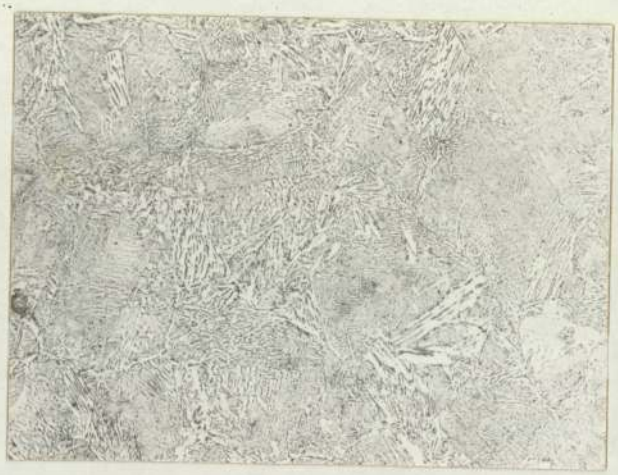

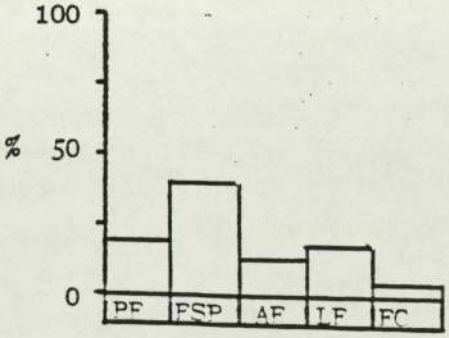

B. Specimen DD15.
CR, 11.4 C/sec.

Mag. X160.
Etchant 2% Nital.

Figure No. 4.83

Representative Photomicrographs Showing The Microstructures Formed In The 0.020%wt Ti Concentration, (SeriesDD) Simulated Low Oxygen Reheated Weld Metal, With Increasing Cooling Rate.

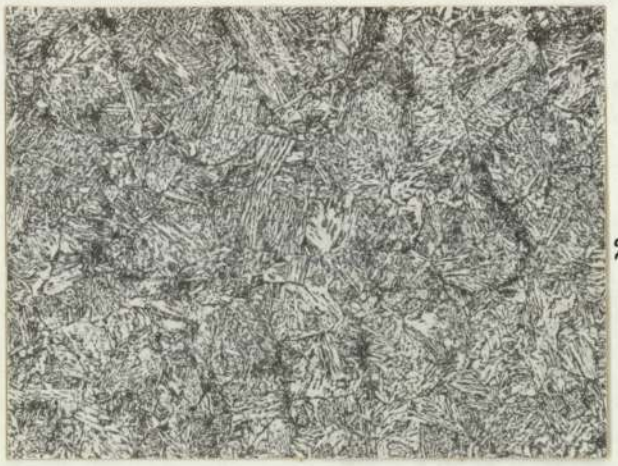

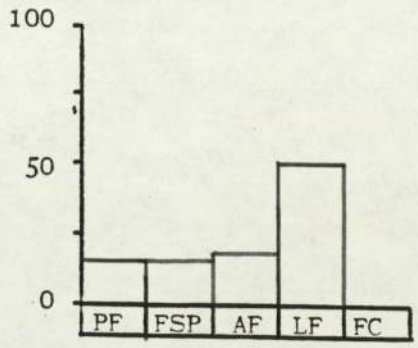

A. Specimen DE15.
Cooling Rate(CR),
4.1°C/sec.

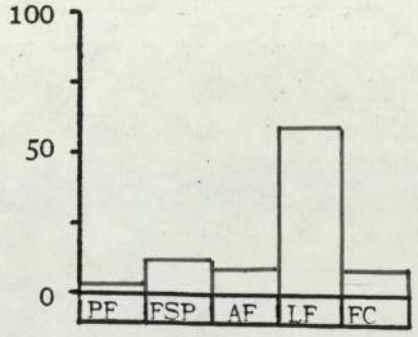

B. Specimen DE5.
CR, 11.4°C/sec.

Mag. X160.
Etchant 2% Nital.

Figure No. 4.84

Representative Photomicrographs Showing The Microstructures Formed In The 0.063%wt Ti Concentration, (Series DE) Simulated Low Oxygen Reheated Weld Metal, With Increasing Cooling Rate.

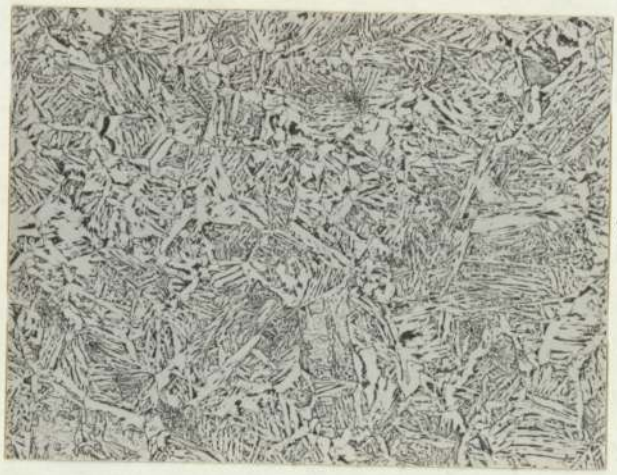

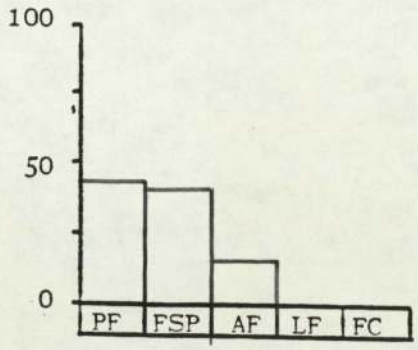

A. Specimen DF9.
Cooling Rate(CR),
4.3°C/sec.

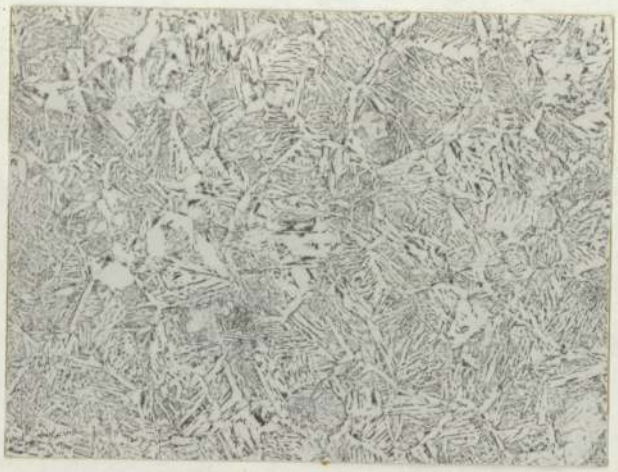

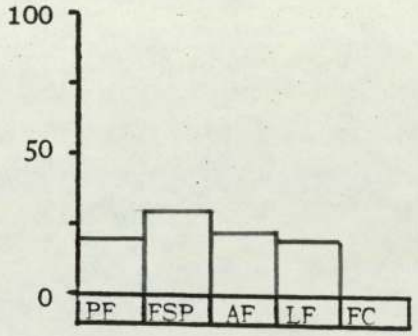

B. Specimen DF11.
CR, 11.5°C/sec.

Mag. X160.
Etchant 2% Nital.

Figure No. 4.85

Representative Photomicrographs Showing The Microstructures Formed In The 0.021%wt Nb Concentration, (Series DF) Simulated Low Oxygen Reheated Weld Metal, With Increasing Cooling Rate.

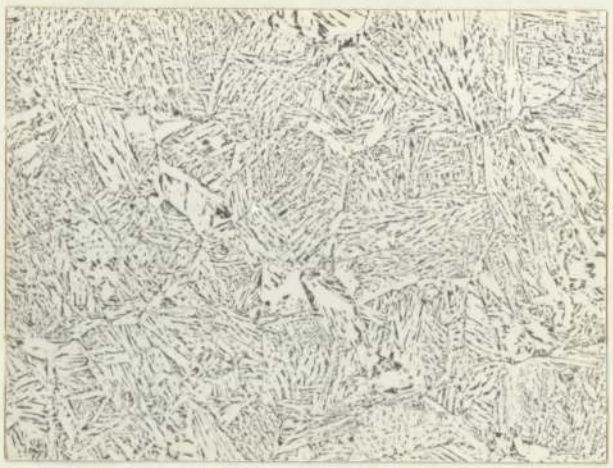

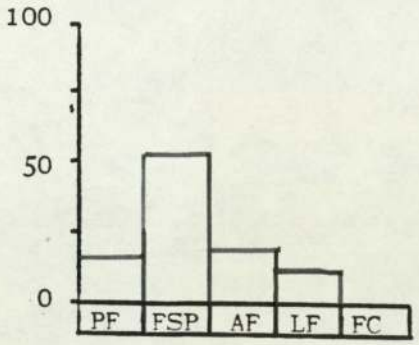

A. Specimen DG7.
Cooling Rate(CR),
4.6°C/sec.

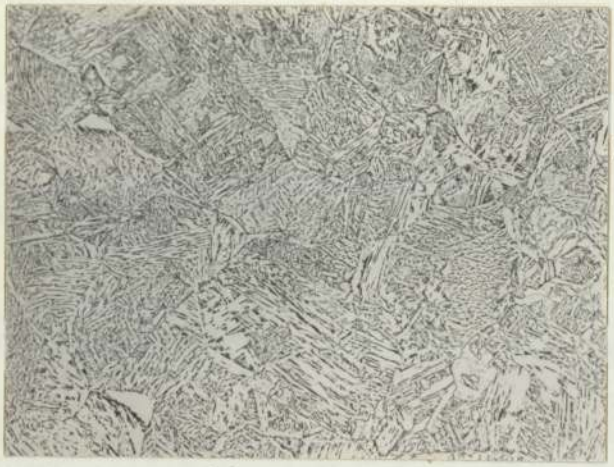

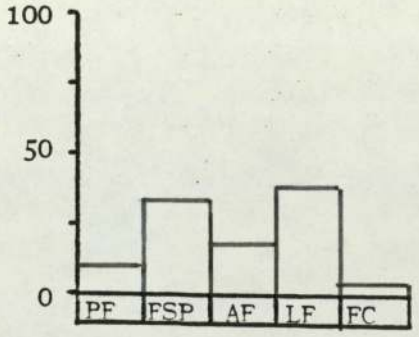

B. Specimen DG1.
CR, 12.3°C/sec.

Mag. X160.
Etchant 2% Nital.

Figure No. 4.86

Representative Photomicrographs Showing The Microstructures Formed In The 0.053%wt Nb Concentration, (Series DG) Simulated Low Oxygen Reheated Weld Metal, With Increasing Cooling Rate.

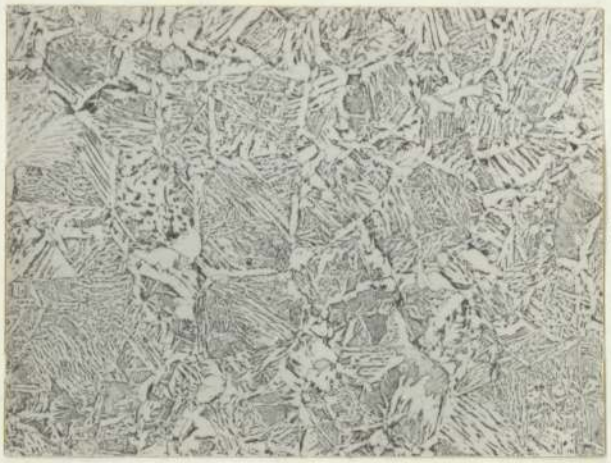

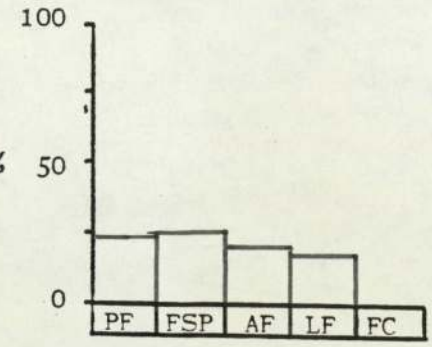

A. Specimen DH2.
Cooling Rate(CR),
4.9°C/sec.

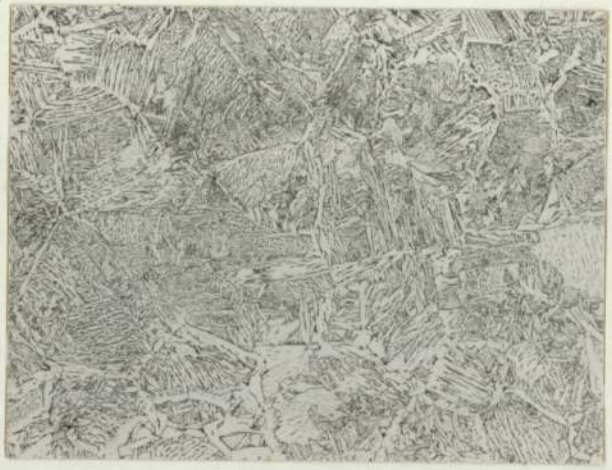

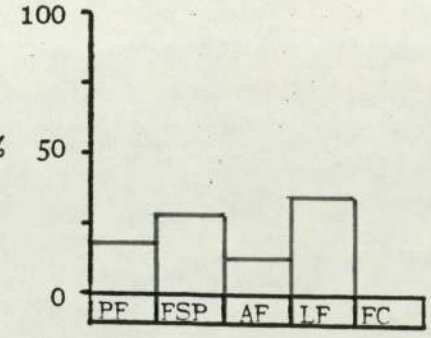

B. Specimen DH16.
CR, 13.2°C/sec.

Mag. X160.
Etchant 2% Nital.

Figure No. 4.87

Representative Photomicrographs Showing The Microstructures Formed In The 0.024%wt Al Concentration, (Series DH) Simulated Low Oxygen Reheated Weld Metal, With Increasing Cooling Rate.

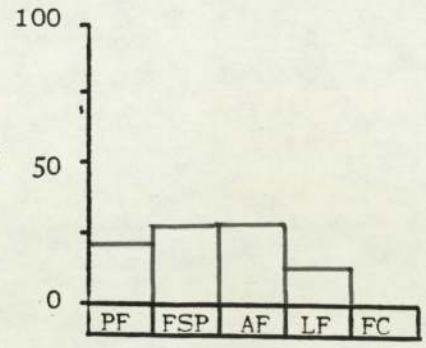

A. Specimen DI2.
Cooling Rate(CR),
4.1°C/sec.

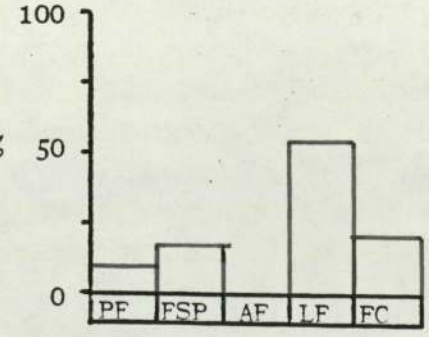

B. Specimen DI10.
CR, 12.3°C/sec.

Mag. X160.
Etchant 2% Nital.

Figure No. 4.88

Representative Photomicrographs Showing The Microstructures Formed In The 0.063%wt Al Concentration, (SeriesDI) Simulated Low Oxygen Reheated Weld Metal, With Increasing Cooling Rate.

Base Alloy, Series DA.
Cooling Rate (CR) 4.2°C/sec.

0.027 %wt V, Series DC.
CR, 4.1°C/sec.

Mag. X1200.
Etchant, Picral.

Figure No. 4.89

Photomicrographs Showing The Effect Of V Additions On The Microphases Formed In Simulated Reheated Weld Metal.

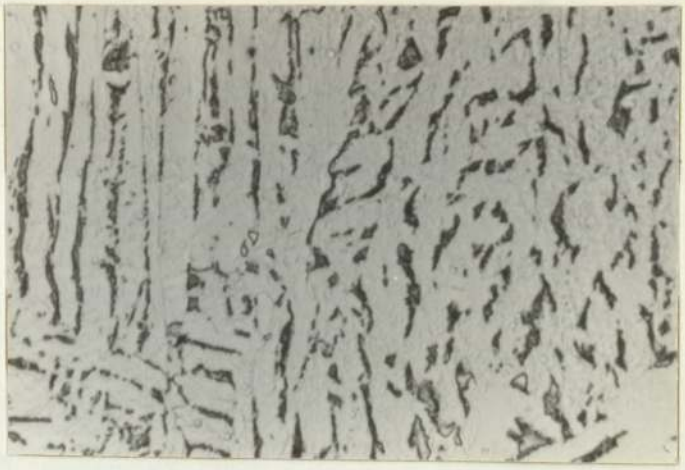

0.020 %wt Ti, Series DD.
Cooling Rate (CR) 3.9 °C/sec.

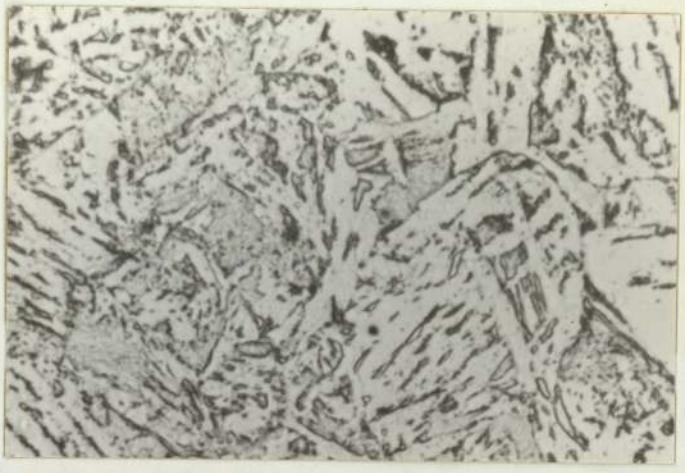

0.063 %wt Ti, Series DE.
CR 4.1°C/sec.

SEE FIGURE 4.89 FOR BASE ALLOY.

Mag. X1200.
Etchant, Picral.

Figure No. 4.90

Photomicrographs Showing The Effect Of Ti Addition On The Microphases Formed In The Simulated Reheated Weld Metal.

0.021 %wt Nb, Series DF.
Cooling Rate (CR)4.3 °C/sec.

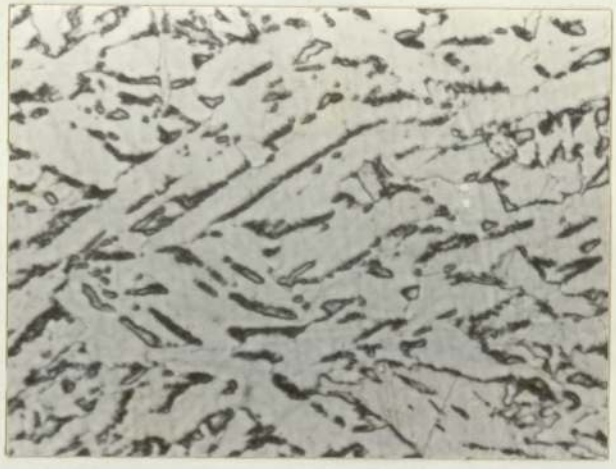

0.053 %wt Nb, Series DG.
CR, 4.6 °C/sec.

SEE FIGURE 4.89 FOR BASE ALLOY.

Mag. X1200.
Etchant, Picral.

Figure No. 4.91

Photomicrographs Showing The Effect Of Nb Addition On The Microphases Formed In The Simulated Reheated Weld Metal.

0.024 %wt Al, Series DH,
Cooling Rate (CR) 4.9 °C/sec.

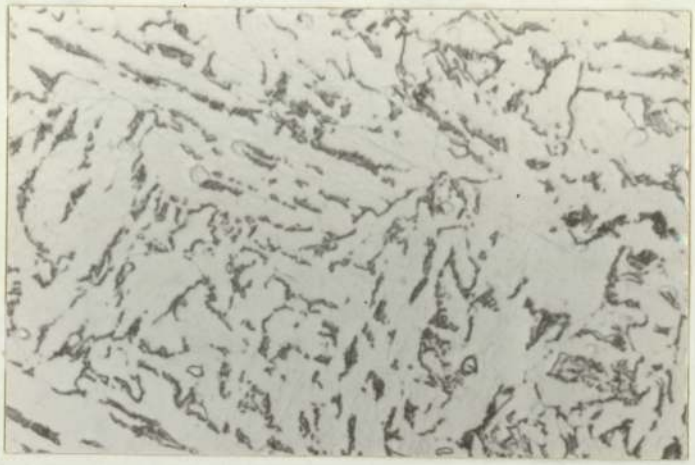

0.063 %wt Al, Series DI
CR, 4.1 °C/sec.

SEE FIGURE 4.89 FOR BASE ALLOY.

Mag. X1200.
Etchant, Picral.

Figure No. 4.92

Photomicrographs Showing The Effect Of Al Addition On The Microphases Formed In The Simulated Reheated Weld Metal.

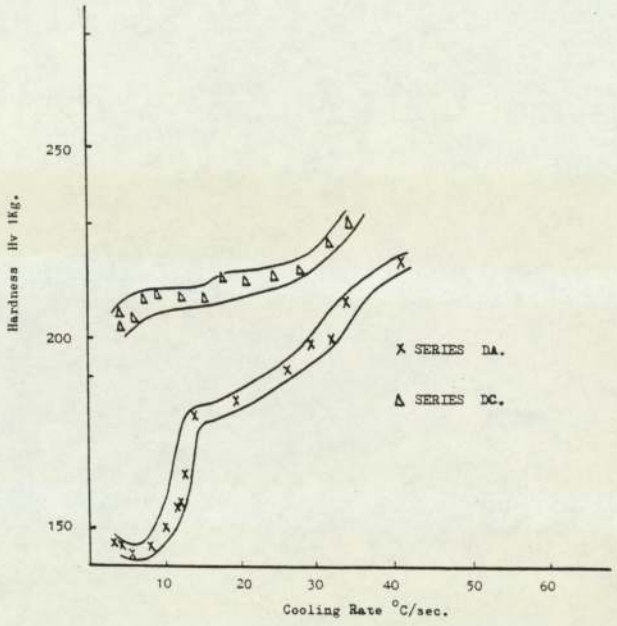

Figure No. 4.93

The Influence Of Vanadium On The Hardness Of Low Oxygen Content Simulated Reheated Weld Metal.

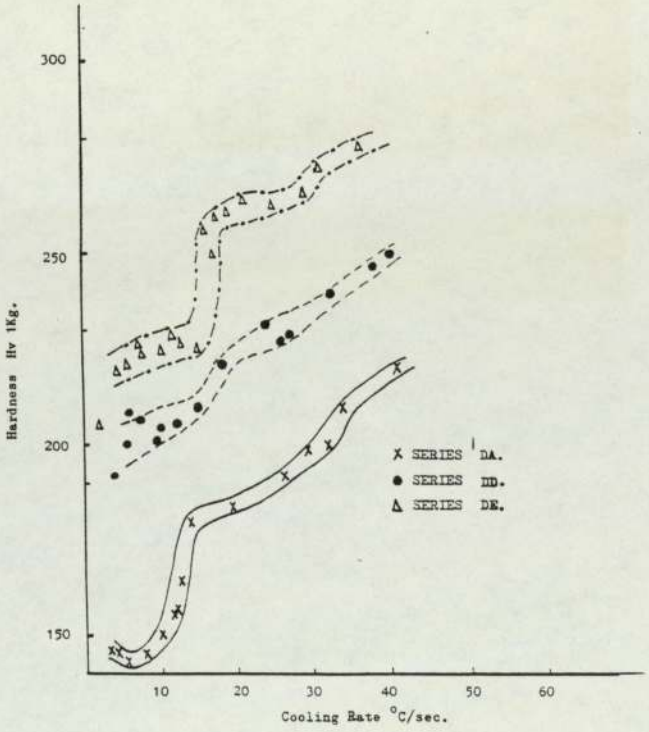

Figure No.. 4.94

The Influence Of Titanium On The Hardness Of Low Oxygen Content Simulated Reheated Weld Metal.

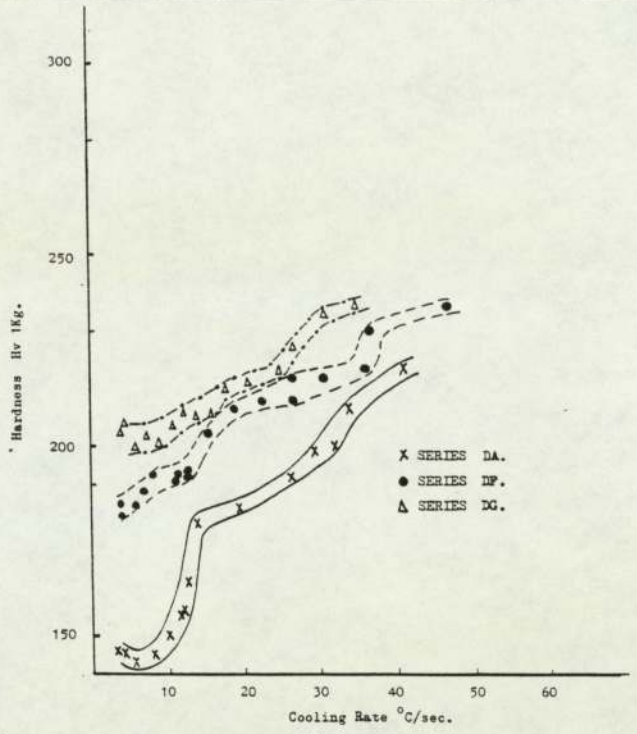

Figure No. 4.95

The Influence Of Niobium On The Hardness Of Low Oxygen Content Simulated Reheated Weld Metal.

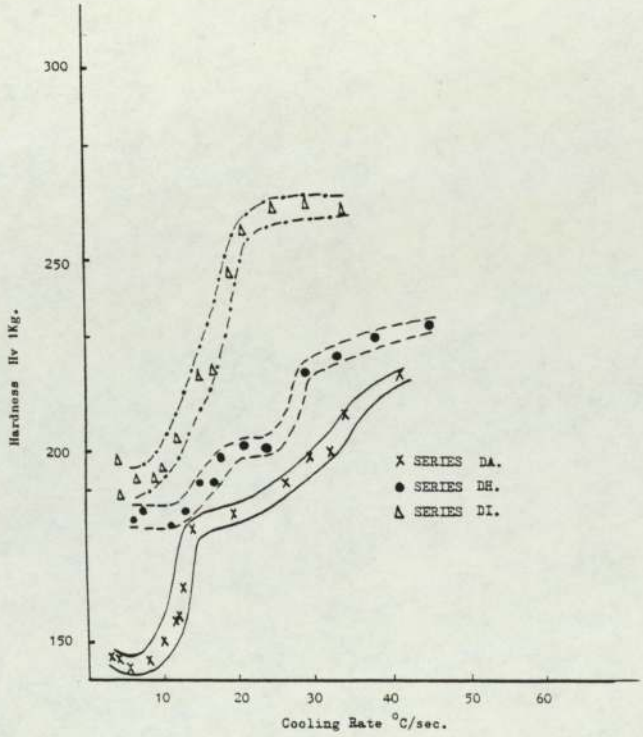

Figure No.4.96

The Influence Of Aluminium On The Hardness Of Low Oxygen Content Simulated Reheated Weld Metal.

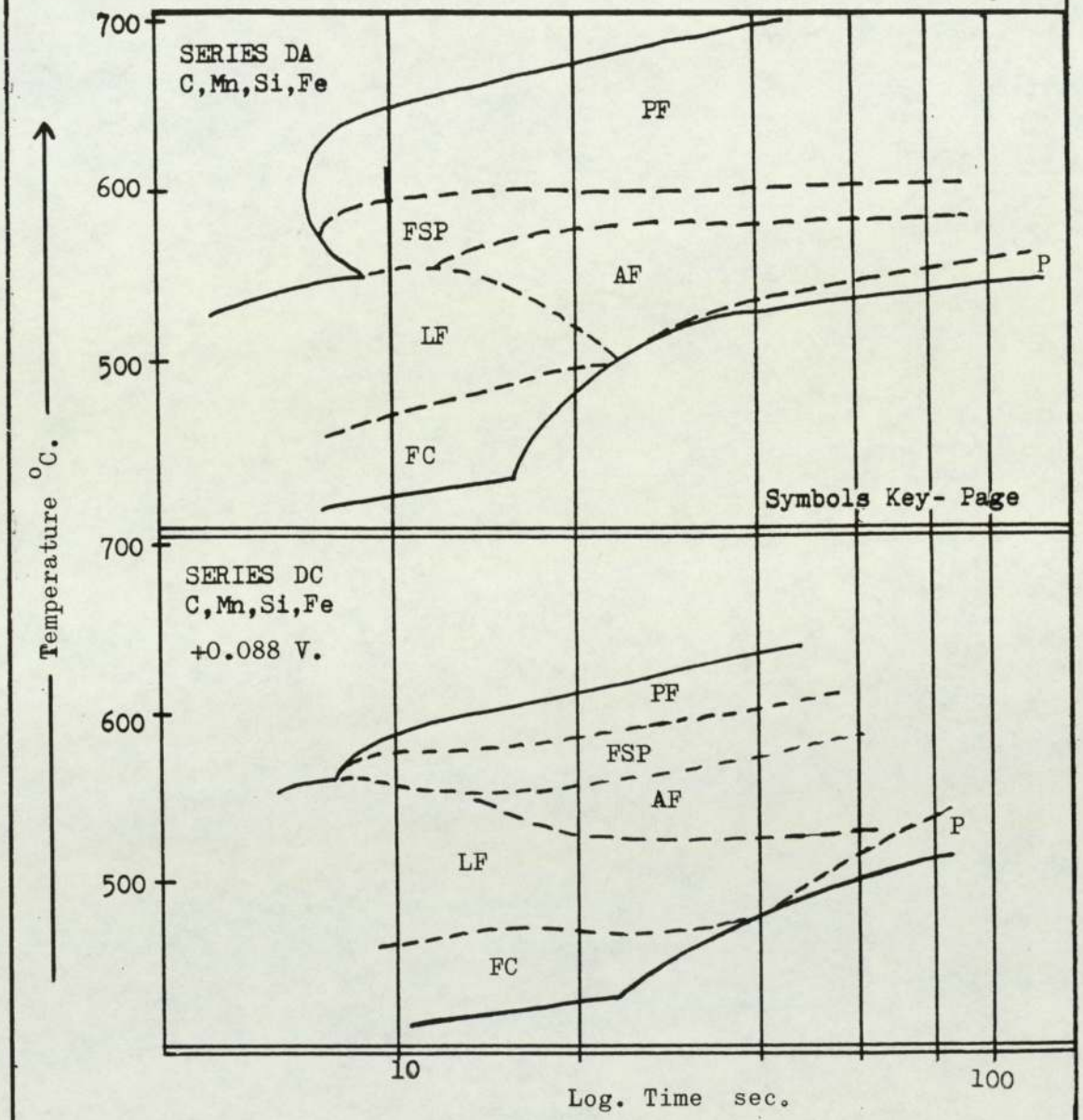

Figure No. 4.97

CCT Diagrams Showing The Effect Of Increased V Concentration On The Transformation Temperatures And Ferrite Constituents Formed In Simulated Reheated Weld Metal, With Low Oxygen Content.

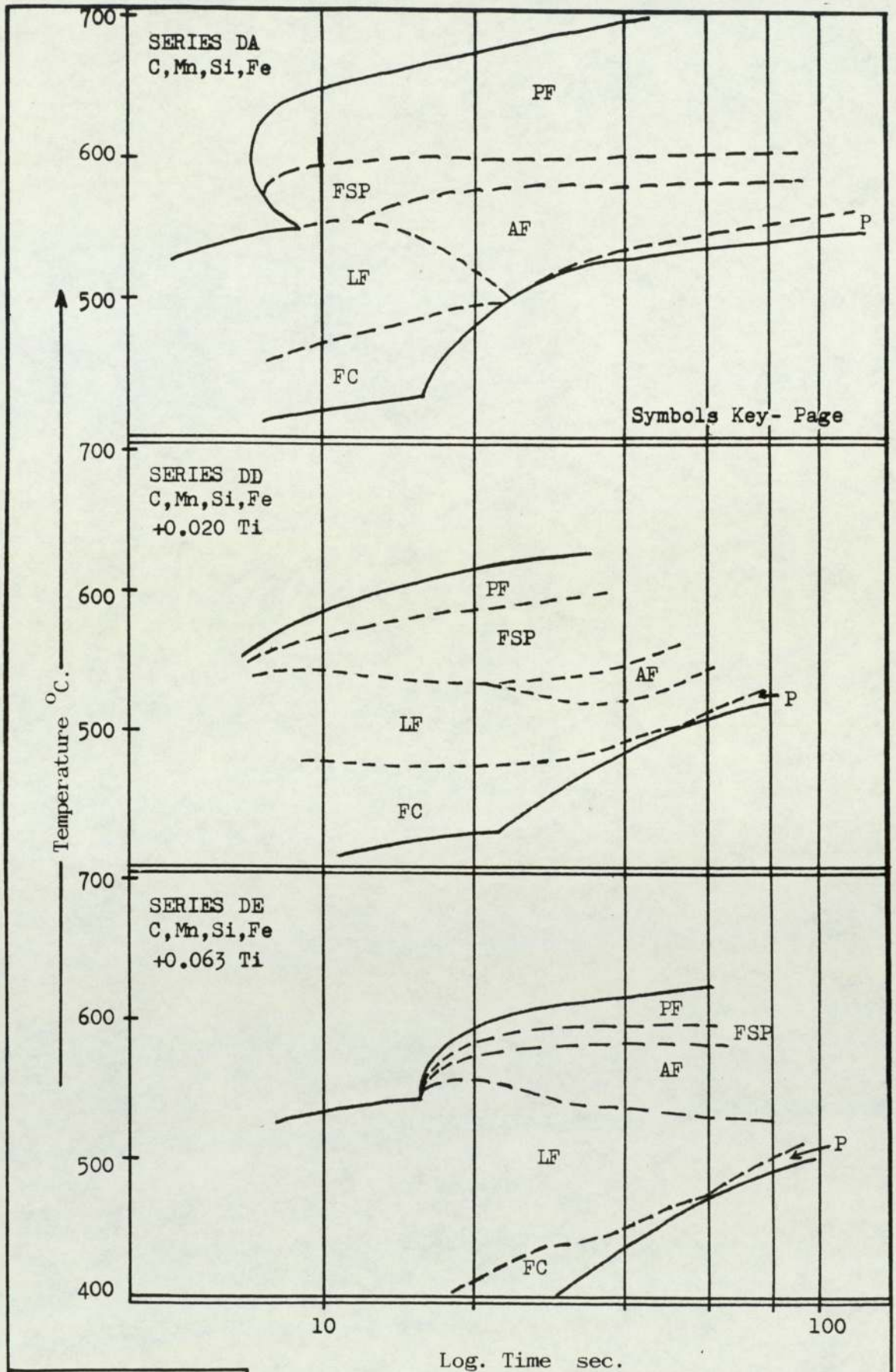

Figure No. 4.98

CCT Diagrams Showing The Effect Of Increased Ti Concentration On The Transformation Temperatures And Ferrite Constituents Formed In Simulated Reheated Weld Metal, With Low Oxygen Content.

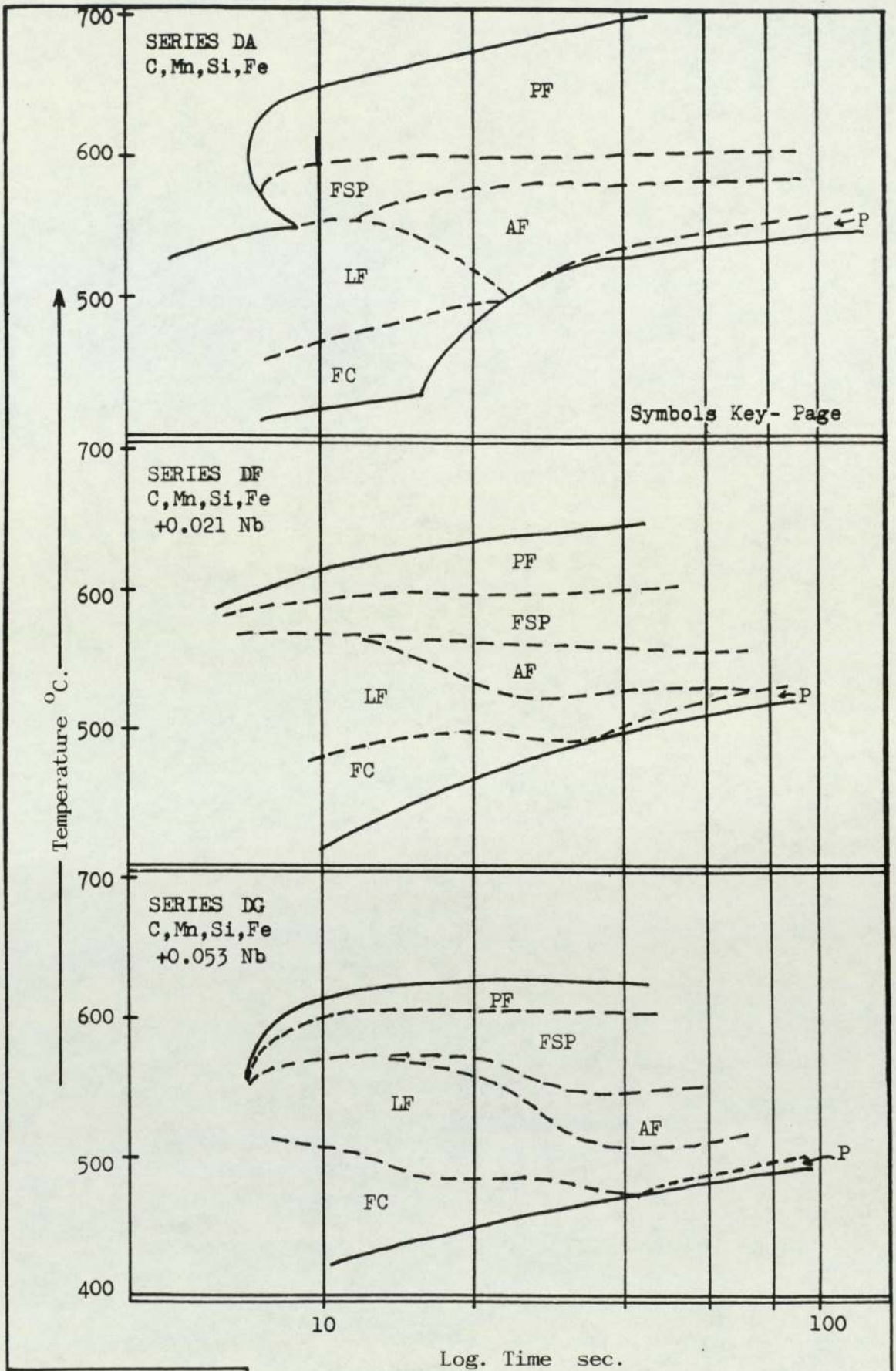

Figure No. 4.99

CCT Diagrams Showing The Effect Of Increased Nb Concentration On The Transformation Temperatures And Ferrite Constituents Formed In Simulated Reheated Weld Metal, With Low Oxygen Content.

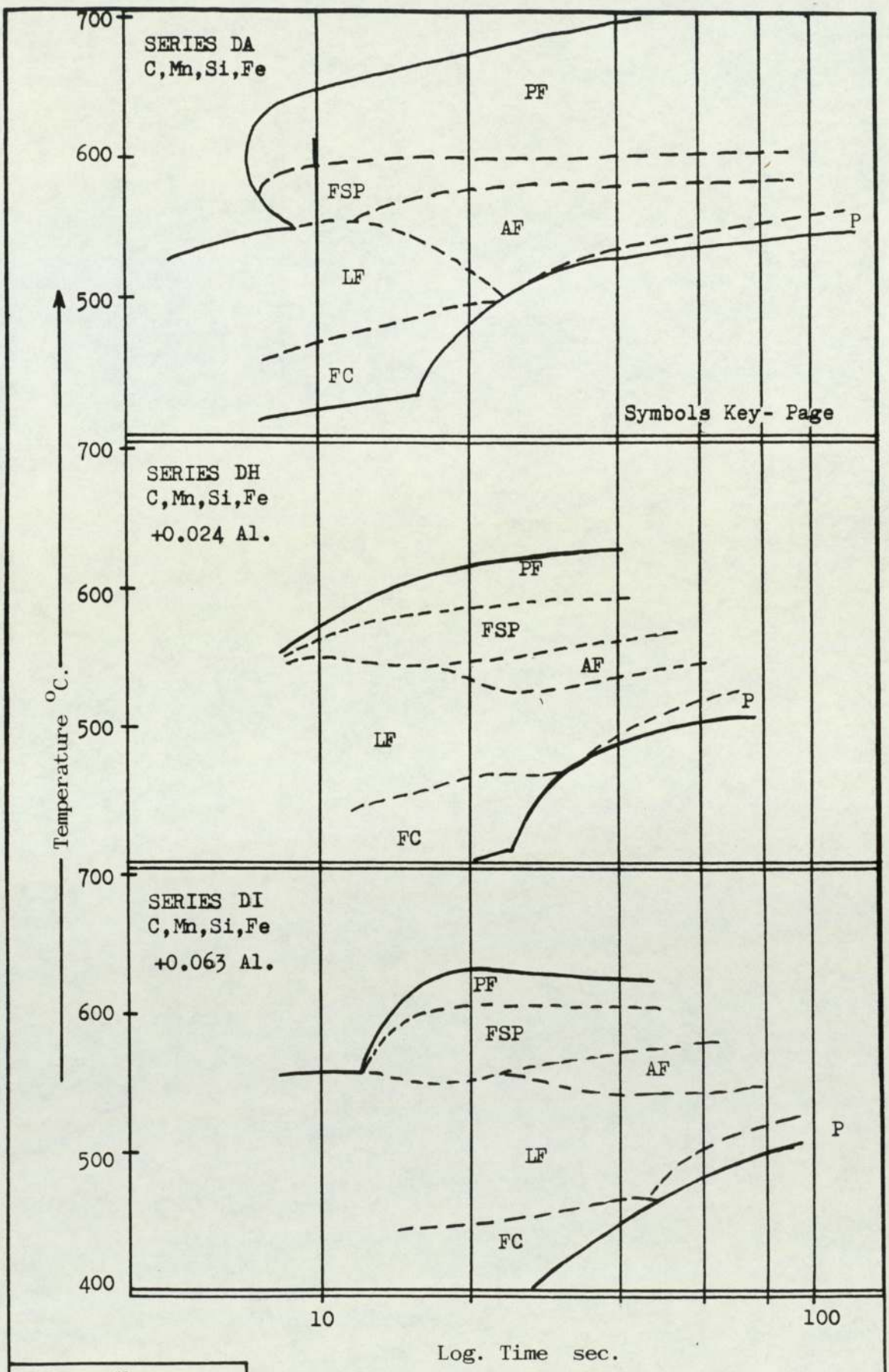

Figure No. 4.100

CCT Diagrams Showing The Effect Of Increased Al Concentration On The Transformation Temperatures And Ferrite Constituents Formed In Simulated Reheated Weld Metal, With Low Oxygen Content.

COMPOSITION					
% WEIGHT				PPM.	
C	Mn	Si	-	O_2	N_2
0.15	1.52	0.24	-	10	30

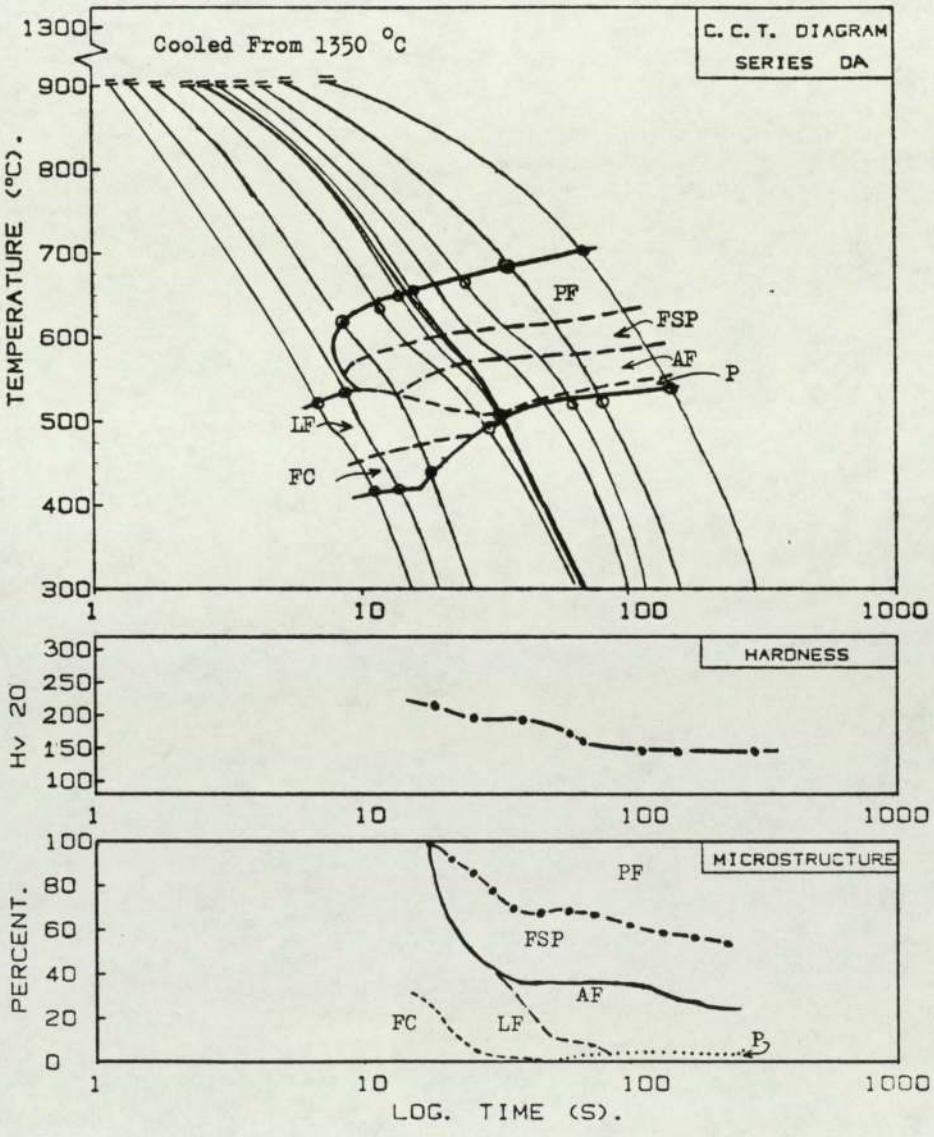

Figure No. 4.101

CCT Diagram For The Plain Carbon Manganese Steel (series DA) Simulated Reheated Weld Metal With Low Oxygen Content, Showing The Transformation Characteristics And Hardness.

COMPOSITION					
% WEIGHT				PPM	
C	Mn	Si	V	O_2	N_2
0.15	1.50	0.25	0.088	10	38

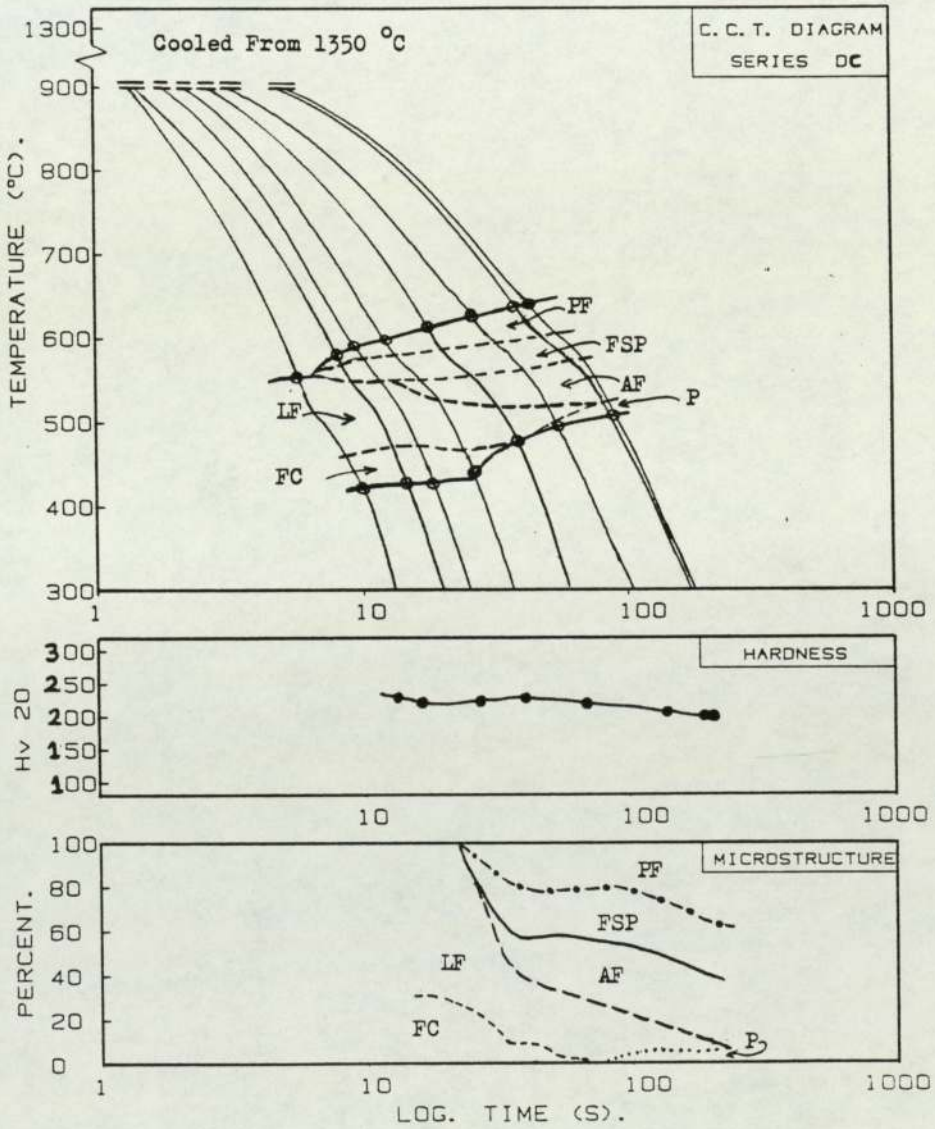

Figure No. 4.102

CCT Diagram Showing The Influence Of 0.088 %Wt V Concentration On The Transformation Characteristics And Hardness Of Simulated Reheated Steel Weld Metal, With Low Oxygen Content.

COMPOSITION					
% WEIGHT				PPM	
C	Mn	Si	Ti	O_2	N_2
0.15	1.46	0.24	0.020	10	38

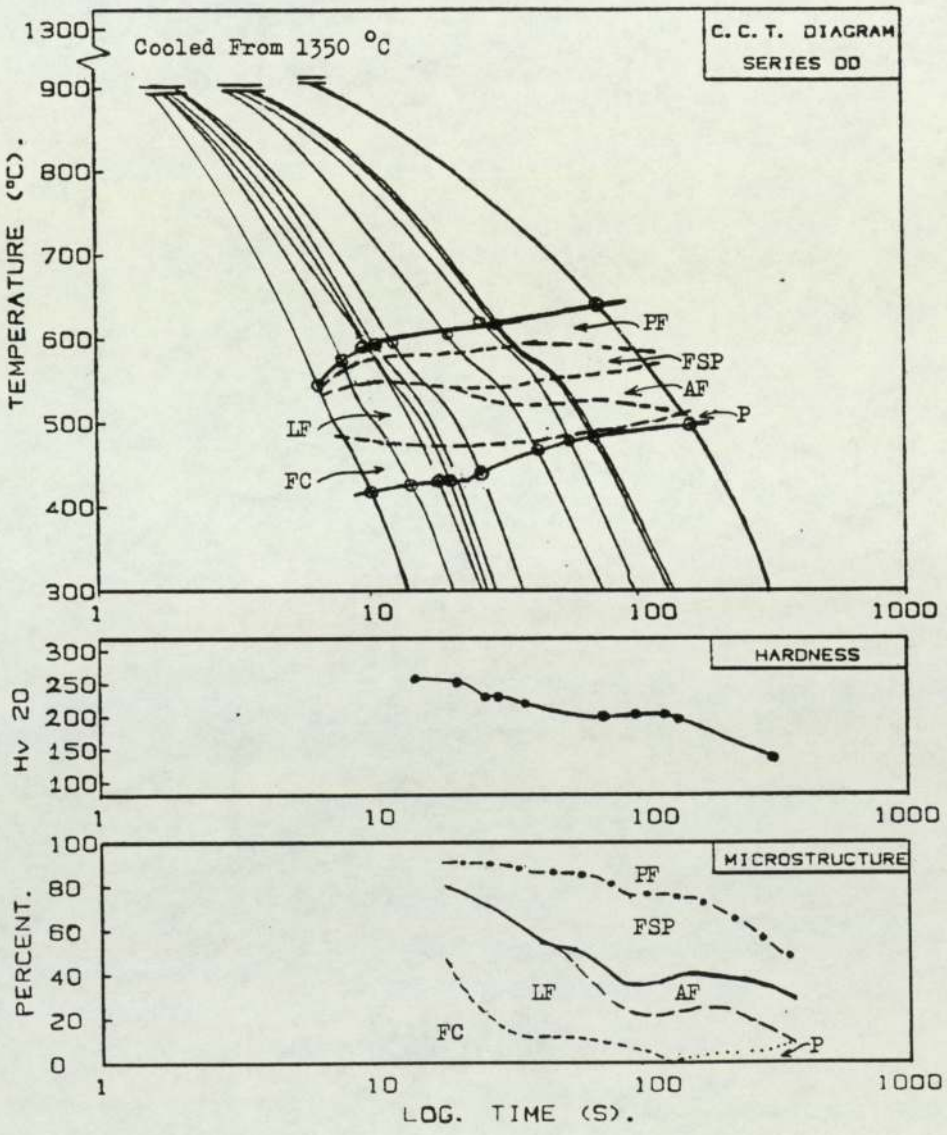

Figure No. 4.103

CCT Diagram Showing The Influence Of 0.020 %wt Ti Concentration On The Transformation Characteristics And Hardness Of Simulated Reheated Steel Weld Metal, With Low Oxygen Content.

COMPOSITION					
% WEIGHT				PPM	
C	Mn	Si	Ti	O_2	N_2
0.15	1.42	0.24	0.063	10	40

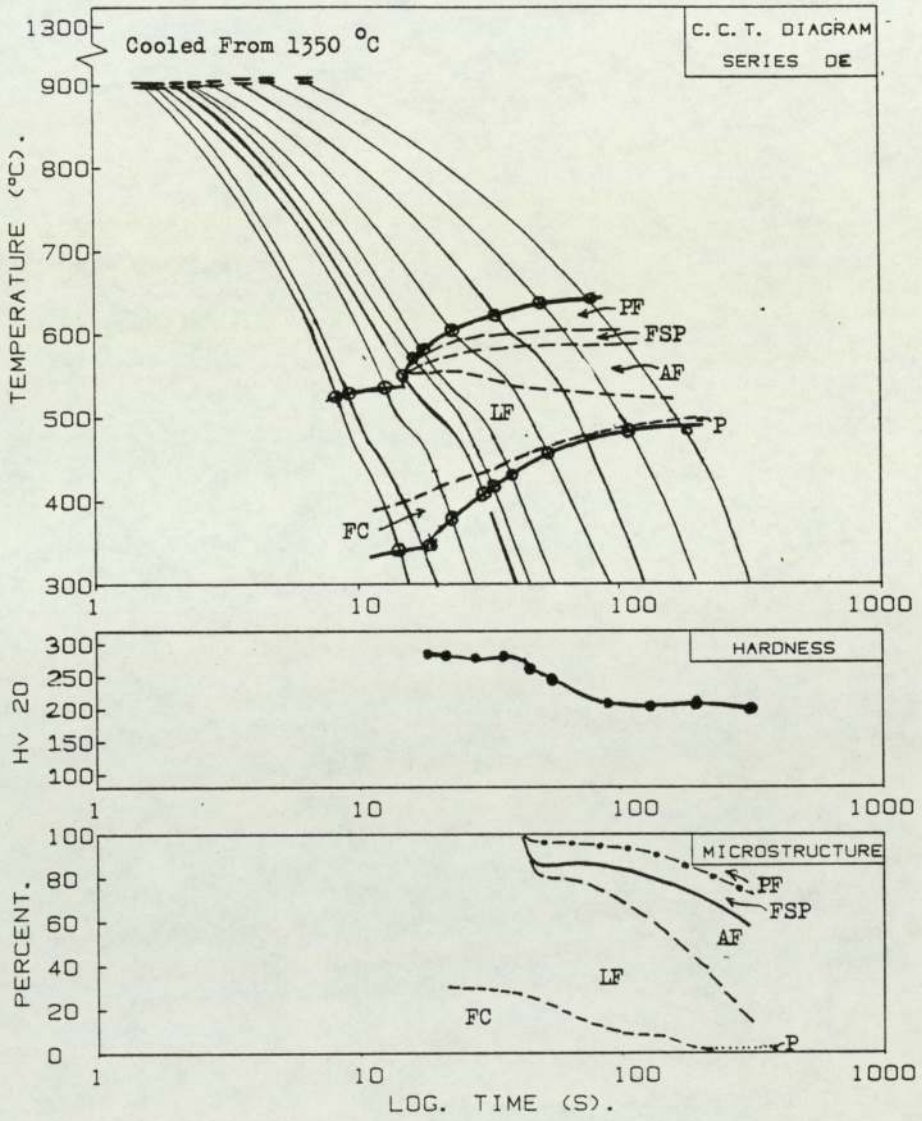

Figure No. 4.104

CCT Diagram Showing The Influence Of 0.063 %Wt Ti Concentration On The Transformation Characteristics And Hardness Of Simulated Reheated Steel Weld Metal, With Low Oxygen Content.

COMPOSITION					
% WEIGHT				PPM	
C	Mn	Si	Nb	O_2	N_2
0.15	1.44	0.24	0.021	10	37

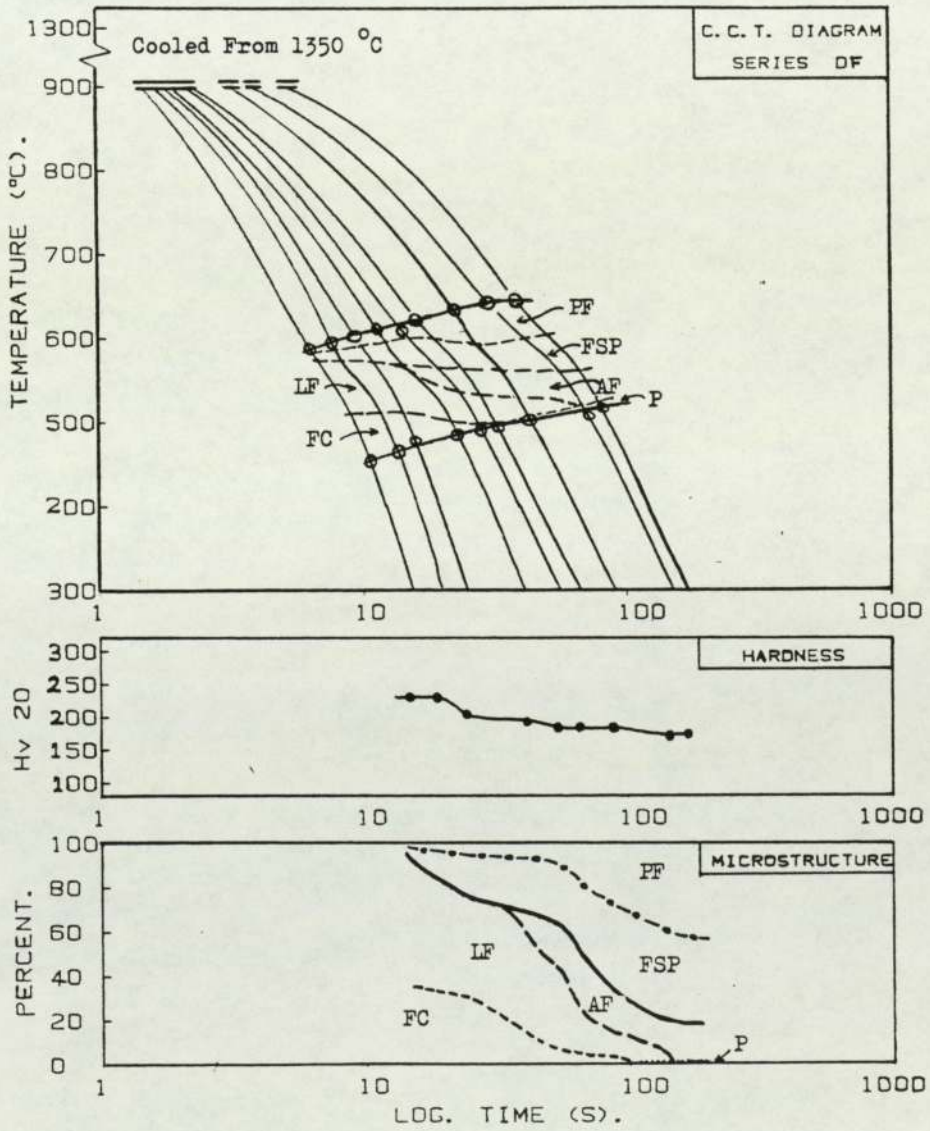

Figure No. 4.105

CCT Diagram Showing The Influence Of 0.021 %Wt Nb Concentration On The Transformation Characteristics And Hardness Of Simulated Reheated Steel Weld Metal, With Low Oxygen Content.

COMPOSITION					
% WEIGHT				PPM	
C	Mn	Si	Nb	O_2	N_2
0.15	1.46	0.25	0.053	10	38

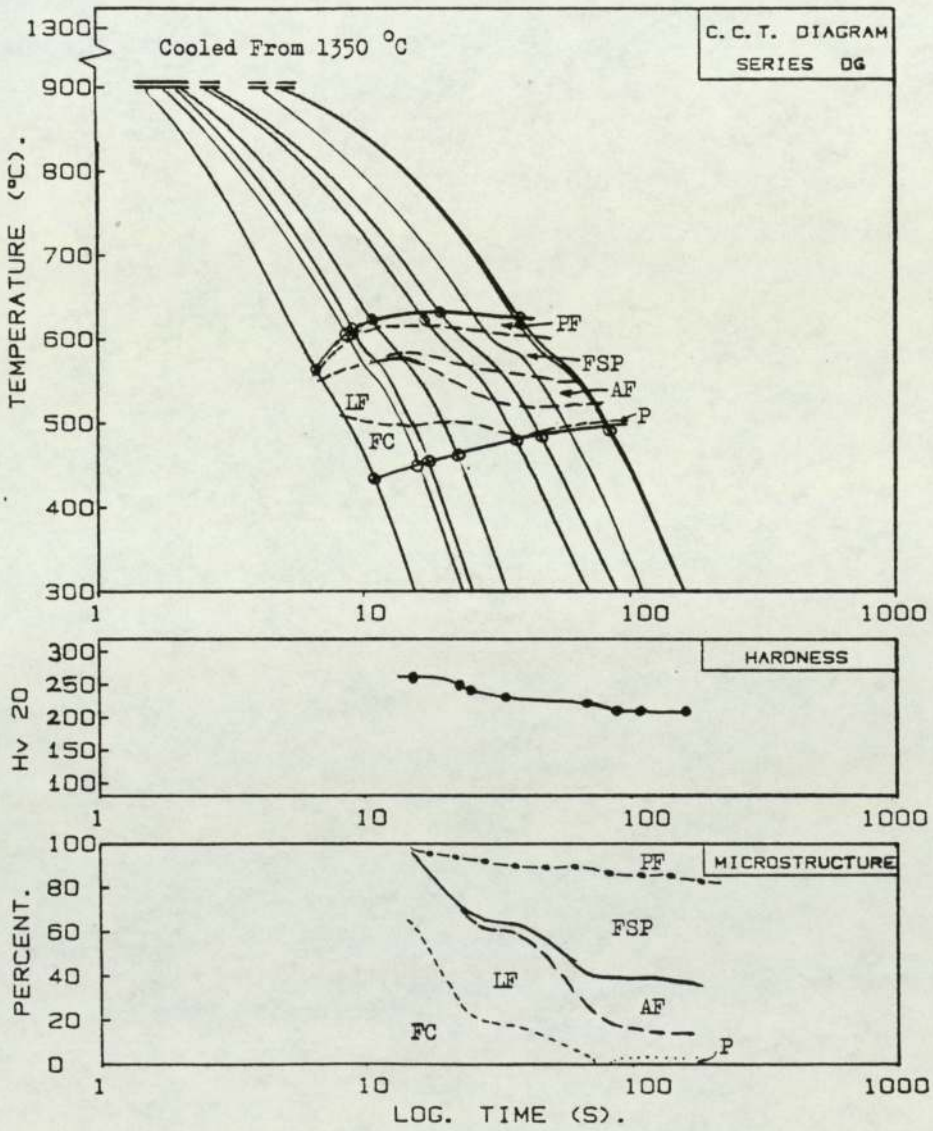

Figure No. 4.106

CCT Diagram Showing The Influence Of 0.053 %Wt Nb Concentration On The Transformation Characteristics And Hardness Of Simulated Reheated Steel Weld Metal, With Low Oxygen Content.

COMPOSITION					
% WEIGHT				PPM	
C	Mn	Si	Al	O_2	N_2
0.174	1.51	0.25	0.024	20	39

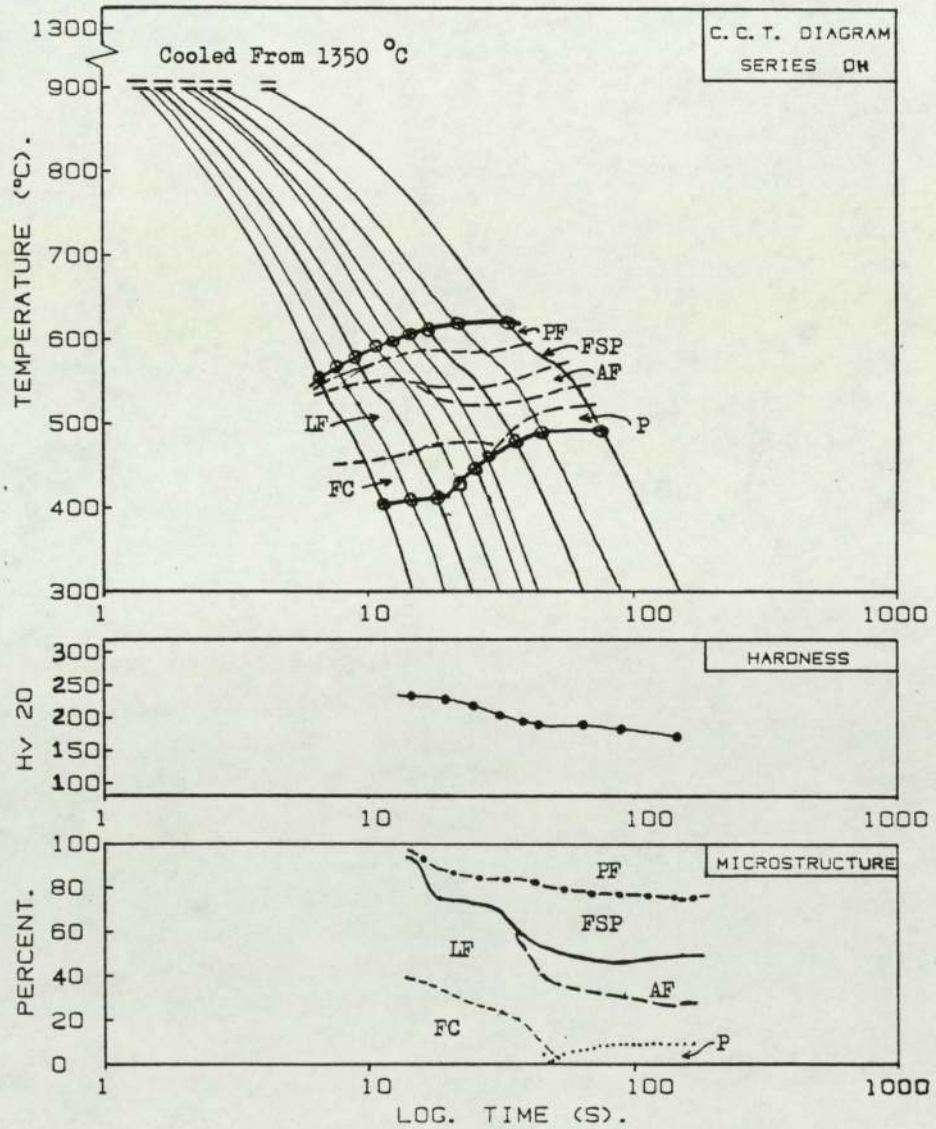

Figure No. 4.107

CCT Diagram Showing The Influence Of 0.024 %Wt Al Concentration On The Transformation Characteristics And Hardness Of Simulated Reheated Steel Weld Metal, With Low Oxygen Content.

COMPOSITION					
% WEIGHT				PPM	
C	Mn	Si	Al	O_2	N_2
0.178	1.52	0.25	0.063	23	40

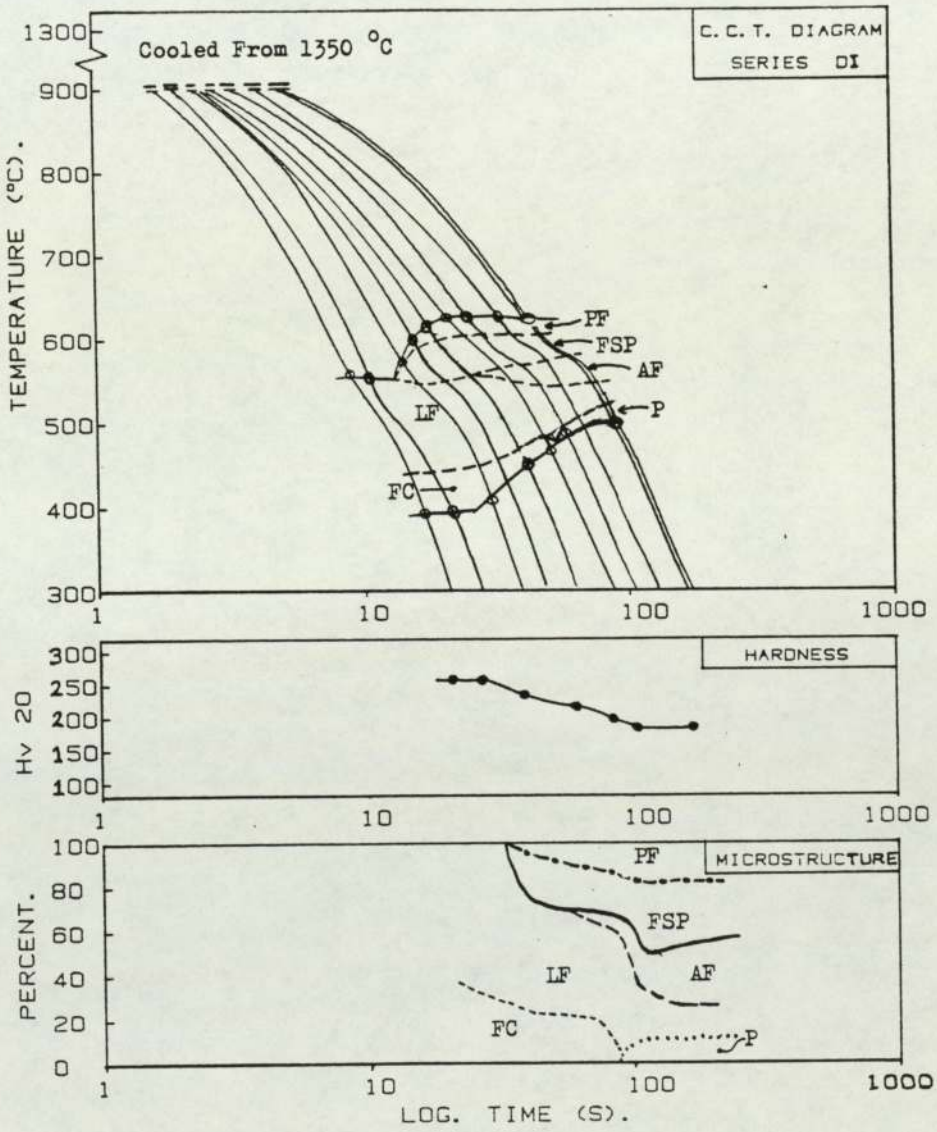

Figure No. 4.108

CCT Diagram Showing The Influence Of 0.063 %Wt Al Concentration On The Transformation Characteristics And Hardness Of Simulated Reheated Steel Weld Metal, With Low Oxygen Content.

FIGURES FOR CHAPTER 5.

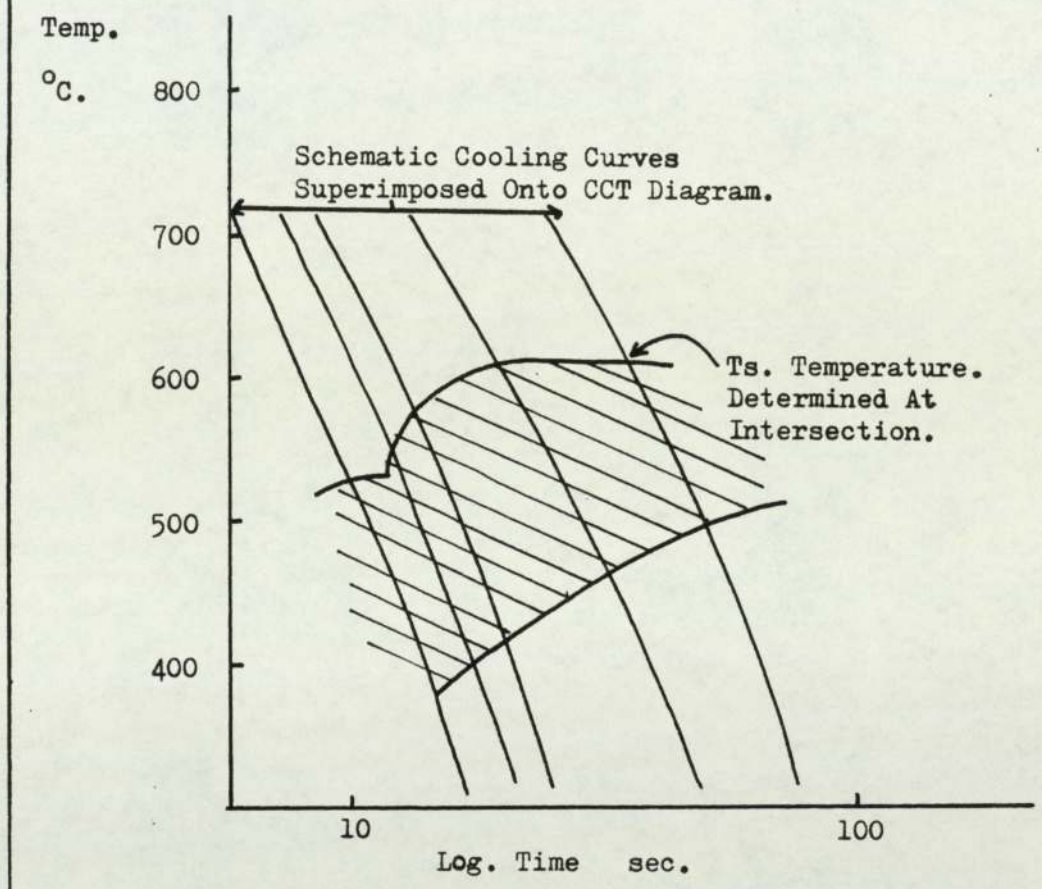

Figure No. 5.1

Determination Of Transformation Start Temperatures (Ts.) Using Schematic Cooling Curves, To Allow Direct Comparison Between Alloys.

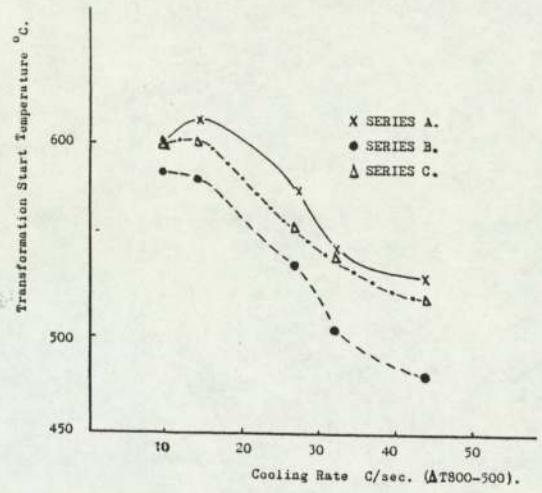

A. 0.027%wt V (Series B)
And 0.088%wt V (Series C).

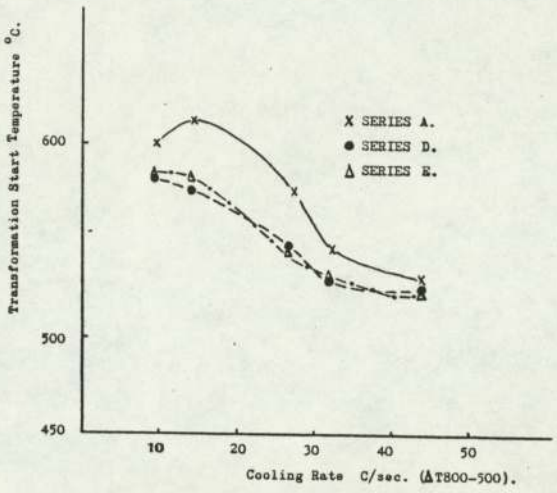

B. 0.020%wt Ti (Series D)
And 0.063%wt Ti (Series E).

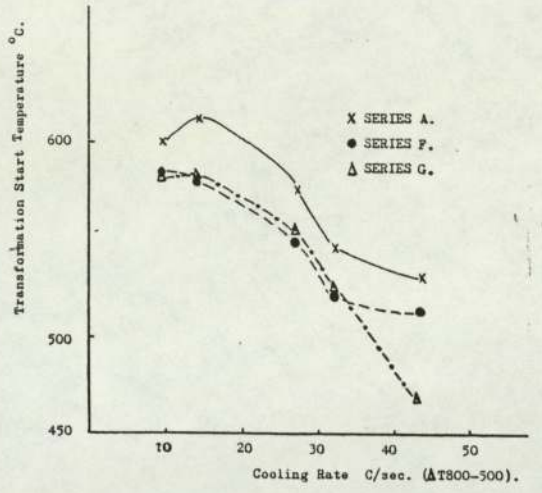

C. 0.021%wt Nb (Series F)
And 0.053%wt Nb (Series G).

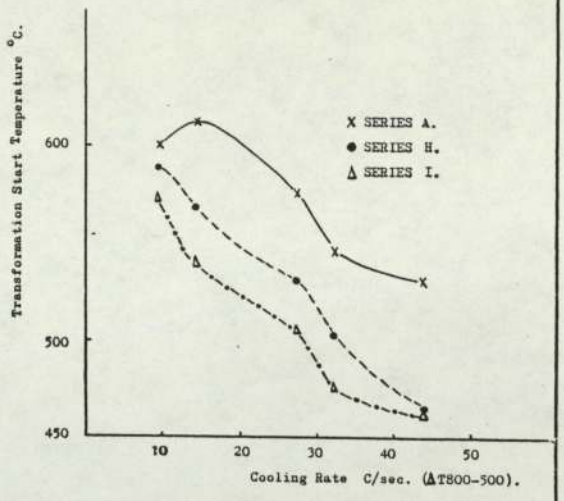

D. 0.024%wt Al (Series H)
And 0.063%wt Al (Series I).

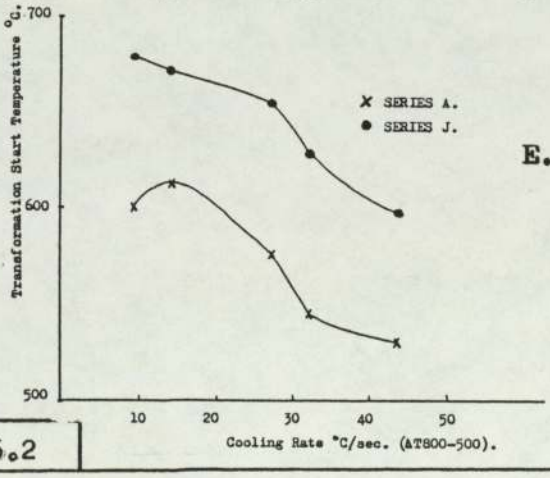

E. 0.05%wt C (Series J).

Figure No. 5.2

Comparison Of The Influence Of Microalloy Additions On The Transformation Start Temperatures In Low Oxygen Simulated As-Deposited Weld Metal.

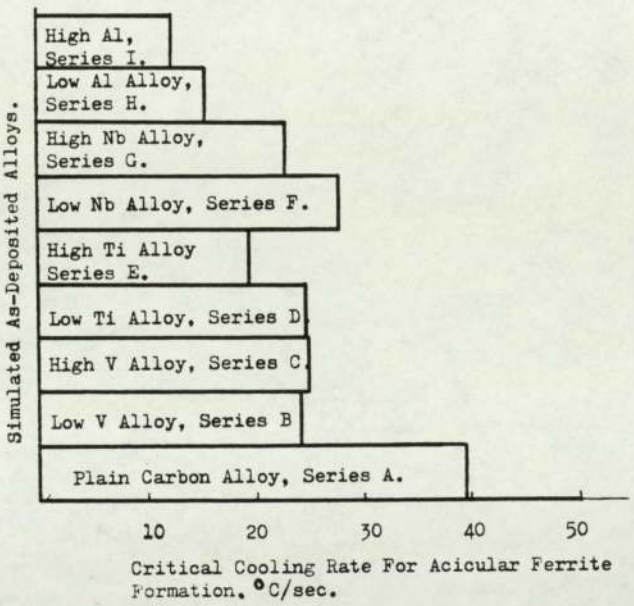

Figure No. 5.3

Comparison Of The Influence Of Microalloying Additions On The Critical Cooling Rate For Acicular Ferrite Formation In Low Oxygen Content Simulated As-Deposited Weld Metal.

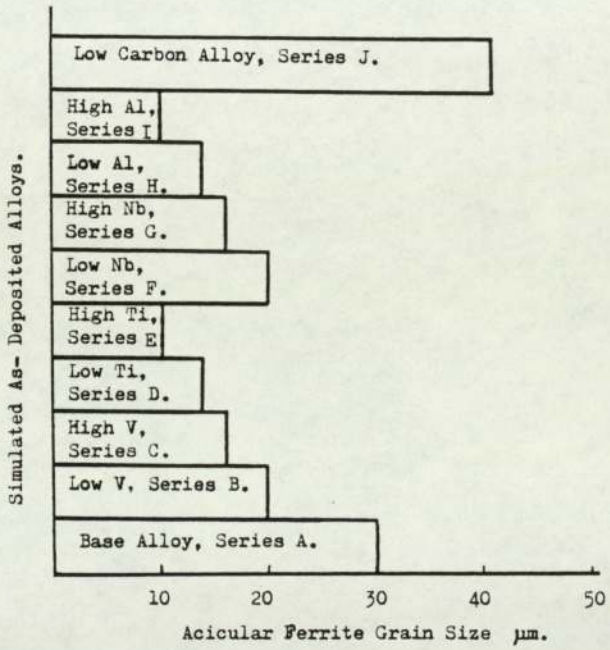

Figure No. 5.4

The Influence Of Microalloy Additions On The Acicular Ferrite Grain Size In Low Oxygen Content Simulated As-Deposited Weld Metal.

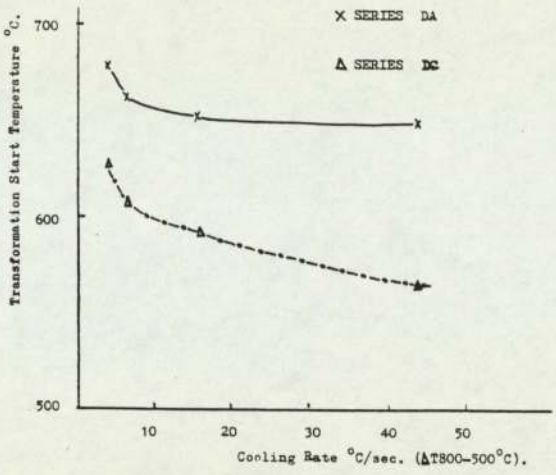

A. 0.088%wt V (Series DC).

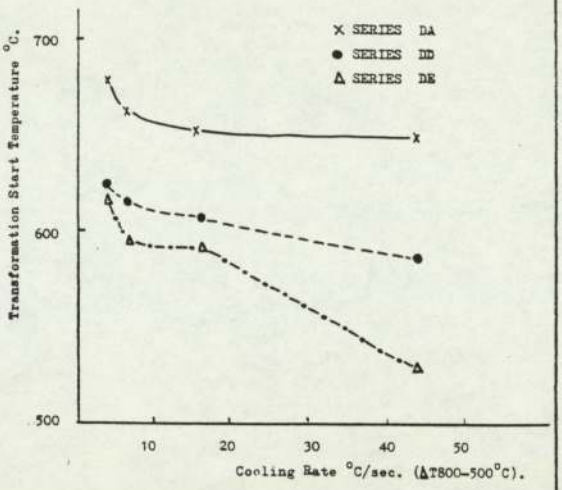

B. 0.020%wt Ti (Series DD)
And 0.063%wt Ti (Series DE).

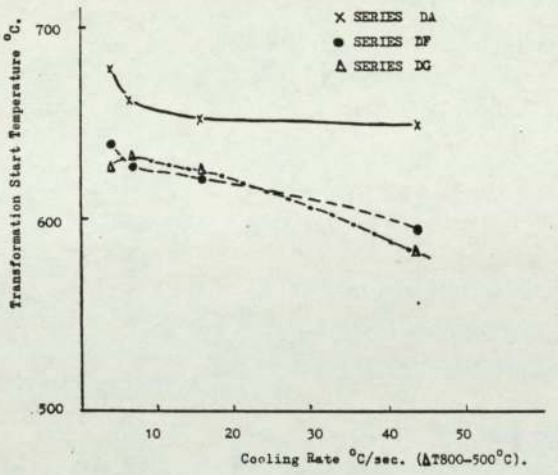

C. 0.021%wt Nb (Series DF)
0.053 %wt Nb (Series DG).

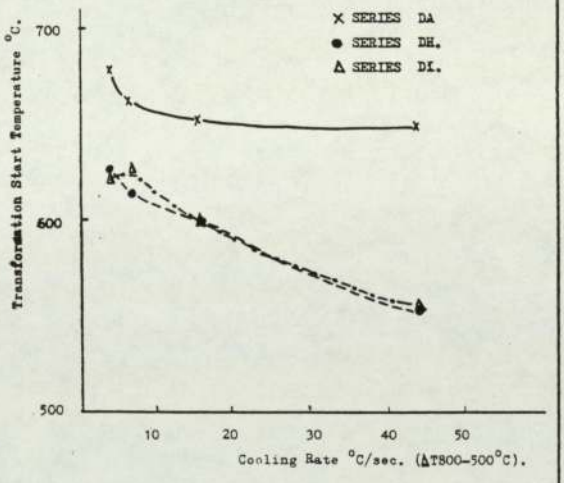

D. 0.024%wt Al (Series DH)
0.063%wt Al (Series DI).

Figure No. 5.5

Comparison Of The Influence Of Microalloy Additions On The Transformation Start Temperatures In Low Oxygen Content Simulated Reheated Weld Metal.

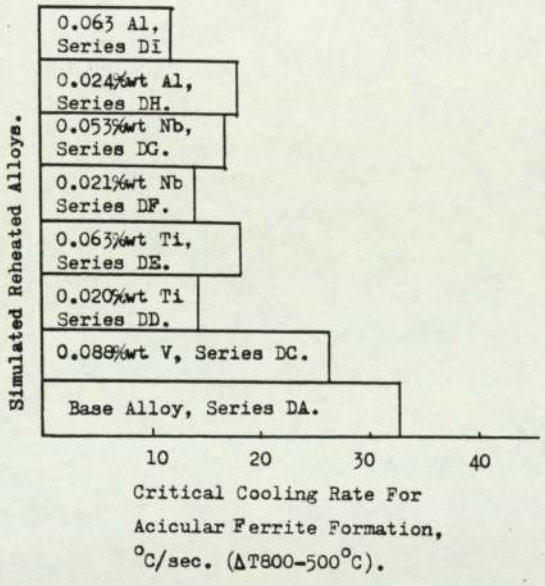

Figure No. 5.6

The Influence Of Microalloying Additions On The Critical Cooling Rate For Acicular Ferrite Formation In The Low Oxygen Content Simulated Reheated Weld Metal.

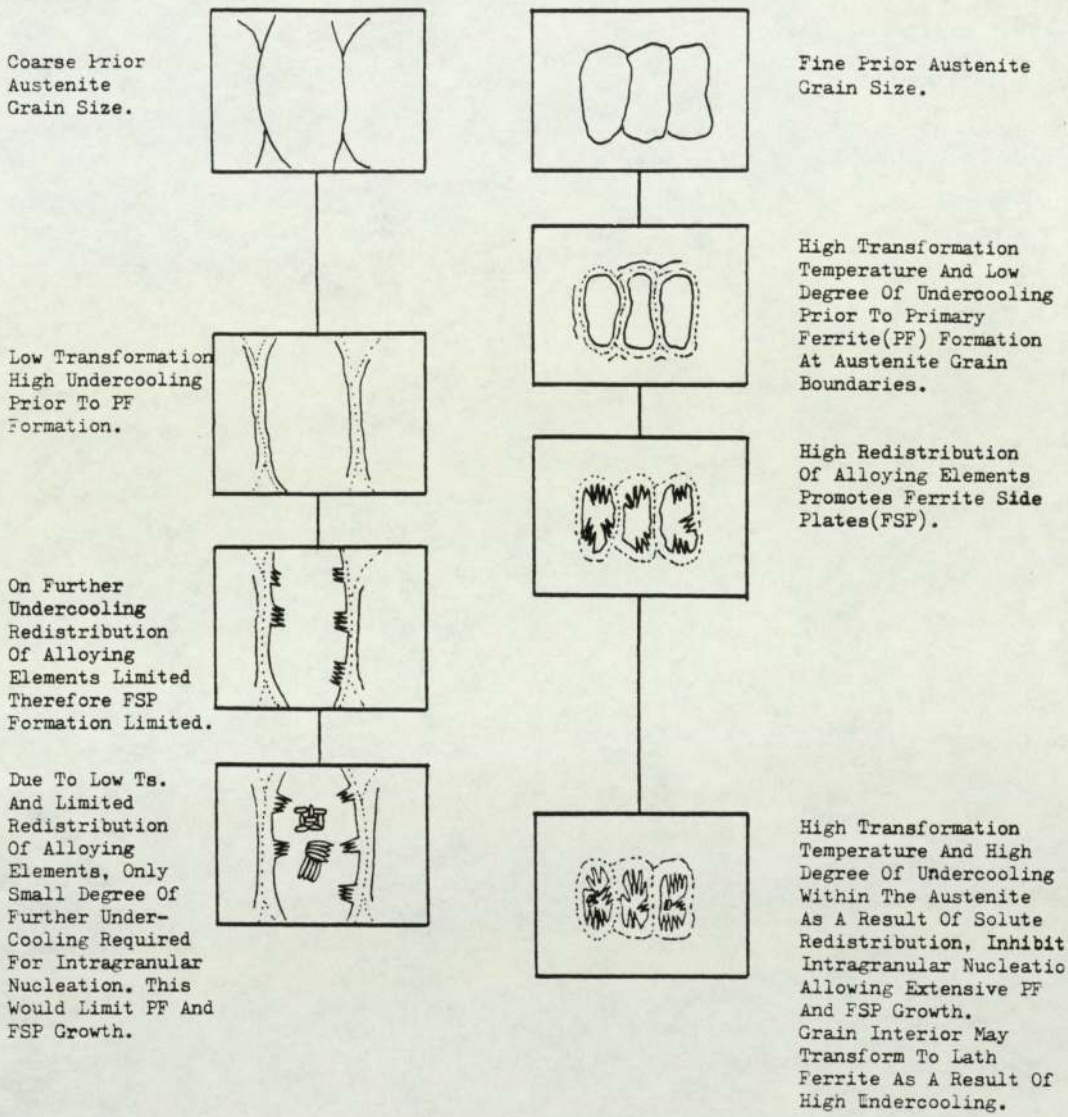

Figure No. 5.7

Schematic Diagram Showing The Influence Of Prior Austenite Grain Size On Microstructural Development In Weld Metal.

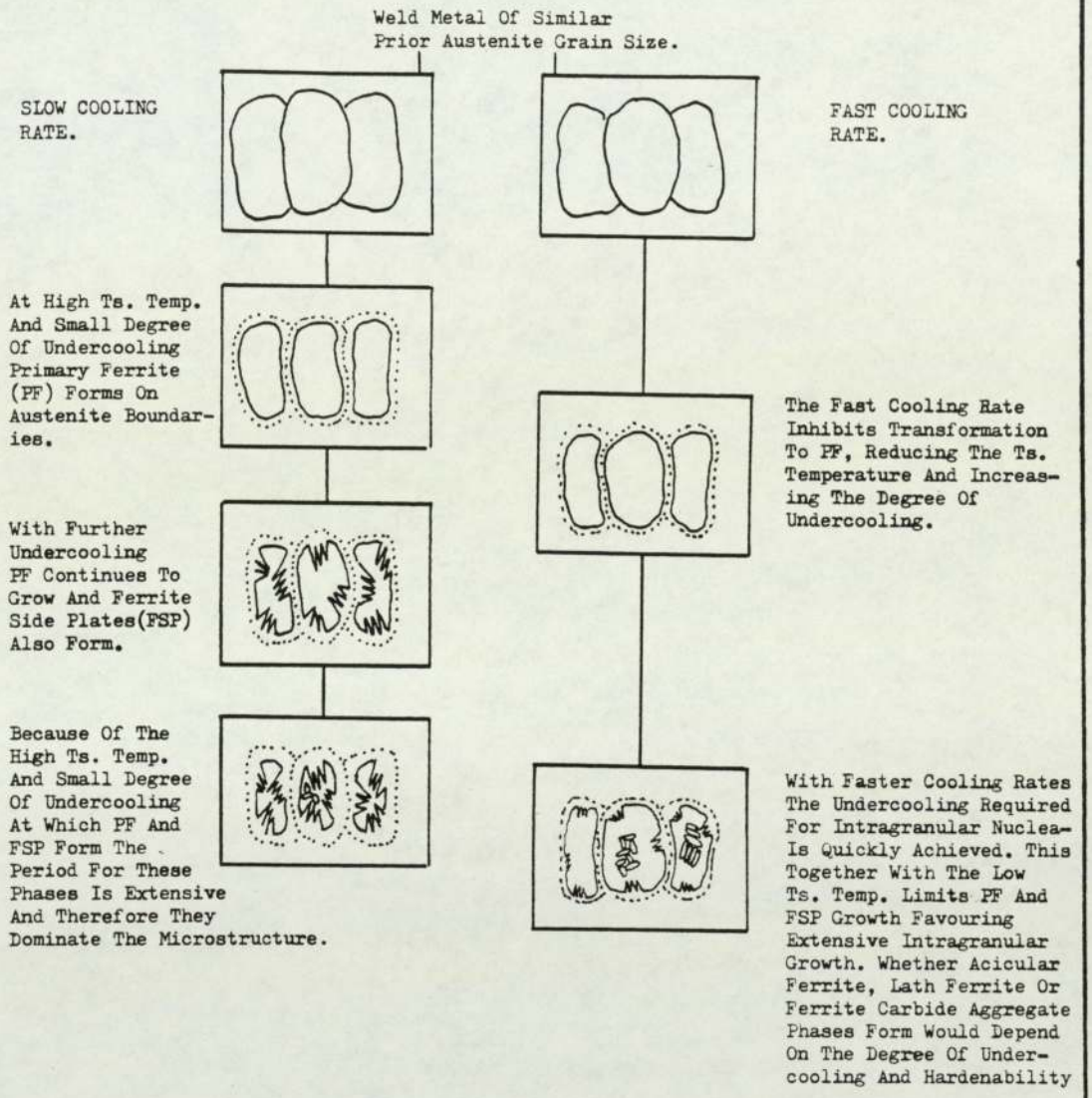

Figure No. 5.8

Schematic Diagram Showing The Influence Of Cooling Rate On Microstructural Development In Weld Metal.

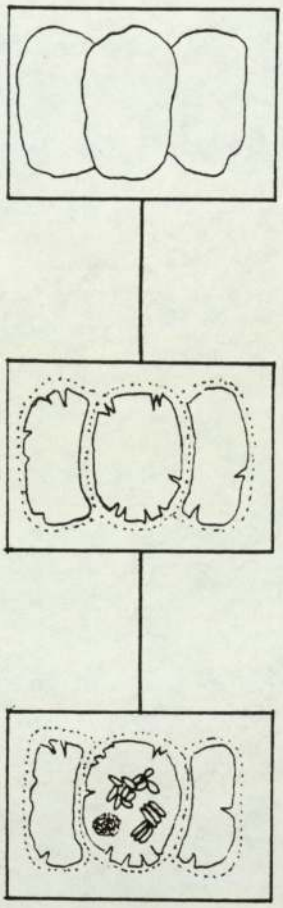

Microalloyed Weld Metal.

Columnar Prior Austenite Grains Of Similar Size To Weld Metal In Figure 5.8.
Slow Cooling Rate.
Microstructural Development May Be Compared With Plain Carbon Alloy, Figure 5.8.

Primary Ferrite(PF) Would Form At The Austenite Boundaries, But The Microalloying Element Increase Hardenability And Therfore Reduces The Ts. Temp. Microalloy Also Inhibit PF Growth, Which May Promote Ferrite Side Plate (FSP) Structures.

However The Reduced Ts. Temp. Would Suggest That Only Limited Further Undercooling Would Be Required For Intragranular Transformation To Occur And This Could Inhibit FSP Growth By Mutual Impingement. The Intragranular Phases That Form Would Depend On The Degree Of Undercooling And Hardenability.

Higher Microalloy Concentrations Would Increase Hardenability And Favour Lower Temperature Transformation Products.

Figure No. 5.9

Schematic Diagram Showing The Influence Of Microalloying Additions On Microstructural Development In Weld Metal.

REFERENCES.

REFERENCES.

1. DUBE, C.A., ARRONSON, H.I., MEHL, R.F, "The Formation Of Proeutectoid Ferrite In Plain Carbon Steels", Rev. Met., Vol.55, p.201, 1958.

2. AARONSON, H.I. "Decomposition of Austenite by Diffusional Processes", AIME, Philadelphia, 389, 1960.

3. COCHRAINE, R.C., "Weld Metal Microstructure and Terminlogy", BSC Report T/PDM/462/1/77/C, 1977 And IIW Doc. A-44-78, 1978.

4. WIDGERY, D.J., "Deoxidation Practice For Mild Steel Weld Metal", Welding Research Supplement, March, p.57-68, 1976.

5. ABSON, D.J., DOLBY, R.E., "A Scheme For The Quantitative Description Of Ferritic Weld Metal Microstructures", Welding Institute Research Bullitin, April, p.100-103, 1980.

6. IIW Sub-Commission IXJ, "Guidelines For The Classification Of Ferritic Steel Weld Metal Microstructural Constituents Using A Light Microscope", IIW Doc. IX-1377-85.

7. CHOI, C.L., HILL, D.C., "A Study Of Microstructural Progression In As-Deposited Weld Metal", Welding Institute Research Supplement, August, p.232-236, 1978.

8. ITO, Y., NAKAISHI, M., KOMIZO YU-ICHI., "Effect Of Oxygen On Low Carbon Steel Weld Metal", Metal Construction, September, p.472-478, 1982.

9. WATSON, M.N., HARRISON, P.L., FARRAR, R.A., "How Niobium Influences Submerged Arc Mild Steel Weld Metal", Welding And Metal Fabrication, March, Part 1, p.101-108, 1981.

10. GLOVER, A.G., McGRATH, J.T., TINKLER, M.J., WEATHERLY, G., "The Influence Of Cooling Rate And Composition On Weld Metal Microstructure In Carbon/Manganese And HSLA Steel", Welding Research Supplement, September, p.267-273, 1977.

11. DOLBY, R.E., "The Weldability Of Low Carbon Structural Steel", Welding Research Bullitin, August, p.209-215, 1977.

12. HARRISON, P.L., WATSON, M.N., FARRAR, R.A., "How Niobium Influences Submerged Arc weld Metal, Welding And Metal Fabrication, April, Part 2, p161-169, 1981.

13. RICKS, R.A., HOWELL, P.R., BARRITE, G.S., "The Nature Of Acicular Ferrite In HSLA Steel Weld Metal", Journal Of Materials Science, Vol.17, p732-740, 1982.

14. WATSON, M.N., "The Mechanical Properties And Transformation Behaviour Of SA Weld Metal Containing Niobium", PhD Thesis, Southampton University, 1980.

15. WIDGERY, D.J., "Microstructures In Steel Weld Metal", Welding Institute Research Bulletin, October, p.277-281, 1975.

16. GARLAND, J.G., KIRKWOOD, P.R., "Towards Improved Submerged Arc Weld Metal", Metal Construction, June, 1975.

17. LEVINE, E., HILL, D.C. "Structure Property Relationships In Low Carbon Weld Metal", Metallurgical Transactions, Vol. 8a, September, p.1453-1463, 1977.

18. TULIANI, S.S., BONISZEWSKI, T., EATON, N.F., "Notch Tougness Of Commercial SAW Metal", Welding And Metals Fabrication, Vol. 37, August, p.327, 1969.

19. PETCH, N.J., "Fracture", Proceedings of Swampscott Conference, 54, 1959.

20. PACY, A.J., KERR, H.W., "Minor Phases And Toughness In SAW Of HSLA Welds", Welding And Metal Fabrication, November, p. 613-615, 1978.

21. SAVAGE, W.F., "Solidification, Segregation And Weld Imperfections", Welding In The World, Vol. 18, p.89-104, 1980.

22. EASTERLING, K., Introduction To The Physical Metallurgy Of Welding, Butterworth And Co. (Publishers) Ltd., 1983, ISBN 0-408-01351-6.

23. TILLER, W.A, RUTLER, J.W., "The Effect Of Growth Conditions On The Solidification Of A Binary Alloy", Canadian Journal Of Physics, Vol.34, p.96-121, 1956.

24. FREDRIKSSON, H., STJERNDAHL, J., "Solidification Of Iron-Base Alloys", Metal Science, Vol. 16, December, p.575-585, 1982.

25. VASILJEV, A.D., "The Mechanical Properties Of Single-Pass Weld Metal In Respect Of Its Solidification", Pro. Conf. Weld Pool Chemistry And Metallurgy, London, Paper 23, 15-17 April, 1980.

26. KEVILLE, B.R., "Preliminary Observations Of The Type, Shape And Distribution of Inclusions Found In Submerged Arc Weldment". Welding Research Supplement, September, p.253-260, 1983.

27. WARDELL, N.R., "Cleanliness And Inclusion Alignment In Low Alloy Steel Weld Metal", Paper 42, as ref. 25.

28. OHASHI, T., FUJII, H. NURI, Y., ASANO, K., "The Effect Of Oxides On Nucleation Behaviour In Supercooled Iron", Transactions Of The Iron And Steel Institute Of Japan, Vol. 17., p.262-270, 1977.

29. NISHIO, K., TOKUNAGA, J., KATOH, M., MUKAE, S., "Effects Of Welding Speed And Micro-Alloying Elements On the Weld Solidification Structures Of Steels", Transactions OF The Japan Welding Society, October, 1981.

30. THAULOW, C., "Structural Changes In SAW Metals Of Carbon Manganese Steels Containing Small Amounts Of Titanium", Paper 29, as ref.25.

31. TURNBULL, D., VONNEGUT, R., "Nucleation Catalysis", Industrial Engineering Chemistry, Vol.44, p.1292-1297, 1952.

32. THREADGILL, P.L., BAILEY, N., "The Prospects For Weld Pool Grain Refinement", Paper 33, as ref. 25.

33. BAILEY, N. "Prospects For Grain Refinement During Welding", Welding Institute Research Bulletin, October, p.289-293, 1975.

34. DAVIES, G.S., GARLAND, J.G, "Solidification Structures And Properties Of Fusion Welds", International Metalurgical Reviews, Review No.176, Published By The Metals Society.

35. COCHRANE, R.C., KIRKWOOD, P.R., "The Significance Of The Grain Coarsening Response Of Carbon Manganese Steels In Relation To Weld Metal Solidification", Pro. Int. Conf. Trends In Steel And Consumables For Welding, London, November, Paper 25, 1978.

36. RASENEN, E., TENKULA, J., "Phase Changes In Welded Joints Of Constructional Steels", Scandinavian Journal Of Metallurgy, p. 75-80, 1972.

37. SAVAGE, W.F., NIPPES, E.F., MILLER, T.W., "Microsegregation In the partially Heated region of 70Cu-30Ni Weld Metal", Welding Journal Research Bulletin, 55, July, p.181-187, 1976.

38. CHRISTIAN, J.W., "Theory Of Transformation In Metals And Alloys", Part 1, 2nd Edition, Pergamon Press Ltd, Headington Hill Hall, Oxford.

39. METALS HANDBOOK, VOL. 8. "Metallographic Structures And Phase Diagrams", 8th. Ed. American Society For Metals, Metals Park, Ohio 44073.

40. COCHRANE, R.C., KIRKWOOD, P.R., "The Effect Of Oxygen On Weld Metal Microstructures", Proc. Conf. The Trends In Steels And Consumables For Welding, London 13-16 November, Vol. 1, Paper 35, p.103-121, 1978.

41. COCHRANE, R.C., "Weld Metal Microstructures- A State Of The Art Review", Welding In The World, Vol. 21, No. 1/2, p.16-24, 1983.

42. KIRKWOOD, P.R., "New Observations On Microstructural Toughness Control In Low Carbon Weld Metal", Institute Of Metallurgist Conf. Low Carbon Structural Steels For The Eighties, Publication No. 1001-77-y, pp IIIB/12-20.

43. HAROUN, N.A., "Theory Of Inclusion Controlled Grain Growth", Journal Materials Science, Vol. 15, p.2816-2822, 1980.

44. TOWNSEND, R.D., KIRKALDY, J.S., "Widmanstatten Ferrite Formation In Fe-C Alloys", Transactions American Society For Metals, Vol. 16, p.605-619, 1968.

45. PARGETER, R.J., "Acicular Ferrite And Inclusions In C-Mn Steel Weld Metal", Welding Institute Research Bulletin, July, p.215-220, 1983.

46. ABSON, D.J., DOLBY, R.E., " Microstructural Transformation In Steel Weld Metal", Welding Institute Research Bulletin, July, 1978.

47. INAGAKI, M., SEKIGUCHI, H.,"Transaction Of The National Institute Of Metals, Vol. 2, p.40, 1960.

48. CHRISTIANSEN, N., " Transformation Behaviour Of C-Mn Weld Metal", Scandinavian Journal Of Metallurgy, Vol. 10, p.147-156, 1981.

49. RODRIGUES, P.E.L.B., ROGERSON, J.H., "How Weld Metal Thermal Cycles Determine The Toughness Of SAW", Welding And Metals F, April, p.183-192, 1980.

50. HARRISON, P.L., "Continuous Cooling Transformation Kinetics And Microstructures Of Mild And Low Alloy Steel Weld Metal", PhD Thesis, Southampton University, 1982.

51. BLAKE, P.D., "Oxygen In Steel Weld Metal", Metal Construction, March, p.118-120, 1979.

52. WIDGERY, D.J., "Deoxidation Practice And Toughness Of Mild Steel Weld Metal", Welding Research Int, Vol. 4,No.2, Part 1, p.54-80, 1974.

53. EAGER, T.W., "Sources Of Weld Metal Oxygen Contamination During SA Welding", Welding Journal Research Supplement, Vol. 57, March, p.76s-80s, 1978.

54. ABSON, D.J., DOLBY, R.E., HART, P.H.M., "Investigation Into The Role Of None Metallic Inclusions, On Ferrite Nucleation In Carbon Steel Weld Metal", The Welding Instutute, Report No. 67/1978/M, 1978.

55. COCHRANE, R.C, KIRKWOOD, P.R., "The Effect Of Oxygen On Weld Metal Microstructures", Proc. Conf. The Trends In Steels And Consumables For Welding, London 13-16 November, Vol. 1, Paper 35, p.103-121. 1978.

56. FARRAR, R.A., WATSON, M.N., "The Efect Of Oxygen And Manganese On SAW Metal Microstructures", Metal Construction, June, p.285-286, 1979.

57. PARGETER, R.J., "Investigation Of SAW Metal Inclusions", The Welding Institute, Report No. 7702/81/260.3, July, 1981.

58. BOOTHBY, P.J., "Inclusions And Microstructure In Gas Shielded Weld Metal", Welding Institute Research Bulletin, October, p.281-286, 1981.

59. TERASHIMA, H., HART, P.H.M., "The Effect Of Aluminium In C-Mn Steels, On Microstructure And Toughness Of SAW Metal", The Welding Institute, Report No. 213/1983, April, 1983.

60. BARRITE, G.S., "The Microstructure And Toughness Of HSLA Steel Weld Metal", Svetsaren, A Welding Review, Part 1, p.8-11, 1983

61. HARRISON, P.L., FARRAR, R.A., " The Influence Of Oxygen Rich Inclusions On the Phase Transformation In HSLA Steel Weld Metal", Journal Of Materials Science, p.2208-2226, 1981

62. IWAMOTO, N., MAKINO, Y., "Inclusion Morphology In SAW Metal Using Fluxes Of the System (CaO)-MnO-SiO", Transaction Of The Japan Welding Research Institute, Vol. 8, December, p,165-168, 1978.

63. NORTH, T.H., BELL, H.B., KOUKABI, A., CRAIG, I., "Notch Toughness Of Low Oxygen Content Submerged Arc Deposits", Welding Journal, December, p.343-354, 1979.

64. HARRISON, P.L., "CCT Diagrams For C-Mn And Niobium Bearing HSLA Steel Weld Metal, Dept. Mechanical And Production Engineering, Report No. ME 79/24, October, 1979.

65. KOR, G.J., TURKOGEN, E.T., "Sulphides And Oxides In Fe-Mn Alloys", Metal Transactions, Vol. 3, 1972.

66. DORSCHU, K.E., STOUT, R.D., "Some Factors Affecting Notch Toughness Of Steel Weld Metal", Welding Journal Research Supplement, Vol. 40, p.97s-105s, 1961.

67. SHIGHA, A., IMURA, H., TSUBOI, J., "Notch Toughness Of Niobium Bearing Steel Weld Metal", IIW Document IX 880-74, 1974.

68. ABSON, D.J., "A Study Of The Influence Of Carbon And Silicon On The Microstructure And Toughness Of SAW Metal", Welding Journal, 68/1978/M, July, 1978.

69. EVANS, G.M., "Effect Of Manganese On The Microstructure And Properties Of All Weld Metal Deposits", Welding Journal Research Supplement, March, 1980.

70. TAYLOR, D.S., "The Effect Of Manganese On The Toughness Of E7016 Type Weld Metal", Welding And Metals Fabrication, November, p.452-460, 1982.

71. TULIANI, S.S., FARRAR, R.A., "The Effect Of Silicon In SA Weld Metals At Low Concentrations", Welding And Metals Fabrication, September, p.553-557, 1975.

72. YOSHINO, Y., STOUT, R.D, "Effect Of Microalloy Elements On The Notch Toughness Of Line Pipe Steel", Welding Journal Research Supplement, Vol.58, March, p.59s-68s, 1979.

73. ABE, N., KITADA, T., MIYATA, S., "Effect Of Alloying Elements On The Toughness And Microstructure Of High Current Density Gas Shielded Arc Process Weld Metal", Transactions Of The Japan Welding Society, Vol. 11, No. 1, April, 1980.

74. GARLAND, J.G., KIRKWOOD, P.R., BSC Report PROD/8 32/1/79/C, 1976.

75. LEVINE, E., HILL, D.C. "A Review Of The Structure And Properties Of Welds In Nb Or V Containing HSLA Steels", Welding Institute Research Bulletin, No.213, 1976.

76. SAWHILL, J.M., WADA, T., "Properties Of Welds In Low Carbon Mn-Mo-Nb Line Pipe Steels", Welding Journal Research Supplement, January, p.1s-11s, 1975.

77. JESSEMAN, R.J., "Columbium Pick-Up In High Dilution SAW Deposits", Proc. Int. Symp. Microalloy 75, Washington USA, Union Carbide, October 1-3, p.578, 1975.

78. DOLBY, R.E., "Review Of The Work Of The Influence Of Nb On The Microstructure And Toughness Of Ferritic Steel Weld Metal", Welding In The World, Vol.19, No.7/8, p.126-141, 1980.

79. ABSON, D.J., HART, P.H.M., " An Investigation Into The Influence Of Nb And V On The Microstructure And Mechanical Properties Of SAW In C-Mn Steels", The Welding Institute, Report No. 122/1980, Phase 1, September, 1980.

80. KIRKWOOD, P.R., GARLAND, J.G., "The Influence Of Vanadium On SAW Metal Toughness", Welding And Metals Fabrication, Parts 1/2, January/February, p.17-28/93-99, 1977.

81. GARLAND, J.G., KIRKWOOD, P.R., "Metallurgical Factors Controlling Weld Metal Toughness In Seam Welding Of Line Pipe Steel", Welding Research Council, Welding Of Line Pipe Steels, Published United Engineering Centre, 345 East 47th St., New York, NY, 10017.

82. WEGERZYN, J., DZIUBINSKI, J., "The Effect Of Minor Additions Of V And Nb In SAW Metal On The Mechanical Properties And Resistance To Brittle Fracture", International Institute Of Welding, IIW Doc. XIIA-145-77, December 1976.

83. MATROSOV, YU.I., SOROKIN, A.N., "Effects Of Vanadium On The Mechanical Properties, Phase Composition And Structure Of Low Pearlite Steel" Translated From Met. Term. Obra. Met., No.5, May, p.16-19, 1981.

84. HANNERZ, N.E., JONSSON-HOLMQUIST, B.M., "Vanadium In Mild Steel Weld Metal", Metal Construction, Vol.6, No.2, p.64-67, 1974.

85. HIRABAYASHI, K., TAIRA, T., YAMAGUCHI, T., TAKESSHIGE, K., "Improvement Of Toughness Of SAW Metal Of Low Temperature Service Line Pipe", Paper Presented TO The Symposium On "Physical Metallurgy Of Weldments", TMS-AIME, Niaghra Falls NY, September, 1976.

86. LEVINE, E., HILL, D.C., "Toughness In HSLA Steel Weldments", Metal Construction, August, p.346-352, 1977.

87. ABSON, D.J., HART, P.H.M., "An Investigation Into The Effects Of Nb And V On The Mechanical Properties Of SAW In C-Mn Steels", The Welding Institute, Report No. 162/1981, Phase 2, October, 1981.

88. DOLBY, R.E., "The Influence Of V On The Microstructure And Toughness Of Ferritic Steel Weld Metal - A Review", Metal Construction, March, p.148-153, 1982,

89. KIRKWOOD, P.R., GARLAND, J.G., "Metallurgical Factors Controlling Weld Metal Toughness In The Steam Welding Of Line Pipe", Symposium On Pipeline Welding, American Welding Society, St. Louis, May, 1976.

90. BONISZEWSKI, T., "Titanium In Steel Wires For CO Welding", Metal Construction, Vol. 1, No.3, May, p.225-229, 1969.

91. SNYDER, J.P., PENSE, A.W., "The Effect Of Titanium On SAW Metal", Welding Research Supplement, July, p.201S- 211S, 1982.

92. WIDGERY, D.J., As Reference 52, Part 2.

93. ITO, Y., NAKANISHI, M., "Study Of Charpy Impact Properties Of Weld Metal With SAW", The Suminoto Search, Vol.15, p.52, 1976.

94. WATANABE, I., SUZUKI, M., KOJIMA, T., "Applicability Of Large Current MIG Welding Techniques", Int. Conf. On Welding Research In The Eighties, Osaka, Japan, Section B, Paper B8, 1980.

95. MORI, N., "Mechanisms Of Notch Toughness Improvements In Ti-B Bearing Weld Metal", IIW Doc. No. IX 1196/81, 1981.

96. TENKULA, J., HEIKKINEN, V.K., "The Effect Of Parent Plate Aluminium On The Properties Of Two Wire SAW Metal In Nb Microalloyed Steels", Welding Research International Bulletin, Vol.8, p.369-376, 1978.

97. HANNERZ, N.E., WEREFORST, T., "The Influence Of Parent Plate Aluminium Content On Microstructure, Inclusion Distribution And Mechanical Properties Of SAW Metal", Paper 25, As Ref. 25.

98. NORTH, T.H., BELL. H.B., NOWICKI, A., CRAIG, I., "Slag/Metal Interaction, Oxygen And Toughness In SAW", Welding Journal, Vol.57, No.3, p.63-75, 1978.

99. SAVCHENKOV, V.A., TERLYSHNAYA, N.K., Welding Production, Vol.23, No.1, 1976.

100. TERASHIMA, H., HART, P.H.M., "Effect Of Aluminium In C-Mn Steels On The Microstructure And Toughness Of SAW Metal", Welding Institute Research Report, No.213/1983, April, 1983.

101. HANNERZ, N.E., "The Influence Of Deoxidation Of Structural Steel On Weld Metal Properties", Welding In The World, Vol.22, No.7/8, p.196-206, 1984.

102. GLADMAN, T., "On The Theory And Effect Of Precipitate Particles On Grain Growth In Metals", Proceedings Of The Royal Society, 294, p.298, 1966.

103. DOLBY, R.E., "Review Of The Work On The Influence Of Nb ON The Microstructure And Toughness Of Ferritic Steel Weld Metal". Welding Institute Research Bulletin, April, 1980.

104. TANINO, O., "The Precipitation Behaviour And Strengthening Effects Of NbC During Tempering And Continuous Cooling", Transactions ISIJ, p.337, 1968.

105. GRAY, J.M., "Weldability Of Niobium Containing HSLA Steel", Welding Research Council Bulletin, No.213, February, 1976.

106. TWEED, J.H., KNOTT, J.F., "Effecting Of Reheating On Microstructure And Toughness Of C-Mn weld Metal ", Metal Science, Vol.17, February, p.45-54, 1983.

107. B.S.1515. "Fusion Welding Of Pressure Vessels For use On The Chemical, Petroleum And Allied Industry".

108. GARLAND, J.G., KIRKWOOD, P.R., British Steel Report, PROD/449/1/74/C, 1974.

109. FARRAR, R.A., WONG, S.Y., WATSON, M.N., "How Stress Relief Affects Submerged Arc Weld Metal Containing Niobium", Welding And Metals Fabrication, Jan/Feb., p.21-23, 1980.

110. FICK, J.I.J., ROGERSON, J.H., "The Effect Of Stress Relief Heat Treatment On The Toughness Of C-Mn Submerged Arc Weld Metal", Welding And Metals F, March, p.85-89, 1978.

111. STEMBERA, V., MRAZ, L., "A Direct Method For The Examination Of Phase Transformation And Construction Of Austenite Breakdown Diagrams For Weld Metal", Svar. Prioz., No.4, p.5-8, 1981.

112. BARLOW, J.A., "Measurement And Analysis Of Thermal Cycles In SAW", Welding Institute Research Bulletin, January, p.5-8, 1982.

113. ELDIS, G.T., HAGEL, W.C., "Hardenability Concepts with Application To Steel", Proc. Symp. Metals Society AIME, Chicago, 1977.

114. GLADMAN, T., WOODHEAD, J.H.,"The Accuracy Of Point Counting In Metallographic Examinations", Journal Of The Iron And Steel Institute, No.194, p.189, 1960.

115. HAUSNER. H.H., Handbook Of Powder Metallurgy, Chemical Publishing Company Co. Inc., New York, 1973.

116. ASTM "General Methods And Instrumentation", Vol 14.01, Temperature Measurement.